Husky Energy

Final Report

White Rose Physical Environmental Data

for Production Systems (2011)

Prepared by: **Oceans Ltd.**

Oceans Contact: **Judith Bobbitt**

85 LeMarchant Rd.
St. John's, NL
A1C 2H1
Telephone: (709) 753-5788
Facsimile: (709) 753-3301
Email: oceans@oceansltd.com

Husky Contact: **Mike Rudofsky**

Development Group
Tel (709)-724-4684
mike.rudofsky@huskyenergy.com

NOTICE TO READER:

Report intended as reference material for the General Parameters document used as guidance for Phase 2 WREP work.

		[redacted]	
Initial Last Name / Title	Oceans Ltd.	Mike Rudofsky	May 31st, 2011
	Prepared By	Accepted By	Acceptance Date

				Document No.:	DG-DVG-RP-0079	Version No:	-

White Rose Physical Environmental Data for Production Systems (2011)

Submitted to
Husky Energy
Suite 901, Scotia Centre
235 Water Street
St. John‟s, NL

by

Oceans LTD.

85 LeMarchant Rd.
St. John‟s, NL
A1C 2H1

Telephone: (709) 753-5788
Facsimile: (709) 753-3301
Email: oceans@oceansltd.com

May 2011

Table of Contents

Table of Figures

Table of Tables

1.0 Introduction

The White Rose oilfield is situated on the northeastern part of the Grand Banks, in an open ocean site located approximately 350 km east of the island of Newfoundland as shown in Figure 1.1. The site is located near the edge of the Continental Shelf in a water depth of approximately 120 m. As a result of its climate, sea state, strong currents, wave and current conditions, and its susceptibility to seasonal intrusions of sea ice and icebergs, the project area is situated in a harsh oceanic environment.

This document has been prepared as a guide for design engineers who are designing and constructing sea installations at White Rose. It is an update to a previous document "Physical Environmental Data for Production System" prepared in 2001 by Oceans Ltd. for Husky Oil. This report contains a comprehensive description of normal and extreme environmental conditions at the White Rose location. In many cases, the site has equivalent environmental conditions to that at other platforms on the Grand Banks.

The report is divided into eleven sections. Section 2 deals with winds, and Section 3 with other atmospheric conditions. Waves are dealt with in Section 4, together with peak enhancement factors and fatigue wave analysis. Extreme wind and waves for return periods of 1-year, 10-year, 50-year, and 100-year are presented in Section 5. The extremes are given for each month as well as for the complete year. Section 6 presents currents for the site, and Section 7 deals with tides together with storm surges and tsunamis. Water properties are presented in Section 8. Sea ice and iceberg conditions are presented in Section 9 together with information on superstructure icing from spray and freezing precipitation. Information on earthquakes and design accelerations has been mainly extracted from the Terra Nova development study and summarized in Section 10. Section 11 deals with climate change and Section 12 details the changes from the last report as a result of having 10 additional years of environmental data.

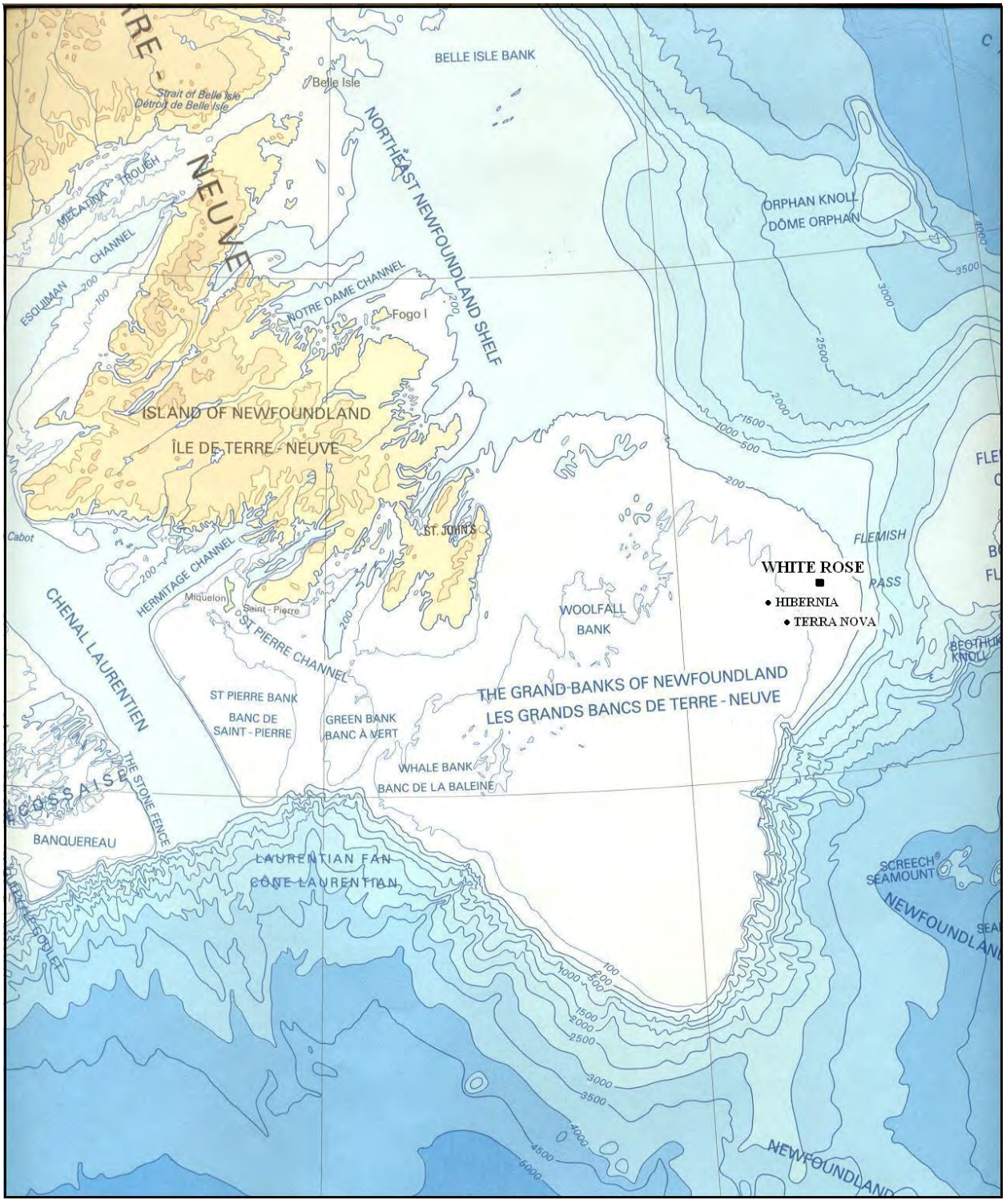

Figure 1.1 Grand Banks and Flemish Cap Bathymetric Features

2.0 Winds

2.1 General Description of Weather Systems

The White Rose area experiences weather conditions typical of a marine environment with the surrounding waters having a moderating effect on temperature. In general, marine climates experience cooler summers and milder winters than continental climates and have a much smaller annual temperature range. Furthermore, a marine climate tends to be fairly humid, resulting in reduced visibilities, low cloud heights, and significant amounts of precipitation.

The climate of the White Rose area is very dynamic, being largely governed by the passage of high and low pressure circulation systems. These circulation systems are embedded in, and steered by, the prevailing westerly flow that typifies the upper levels of the atmosphere in the mid-latitudes, which arises because of the normal tropical to polar temperature gradient. The mean strength of the westerly flow is a function of the intensity of this gradient, and as a consequence is considerably stronger in the winter months than during the summer months, due to an increase in the south to north temperature gradient. [Meteorological convention defines seasons by quarters; e.g., winter is December, January, February, etc.]

At any given time, the upper level flow is a wave-like pattern of large and small amplitude ridges and troughs. These ridges and troughs tend to act as a steering mechanism for surface features and therefore their positions in the upper atmosphere determine the weather at the earth‟s surface. Upper ridges tend to support areas of high pressure at the surface, while upper troughs lend support to low pressure developments. The amplitude of the upper flow pattern tends to be higher in winter than summer, which is conducive to the development of more intense storm systems.

During the winter months, an upper level trough tends to lie over Central Canada and an upper ridge over the North Atlantic resulting in three main storm tracks affecting the region: one from the Great Lakes Basin, one from Cape Hatteras, North Carolina and one from the Gulf of Mexico. These storm tracks, on average, bring eight low pressure systems per month over the area. The intensity of these systems ranges from relatively weak features to major winter storms. Recent studies (Archer and Caldeira, 2008) have shown that there exists a poleward shift of the jet stream, and consequently storm tracks, at a rate of 0.17 to 0.19 degrees/decade in the northern hemisphere. This shift has been related to an increase in the equator-to-pole temperature gradient. McCabe (2001) obtained similar results, finding that there has been a decrease in mid-latitude cyclone frequency and an increase in high-latitude cyclone frequency. In addition, McCabe (2001) found that storm intensity has increased in both the high and mid-latitudes.

In the case where the upper level long wave trough lies well west of the region, the main storm track will lie through the Gulf of St. Lawrence or Newfoundland. Under this regime, an east to southeast flow ahead of a warm front associated with a low will give way to winds from the south in the warm sector of the system. Typically, the periods of southerly winds and mild conditions will be of relatively long duration, and in general, the incidence of extended storm conditions is likely to be relatively infrequent. Strong frictional effects in the stable flow from the south results in a marked shear in the surface boundary layer and relatively lower winds at the sea surface. As a consequence, local

wind wave development tends to be inhibited under such conditions. Precipitation types are more likely to be in the form of rain or drizzle, with relatively infrequent periods of continuous snow, although periods of snow showers prevail in the unstable air in the wake of cold fronts associated with the lows. Visibility will be reduced at times in frontal and advection fogs, in snow, and in snow shower activity.

At other times, with the upper long wave trough situated further to the east, the main storm track may lie through or to the east of the Grand Banks. With the lows passing closer to the site and a higher potential for storm development, the incidence of strong gale and storm conditions is greater. Longer bouts of cold, west to northwest winds behind cold fronts occur more frequently, and because the flow is colder than the surface water temperatures, the surface layer is unstable. The shear in the boundary layer is lower, resulting in relatively higher wind speeds near the surface, and consequently relatively higher sea state conditions. With cold air and sea surface temperatures coupled with high winds, the potential for freezing spray will occur quite frequently. In this synoptic situation, a greater incidence of precipitation in the form of snow is likely to occur. Freezing precipitation, either as rain or drizzle, occurs rather infrequently on the Grand Banks. Visibility will be reduced in frontal and advection fogs, and relatively more frequently by snow.

Frequently, intense low pressure systems become „captured" and slow down or stall off the coast of Newfoundland and Labrador. This may result in an extended period of little change in conditions that may range, depending on the position, overall intensity and size of the system, from the relatively benign to heavy weather conditions.

By summer, the main storm tracks have moved further north than in winter. Low-pressure systems are less frequent and much weaker. With increasing solar radiation during spring, there is a general warming of the atmosphere that is relatively greater at higher latitudes. This decreases the north-south temperature contrast, lowers the kinetic energy of the westerly flow aloft and decreases the potential energy available for storm development. Concurrently, there is a northward shift of the main band of westerly winds at upper levels and a marked development of the Bermuda-Azores sub-tropical high-pressure area to the south. This warm-core high-pressure cell extends from the surface through the entire troposphere. The main track of the weaker low-pressure systems typically lies through the Labrador region and tends to be oriented from the west-southwest to the east-northeast.

With low pressure systems normally passing to the north of the region in combination with the northwest sector of the sub-tropical high to the south, the prevailing flow across the Grand Banks is from the southwest during the summer season. Wind speed is lower during the summer and the incidence of gale or storm force winds relatively infrequent. There is also a corresponding decrease in significant wave heights.

The prevailing southwesterly flow during the late spring and early summer tends to be moist and it is relatively warmer than the underlying surface waters on the Grand Banks.

Rapidly deepening storms are a problem south of Newfoundland in the vicinity of the warm water of the Gulf Stream. Sometimes these explosively deepening oceanic cyclones develop into a "weather bomb", defined as a storm that undergoes central pressure falls greater than 24 mb over 24 hours. Hurricane force winds near the center,

the outbreak of convective clouds to the north and east of the center during the explosive stage, and the presence of a clear area near the center in its mature stage (Rogers and Bosart, 1986) are typical of weather bombs. After development, these systems will either move across Newfoundland or to the east of Newfoundland producing gale to storm force winds from the southwest to south over the Grand Banks.

In addition to extratropical cyclones, tropical cyclones often retain their tropical characteristics as they enter the study area. Tropical cyclones account for the strongest sustained surface winds observed anywhere on earth. The hurricane season in the North Atlantic basin normally extends from June through November, although tropical storm systems occasionally occur outside this period. Once formed, a tropical storm or hurricane will maintain its energy as long as a sufficient supply of warm, moist air is available. Tropical storms and hurricanes obtain their energy from the latent heat of vapourization that is released during the condensation process. These systems typically move east to west over the warm water of the tropics; however, some of these systems turn northward and make their way towards Newfoundland. Since the capacity of the air to hold water vapour is dependent on temperature, as the hurricanes move northward over the colder ocean waters, they begin to lose their tropical characteristics. By the time these weakening cyclones reach Newfoundland, they are usually embedded into a mid-latitude low and their tropical characteristics are usually lost.

A significant number of tropical cyclones which move into the mid-latitudes will undergo transition into extratropical cyclones. On average, 46% of tropical cyclones which formed in the Atlantic transform into extratropical cyclones. During this transformation, the system loses tropical characteristics and becomes more extratropical in nature. These systems frequently produce large waves, gale to hurricane force winds and intense rainfall. The likelihood that a tropical cyclone will undergo transition increases toward the second half of the tropical season, with October having the highest probability of transition. In the Atlantic, extratropical transition occurs at lower altitudes in the early and late hurricane season and at higher latitudes during the peak of the season (Hart and Evans, 2001).

2.2 Data Sources

The data sources to describe the wind climatology at White Rose came from three main sources: the International Comprehensive Ocean-Atmosphere Data Set (ICOADS), rig observations and the MSC50 North Atlantic wind and wave climatology data base. The locations of the climate data sources are presented in Figure 2.1.

It should also be noted that wind speeds from the MSC50 and ICOADS data sets are not directly comparable to each other due to their sampling period and the heights at which they were measured. Wind speed is dependent on height since the wind speed increases at increasing heights above sea level. Methods to reduce wind speeds from anemometer level to 10 m have proven ineffective due to atmospheric stability issues. Winds in the ICOADS data set were either estimated or measured by anemometers at various heights above sea level.

Winds speeds from each of the data sources have different averaging periods. The MSC50 winds are 1-hour averages while the ICOADS and MANMAR winds are 10-minute average winds. For consistency, the MSC50 wind speeds have been adjusted to 10-minute wind speeds. The adjustment factor to convert from 1-hour mean values to 10-minute mean values is usually taken as 1.06 (U.S. Geological Survey, 1979).

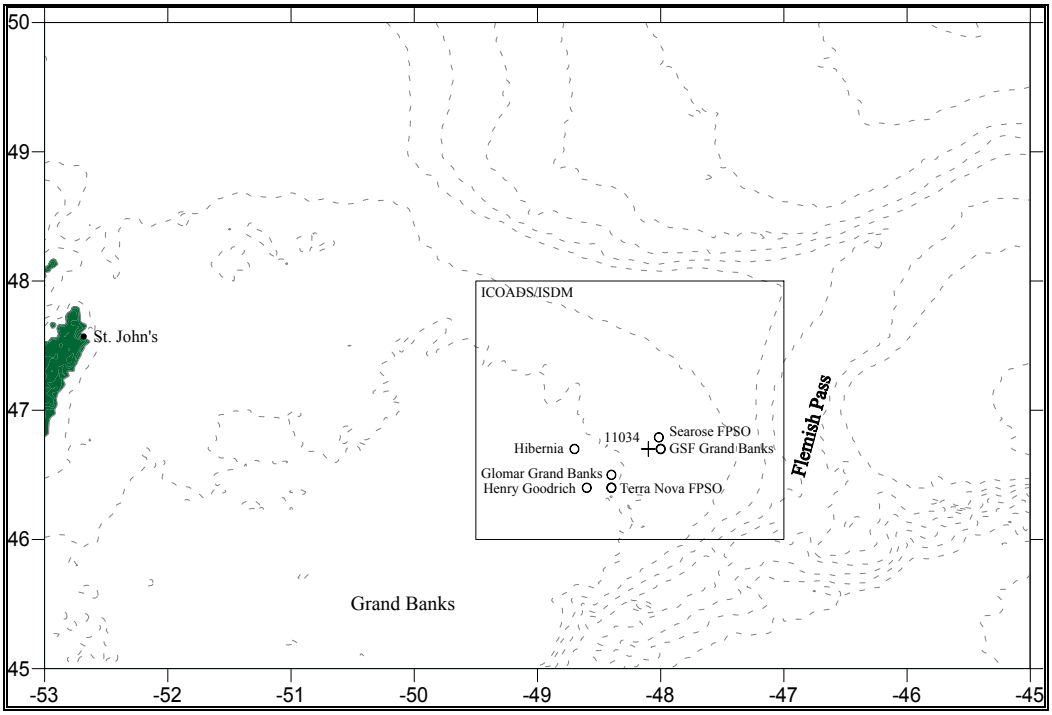

Figure 2.1 Locations of the Climate Data Sources

ICOADS

Air temperature, sea surface temperature and visibility statistics for the area were compiled using data from the International Comprehensive Ocean-Atmosphere Data Set (ICOADS). A subset of global marine surface observations from ships, drilling rigs, and buoys for the area from 46°00'N to 48°00'N, and 047°00'W to 049°30'W covering the period from January 1980 to January 2011 was used in this report.

The ICOADS data set has certain inherent limitations in that the observations are not spatially or temporally consistent. In addition, the data set is somewhat prone to observation and coding errors, resulting in some erroneous observations within the data set. The errors were minimized by using an outlier trimming level of 5.5 standard deviations for wind speed, and 3.5 standard deviations for air temperature and sea surface temperatures. In an attempt not to exclude valid observations from the data set, any data greater than 4.5 standard deviations for wind speed and 2.8 standard deviations for air and sea surface temperature were flagged and subsequently analyzed for consistency with other data within the same region and same time. Despite this analysis, valid observations may still have been excluded from the data set. Conversely, invalid data

which fell within the limits of the quality control analysis may have been included in the data set.

While the ship-based reports have been quality controlled to the extent possible, they are likely to contain some observation errors in addition to position report errors, particularly for the older reports. As well, the data set is known to contain a „fair weather bias", which arises for the following reasons: ship"s captains may choose to avoid areas of heavy weather, and since the reporting program is voluntary, fewer observations are likely to be taken under adverse weather and sea state conditions. This bias is more likely to be present during the winter season and over temperate and northern seas where vessel traffic is light.

Kent et al. (1993) demonstrated various systematic inconsistencies in the meteorological observations from voluntary observing ships. These inconsistencies were mostly dependent on the method of estimation that was used. Sea surface temperature data from engine intake thermometers were found to be biased high by an average of 0.3ºC. The dew point temperatures from fixed thermometer screens were biased high compared to psychrometer readings. The magnitude of the bias was of the order of 1ºC and varied with dew point temperature. Wind speeds from anemometers were biased high compared to visual winds by about two knots for winds up to about 25 knots. It was unknown whether visual winds or anemometer winds were more accurate. Compared to daytime values, visual winds at night were underestimated by about 1 m/s at 15 m/s and 5 m/s at 25 m/s.

Rig Observations

Wind statistics were also compiled using MANMAR data from several offshore platforms located in the region. The location, period of observation and anemometer height for each of these stations is presented in Table 2.1. Note that the Glomar Grand Banks and the GSF Grand Banks are the same platform under different names at the time of the observations.

Table 2.1 Locations of MANMAR Observations

	Latitude	Longitude	Anemometer Height (m)	Period
Sea Rose FPSO	46.8°N	48.0°W	42	Nov 04, 2005 – Mar 30, 2010
Terra Nova FPSO	46.4°N	48.4°W	50	Aug 12, 2007 - Dec 31, 2010
Glomar Grand Banks	46.5°N	48.4°W	82.5	Dec 31, 1998 - Jul 02, 2000
GSF Grand Banks	46.7°N	48.0°W	82.5	July 16, 2003 – Dec 31, 2010
Henry Goodrich	46.4°N	48.6°W	95	Feb 23, 2000 - Jun 30, 2009
Hibernia	46.7°N	48.7°W	139	Jan 01, 1999 - Dec 31, 2010
Ocean Ranger	46.5°N	48.4°W	N/A	Dec 04, 1980 – Feb 09, 1982

MSC50 Data Set

Wind climate statistics for the area were extracted from the MSC50 North Atlantic wind and wave climatology data base compiled by Oceanweather Inc under contract to

Environment Canada. The MSC50 data base consists of continuous wind and wave hindcast data in 1-hour time steps from January 1954 to December 2009, on a 0.1° latitude by 0.1° longitude grid. Winds from the MSC50 data set are 1-hour averages of the effective neutral wind at a height of 10 m (Harris, 2007). Grid point 11034 was chosen to represent conditions within the area of interest.

The MSC50 project followed the same basic methodology as was applied in the AES40 hindcast with notable improvements and upgrades. The temporal resolution was changed from a 6-hour time base to a 3-hour analysis. This increased resolution resulted in improved modeling of rapidly deepening winter storms which develop off the US Eastern Seaboard and track northeast across the Grand Banks.

2.3 Wind Speeds and Directions at White Rose

The White Rose area experiences predominately southwest to west flow throughout the year. There is a strong annual cycle in the wind direction. West to northwest winds which are prevalent during the winter months begin to shift counter-clockwise during March and April, resulting in a predominant southwest wind by the summer months. As autumn approaches, the tropical-to-polar temperature gradient strengthens and the winds shift slightly, becoming predominately westerly again by late fall and into winter. Low pressure systems crossing the area are more intense during the winter months. As a result, mean wind speeds tend to peak during this season.

In addition to mid-latitude low pressure systems crossing the Grand Banks, tropical cyclones often move northward out of the influence of the warm waters of the Gulf Stream, passing near the Island of Newfoundland. Once the cyclones move over colder waters they lose their source of latent heat energy and often begin to transform into a fast-moving and rapidly developing extratropical cyclone producing large waves and sometimes hurricane force winds.

Low pressure systems crossing the area are more intense during the winter months. As a result, mean wind speeds tend to peak during this season. Wind speed typically increases with increasing heights above sea level. Statistics in Table 2.2 are presented in order of increasing height above sea level with the MSC50 data set being the lowest and the Hibernia Platform being the highest. The anemometer heights for each platform are found in Table 2.1. Statistics for each anemometer level are presented to give a better idea of winds at varying levels above sea level.

A wind rose of the annual wind speed for Grid Point 11034 is presented in Figure 2.2 and the associated histogram of the wind speed frequency in Figure 2.3. Monthly wind roses along with histograms of the percentage occurrence of wind speeds can be found in Appendix 1. Percentage frequency of wind direction by month is presented in Table 2.3.

Table 2.2 Mean Wind Speed (m/s) Statistics

	MSC50 Grid Point 11034	ICOADS	Ocean Ranger	Sea Rose FPSO	Terra Nova FPSO	Glomar Grand Banks	GSF Grand Banks	Henry Goodrich	Hibernia
January	11.1	14.2	13.8	13.2	14.3	12.9	14.0	15.4	16.9
February	10.9	13.6	13.0	12.0	13.3	11.9	13.0	15.3	16.0
March	9.9	12.5	-	11.1	12.3	11.9	12.6	14.0	14.6
April	8.3	11.7	-	10.3	11.5	11.4	12.2	12.7	13.7
May	7.0	10.6	-	8.9	11.0	9.7	11.4	11.8	12.8
June	6.5	10.5	-	8.8	10.0	9.4	9.9	11.6	12.1
July	6.1	10.2	-	8.4	9.4	9.5	9.4	11.1	11.5
August	6.4	9.4	-	10.7	9.4	8.4	8.9	9.8	10.8
September	7.5	10.4	-	10.8	10.6	10.3	10.0	10.4	11.9
October	8.8	11.7	-	12.5	11.8	12.8	11.4	12.2	13.6
November	9.5	12.3	14.1	12.7	12.3	11.0	12.1	12.7	14.5
December	10.7	14.0	12.3	13.9	14.5	12.6	13.4	14.4	16.1

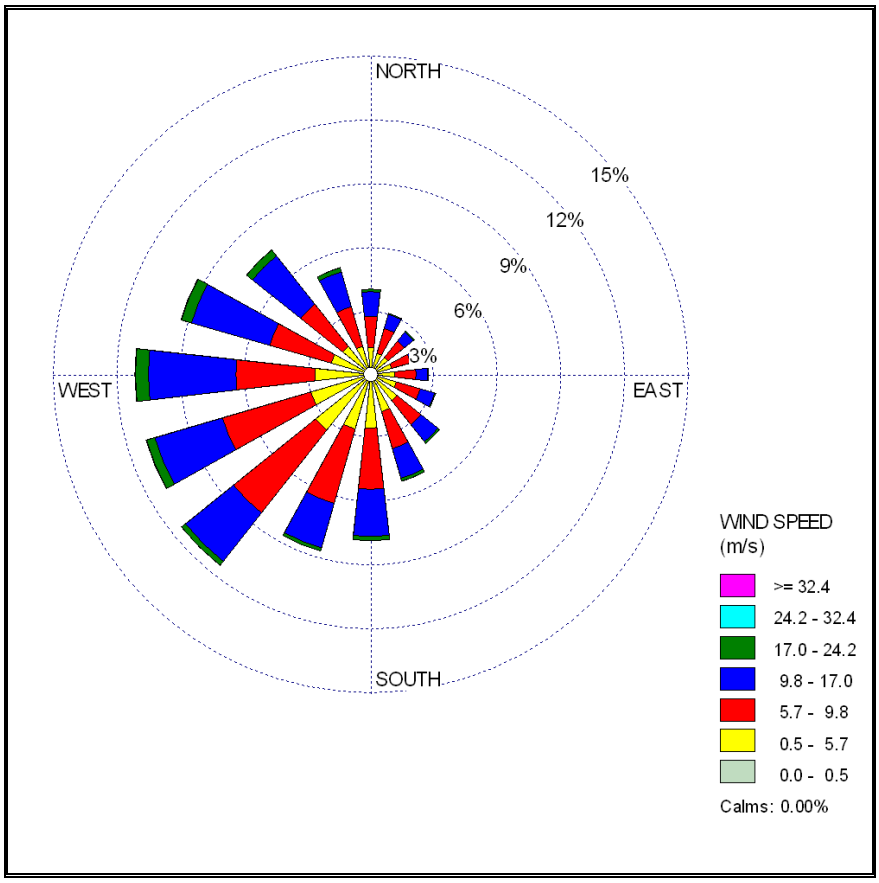

Figure 2.2 Annual Wind Rose for MSC50 Grid Point 11034 located near 46.7°N; 48.1°W. 1954 – 2009

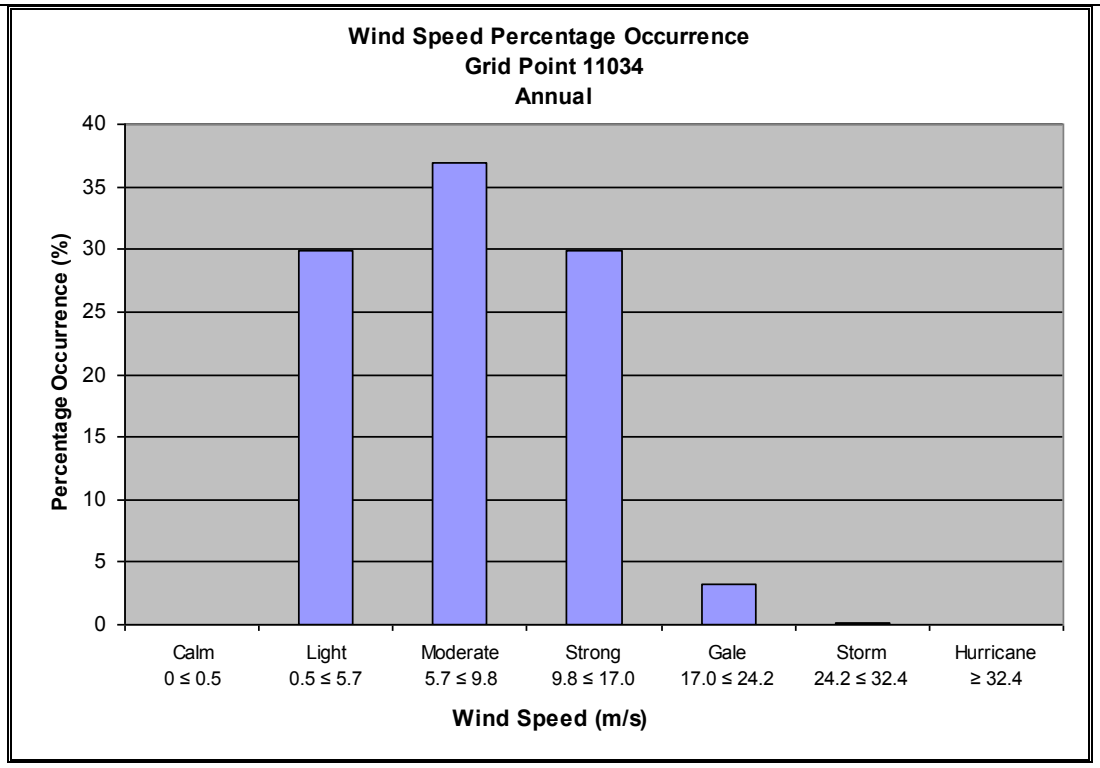

Figure 2.3 Annual Percentage Frequency of Wind Speeds for MSC50 Grid Point 11034 located near 46.7°N; 48.1°W. 1954 – 2009

Table 2.3 Monthly and Annual Percentage Frequency of Wind Speed by Direction (MSC50 Grid Point 11034)

	Direction							
Month	**NE**	**E**	**SE**	**S**	**SW**	**W**	**NW**	**N**
January	4.2	5.0	7.8	11.7	17.7	29.0	17.6	6.9
February	5.1	6.0	8.6	11.9	15.2	27.1	18.3	7.9
March	7.4	7.0	8.0	12.2	16.5	21.6	16.6	10.8
April	7.5	9.0	10.0	12.6	17.7	18.1	14.9	10.2
May	7.7	7.3	9.2	15.4	20.5	17.1	13.3	9.6
June	5.0	5.4	7.8	16.9	30.6	17.0	9.8	7.6
July	2.7	3.6	6.9	21.7	37.8	16.4	6.9	4.0
August	4.4	4.2	8.3	18.4	30.3	18.7	9.2	6.7
September	5.8	4.7	6.8	14.8	21.5	21.3	15.8	9.4
October	4.7	5.3	7.3	13.2	17.9	22.5	19.5	9.6
November	5.0	5.5	9.1	14.3	17.2	21.9	18.9	8.1
December	4.1	5.0	8.2	12.9	16.3	26.8	18.5	8.2
Annual	5.3	5.6	8.2	14.7	21.6	21.5	14.9	8.2

Wind speeds are much lower in the summer than in winter. The percentage exceedance of wind speeds at grid point 11034 is presented in Table 2.4 and Figure 2.4. Winds of gale force or greater are observed in 9.41% of the January observations and in only 0.02% of the July observations. Gale force winds or greater winds (>17.0m/s) occurred at the 10-metre level only 3.4% of the time annually.

Table 2.4 Percentage Exceedance of Wind Speed by Beaufort Category at Grid Point 11034

	Percent Winds > 0.5 m/s	Percent Winds > 5.7 m/s	Percent Winds > 9.8 m/s	Percent Winds > 17.0 m/s	Percent Winds > 24.2 m/s	Percent Winds > 32.4 m/s	Total Wind Samples
January	100.0	86.1	57.0	9.6	0.3	0.0	41664
February	100.0	86.0	55.9	8.7	0.4	0.0	37968
March	100.0	80.6	47.0	4.8	0.1	0.0	41664
April	100.0	70.5	31.5	1.8	0.0	0.0	40320
May	99.9	59.1	18.8	0.5	0.0	0.0	41664
June	100.0	54.6	13.6	0.1	0.0	0.0	40320
July	99.9	50.8	8.4	0.0	0.0	0.0	41664
August	100.0	52.9	11.7	0.2	0.0	0.0	41664
September	100.0	63.3	22.7	1.0	0.0	0.0	40320
October	100.0	75.1	36.4	2.3	0.1	0.0	41664
November	100.0	79.2	42.8	3.9	0.1	0.0	40320
December	100.0	84.3	53.8	7.5	0.3	0.0	41664
Annual	100.0	70.1	33.2	3.4	0.1	0.0	490896

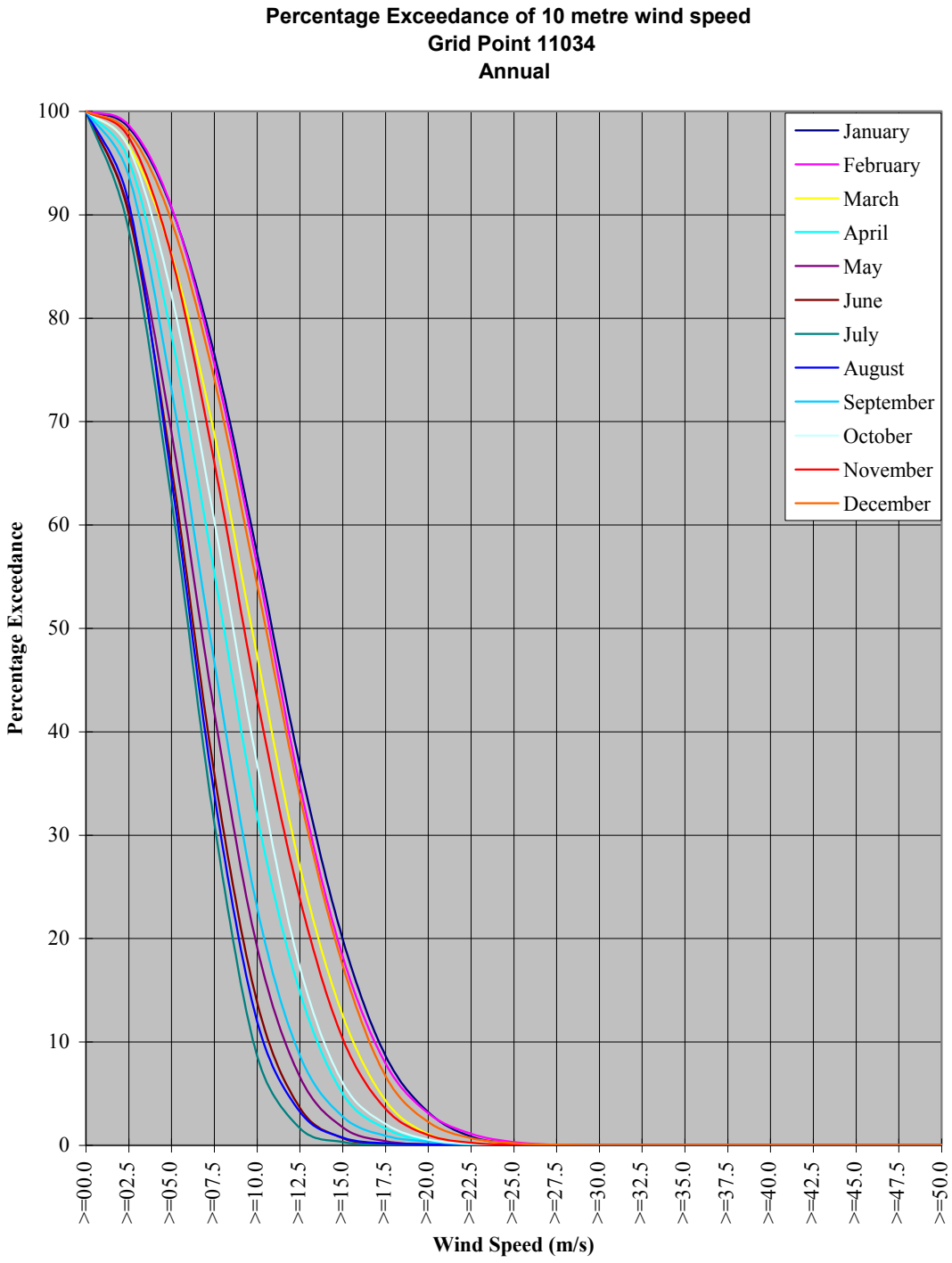

Figure 2.4 Percentage Exceedance of 10 metre Wind Speed at Grid Point 11034 Located Near 46.7°N; 48.1°W . 1954 to 2009

A table of monthly maximum wind speeds for each of the data sets is presented in Table 2.5 and the monthly maximum wind speed by direction from the MSC50 data base in Table 2.6. Rapidly deepening storm systems known as weather bombs frequently cross the Grand Banks. These storm systems typically develop in the warm waters of Cape Hatteras and move northeast across the Grand Banks. At 00Z on February 11, 2003 a 987 mb low pressure off Cape Hatteras deepened to 949 mb as it moved northeast, crossing eastern Newfoundland near 18Z. The low then began to weaken as it moved north of the forecast waters in the evening. There were no observations on the White Rose field during this event. Wind speeds of 49.4 m/s and 50.9 m/s from the southwest were recorded by the Hibernia and the Henry Goodrich anemometers, respectively as this system passed. The values from the Hibernia Platform do not give a true indication of the winds during this event, as the anemometer reached its maximum speed for a period of time. Furthermore, wind speeds reported in both the Henry Goodrich and Hibernia MANMAR"s are every three hours and as such probably did not capture the highest wind speeds measured during this event. The anemometers on all platforms on the Grand Banks; the Henry Goodrich, Terra Nova FPSO, and Hibernia registered the maximum speeds the anemometers could record during gusts. While wind speeds at the surface were estimated to be high, the wind speeds measured at the anemometers were not related to the surface winds and therefore adjustment factors to adjust wind speeds from the anemometers to the surface are not valid. The extreme wind speeds measured during this event were due to a combination of a very low central pressure which resulted in the surface boundary layer lowering to below anemometer heights. As a consequence, the anemometers were subject to a very strong low-level jet associated with the low pressure system.

A wind speed of 43.7 m/s was recorded by the Sea Rose FPSO at 00Z and 03Z on October 15, 2009. This occurred as another storm following a similar track to the February 10th storm passed over the area. During this event, the low pressure deepened from 1002 mb at 00Z on October 14th to 963 mb as the system passed northeast of the Avalon on October 15th.

2.4 Tropical Systems

The hurricane season in the North Atlantic basin normally extends from June through November, although tropical storm systems occasionally occur outside this period. While the strongest winds typically occur during the winter months and are associated with mid-latitude low pressure systems, storm force winds may occur at any time of the year, as a result of tropical systems. Once formed, a tropical storm or hurricane will maintain its energy as long as a sufficient supply of warm, moist air is available.

Tropical storms and hurricanes obtain their energy from the latent heat of vapourization that is released during the condensation process. These systems typically move east to west over the warm water of the tropics. However, some of these systems turn northward and make their way towards Newfoundland and the project area. Since the capacity of the air to hold water vapour is dependent on temperature, the hurricanes begin to lose their tropical characteristics as they move northward over the colder ocean waters. By

the time these weakening cyclones reach Newfoundland, they are usually embedded into a mid-latitude low and their tropical characteristics are usually lost.

Table 2.5 Maximum Wind Speed (m/s) Statistics

	MSC50 Grid Point 11034	ICOADS	Ocean Ranger	Sea Rose FPSO	Terra Nova FPSO	Glomar Grand Banks	GSF Grand Banks	Henry Goodrich	Hibernia
January	29.0	43.7	34.5	25.7	31.9	30.9	37.6	44.2	43.2
February	32.0	46.3	37.0	25.7	31.4	26.8	35.5	52.5	49.4
March	28.4	38.0	-	23.7	29.8	23.7	31.4	32.9	37.6
April	25.0	37.0	-	24.7	23.2	26.8	28.3	30.9	32.9
May	22.5	33.9	-	21.6	25.2	22.1	25.7	32.9	32.4
June	23.4	35.5	-	18.5	24.2	21.1	27.3	28.3	35.5
July	19.6	31.9	-	18.0	23.2	20.1	25.2	26.2	31.9
August	28.9	26.0	-	33.4	29.8	25.7	34.0	28.8	41.2
September	24.6	37.6	-	30.9	34.5	29.3	26.8	28.3	43.2
October	27.0	41.1	-	43.7	31.9	32.9	30.9	27.8	44.8
November	27.5	41.2	28.8	25.2	28.3	25.7	29.3	32.4	38.1
December	30.1	47.8	28.8	24.7	37.6	27.3	35.5	38.1	39.1

Source: MANMAR observations from rigs and platforms
ICOADS data set

Table 2.6 Monthly Maximum Anemometer Wind Speed (m/s) by Direction

	Direction								Monthly	
Month	NE	E	SE	S	SW	W	NW	N	Min	Max
January	21	23	24	26	29	27	27	25	21	29
February	23	22	25	30	30	30	32	24	22	32
March	22	25	24	22	24	28	28	24	22	28
April	22	20	21	25	24	23	24	24	20	25
May	16	18	17	19	20	19	22	19	16	22
June	16	17	20	18	18	21	23	15	15	23
July	14	16	17	20	17	17	17	15	14	20
August	17	18	19	29	28	23	29	24	17	29
September	21	21	22	23	25	23	21	21	21	25
October	22	22	24	27	27	27	25	23	22	27
November	21	23	23	27	23	27	28	26	21	28
December	22	22	25	23	28	28	30	25	22	30
Years Max	23	25	25	30	30	30	32	26		

Source: MSC50 data base

There has been a significant increase in the number of Hurricanes that have developed within the Atlantic Basin during the last 15 years. Figure 2.5 shows the 5-year average of tropical storms which have developed within the Atlantic Basin since 1961. This increase in activity has been attributed to naturally occurring cycles in tropical climate patterns near the equator called the tropical multi-decadal signal (Bell and Chelliah, 2006). As a result of the increase in tropical activity in the Atlantic Basin, there has also been an increase in tropical storms or their remnants entering the Canadian Hurricane Centre Response zone. There is little change in the 5-year trend for hurricanes coming within the project area. It should be noted that the unusually high number of tropical storms in 2005 may be skewing the results for the 2001 to 2005 season.

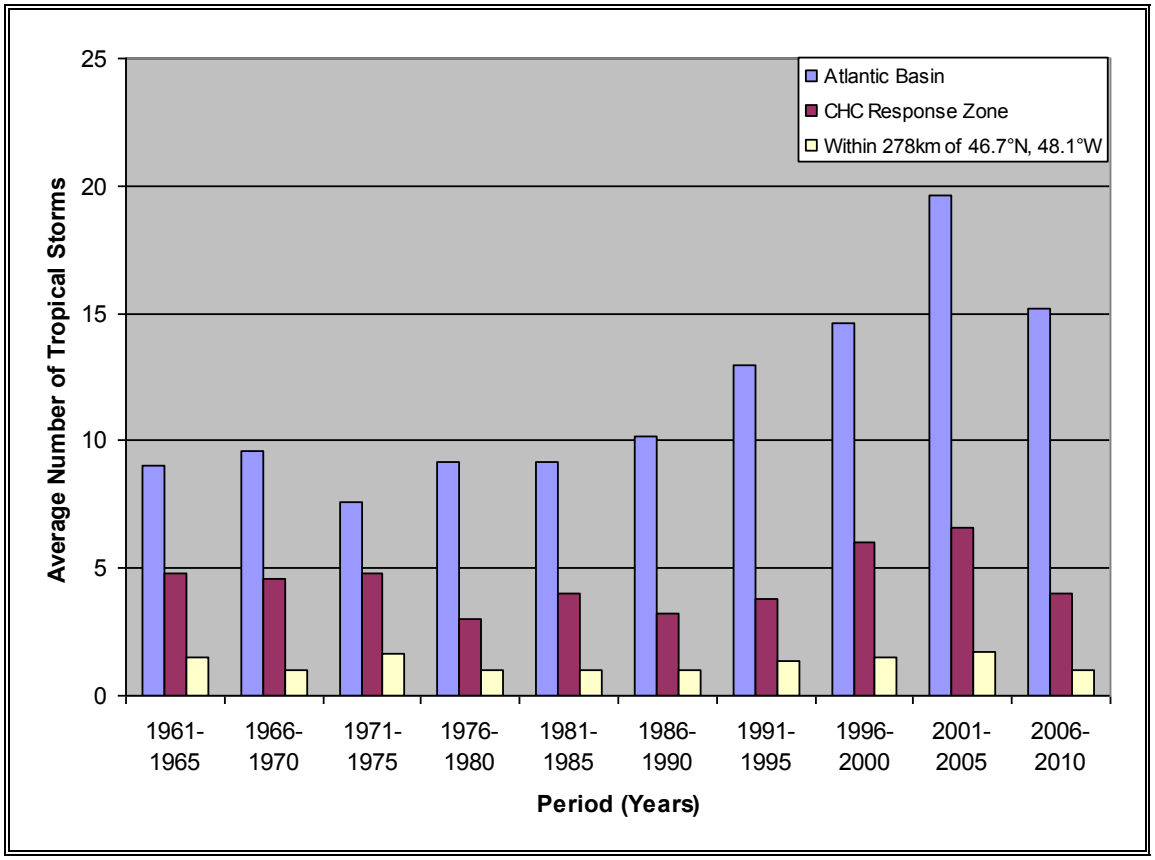

Figure 2.5 5-Year Average of the Number of Tropical Storms which formed in the Atlantic Basin since 1961

A significant number of tropical cyclones which move into the mid-latitudes transform into extratropical cyclones. On average, 46% of tropical cyclones which formed in the Atlantic transform into extratropical cyclones. During this transformation, the system loses tropical characteristics and becomes more extratropical in nature resulting in an increase in size which produces large waves, gale to hurricane force winds and intense rainfall. The likelihood that a tropical cyclone will undergo transition increases toward the second half of the tropical season; with October having the highest probability of

transition. In the Atlantic, extratropical transition occurs at lower latitudes in the early and late hurricane season and at higher latitudes during the peak of the season (Hart and Evans, 2001).

Since 1958, 32 tropical systems have passed within 278 km of 46.7ºN; 48.1ºW. The names are given in Table 2.7 and the tracks are shown in Figure 2.6. It should be noted that the values in Table 2.7 are the maximum 1-minute mean wind speeds occurring within the tropical system at the 10-m reference level as it passed within 278 km of the location.

Table 2.7 Tropical Systems Passing within 278 km of 46.7ºN, 48.1ºW (1958 to 2010)

Year	Month	Day	Hour	Name	Latitude	Longitude	Wind (m/s)	Pressure	Category
1963	8	28	0000	Beulah	45.8	-48.3	36.0	N/A	Category 1
1963	10	12	1800	Flora	45.2	-47.5	38.6	N/A	Extratropical
1964	9	4	1800	Cleo	46.9	-49.8	36.0	N/A	Category 1
1967	9	4	0600	Arlene	45.8	-48.6	30.9	N/A	Tropical Storm
1969	8	13	0000	Blanche	47.1	-49.0	25.7	N/A	Extratropical
1971	7	7	1800	Arlene	46.5	-53.0	23.1	N/A	Extratropical
1971	8	6	1200	Unnamed	55.7	-43.8	36.0	974	Category 1
1974	7	20	0600	Subtrop 2	46.7	-48.0	20.6	N/A	Extratropical
1975	7	4	0600	Amy	44.5	-51.6	25.7	986	Tropical Storm
1975	10	3	1200	Gladys	46.6	-50.6	43.7	960	Category 2
1976	8	24	0000	Candice	45.9	-48.7	33.4	N/A	Category 1
1978	9	5	0600	Ella	47.2	-50.2	41.2	975	Category 1
1979	8	6	0600	Unnamed	48.2	-50.6	12.9	N/A	Tropical Depression
1980	9	8	1200	Georges	45.6	-51.1	34.5	993	Category 1
1982	9	19	0600	Debby	47.0	-50.5	38.6	979	Category 1
1984	9	2	1984	Cesar	46.0	-50.4	25.7	994	Tropical Storm
1990	9	3	0000	Gustav	46.0	-46.5	28.3	993	Tropical Storm
1992	10	26	1800	Frances	46.0	-46.9	28.3	988	Tropical Storm
1993	9	10	0600	Floyd	45.4	-48.3	33.4	990	Category 1
1995	7	20	1200	Chantal	45.4	-48.8	25.7	1000	Extratropical
1995	8	22	1200	Felix	46.8	-50.8	25.7	985	Tropical Storm
1999	10	19	1200	Irene	48.0	-48.0	41.2	968	Extratropical
2000	9	25	1200	Helene	44.0	-55.5	28.3	988	Tropical Storm
2001	8	29	0000	Dean	47.0	-48.5	23.1	999	Extratropical
2001	9	20	0000	Gabrielle	48.5	-48.5	30.9	988	Extratropical
2001	11	6	1200	Noal	43.0	-48.5	25.7	996	Extratropical
2003	10	7	1800	Kate	47.5	-47.2	30.9	980	Tropical Storm
2004	8	6	0000	Alex	44.5	49.3	38.6	978	Category 1
2004	9	2	0000	Gaston	47.0	-50.0	23.1	997	Extratropical
2005	7	30	1800	Franklin	46.4	-48.8	20.6	1006	Extratropical
2008	10	1	1800	Laura	47.5	-46.3	20.6	995	Extratropical
2009	8	24	0900	Bill	48.6	-50.2	36.0	980	Tropical Storm

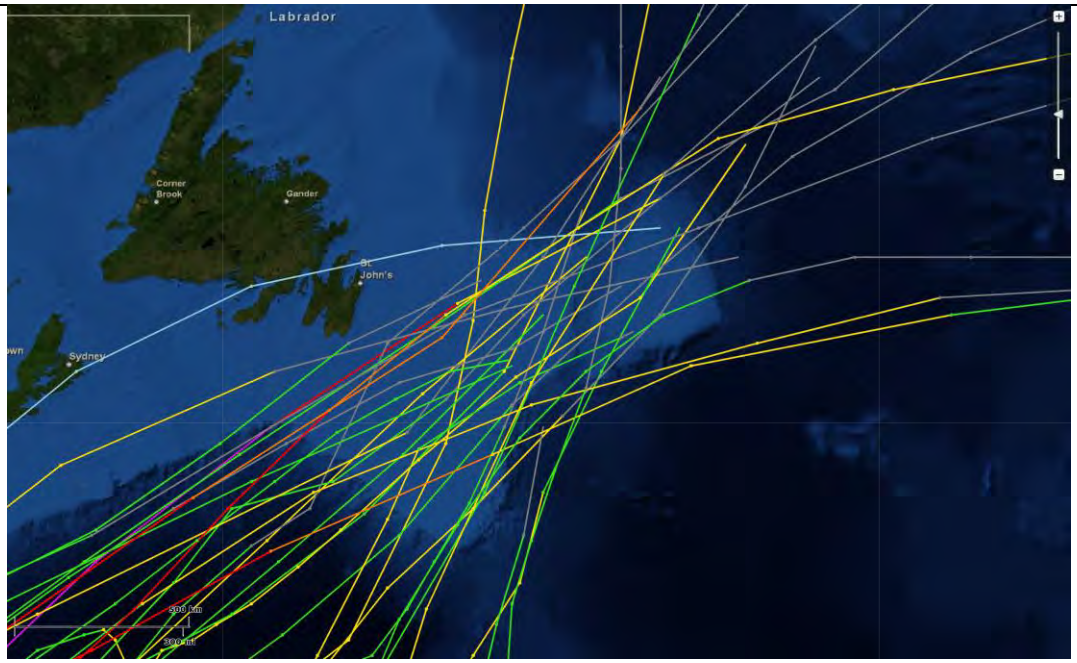

Figure 2.6 Storm Tracks of Tropical Systems Passing within 278 km of 46.7ºN, 48.1ºW (1958 to 2010)

On occasion, these systems still maintain their tropical characteristics when they reach Newfoundland. Nine Category 1 and one Category 2 hurricanes crossed within 278 km during the period from 1958 to 2008. The most intense of these storms was Hurricane Gladys which crossed at 12Z on October 03, 1975 with maximum sustained wind speeds of 43.7 m/s and a central pressure of 960 mb. Hurricane Gladys underwent extratropical transition over the following hours and moved northeast of the area as an extratropical storm with wind speeds of 38.6 m/s.

3.0 Weather Variables

3.1 Air and Sea Surface Temperature

The moderating influence of the ocean serves to limit both the diurnal and the annual temperature variation on the Grand Banks. Diurnal temperature variations due to the day/night cycles are very small. Short-term, random temperature changes are due mainly to a change of air mass following a warm or cold frontal passage. In general, air mass temperature contrasts across frontal zones are greater during the winter than during the summer season.

Air and sea surface temperatures for the area were extracted from the ICOADS data set. A monthly plot of air temperature versus sea surface temperature is presented in Figure 3.1. Air and Sea Surface Temperature statistics presented in Table 3.1 and Table 3.2 show that the atmosphere is coldest in the month of February with a mean monthly air temperature of -0.4°C, and warmest in August with a mean monthly air temperature of 14.3°C. Similarly, sea surface temperature is warmest in August with a mean monthly temperature of 13.7°C and coldest in February and March with mean monthly temperatures of 0.3°C. The mean sea surface temperature is cooler than the mean air temperature from March to August, with the greatest difference occurring in the month of July. From September to February, sea surface temperatures are warmer than the mean air temperature. The colder sea surface temperatures from March to August have a cooling effect on the atmosphere, while relatively warmer sea surface temperatures from September to February tend to warm the overlying atmosphere.

Monthly mean daily maximum and minimum temperature statistics are also presented for the ICOADS data set. Mean temperatures for each month are the mean of all temperatures recorded at the site during that month. The maximum and minimum temperatures are the highest and lowest temperatures, respectively, recorded during the month over the entire data set. The mean daily maximum is the average of all maximum temperatures recorded during the specified month, while the mean daily minimum is the average of all minimum temperatures recorded during the specified month.

Table 3.1 ICOADS Air Temperature (°C) Statistics

Month	Mean	Maximum	Minimum	Standard Deviation (°C)	Mean Daily Maximum	Mean Daily Minimum
January	0.1	12.0	-12.0	3.2	2.6	-2.2
February	-0.4	10.4	-12.1	3.1	1.9	-2.9
March	0.3	15.3	-17.3	2.8	2.5	-1.7
April	1.9	11.4	-7.3	2.4	4.1	0.1
May	4.1	13.0	-10.0	2.3	6.2	2.3
June	7.1	16.8	-1.2	2.4	9.3	5.3
July	11.9	25.3	-3.2	2.6	13.5	9.7
August	14.3	23.6	5.5	2.3	16.1	12.4
September	12.6	20.5	-4.0	2.5	14.7	10.7
October	8.8	18.4	-1.0	3.0	11.1	6.9
November	5.1	15.3	-4.6	3.0	7.5	3.2
December	2.1	12.8	-13.5	3.3	4.5	0.1

Table 3.2 ICOADS Sea Surface Temperature (°C) Statistics

Month	Mean	Maximum	Minimum	Standard Deviation	Mean Daily Maximum (°C)	Mean Daily Minimum (°C)
January	1.0	7.0	-2.0	1.5	2.3	0.2
February	0.3	6.0	-2.0	1.7	1.6	-0.4
March	0.3	6	-2.0	1.4	1.5	-0.4
April	1.0	7.5	-2.0	1.6	2.0	0.2
May	3.0	9.6	-2.0	1.8	4.2	1.8
June	5.9	14.0	-2.0	2.4	7.1	4.4
July	10.5	19.0	2.3	2.5	11.4	8.8
August	13.7	20.5	6.0	2.2	14.7	11.9
September	12.7	20.0	4.0	2.4	13.9	10.8
October	9.1	17.0	1.0	2.7	10.8	7.2
November	5.5	13	-1.9	2.6	7.25	3.9
December	2.7	10.2	-2.0	2.11	4.3	1.6

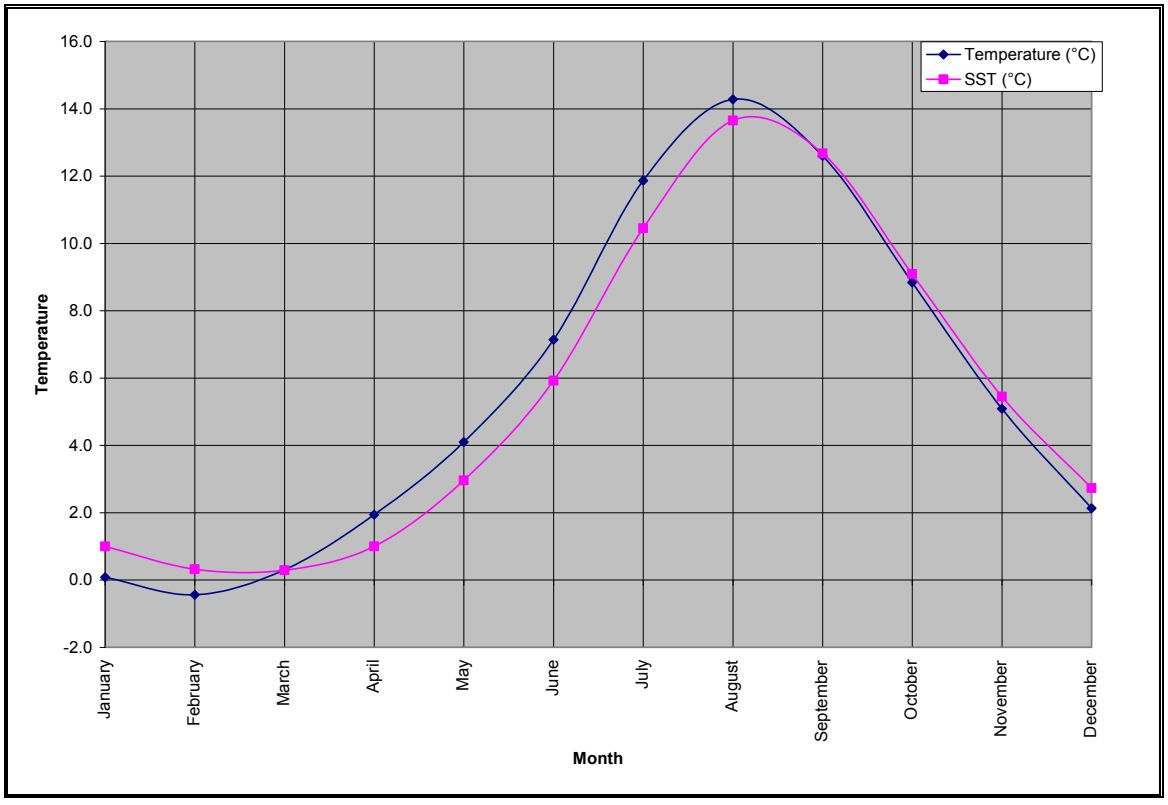

Figure 3.1 Monthly Mean Air and Sea Surface Temperature (°C) for the ICOADS data set

3.2 Extreme Air Temperatures

The ICOADS data set was analyzed to determine the number of days each year that specified thresholds were met. The results are presented in Table 3.3. There were 544 days when the minimum daily temperature decreased below -5°C. Of these, 224 days occurred during the 1980"s, 142 occurred during the 1990"s and 178 during the 2000"s. The temperature decreased below -10°C on only 36 days; half of which occurred during the 1980"s. The temperature decreased to below -15°C on only 2 days. The two days when the temperature decreased below -15°C occurred on March 10-11th, 1986 when temperatures dropped to -17.3°C. This cold temperature occurred because of pack ice in the area (Figure 3.2) and winds from the northwest.

Table 3.3 Number of Days below Threshold

Year	days <= -5°C	days <= -10°C	days <= -15°C	Minimum Temperature (°C)
1980	15	1	0	-11.5
1981	6	1	0	-10.0
1982	30	0	0	-9.5
1983	22	1	0	-10.0
1984	27	5	0	-13.5
1985	30	4	0	-11.8
1986	29	3	2	-17.3
1987	12	0	0	-7.2
1988	23	2	0	-10.5
1989	30	2	0	-12.0
1990	32	2	0	-11.0
1991	30	5	0	-11.0
1992	22	1	0	-10.0
1993	15	2	0	-11.2
1994	11	0	0	-7.5
1995	5	0	0	-7.0
1996	6	0	0	-8.0
1997	6	0	0	-8.3
1998	11	0	0	-8.4
1999	4	0	0	-8.0
2000	10	0	0	-8.2
2001	15	1	0	-10.1
2002	27	2	0	-11.5
2003	37	4	0	-12.0
2004	6	0	0	-7.9
2005	12	0	0	-7.9
2006	6	0	0	-9.2
2007	19	0	0	-8.3
2008	22	0	0	-8.8
2009	17	0	0	-8.1
2010	7	0	0	-8.7

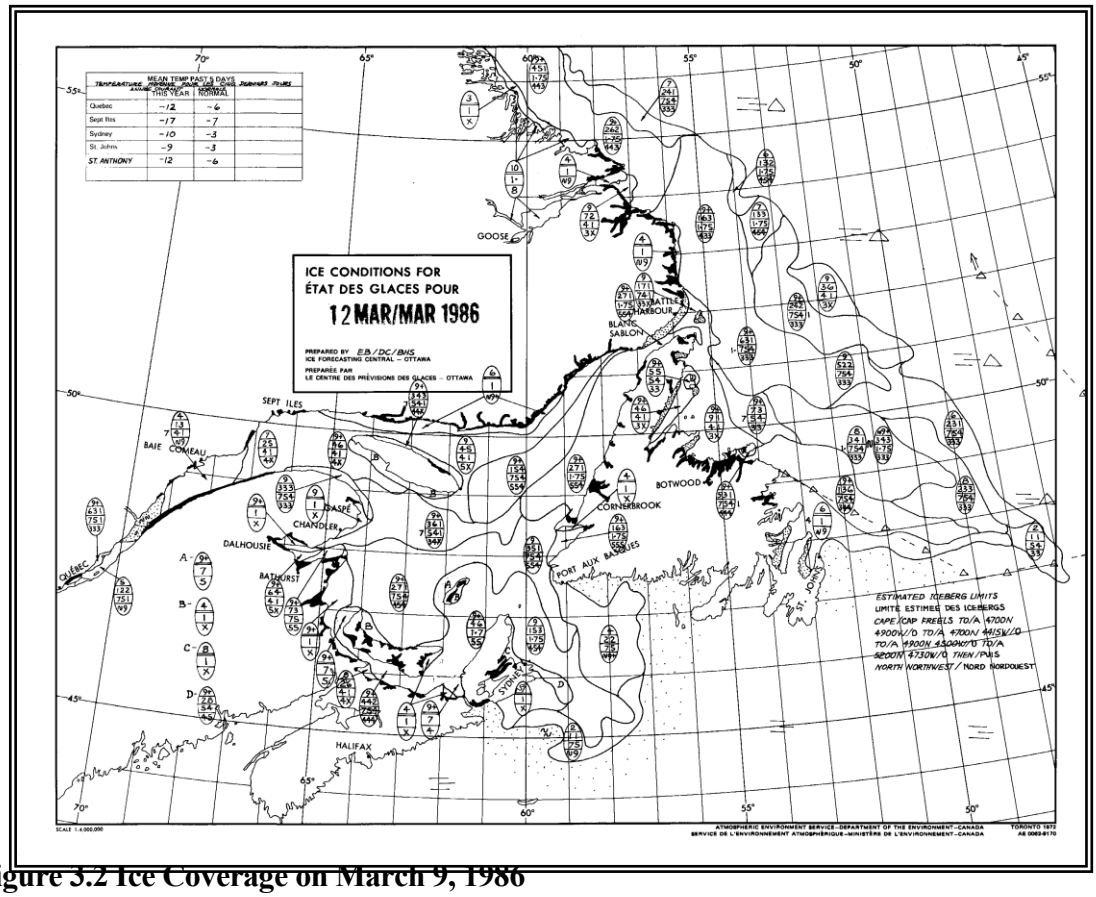

Figure 3.2 Ice Coverage on March 9, 1986

The extreme temperature analysis was carried out using the ICOADS data set supplemented by observations from different vessels and rigs from February 1984 to August 1988 that were not included in the ICOADS data set.

3.2.1 Minimum Temperature

There are two design specifications for offshore structure. The DNV Standard is the "lowest daily mean temperature to which the structure may be exposed". The CSA Standard is "the minimum temperature with an annual probability of exceedance of 0.5".

CSA Standard

According to CSA Standard for Steel Structures S473-04 the Toughness Design Temperature is defined as "The minimum temperature to which a structural element is subject, established on the basis of an annual probability of exceedance of 0.5. The temperature is that actually experienced by the element, taking into account thermal inertia and all sources of heat".

For the minimum temperature analysis, the daily minimum temperature was found for each day in the data set. The 30 lowest minimum temperature events were then chosen with one restriction; no event could occur within 5 days of another. This restriction

ensures that all the chosen events were independent of each other. The lowest minimum temperature event chosen was -17.3°C, which occurred on March 10th, 1986. These temperature events were fitted to a Gumbel distribution and extreme value estimates for minimum temperature were calculated for return periods of 2-years, 10-years, 25-years, 50-years and 100-years. These values are given in Table 3.4 together with the 95% confidence intervals.

Table 3.4 Extreme Minimum Temperature Estimates for Return Periods of 2, 10, 25, 50 and 100 Years

Return Period (years)	Annual Probability of Exceedance	Extreme Minimum Temperature (°C)	95% Lower Confidence Bound (°C)	95% Upper Confidence Bound (°C)
2	0.5	-11.8	-12.4	-11.3
10	0.1	-14.8	-16.2	-13.3
25	0.04	-16.3	-18.3	-14.3
50	0.02	-17.4	-19.8	-15.0
100	0.01	-18.5	-21.3	-15.7

DNV Standard

According to the DNV Offshore Standard DNV-OS-C101 Design of Offshore Steel Structure, the Design Temperature is defined as the "The lowest mean daily temperature to which the structure may be exposed to during installation and operation".

The lowest mean temperature analysis was carried out using reported temperature data from the ICOADS data set. This data spans a 31-year period from January 01, 1980 to December 31, 2010.

Observations in the ICOADS data set are marine weather observations (as opposed to aviation observations) and are normally taken every three hours starting at 00:00 UTC.

As an example of the methodology, all the observations (if available) for January 1st 1981 were extracted from the data and an average temperature was calculated for the day (00:00 to 23:59 UTC). A mean was then calculated from all the January 1st average temperatures over a 31-year period. This mean temperature is plotted in Figure 3.3 together with the mean daily temperatures for every day of the year.

The lowest mean daily average temperature of -1.8°C occurred on January 23rd. The January 23rd mean was based on 582 observations over a time period of 31 years. There were two years during this period without any data for January 23rd.

On March 10th, 1986, when the lowest minimum temperature of -17.3°C was recorded the daily mean temperature was -10.2°C.

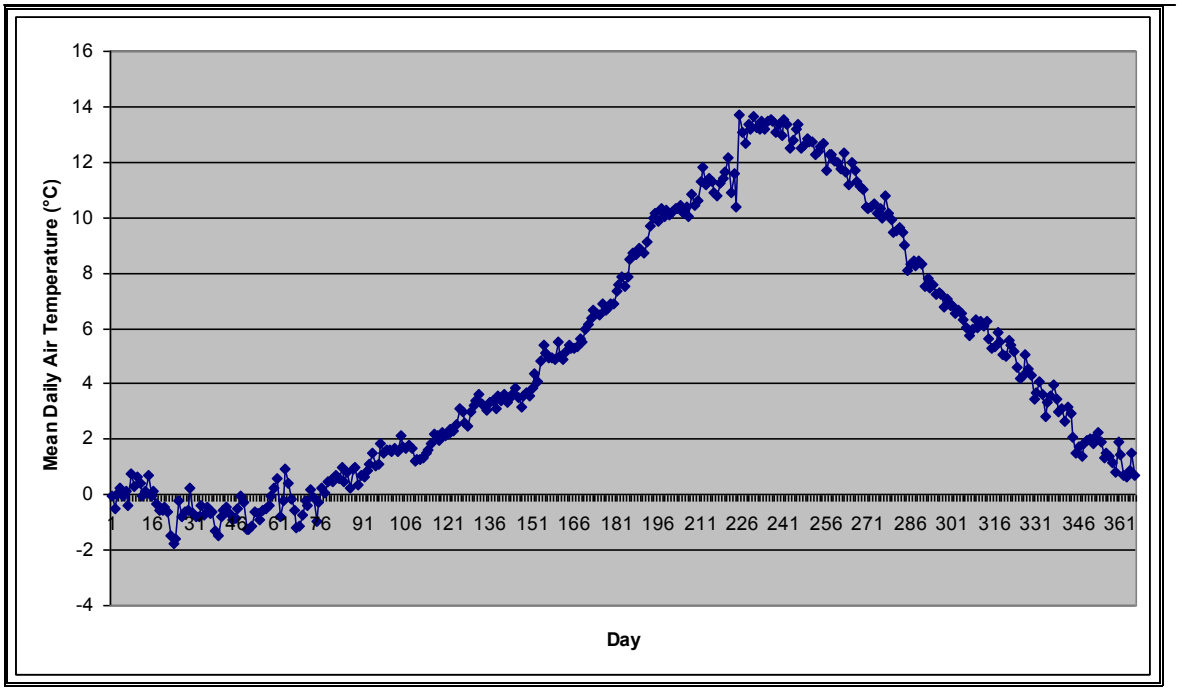

Figure 3.3 Mean Daily Average Temperatures

3.2.2 Maximum Temperature

For the maximum temperature analysis, the daily maximum temperature was found for each day in the data set. The 30 highest maximum temperature events were then chosen with one restriction; no event could occur within 5 days of another. This restriction ensures that all the chosen events were independent of each other. The highest maximum temperature event chosen was 22.5°C, which occurred on August 29, 2005. These temperature events were fitted to a Gumbel distribution and extreme value estimates for maximum temperature were calculated for return periods of 2-years, 10-years, 25-years, 50-years and 100-years. These values are given in Table 3.4 together with the 95% confidence intervals.

Table 3.5 Extreme Maximum Temperature Estimates for Return Periods of 2, 10, 25, 50 and 100 Years

Return Period (years)	Extreme Maximum Temperature (°C)	95% Lower Confidence Bound (°C)	95% Upper Confidence Bound (°C)
2	20.71	21.09	20.33
10	22.65	23.60	21.70
25	23.63	24.93	22.33
50	24.35	25.92	22.79
100	25.07	26.90	23.24

3.3 Relative Humidity

Relative Humidity is the ratio, expressed as a percentage, of the amount of water vapour present in the air to the amount of water vapour which would be present if the air were saturated with respect to water at the same temperature and pressure. Relative humidity was computed from a combination of MANMAR data from the various platforms located in the Jean d"Arc Basin.

Monthly percent exceedances of relative humidity were computed and shown in Table 3.6. It is evident that the surface air is generally more moist during the spring and summer season in comparison to the colder months. Monthly exceedance plots are shown in Figure 3.4.

Table 3.6 Percent Exceedance of Relative Humidity

Relative Humidity (%)	Jan	Feb	Mar	Apr	May	Jun	Jul	Aug	Sep	Oct	Nov	Dec
≥ 0	100.0	100.0	100.0	100.0	100.0	100.0	100.0	100.0	100.0	100.0	100.0	100.0
≥ 5	100.0	100.0	100.0	100.0	100.0	100.0	100.0	100.0	100.0	100.0	100.0	100.0
≥ 10	100.0	100.0	100.0	100.0	100.0	100.0	100.0	100.0	100.0	100.0	100.0	100.0
≥ 15	100.0	100.0	100.0	100.0	100.0	100.0	100.0	100.0	100.0	100.0	100.0	100.0
≥ 20	100.0	100.0	100.0	100.0	100.0	100.0	100.0	100.0	100.0	100.0	100.0	100.0
≥ 25	100.0	100.0	100.0	100.0	100.0	100.0	100.0	100.0	100.0	100.0	100.0	100.0
≥ 30	100.0	100.0	100.0	100.0	100.0	100.0	100.0	100.0	100.0	100.0	100.0	100.0
≥ 35	100.0	100.0	100.0	100.0	99.9	100.0	100.0	100.0	100.0	100.0	100.0	100.0
≥ 40	100.0	100.0	100.0	100.0	99.9	100.0	100.0	100.0	100.0	100.0	99.9	100.0
≥ 45	99.9	99.9	99.9	100.0	99.9	100.0	100.0	100.0	100.0	100.0	99.9	99.9
≥ 50	99.9	99.8	99.9	100.0	99.8	100.0	99.9	100.0	99.9	99.9	99.8	99.9
≥ 55	99.8	99.6	99.7	99.9	99.7	99.9	99.9	100.0	99.5	99.7	99.4	99.6
≥ 60	98.9	98.7	99.4	99.7	99.5	99.8	99.8	100.0	98.4	98.3	97.9	98.3
≥ 65	96.0	96.5	97.9	99.0	99.1	99.6	99.7	99.7	96.0	95.0	94.0	94.2
≥ 70	89.4	91.2	94.7	97.4	98.3	99.2	99.5	98.5	91.8	88.4	86.8	86.8
≥ 75	78.0	80.8	87.6	92.5	95.7	98.2	98.7	96.1	85.3	78.6	77.5	78.0
≥ 80	63.7	67.1	75.9	86.0	91.5	95.4	96.6	91.2	75.4	66.4	67.9	67.3
≥ 85	48.4	53.2	61.4	75.4	83.6	89.7	93.2	82.3	63.3	54.2	55.9	54.6
≥ 90	35.5	39.1	45.9	62.4	72.0	78.1	85.3	68.2	47.2	39.6	42.1	40.1
≥ 95	21.1	23.5	27.2	40.6	51.3	59.0	71.1	49.5	29.8	25.3	27.7	24.0
≥100	9.8	11.4	12.8	19.1	24.0	28.9	36.7	20.2	11.2	9.8	12.8	9.2

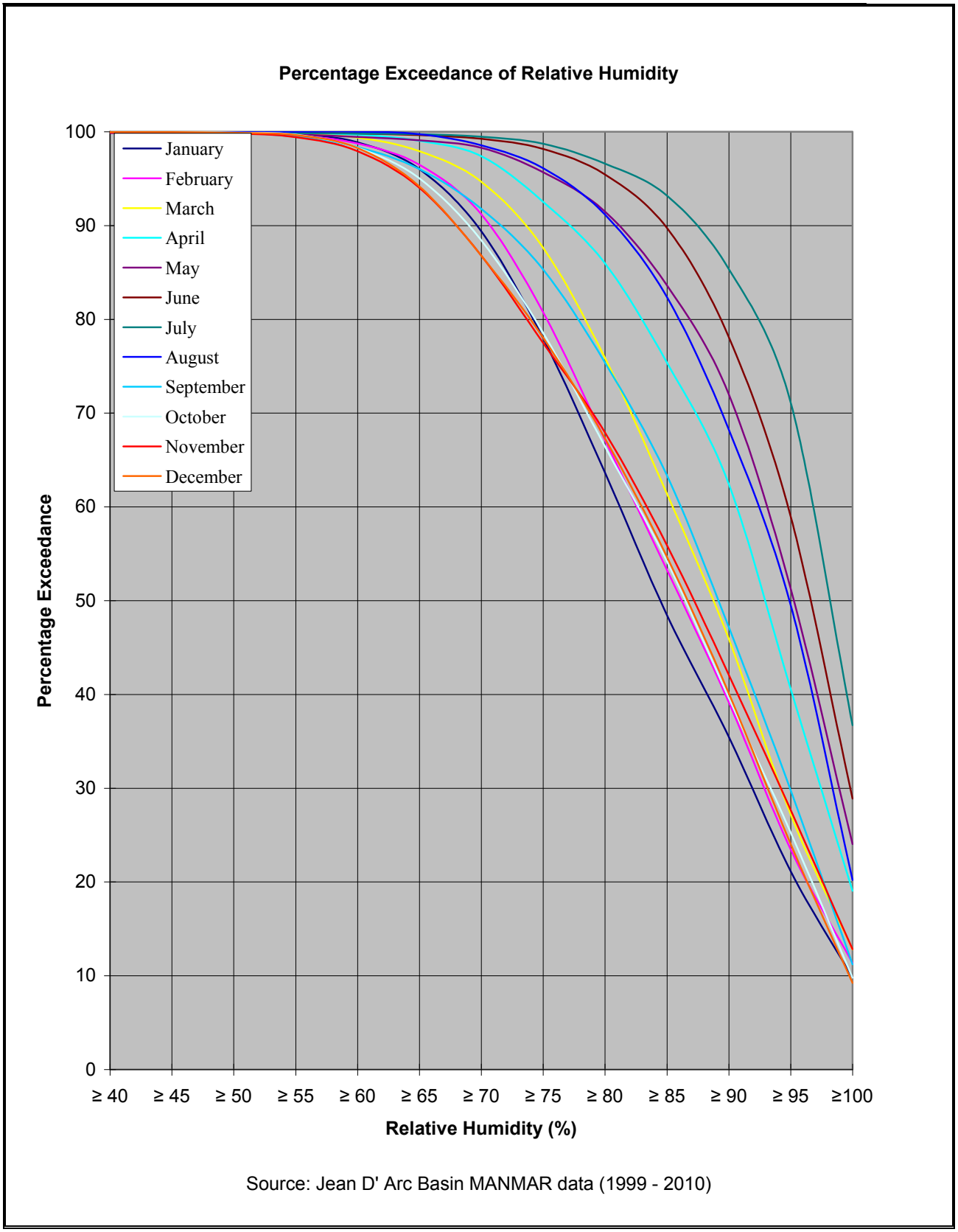

Figure 3.4 Percent Exceedance of Relative Humidity

3.4 Precipitation Types

Precipitation can come in three forms and are classified as liquid, freezing or frozen. Included in the three classifications are;

Liquid Precipitation
- Drizzle
- Rain

Freezing Precipitation
- Freezing Drizzle
- Freezing Rain

Frozen Precipitation
- Snow
- Snow Pellets
- Snow Grains
- Ice Pellets
- Hail
- Ice Crystals

The migratory high and low pressure systems transiting the temperate middle latitude of the Northern Hemisphere cause a variety of precipitation types in their paths. The frequency of precipitation type for the project area was calculated using data from the ICOADS data set, with each occurrence counting as one event. Precipitation statistics for these regions may be low due to a fair weather bias. That is, ships tend to either avoid regions of inclement weather, or simply do not report during these events.

The percentage of occurrences of freezing precipitation data was also calculated from the ICOADS data set. Freezing precipitation occurs when rain or drizzle aloft enters negative air temperatures near the surface and becomes super-cooled so that the droplets freeze upon impact with the surface. This situation typically arises ahead of a warm front extending from low pressure systems passing west of the area. The frequency of freezing precipitation was slightly higher in the winter months than during the spring.

The frequency of precipitation type (Table 3.7) shows that annually, precipitation occurs 22.1% of the time. Winter has the highest frequency of precipitation with 34.6 % of the observations reporting precipitation. Snow accounts for the majority of precipitation during the winter months, accounting for 59.0% of the occurrences of winter precipitation. Summer has the lowest frequency of precipitation with a total frequency of occurrence of only 12.9%. Snow has been reported in each month. However, this is probably due to coding errors rather than the actual presence of snow.

Thunderstorms occur relatively infrequently over the project area though they may occur in any month of the year. It should be noted that hail only occurs in the presence of severe thunderstorms, yet in Table 3.7 the frequency of hail is higher than the frequency of thunderstorms during the months of November to January. This may be due to observer inexperience, classifying what should be ice pellets (formed through entirely different atmospheric processes) as hail or through coding error.

Table 3.7 Percentage Frequency (%) Distribution of Precipitation for ICOADS data set

	Rain / Drizzle	Freezing Rain / Drizzle	Rain / Snow Mixed	Snow	Thunder storm	Hail	Total
January	12.7	0.5	0.6	23.3	0.0	0.2	37.3
February	10.1	0.8	0.4	22.5	0.0	0.0	33.9
March	11.8	0.9	0.3	14.5	0.0	0.0	27.6
April	13.2	0.2	0.2	5.0	0.0	0.0	18.7
May	14.1	0.0	0.1	1.1	0.0	0.0	15.3
June	13.1	0.0	0.0	0.1	0.1	0.0	13.3
July	10.9	0.0	0.0	0.0	0.1	0.0	11.0
August	14.2	0.0	0.0	0.1	0.2	0.0	14.5
September	15.5	0.0	0.0	0.1	0.1	0.0	15.7
October	20.2	0.0	0.1	1.1	0.1	0.1	21.6
November	19.3	0.0	0.4	5.9	0.0	0.2	25.8
December	15.9	0.1	0.6	15.4	0.1	0.3	32.4
Winter	13.0	0.5	0.5	20.4	0.0	0.2	34.6
Spring	13.1	0.4	0.2	6.6	0.0	0.0	20.2
Summer	12.7	0.0	0.0	0.1	0.1	0.0	12.9
Autumn	18.3	0.0	0.2	2.4	0.1	0.1	21.1
Total	14.3	0.2	0.2	7.3	0.1	0.1	22.1

3.5 Visibility

Visibility is defined as the greatest distance at which objects of suitable dimensions can be seen and identified. Horizontal visibility may be reduced by any of the following phenomena, either alone or in combination:

- Fog (visibility less than 1 km)
- Mist (visibility less than 10 km)
- Haze
- Smoke
- Liquid Precipitation (e.g., drizzle)
- Freezing Precipitation (e.g., freezing rain)
- Frozen Precipitation (e.g., snow)
- Blowing Snow

During the winter months, the main obstruction is snow; however, mist and fog may also reduce visibilities at times. As spring approaches, the amount of visibility reduction attributed to snow decreases. As the air temperature increases, so does the occurrence of advection fog. Advection fog forms when warm moist air moves over cooler waters. By April, the sea surface temperature south of Newfoundland is cooler than the surrounding air. As warm moist air from the south moves over the colder sea surface, the air cools and its ability to hold moisture decreases. The air will continue to cool until it becomes saturated and the moisture condenses to form fog. The presence of advection fog increases from April through July. The month of July has the highest percentage of obscuration to visibility, most of which is in the form of advection fog, although frontal fog can also contribute to the

reduction in visibility. In August, the temperature difference between the air and the sea begins to decrease and by September, the air temperature begins to fall below the sea surface temperature. As the air temperature drops, the occurrence of fog decreases. Reduction in visibility during autumn and winter is relatively low and is mainly attributed to the passage of low-pressure systems. Fog is the main cause of the reduced visibilities in autumn, and snow is the main cause of reduced visibilities in the winter. September and October have the lowest occurrence of reduced visibility since the air temperature has, on average, decreased below the sea surface temperature and it is not yet cold enough for snow.

Fog also occurs at White Rose as relatively warm rain falls through cooler air beneath a frontal surface. Typically, the base of the cloud layer lowers as the air becomes saturated and condensation occurs. If the cloud base reaches the surface, frontal fog occurs. Most frequently, frontal fog occurs ahead of a warm front associated with a frontal disturbance. As the front moves through, clearing of the fog may occur but frequently, frontal fog gives way to advection fog in the warm sector of a low pressure system. Typically, fog clears as drier air is advected into the region from continental source regions to the west.

A plot of the frequency distribution of visibility from the ICOADS data set is presented in Figure 3.5. This figure shows that obstructions to vision can occur in any month. Annually, 47.8% of the observations had reduced visibilities less than10 km. The percent frequency of visibilities less than 1 km is shown in Figure 3.6.

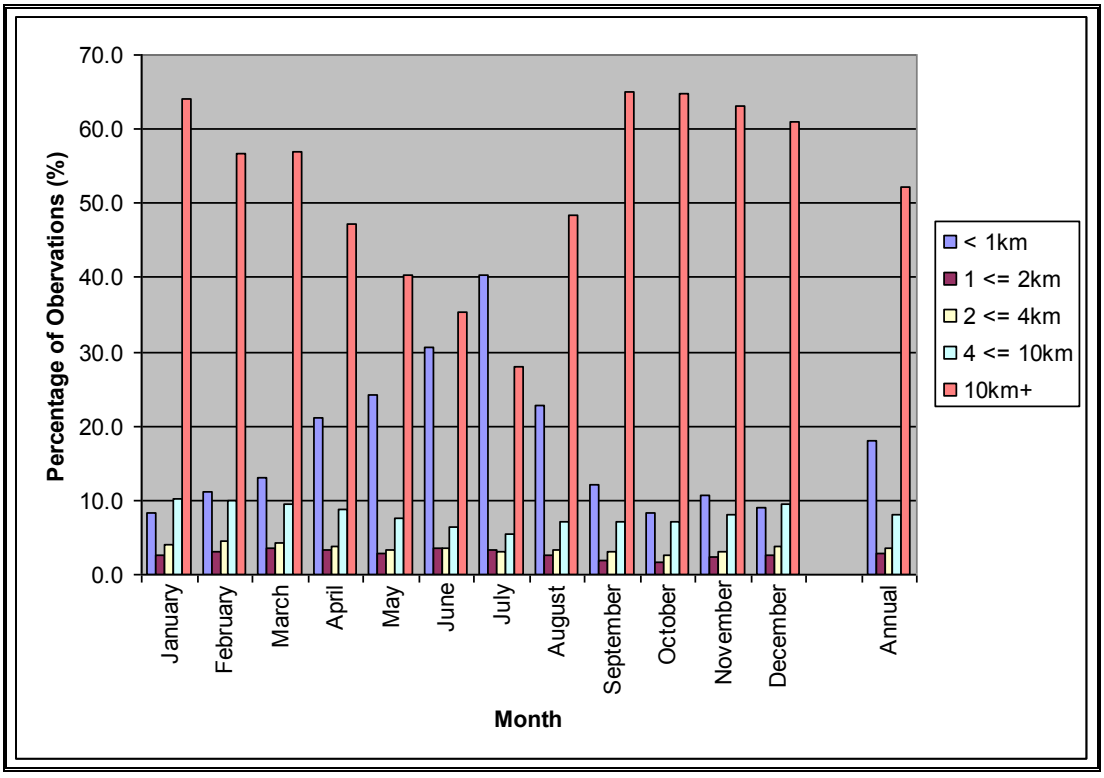

Figure 3.5 Monthly and Annual Percentage Occurrence of Visibility in Region 1 (Source: ICOADS Data set (1980-2010))

3.6 Flying Weather

Flying weather statistics valid for the Grand Banks generally are given in Table 3.8. The statistics were computed from aviation weather observations taken on board various drilling rigs operating in the vicinity of the White Rose field between December 1985 and December 2010. In general, aviation observations were taken during the early morning hours and throughout the daylight hours. The table gives the percent frequency of the joint occurrence of four combinations of cloud ceiling height and visibility limits on a monthly basis.

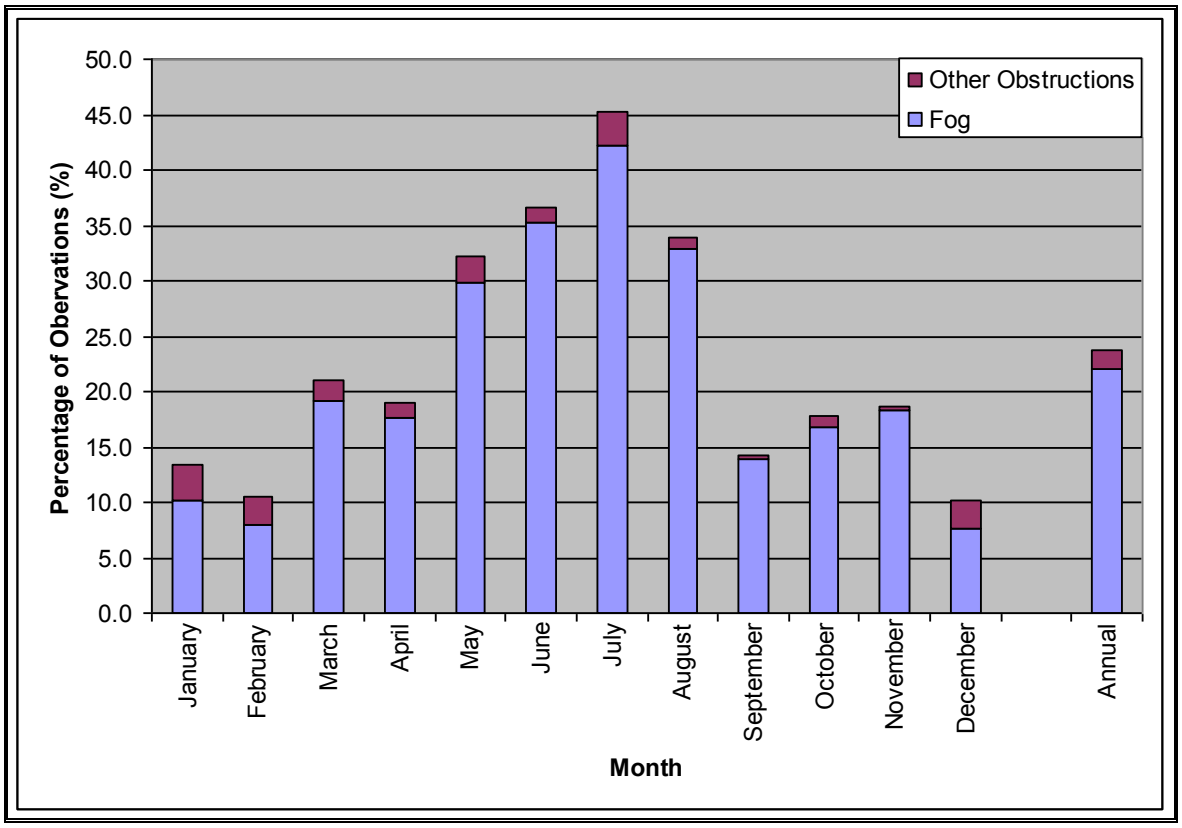

Figure 3.6 Percent Frequency of Visibility Observations less that 1 km (0.5nm) due to Fog and other Obstructions to Visibility

Table 3.8 Flying Weather Cloud Ceiling and Visibility Statistics near the White Rose Field

	Number of Valid Observations	Percent Frequency of Valid Observations			
		Ceiling >= 300m Visibility >= 1km	Ceiling >= 300m Visibility < 1km	Ceiling < 300m Visibility >= 1km	Ceiling < 300m Visibility < 1km
January	2335	75.1	0.5	15.0	9.4
February	2481	73.6	0.6	19.1	6.8
March	2394	63.7	2.3	17.7	16.2
April	2258	44.4	0.8	41.1	13.7
May	3158	34.0	2.1	38.2	25.7
June	3157	32.5	1.9	34.9	30.8
July	3097	22.2	2.5	36.4	39.0
August	2890	33.4	2.5	36.0	28.1
September	3291	56.9	0.9	30.8	11.3
October	2635	62.8	0.9	22.5	13.8
November	1872	67.1	1.4	17.6	13.9
December	2449	77.0	0.4	15.9	6.7
Annual	32017	51.6	1.4	28.0	18.9

4.0 Waves

4.1 General Description

The main parameters for describing wave conditions are the significant wave height, the maximum wave height, the peak spectral period, and the characteristic period. The significant wave height is defined as the average height of the 1/3 highest waves, and its value roughly approximates the characteristic height observed visually. The maximum height is the greatest vertical distance between a wave crest and adjacent trough. The spectral peak period is the period of the waves with the largest energy levels, and the characteristic period is the period of the 1/3 highest waves. The characteristic period is the wave period reported in ship observations, and the spectral peak period is reported in the MSC50 data set.

A sea state may be composed of the wind wave alone, swell alone, or the wind wave in combination with one or more swell groups. A swell is a wave system not produced by the local wind blowing at the time of observation and may have been generated within the local weather system, or from within distant weather systems. The former situation typically arises when a front, trough, or ridge crosses the point of concern, resulting in a marked shift in wind direction. Swells generated in this manner are usually of low period. Swells generated by distant weather systems may propagate in the direction of the winds that originally produced the waves to the vicinity of the observation area. These swells may travel for thousands of miles before dying away. As the swell advances, its crest becomes rounded and its surface smooth. As a result of the latter process, swell energy may propagate through a point from more than one direction at a particular time.

The wave climate of the Grand Banks is dominated by extra-tropical storms, primarily during October through March. Severe storms may, on occasion, occur outside these months. Storms of tropical origin may occur during the early summer and early winter, but most often from late August through October. Hurricanes are usually reduced to tropical storm strength or evolve into extra-tropical storms by the time they reach the area but they are still capable of producing storm force winds and high waves.

During autumn and winter, the dominant direction of the combined significant wave height is from the west. This corresponds with a higher frequency of occurrence of the wind wave during these months, suggesting that during the late fall and winter, the wind wave is the main contributor to the combined significant wave height. During the months of March and April, the wind wave remains predominately westerly while the swell begins to come from a southerly direction, resulting in the vector mean direction of the combined significant wave heights being southwesterly. A mean southwesterly direction for the combined significant wave heights during the summer months is a result of a mainly southwesterly wind wave and a southwesterly swell. As winter approaches again, during the months of September and October, the wind wave will veer to the west and become the more dominant component of the combined significant wave height. This will result in the frequency of occurrence of the combined significant wave heights being westerly once again.

Wave statistics were also compiled from wave data measured in and near the project area. The Hibernia wave data set has been divided into two periods due to changes in the

sampling period. The sampling period changed from a 60-minute average updated every 20 minutes, to a 60-minute average updated every 2.5 minutes. In addition, the White Rose data set from October 2003 – December 2010 has been split due to the change in measuring equipment from a TRYAXIS directional waverider buoy to a Datawell Directional waverider Buoy. A non-directional Datawell waverider buoy was used on the White Rose Field for the period of March 31, 1999 to June 25, 2000. The location and observation period of these stations is presented in Table 4.1.

Table 4.1 Locations of wave observations

	Latitude	Longitude	Period
Terra Nova	46.4°N	48.4°W	July 13, 1999 – September 30, 2009
White Rose	46.8°N	48.0°W	March 31, 1999 – June 25, 2000
White Rose	46.8°N	48.0°W	October 06, 2003 – August 18, 2007
White Rose	46.8°N	48.0°W	August 15, 2007 – December 31, 2010
Ocean Ranger	46.5°N	48.4°W	December 04, 1980 – February 09, 1982
Buoy 44153	46.7°N	48.8°W	July 02, 1994 – March 11, 1998
Hibernia	46.7°N	48.7°W	January 01, 1998 - December 08, 2004
Hibernia	46.7°N	48.7°W	January 01, 2004 - December 31, 2010

4.2 Data Sources

The data sources to describe the wave climatology at White Rose came from the Integrated Science Data Management (ISDM) data base and the MSC50 North Atlantic wind and wave climatology data base. The locations of the climate data sources are presented in Figure 2.1.

MSC50 Data Set

Wave climate statistics for the White Rose were extracted from the MSC50 North Atlantic wind and wave climatology data base compiled by Oceanweather Inc under contract to Environment Canada. The MSC50 data base consists of continuous wind and wave hindcast data in 1-hour time steps from January 1954 to December 2009, on a 0.1° latitude by 0.1° longitude grid. Grid point 11034 was chosen to represent conditions within the area of interest. Wave heights and periods in the MSC50 data base are computed using a Pierson Moskowitz spectrum.

The MSC50 analysis followed the same basic methodology as was applied in the AES40 hindcast with notable improvements and upgrades. The temporal resolution was changed from a 6-hour time base to a 3-hour analysis. This increased resolution resulted in improved modeling of rapidly deepening winter storms which develop off the US Eastern Seaboard and track northeast across the Grand Banks.

Prior to 1962, mean monthly ice statistics were used when calculating the wave heights in the MSC50 data set. As a result, if the mean monthly ice coverage for a particular grid point is greater than 50% for a particular month, the whole month (from the 1st to the 31st) gets "iced out"; meaning that no forecast wave data has been generated for that month. This sometimes results in gaps in the wave data. Since 1962, weekly ice data supplied by

the Canadian Ice Service was used allowing the MSC50 hindcast to better represent the changing ice conditions (Swail et al., 2006).

Integrated Science Data Management Data Base

While drilling operations are being conducted, a wave buoy is normally deployed within the region. Wave buoys provide real-time measured wave data, which are incorporated into the marine weather reports. Normally, the significant wave height and average period derived from the buoy data are archived for use in determining wave climate statistics for the area. The Integrated Science Data Management (ISDM) has been collecting, archiving and providing spectral wave data since 1970 and archives over 6 million observed wave spectra from 500 locations. ISDM performs a quality inspection (QC) of each observed wave spectra prior to update into the data base. Flags are assigned to the observed and derived parameters reflecting data quality. Quality control is performed by ISDM by examining the energy distribution of the power spectrum and comparing relative values of significant wave height and peak period between neighboring buoys.

4.3 Wave Analysis Results

The annual wave rose from the MSC50 grid point 11034 is presented in Figure 4.1. The wave rose shows that the majority of wave energy comes from the west-southwest to south-southwest, and accounts for 36.0% of the waves. Waves were "iced out" for 1.36% of the time at grid point 11034 over the 55-year record.

The annual percentage frequency of significant wave heights is presented in Figure 4.2. This figure shows that the majority of significant wave heights lie between 1.0 and 3.0 m. There is a gradual decrease in frequency of wave heights above 3.0 m and only a small percentage of the wave heights exceed 7.0 m. Monthly rose histograms of frequency distributions of wave heights can be found in Appendix 2.

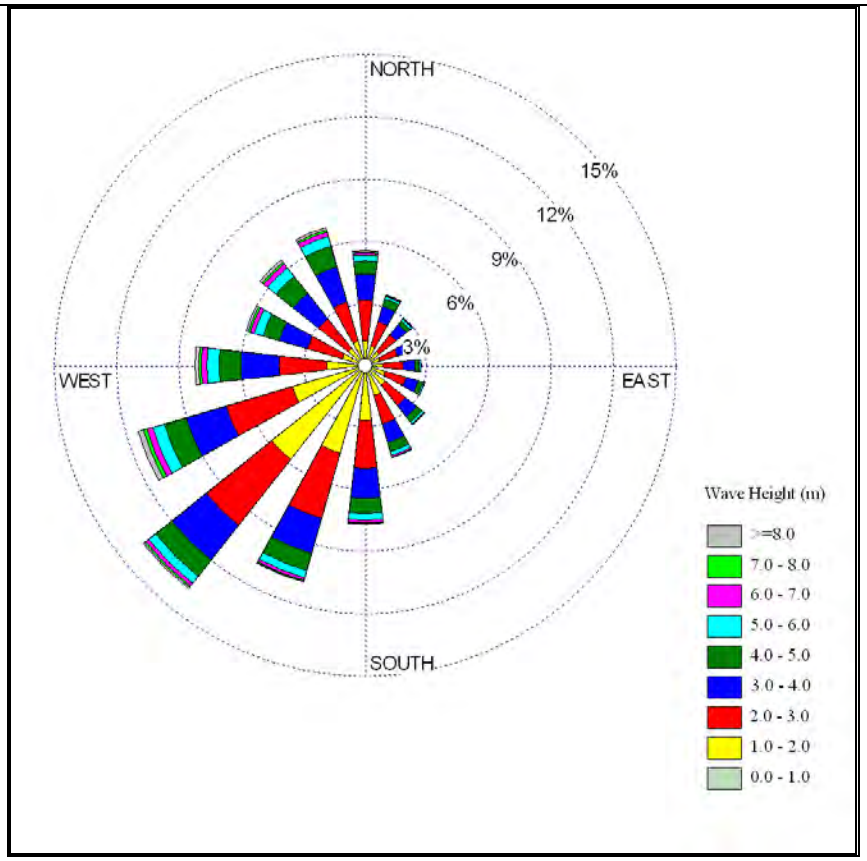

Figure 4.1 Annual Wave Rose for MSC50 Grid Point 11034 Located near 46.7°N; 48.1°W. 1954 to 2009

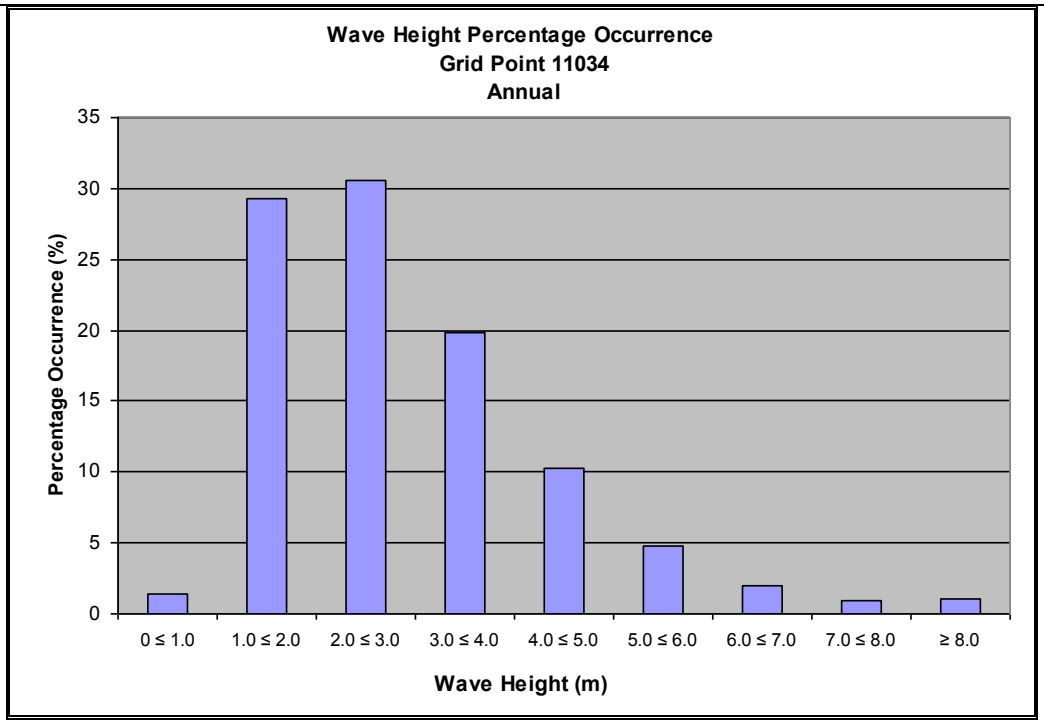

Figure 4.2 Annual Percentage Frequency of Wave Height for MSC50 Grid Point 11034 Located near 46.7°N; 48.1°W. 1954 to 2009

Significant wave heights on the Grand Banks peak during the winter months with Grid Point 11034 having a mean monthly significant wave height of 4.2 m in January. The lowest significant wave heights occur in the summer with July month having a mean monthly significant wave height of only 1.7 m (Table 4.2).

Combined significant wave heights of 10.5 m or more occurred in each month between September and April in the MSC50 data, with the highest waves occurring during the month of February (Table 4.3). The highest significant wave height of 14.8 m in the MSC50 data set occurred on February 15, 1982. The highest combined significant wave heights of 14.6 m and 13.8 m in the Terra Nova and Hibernia data sets, respectively, occurred during the February 11, 2003 storm event previously mentioned. While the maximum significant wave heights tend to peak during the winter months, a tropical system could pass through the area and produce high wave heights during any month.

Table 4.2 Mean Significant Wave Height Statistics (m)

	MSC50 Grid Point 11034	Ocean Ranger	Terra Nova	White Rose (2003-2007)	White Rose (2007-2010)	Hibernia (1998-2004)	Hibernia (2005-2008)	Buoy 44153
January	4.2	5.2	4.1	4.9	4.2	4.0	3.9	N/A
February	3.9	4.4	3.8	4.5	3.8	3.7	3.4	0.2
March	3.4	4.7	3.3	4.3	3.2	3.6	3.1	N/A
April	2.8	3.7	2.6	2.7	2.5	2.8	2.3	N/A
May	2.2	1.7	2.2	2.6	2.4	2.3	1.8	0.7
June	1.9	1.5	1.8	2.6	1.9	2.0	1.8	0.6
July	1.7	1.8	1.5	2.4	1.6	1.6	1.6	0.7
August	1.8	1.8	1.8	2.3	1.9	1.9	1.8	1.0
September	2.4	3.8	2.3	2.8	2.3	2.3	2.4	1.0
October	3.0	3.0	3.0	3.8	3.1	2.6	3.2	1.3
November	3.4	4.8	3.1	3.8	3.0	3.2	2.9	1.6
December	4.0	4.6	3.8	4.2	4.2	3.8	3.6	2.1

Source: ISDM data base
MSC50 data base

Table 4.3 Maximum Combined Significant Wave Height Statistics (m)

	MSC50 Grid Point 11034	Ocean Ranger	Terra Nova	White Rose (2003-2007)	White Rose (2007-2010)	Hibernia (1998 - 2004)	Hibernia (2005 - 2008)	Buoy 44153
January	13.0	10.6	12.5	12.2	11.8	12.2	11.5	N/A
February	14.8	8.3	14.6	11.9	10.2	13.8	9.4	2.1
March	11.4	7.2	9.4	12.8	8.8	9.7	9.3	N/A
April	10.8	7.8	7.1	11.0	5.7	9.4	7.5	N/A
May	10.3	3.8	6.3	10.9	6.6	7.4	6.8	1.5
June	10.0	3.0	6.5	9.2	5.6	7.2	8.4	2.6
July	6.2	4.2	4.1	8.5	3.5	6.4	9.1	2.1
August	9.4	3.3	8.0	9.3	7.3	18.2	8.2	5.2
September	11.7	8.4	10.4	11.1	12.9	9.9	9.8	5.0
October	12.1	5.8	10.4	12.2	9.5	9.0	10.2	5.1
November	11.5	7.0	10.2	11.2	9.4	10.5	9.3	6.0
December	13.8	8.1	11.7	11.1	11.1	10.8	9.3	5.9

Source: ISDM data base
MSC50 data base

Figure 4.3 shows percentage exceedance curves of significant wave heights for Grid Point 11034. Percentage exceedance curves for the months of January through April show that the curves do not reach 100% because of the presence of ice during these months.

The spectral peak period of waves vary with season with the most common period varying from 7 seconds during summer to 11 seconds in winter. Annually, the most

common spectral peak period is 9 seconds, occurring 18.4% of the time at Grid Point 11034. The percentage occurrence of spectral peak period for each month is shown in Table 4.4 and Figure 4.4. The highest percentage for each month in Table 4.4 has been highlighted.

Table 4.4 Percentage Occurrence of Peak Spectral Period of the Total Spectrum at Grid Point 11034 Located near 46.7°N; 48.1°W. 1954 to 2009

	Peak Spectral Period (seconds)															
Month	1	2	3	4	5	6	7	8	9	10	11	12	13	14	15	16
January	0.0	0.0	0.0	0.0	0.2	1.2	4.7	8.6	14.6	18.6	**22.3**	12.7	11.4	4.9	0.6	0.1
February	0.0	0.0	0.0	0.1	0.8	2.4	6.7	10.0	15.8	18.1	**20.1**	12.5	8.3	4.1	0.6	0.3
March	0.0	0.0	0.0	0.3	1.1	3.2	8.5	11.5	17.2	**18.9**	17.9	11.1	5.9	3.7	0.2	0.3
April	0.0	0.0	0.0	0.2	1.3	4.2	9.0	14.7	**23.7**	20.3	14.1	7.5	3.1	1.6	0.2	0.1
May	0.0	0.0	0.0	0.1	1.5	7.1	15.8	**25.3**	22.9	14.7	6.2	4.4	1.4	0.4	0.0	0.0
June	0.0	0.0	0.0	0.2	3.6	10.6	24.7	**27.3**	19.6	8.6	2.2	1.4	1.5	0.2	0.0	0.0
July	0.0	0.0	0.0	0.3	4.3	14.3	**29.3**	27.8	13.9	5.7	1.3	0.8	1.8	0.2	0.1	0.2
August	0.0	0.0	0.0	0.4	4.8	12.7	**28.9**	26.3	14.6	5.5	2.7	2.1	1.6	0.4	0.1	0.1
September	0.0	0.0	0.0	0.1	1.8	6.5	17.0	**21.6**	20.2	10.6	8.4	7.4	4.4	1.3	0.4	0.3
October	0.0	0.0	0.0	0.0	0.9	3.4	10.7	17.5	**22.3**	16.3	12.0	9.2	5.3	1.9	0.2	0.2
November	0.0	0.0	0.0	0.0	0.6	2.6	8.2	12.2	19.9	**20.3**	16.0	9.4	7.5	2.8	0.2	0.2
December	0.0	0.0	0.0	0.0	0.2	1.3	4.7	9.1	15.8	**21.1**	20.9	12.5	9.9	3.9	0.5	0.2
Winter	0.0	0.0	0.0	0.1	0.4	1.6	5.4	9.3	15.4	19.3	**21.1**	12.6	9.9	4.3	0.6	0.2
Spring	0.0	0.0	0.0	0.2	1.3	4.8	11.1	17.2	**21.3**	18.0	12.8	7.7	3.5	1.9	0.1	0.1
Summer	0.0	0.0	0.0	0.3	4.2	12.5	**27.6**	27.2	16.0	6.6	2.1	1.4	1.6	0.2	0.1	0.1
Autumn	0.0	0.0	0.0	0.1	1.1	4.2	12.0	17.1	**20.8**	15.7	12.2	8.7	5.7	2.0	0.3	0.2
Annual	0.0	0.0	0.0	0.2	1.8	5.8	14.0	17.7	**18.4**	14.9	12.0	7.6	5.2	2.1	0.3	0.2

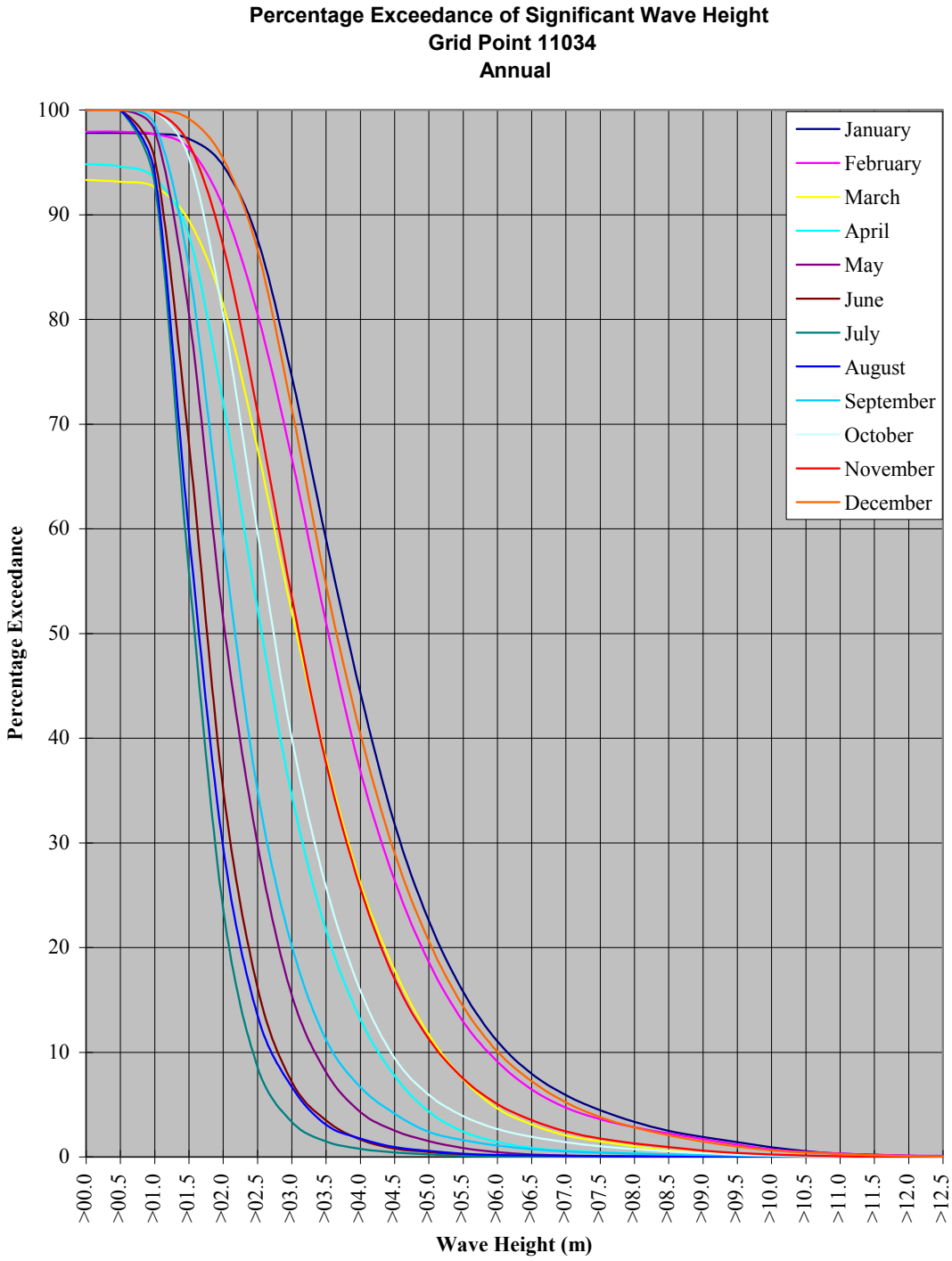

Figure 4.3 Percentage Exceedance of Significant Wave Height at Grid Point 11034 Located near 46.7°N; 48.1°W. 1954 to 2009

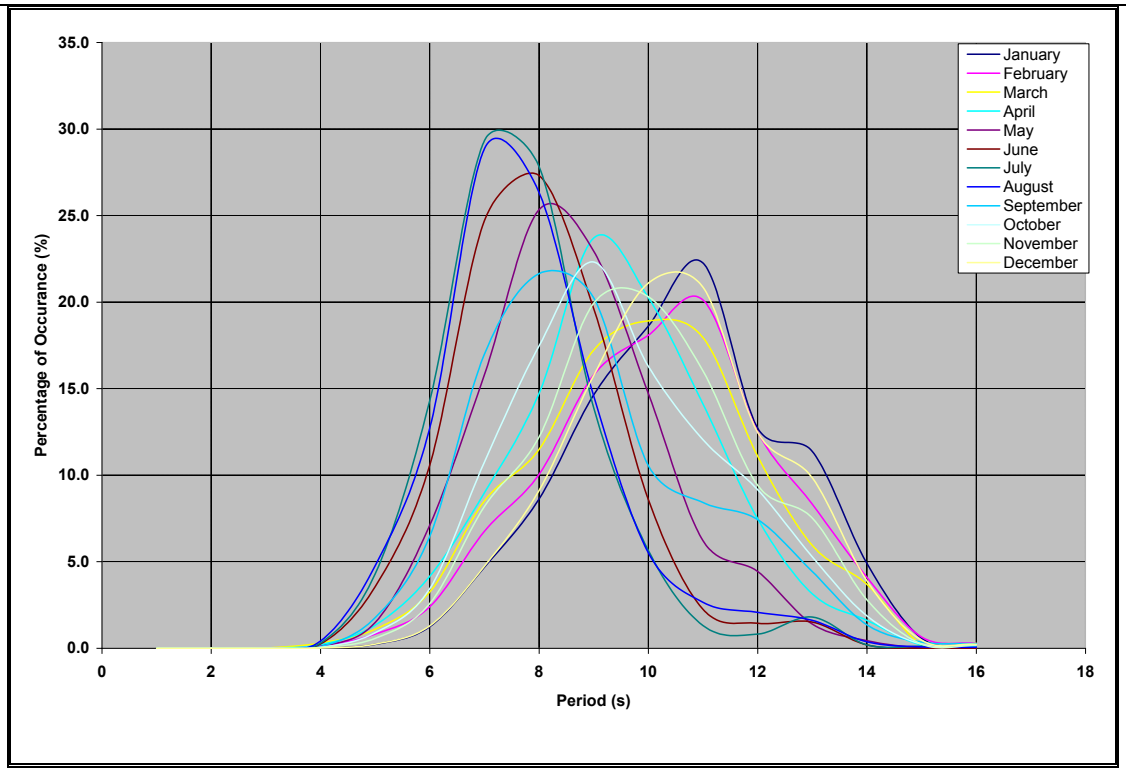

Figure 4.4 Percentage of Occurrence of Peak Wave Period at Grid Point 11034 Located near 46.7°N; 48.1°W. 1954 to 2009

A scatter diagram of the significant wave height versus spectral peak period is presented in Table 4.5. From this table it can be seen that the most common wave at grid point 11034 is 2 m with a peak spectral period of 9 seconds. Note that wave heights in these tables have been rounded to the nearest whole number. Therefore, the 1 m wave bin would include all waves from 0.51 m to 1.50 m.

Table 4.5 Percent Frequency of Occurrence of Significant Combined Wave Height and Peak Spectral Period at Grid Point 11034 located near 46.7°N; 48.1°W

		Wave Height (m)														Total
		<1	1	2	3	4	5	6	7	8	9	10	11	12	13	
Period (s)	0	1.34														1.34
	1	0.00														0.00
	2	0.00														0.00
	3	0.00	0.00													0.00
	4	0.00	0.13	0.03												0.16
	5	0.00	0.97	0.73	0.04	0.00										1.75
	6	0.00	1.60	3.77	0.38	0.02	0.00									5.77
	7	0.00	4.32	5.90	3.43	0.29	0.01									13.96
	8	0.02	4.46	6.48	4.45	1.99	0.15	0.00								17.55
	9	0.00	1.55	8.01	3.96	3.46	1.07	0.07	0.00							18.12

	10	0.00	0.61	4.42	4.26	2.47	2.20	0.59	0.04	0.00						14.60
	11	0.00	0.20	1.99	4.13	2.33	1.41	1.17	0.43	0.07	0.00					11.74
	12	0.00	0.22	1.41	2.12	1.46	0.72	0.52	0.48	0.33	0.15	0.02	0.00			7.42
	13	0.00	0.23	0.71	1.14	1.22	0.67	0.34	0.20	0.19	0.20	0.15	0.03	0.00		5.09
	14		0.04	0.14	0.40	0.58	0.40	0.17	0.08	0.05	0.04	0.07	0.06	0.03	0.00	2.07
	15		0.01	0.02	0.04	0.05	0.07	0.03	0.01	0.00	0.00	0.00	0.01	0.01	0.01	0.26
	16		0.02	0.02	0.03	0.04	0.02	0.01	0.00	0.00	0.00			0.00	0.00	0.15
	17		0.01	0.02	0.01	0.00	0.00	0.00	0.00							0.04
	18		0.00				0.00	0.00								0.00
		1.38	14.37	33.64	24.41	13.91	6.72	2.91	1.25	0.64	0.39	0.24	0.10	0.03	0.01	100.00

Note: The incidence of 0 wave height and <1 wave period is due to the presence of sea ice.

4.4 Swell

Cross Swells

Cross swells are formed when both wind waves and one or more systems of swell waves are present at the same time. A cross swell is determined to be present if the primary swell (greater than 0.25 m in height) has an approximate direction between 45° and 135° from the reported wind direction. A following swell is determined to be present if the primary swell (greater than 0.25 m in height) direction is between approximately 0° and 45° from the reported wind direction. For an opposing swell, the swell direction is between 135° and 180° from the reported wind direction.

Annually, 91.5% of all the MANMAR observations on the White Rose field containing wave information included a primary swell of greater than 0.25 m. Of these observations, 43.7% were cross swells, 39.6% were following swells and 16.7% were opposing swells. This information, along with monthly statistics is presented in Table 4.6.

Table 4.6 Percentage of Observations of Primary Swell (>0.25m) Relative to Wind Direction

Month	Cross[1] Swell (%)	Following[2] Swell (%)	Opposing[3] Swell (%)	Total (%)
January	45.1	43.5	11.3	96.4
February	39.5	45.2	15.3	98.1
March	48.3	30.1	21.5	95.6
April	45.1	35.4	19.6	95.0
May	45.7	35.7	18.6	90.0
June	46.3	39.3	14.4	81.6
July	37.3	44.9	17.8	81.5
August	40.9	40.2	19.0	86.1
September	41.8	39.4	18.8	87.4
October	46.3	40.5	13.2	94.3
November	43.1	35.0	22.0	95.0
December	44.5	46.1	9.4	97.3
Annual	43.7	39.6	16.7	91.5

4.5 Model Wave Spectra and Peak Enhancement Factor

The selection or design of floating drilling/production platforms for use in a particular offshore environment, if responsive to the spectral distribution of wave energy, requires the use of a design wave environment. The JONSWAP wave spectrum formulation (Hasselmann et al., 1973) is frequently employed to describe wave energy distribution as a function of wave frequency (World Meteorological Organization, 1998), or equivalently, wave period. The JONSWAP spectrum is a five-parameter model formulation that is defined in terms of two scaling parameters and three shape parameters. The scaling parameters are significant wave height (H_s) and spectral peak period (T_p). The shape parameters include the so-called JONSWAP peak enhancement factor (γ), and the left and right width parameters (σ_1, σ_2). Previous work has shown that the two width parameters show little variability and are generally taken to be constant; the remaining three factors are classified as free parameters (e.g., Muller, 1976). Following the approach taken by LeBlond et al. (1982), the JONSWAP spectral form used in this report is as follows:

$$S(f) = (A / f^5) \exp(-B/f^4) \gamma^a$$

where:

$$A = (5 H_s^2 f_p^4) / 16$$
$$B = (5 f_p^4) / 4$$
$$a = \exp[-(f-f_p)^2 / (2 \sigma_{1,2}^2 f_p^2)]$$
$$\sigma_1 = 0.07, \text{ for } f <= f_p$$
$$\sigma_2 = 0.09, \text{ for } f > f_p$$

H_s = significant wave height
f_p = spectral peak frequency
f = wave frequency
γ = peak enhancement factor

Oceans Ltd. (2001) analyzed 15 wave spectra from two storms in the fall of 1999 with significant wave heights greater than 9.0 m. Nine of these spectra were recorded at White Rose and six at Terra Nova. The results showed that the peak enhancement factor ranged from 1.0 to 2.7, with a mean value of 1.7.

The wave spectra from Hurricane Gert were from one of the storms that was analyzed. The significant wave height reached 9.85 m at 1550 UTC on September 23, 1999 at White Rose N-30 as Hurricane Gert tracked through the region. The value for γ was 1.1 (Figure 4.5) showing that the wave energy was spread over a broad range of frequencies.

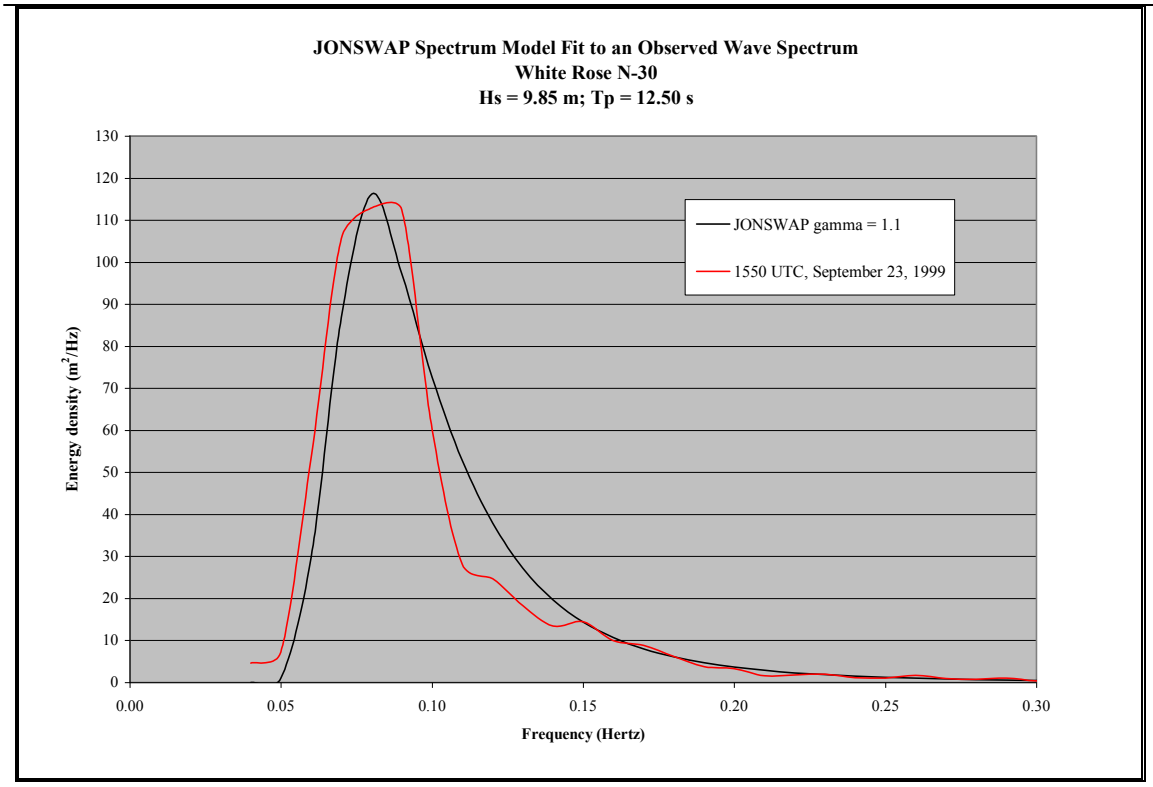

Figure 4.5. Sample JONSWAP Spectral Fit for Wave Spectrum during Hurricane Gert

LeBlond et al. (1982) carried out an investigation in which γ was computed for short time-series of wave observations near Hibernia through two major storm events that affected the Grand Banks in January and February of 1982. In the January storm analyzed by LeBlond, significant wave heights increased from just over 2.4 m to a peak of 10.8 m. Using fourteen spectra fitted at 3-hour intervals, it was found that the peak enhancement factor γ ranged from near 1.0 to 4.2, with a mean of 2.2. In the February storm, twenty-one individual spectra at 20-minute intervals were fitted. During this time the significant wave height increased from 5.1 m to a peak of 12.8 m. The value of γ varied from 1.2 to 4.7 with a mean of 2.3.

Other work that has been carried out has been largely limited to averaged or smoothed wave spectra, an approach that cannot adequately reflect the range of variability that occurs in the marine environment.

4.5.1 Spectral Shape

This report investigates derived peak enhancement factors at White Rose using wave spectra measured with a TRIAXYS waverider buoy over the period October 2003 to December 2006 (data sets are not continuous) and with a Datawell Directional waverider buoy over the period of August 2007 to December 2010, with a focus on high significant wave height events and storm situations. Spectral data was not available for the period of January 2007 to August 2007 and as a result, is not included in the analysis. The analysis

for the period of October 2003 to December 2006 was previously carried out by Oceans (2007). Due to the differences in instrumentation, the spectral data for August 2007 to December 2010 were analyzed separately. For each selected wave spectrum, a range of JONSWAP model forms were compared to the measured spectrum with the peak enhancement factor varying in steps of 0.1. The best-fit spectrum was then selected using a least-squares fitting routine. Three sample JONSWAP fitted spectra are presented below in Figures 4.6 to 4.8 for peak enhancement factors of 5.8, 2.5 and 1.0 respectively.

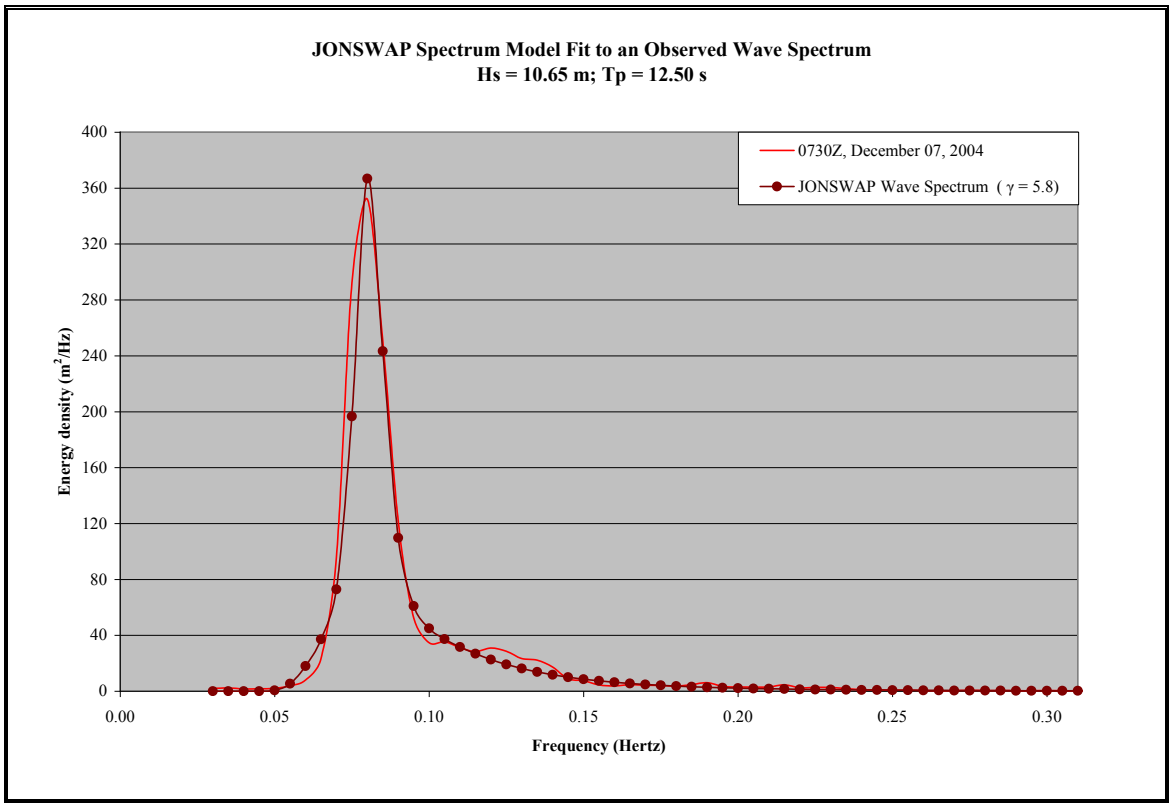

Figure 4.6 Sample JONSWAP Spectral Fit, Dec 07, 2004

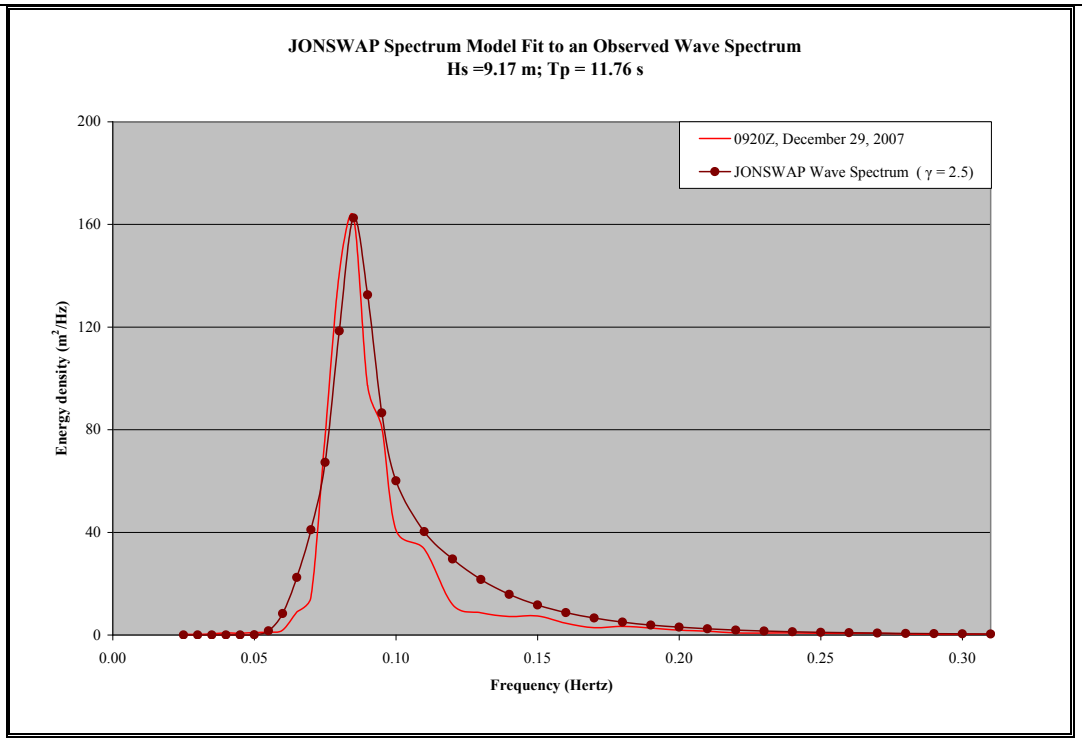

Figure 4.7 Sample JONSWAP Spectral Fit, December 29, 2007

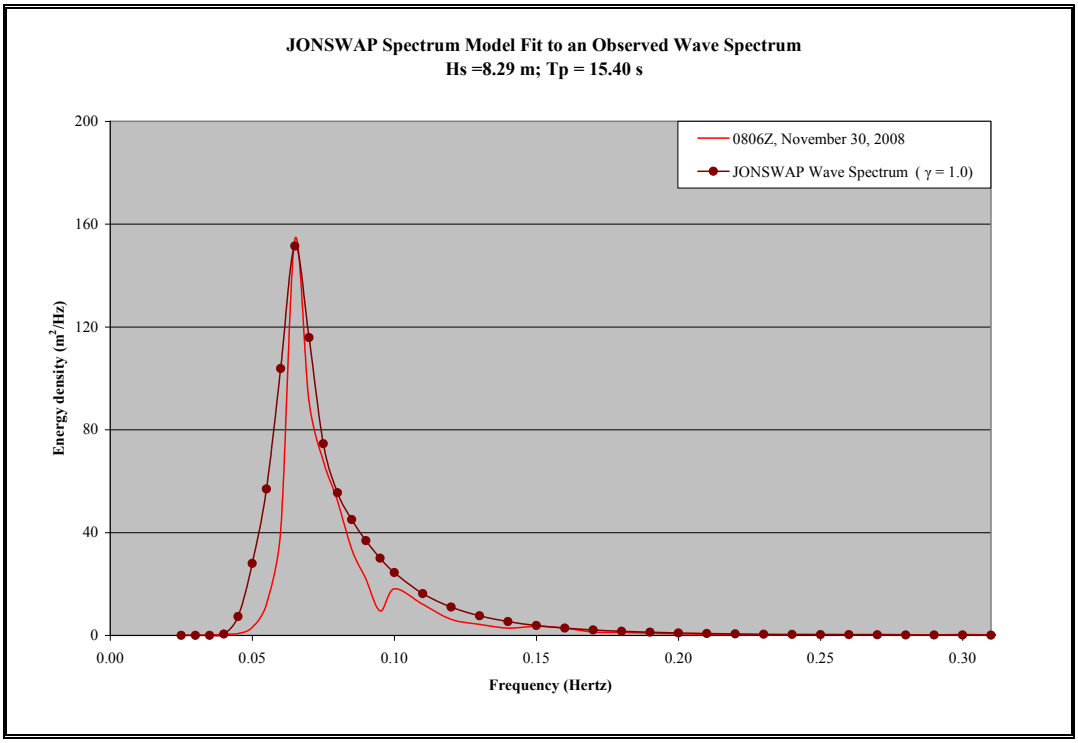

Figure 4.8 Sample JONSWAP Spectral Fit, November 30, 2008

4.5.2 Spectra from the TRIAXYS Waverider Buoy

A significant wave height threshold of 8.0 m was chosen for the analysis, which resulted in 210 wave spectra over 17 storms. In this sample set, H_s ranged from 8.0 to 11.75 m and T_p ranged from 10.5 to 16.7 seconds. Various statistics derived from the data set are presented in Table 4.7.

Table 4.7 White Rose JONSWAP Peak Enhancement Factor Statistics for Hs >= 8.0 metres

Total Samples	210
Minimum	1.0
Maximum	6.4
Mean	2.4
Standard Deviation	1.0
Median	2.3

Values of γ ranged from a low of 1.0 to a high of 6.4, with a mean value of 2.4 and a standard deviation of 1.0. This mean is consistent with the mean values of 2.2 and 2.3 calculated by LeBlond et al. (1982) on his analysis of the spectra occurring over 2 storms and discussed earlier. The highest γ value of 6.4 occurred on November 10, 2003 with a significant wave height of 10.79 m and spectral peak period of 13.3 seconds. Distributions of γ for $H_s \geq 8.0$ m are presented in Figure 4.9 and Figure 4.10. A scatter plot of γ vs. H_s is shown in Figure 4.11.

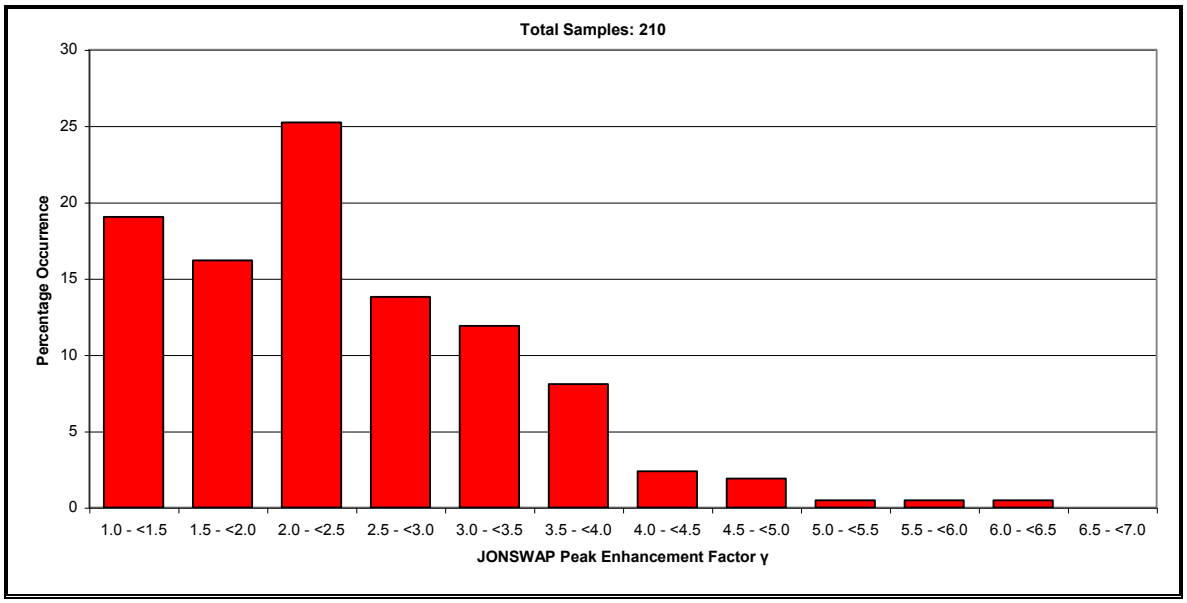

Figure 4.9 Distribution of Peak Enhancement Factors for Hs >= 8.0 metres at White Rose (Percentage Occurrence) for 17 Storms

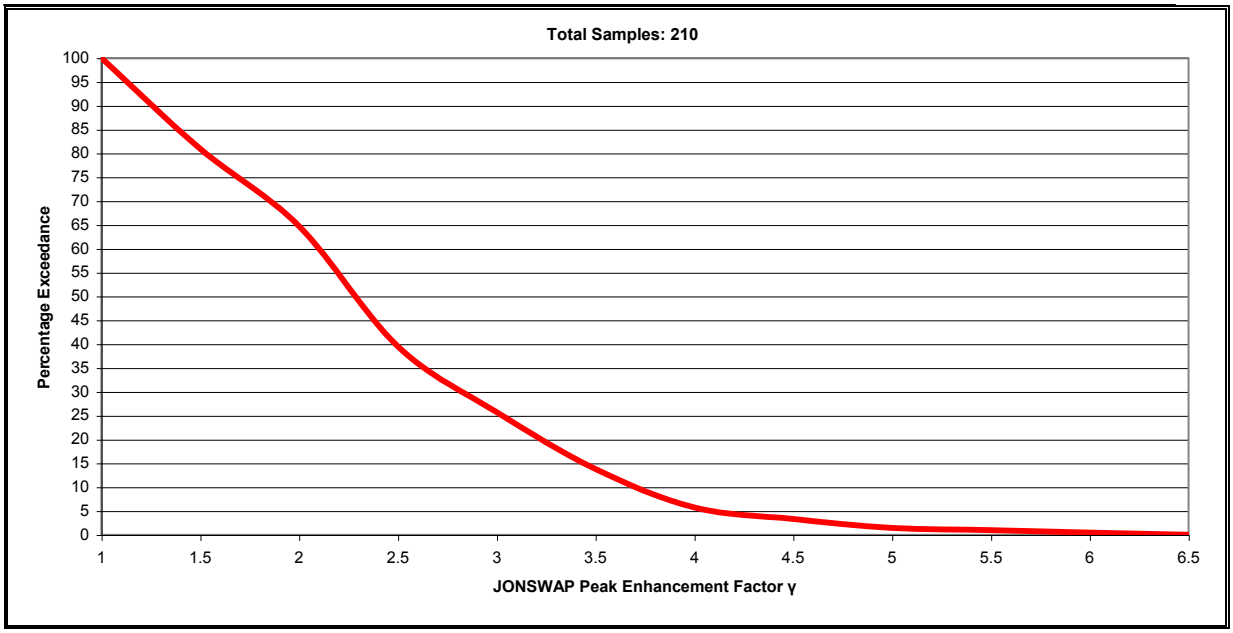

Figure 4.10 Distribution of Peak Enhancement Factors for Hs >= 8.0 metres at White Rose (Percentage Exceedance) for 17 Storms

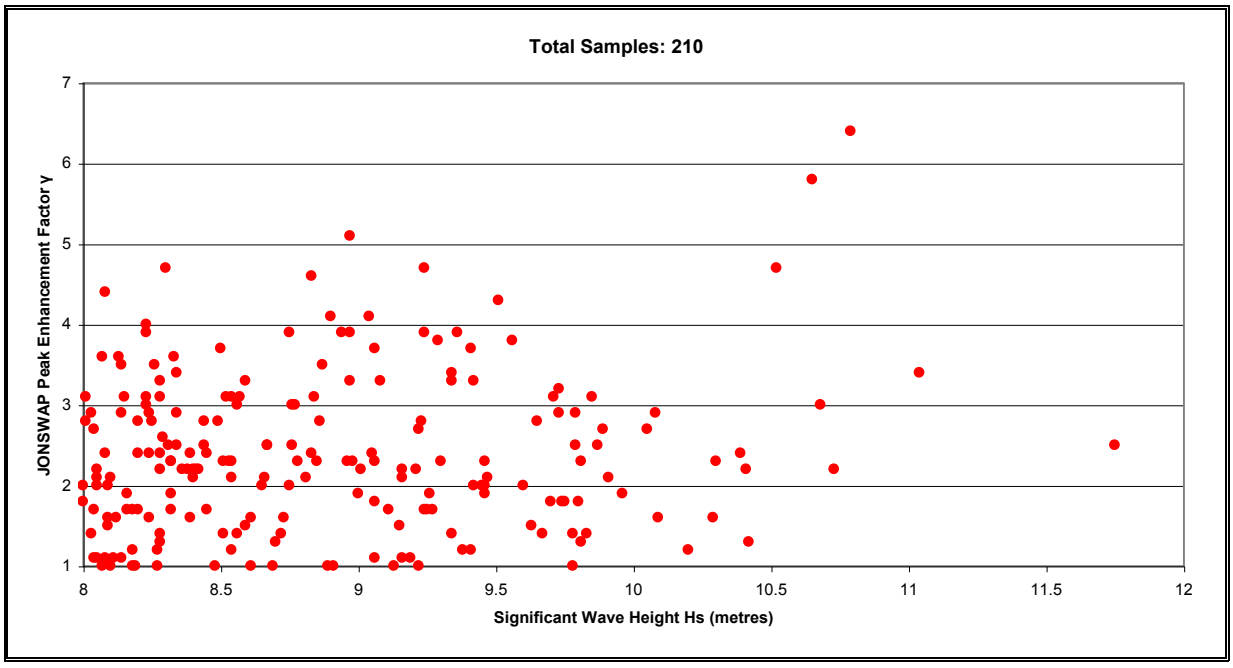

Figure 4.11 White Rose JONSWAP Peak Enhancement Factor vs. Significant Wave Height for Hs >= 8.0 metres for 17 Storms

Peak Enhancement Factor at Storm Peaks

In an effort to determine whether values of γ tend to cluster around any particular value at the peak significant wave height during a storm situation, 17 separate storm events during which H_s reached or exceeded 8.0 m were selected from the waverider data set. At the highest wave height measured during the storm (the „storm peak"), the JONSWAP peak enhancement factor was calculated. Storm peak data are listed in Table 4.8, calculated statistics are given in Table 4.9 and the distribution of γ is presented in Figure 4.12.

Table 4.8 Selected Storm Peaks

Year	Month	Day	Time	Hs	Tp	γ
2003	11	10	0100	10.79	13.30	6.4
2004	01	18	1600	10.60	14.30	3.0
2004	12	07	0730	10.65	12.50	5.8
2004	12	28	1700	8.39	13.30	2.4
2005	01	12	0900	8.34	11.80	2.9
2005	01	13	0400	8.28	14.30	1.4
2005	01	23	1600	8.45	13.30	2.4
2005	03	12	1630	9.78	14.30	1.4
2005	03	14	2230	8.20	15.40	2.8
2005	10	13	0000	11.75	15.40	2.5
2006	01	17	2130	8.28	14.29	1.3
2006	01	23	0500	11.04	14.29	3.4
2006	02	11	1030	8.75	11.11	3.9
2006	02	14	0100	9.29	11.76	3.8
2006	02	25	1000	9.27	14.30	1.7
2006	09	14	0300	9.87	12.50	2.5
2006	12	05	1730	8.65	14.30	2.0

Table 4.9 White Rose JONSWAP Peak Enhancement Factor Statistics for Storm Peaks

Total Samples	17
Minimum	1.3
Maximum	6.4
Mean	3.1
Standard Deviation	1.4
Median	2.8

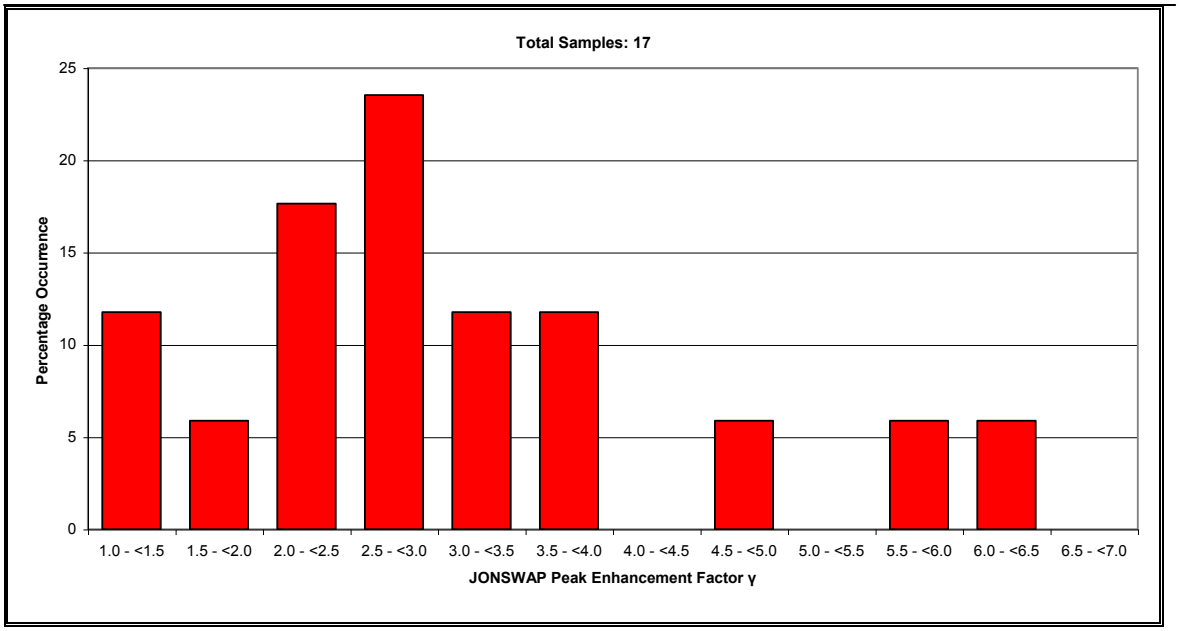

Figure 4.12 Distribution of Peak Enhancement Factor at Storm Peaks

Figure 4.12 shows that there is a relatively large variability in γ at the storm peaks, and little clustering is evident. The most common value of γ falls in the range of 2.5 to 3.0, and the mean, standard deviation and median values are all slightly higher than those given earlier.

4.5.3 Spectra from the Datawell Waverider Buoy

A significant wave height threshold of 8.0 m was chosen for the analysis, which resulted in 260 wave spectra over 17 storms. In this sample set, H_s ranged from 8.0 to 12.86 metres and T_p ranged from 10.0 to 16.7 seconds. Various statistics derived from the data set are presented in Table 4.10.

Table 4.10 White Rose JONSWAP Peak Enhancement Factor Statistics for Hs >= 8.0 metres measured by the Datawell Waverider Buoy

Total Samples	260
Minimum	1.0
Maximum	4.8
Mean	1.9
Standard Deviation	0.8
Median	1.7

Values of γ ranged from a low of 1.0 to a high of 4.8, with a mean value of 1.9 and a standard deviation of 0.8. This mean is consistent with the mean values of 2.2 and 2.3 calculated by LeBlond et al. (1982) on his analysis of the spectra occurring over 2 storms

and discussed earlier. The highest γ value of 4.8 occurred on December 22, 2010, with significant wave height of 8.12 m and peak period of 12.5 seconds. Distributions of γ for $H_s \geq 8.0$ m are presented in Figure 4.13 and Figure 4.14. A scatter plot of γ vs. H_s is shown in Figure 4.15.

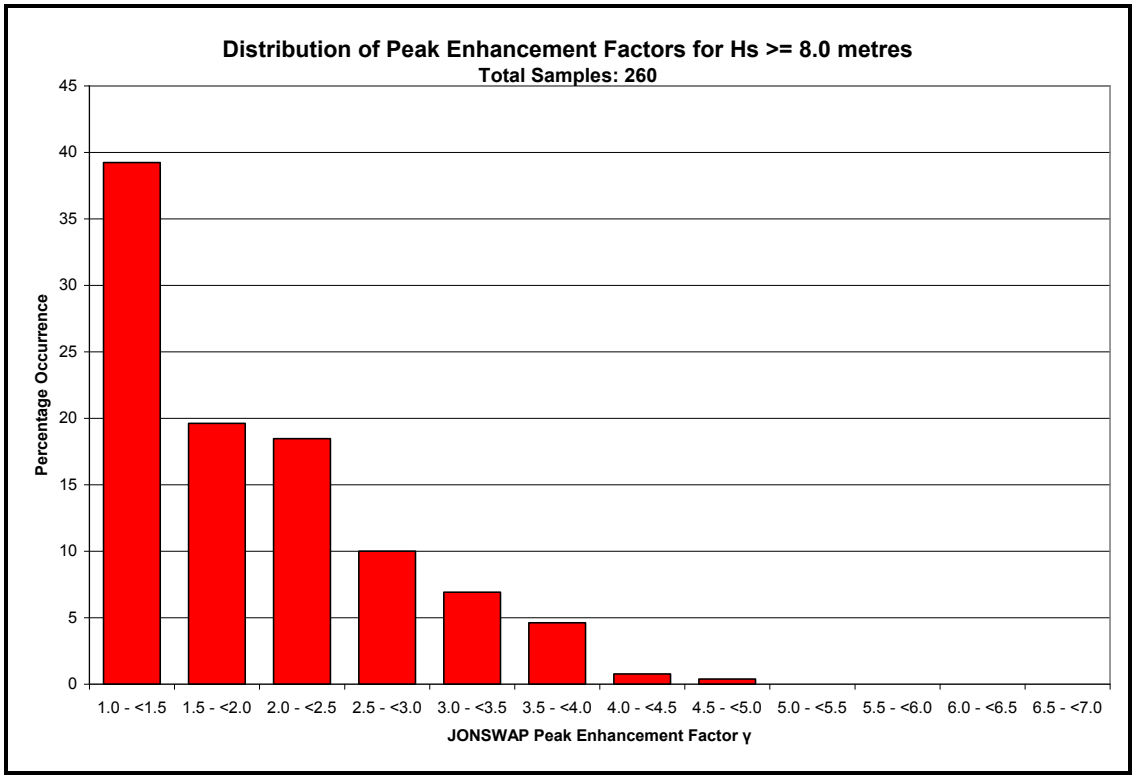

Figure 4.13 Distribution of Peak Enhancement Factors for Hs >= 8.0 metres at White Rose (Percentage Occurrence) for 17 Storms

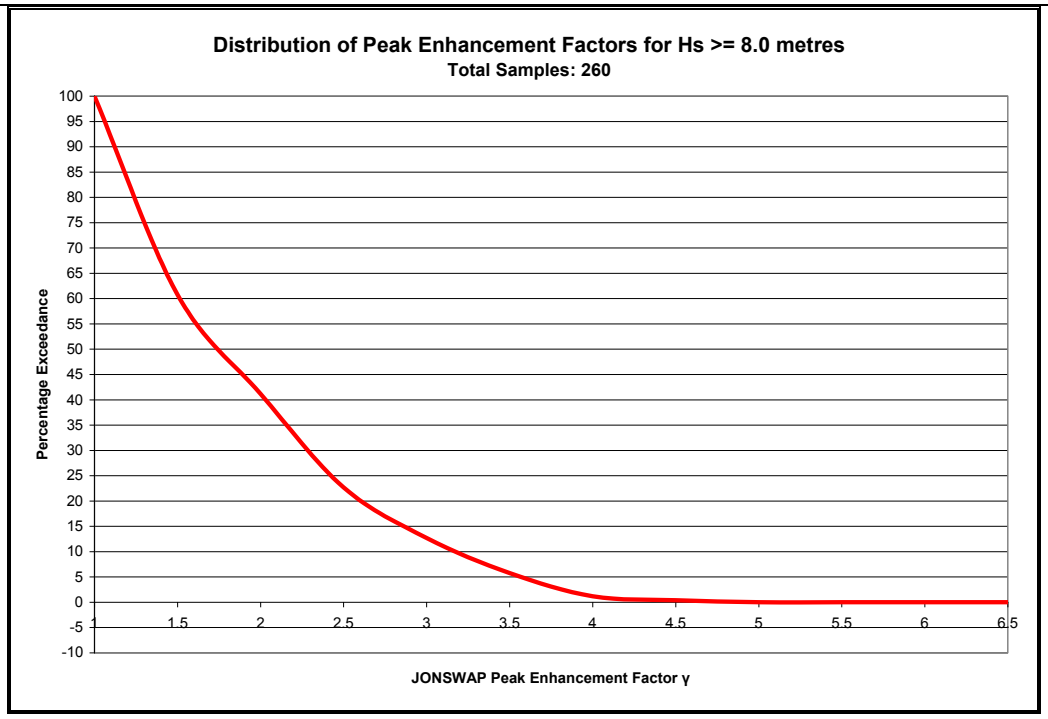

Figure 4.14 Distribution of Peak Enhancement Factors for Hs >= 8.0 metres at White Rose (Percentage Exceedance) for 17 Storms for 17 Storms

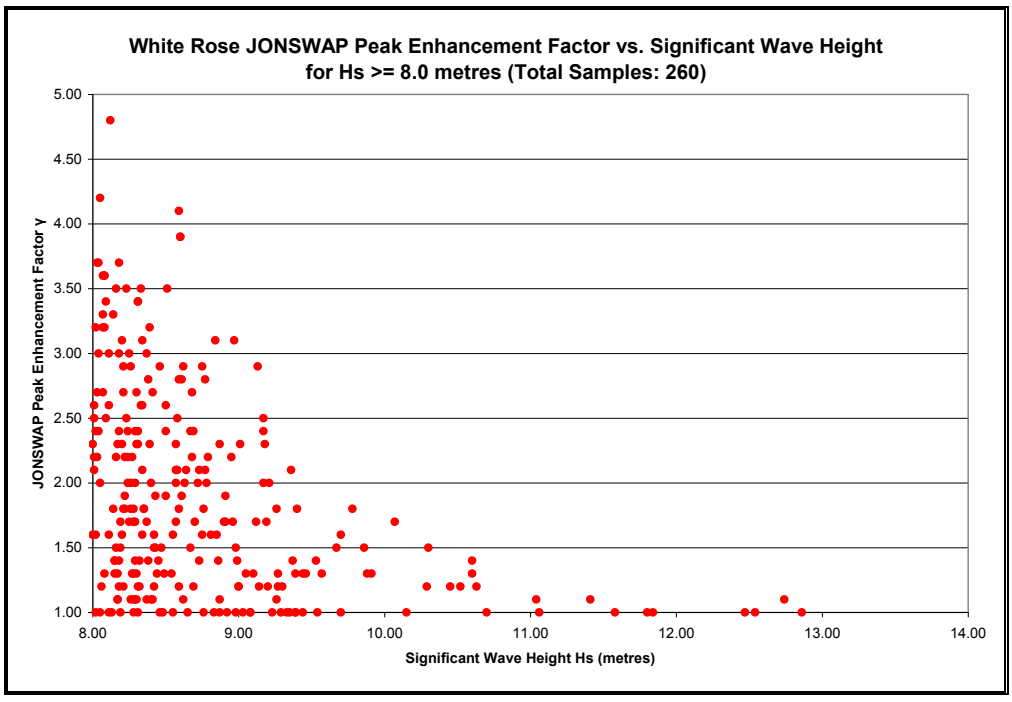

Figure 4.15 White Rose JONSWAP Peak Enhancement Factor vs. Significant Wave Height for Hs >= 8.0 metres

Peak Enhancement Factor at Storm Peaks

In an effort to determine whether values of γ tend to cluster around any particular value at the peak significant wave height during a storm situation, 17 separate storm events during which H_s reached or exceeded 8.0 m were selected from the waverider data set. At the highest wave height measured during the storm (the „storm peak"), the JONSWAP peak enhancement factor was calculated. Storm peak data are listed in Table 4.11, calculated statistics are given in Table 4.12 and the distribution of γ is presented in Figure 4.16.

Table 4.11 Selected Storm Peaks

Year	Month	Day	Time	Hs	Tp	γ
2007	12	04	0350	9.39	16.67	1.0
2007	12	29	0920	9.17	11.76	2.5
2008	01	01	1717	11.84	13.30	1.0
2008	03	14	0844	8.70	13.30	1.7
2008	10	22	1036	8.21	10.50	1.2
2008	11	30	0806	8.29	15.40	2.0
2008	12	23	1136	11.06	14.30	1.0
2009	02	02	0136	10.15	12.50	1.0
2009	02	19	0206	9.30	15.40	1.2
2009	10	15	0135	9.37	11.80	1.4
2009	10	27	0235	9.54	13.30	1.0
2009	12	07	0139	8.64	11.10	2.1
2009	12	22	1739	9.88	15.40	1.3
2010	01	10	2238	8.78	11.76	2.0
2010	02	05	1839	9.86	14.29	1.5
2010	09	21	2029	12.86	16.67	1.0
2010	11	22	1511	9.44	11.76	1.3

Table 4.12 White Rose JONSWAP Peak Enhancement Factor Statistics for Storm Peaks

Total Samples	17
Minimum	1.0
Maximum	2.5
Mean	1.4
Standard Deviation	0.5
Median	1.3

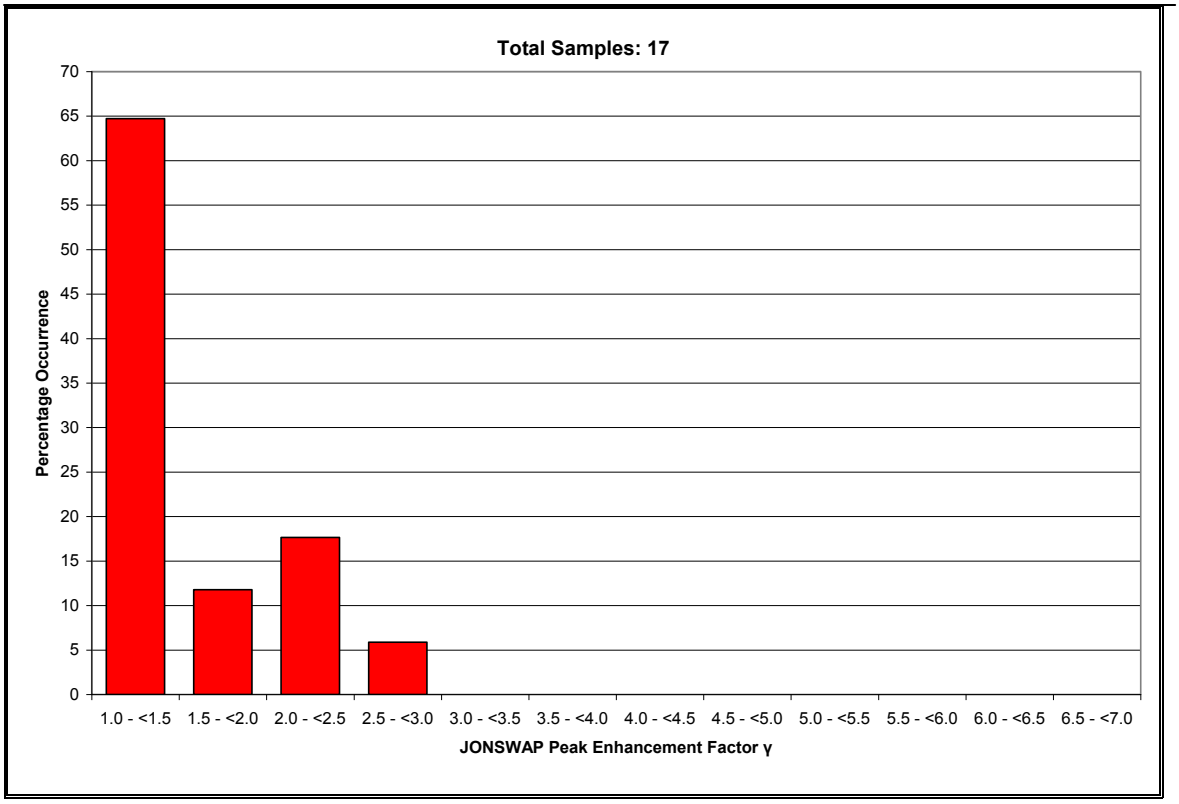

Figure 4.16 Distribution of Peak Enhancement Factor at Storm Peaks

The most common value of γ falls in the range of 1.0 to 1.5, and the mean, standard deviation and median values are all slightly higher than those given for data from the Triaxys buoy.

4.5.4 Evolution of Peak Enhancement Factor during Storm Events

In order to analyze the variability and evolution of γ over the course of a storm event, four separate storm events during which H_s exceeded 8.0 m for a significant period of time were chosen. These events occurred on November 09 to 10, 2003, October 12 to 14, 2005, January 22 to 24, 2006 and January 10 to 11, 2010. The evolution of Hs, Tp and γ over the course of each of these storms is presented in Figure 4.17 to Figure 4.20. It can be seen from each storm that γ can be highly variable and can change significantly over a very short period of time. In these time series, γ often varied by a factor of two or more between fitted spectra 30 minutes apart and, in a limited number of instances, γ varied by a factor of 2.5 or more in 30 minutes.

It is also evident from the results that the variability in γ is highest leading up to the storm peak. After the storm peak, as significant wave heights begin to decrease and the highest peak periods are observed, the values of γ tend to converge to a range between 1.0 and 2.5. This tendency can be seen in all four storm events, but is most evident during the event of January 22 to 24, 2006.

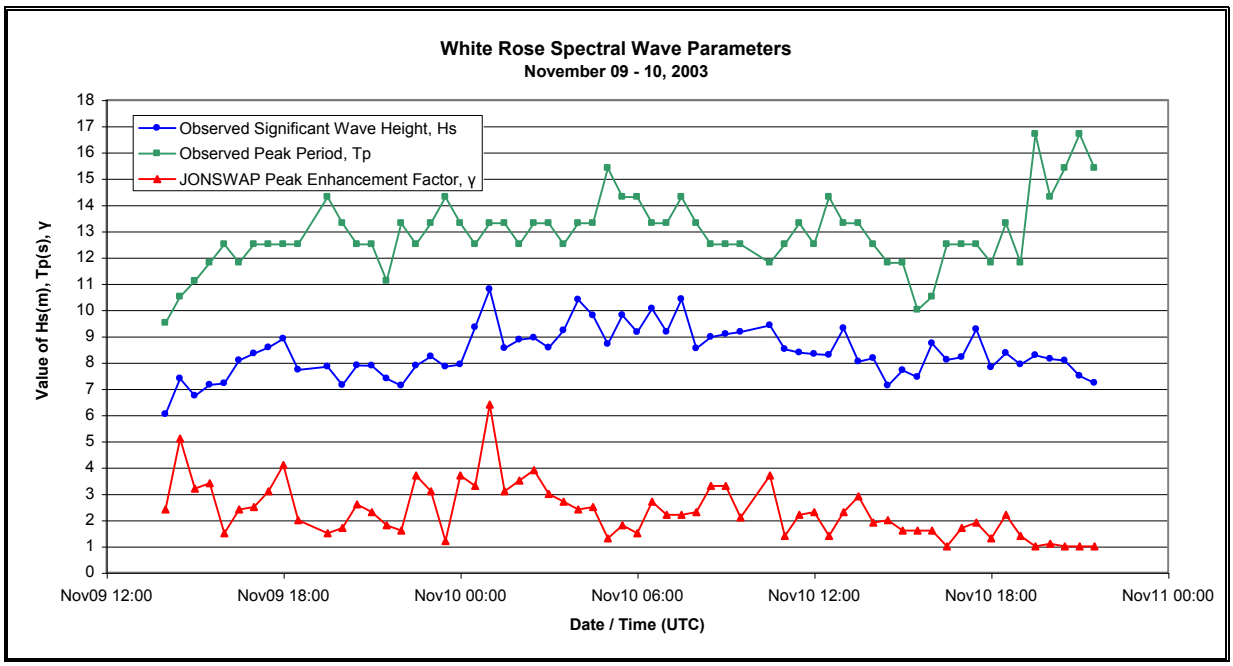

Figure 4.17 Evolution of Hs, Tp and γ, on November 09 to 11, 2003

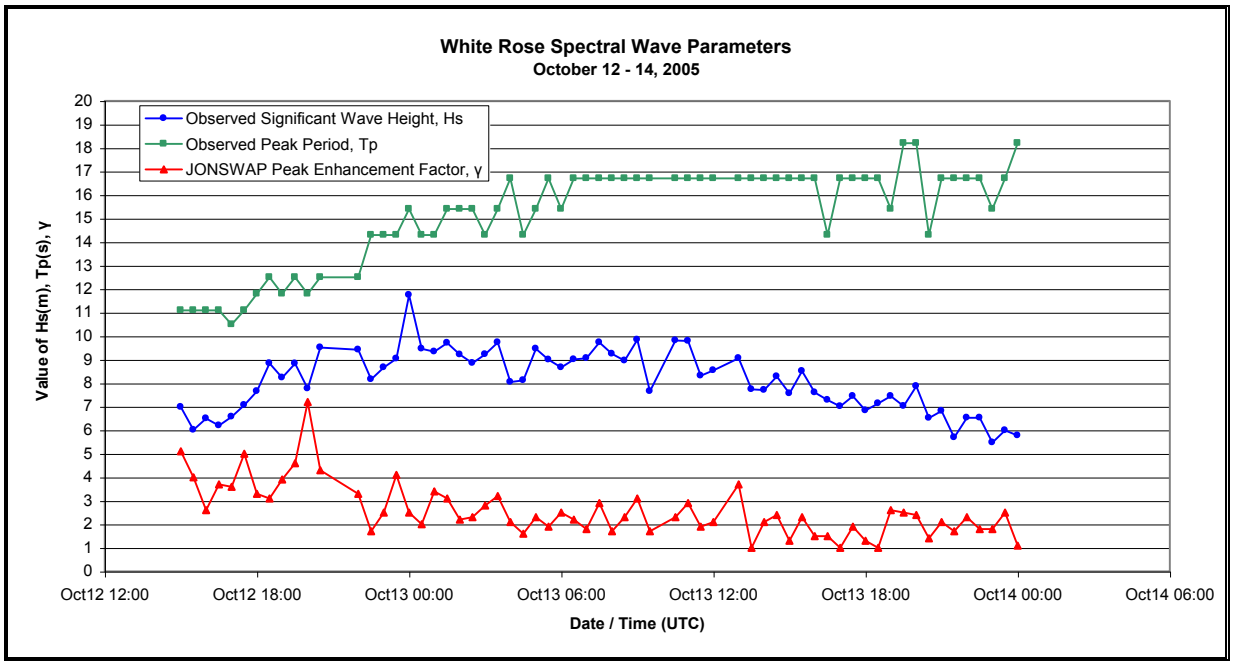

Figure 4.18 Evolution of Hs, Tp and γ, on October 12 to 14, 2005

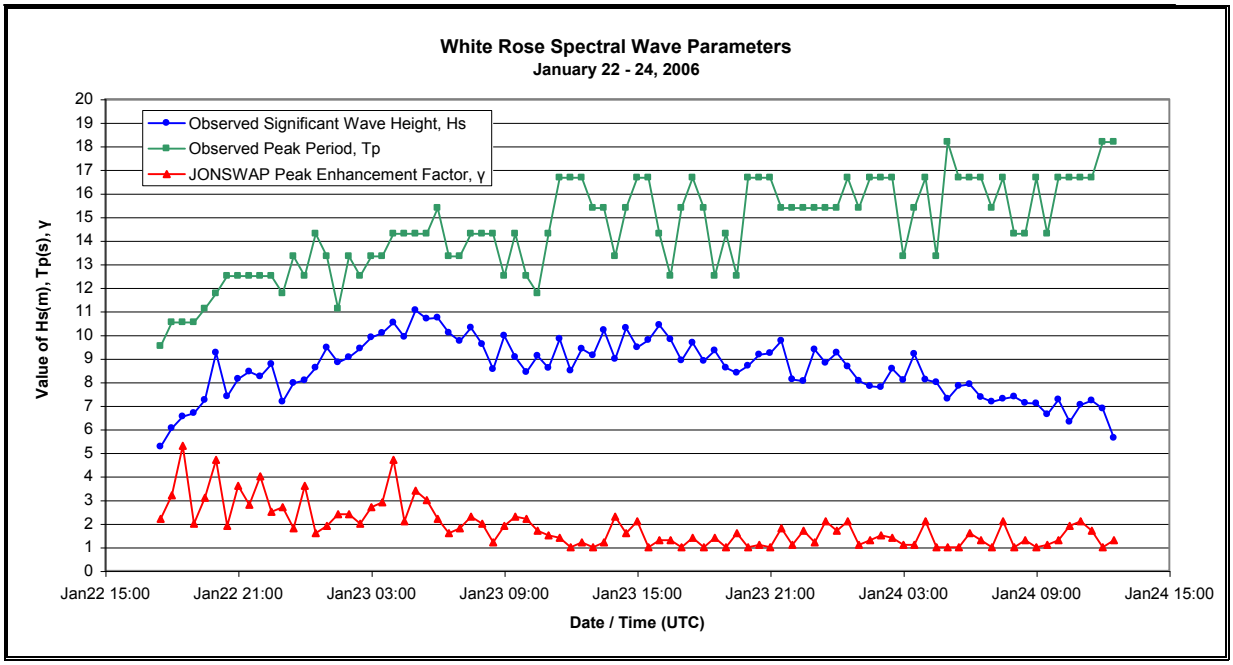

Figure 4.19 Evolution of Hs, Tp and γ, on January 22 to 24, 2006

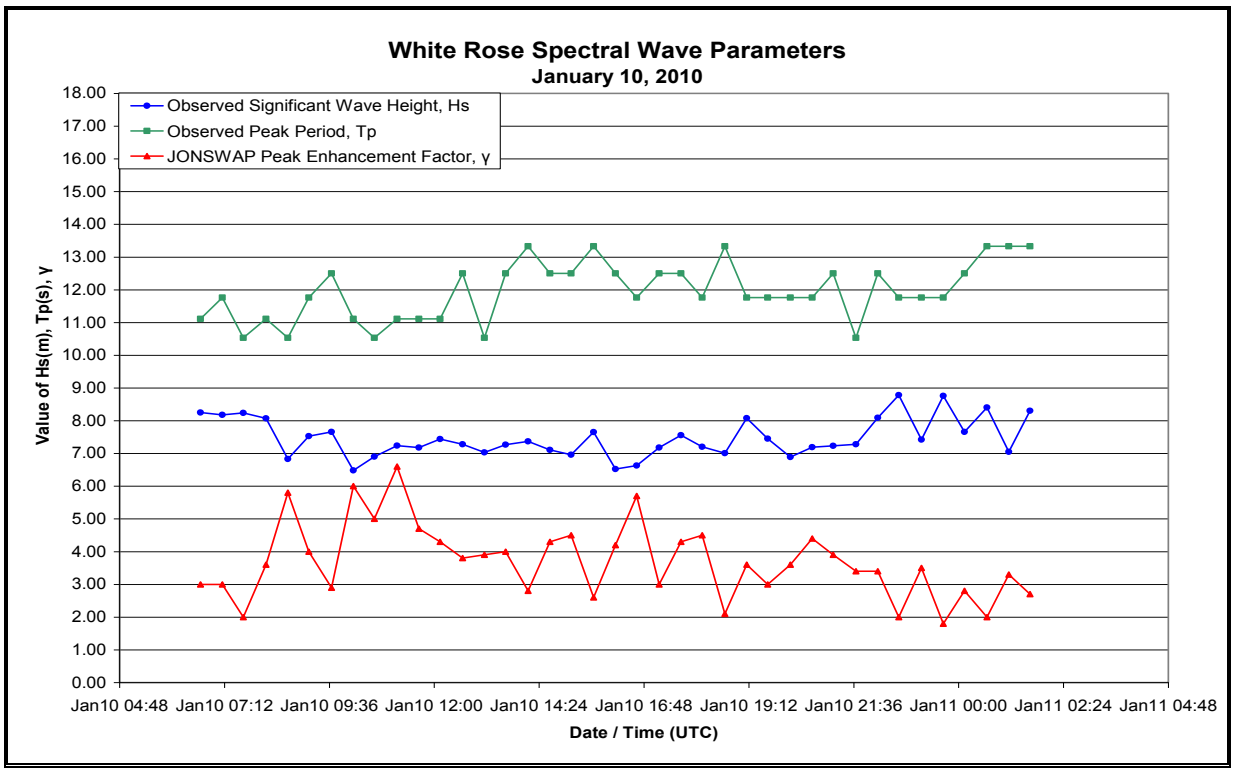

Figure 4.20 Evolution of Hs, Tp and γ, on January 10 to 11, 2010

4.5.5 Summary

An analysis of the wave spectra with Hs≥ 8.0 m measured at White Rose shows different results between the TRIAXYS wave buoy and the Datawell waverider buoy.

The values of γ for the TRIAXYS wave buoy ranged between 1.0 and 6.4 for significant wave height equal or greater than 8 m. For the TRIAXYS wave buoy the most common value of γ lies between 2.0 and 2.5 for all wave spectra that was analyzed. However, during the peak of the storms, the most common value of γ was between 2.5 and 3.0. The analysis of the Datawell waverider spectra gave γ values ranging between 1.0 and 4.8. The most common values are between 1.0 and 1.5 for all wave spectra and for the storm peaks.

There is a considerable spread among the values of γ in the TRIAXYS data, with values ranging from 1.0 to 6.4 with a mean value of 2.4 and a standard deviation of 1.0. The Datawell data has a range of 1.0 to 4.8 with a mean value of 1.9 and standard deviation of 0.8. It is therefore not possible to determine a single value of γ that would be applicable to all situations at White Rose.

It must be noted that in the analysis of wave parameters for the October 12 to 14, 2005 storm situation, a γ value of 7.2 was found at 20:00 UTC on October 12. This spectrum was not included in the analysis of wave spectra with H_s >= 8.0 m because H_s at that time was 7.77 m. A γ value of 7.2 may seem extremely high, but according to Chakrabarti (1987) the JONSWAP peak enhancement factor may vary between a value of 1 and 7. An analysis of the wave parameter and spectral data at that time did not indicate any obvious problems with the data.

Over the course of individual storm events, γ can be highly variable and can change significantly over a very short period of time, often by a factor or 2 or more in a period of 30 minutes. This variability appears to be highest leading up to the storm peak. After the storm peak, as significant wave heights begin to decrease and the highest peak periods are observed, the values of γ tend to converge to a range between 1.0 and 2.5. This fact can be explained by the sea state becoming more fully-developed over the course of the storm as a greater number of wave trains are present, thereby distributing energy over a wider range of frequencies.

4.6 Fatigue Wave Height Distribution by Direction

A 20-year frequency distribution of individual wave heights in the vicinity of White Rose was estimated using the following data as inputs:

- significant wave height by vector mean direction (from) at 1-hour intervals for grid point 11034 from the MSC50 hindcast time-series data set for the period 1954 through 2009;
- mean wave periods for individual waves based on information provided by the client.

The 55-year frequency distribution of significant wave height by direction was proportioned to form an equivalent data set valid for a 20-year period.

Individual wave heights are assumed to follow a Raleigh distribution (World Meteorological Organization, 1988) wherein the probability of wave heights (H) exceeding a given height (H_1) in terms of significant wave heights (Hs) is given by:

$$F(H > H_1) = \exp [-2 (H / Hs)^2]$$

From this, the expected probabilities for individual wave heights in 1 m ranges were computed (F_i) for each significant wave height, and the corresponding mean wave period was assigned to each height range. Total number of waves in the 1-hour period for each wave period was then multiplied by the corresponding wave height range probability (F_i) to obtain an estimate of the number of individual wave heights in each height range. The number of individual wave heights was then summed for all sea states by direction. The results are shown in Table 4.13.

4.7 Wave/Current Interaction

Occasionally, there are reports of vessels encountering exceptionally enormous waves during storms. These reports are most common off the southeast coast of South Africa in the Agulhas current. There have been some reports of these huge "episodic" waves in the North Atlantic. The Queen Mary (81,000 tons) nearly capsized during a North Atlantic storm in 1943 when it was caught broadside by a gigantic wave which ripped gear off the decks and smashed glass windows in the bridge (Teagle, 1978). The 632-foot tanker, Texaco Oklahoma, was broken in two by a giant wave in the North Atlantic south of New York in 1971. Thus other ships of 450 foot length and 12,000 ton displacements (Anita and Norse Variant) were lost in the same area in March 1973, during storms with strong north easterly winds. All three ships were in the Gulf Stream when they encountered the storms. The ocean liner Queen Elizabeth on a trans-Atlantic trooping voyage in 1943, passing over Greenland"s continental shelf met an episodic wave of massive proportions (Dawson, 1977), tearing gear away that was fixed to the forecastle and smashing the glass on the bridge.

Episodic waves are characterized by both their unusual height and very steep slope. They have usually been found near the continental shelf break (Dawson, 1977) indicating that the unusual waves may be the result of storm waves interacting and gaining energy from the current. Long swell propagating against a current can be refracted and steepened while gaining energy from the current flow. Smith (1976) calculated a possible amplification factor of 4 for the wave height of 12 sec waves in the Agulhas current. LeBlond (1982) suggests that similar wave conditions could occur in the Labrador Current.

Anyone carrying out CTD transects across the edge of the Continental Shelf in summer will notice that the waves are noticeably higher across a narrow band (10 to 20 km) on the outside edge of the Grand Banks, in the core of the Labrador current. These higher waves are due to the interaction of waves and current. The wave climate at White Rose is very similar to that at Hibernia and Terra Nova. The question is whether there is a higher risk of larger waves due to being located closer to the core of the Labrador Current. Presumably the higher waves in the Labrador Current region will form by waves propagating from a southerly direction.

Table 4.13 Estimated 20-Year Frequency Distribution of Individual Wave Heights by Direction for White Rose

20-Year Frequency Distribution of Individual Wave Heights by Direction										
Wave Height (m)	Mean Period (s)	True Direction (from)								
		NE	E	SE	S	SW	W	NW	N	Totals
> 0 to < 1	4.0	4180978	4005167	5442882	11214750	12574461	10101318	6974590	6884277	61378423
>= 1 to < 2	5.4	2128561	1998380	2579347	5153688	7471860	5839049	4766739	4176006	34113630
>= 2 to < 3	6.3	769842	698788	917169	1894038	2843029	2551643	2246192	1721147	13641848
>= 3 to < 4	6.8	273542	237475	330042	728622	1066838	1138327	1028549	690862	5494257
>= 4 to < 5	7.3	98020	80610	119558	283515	425553	518152	466034	280002	2271444
>= 5 to < 6	7.8	38194	29556	46117	116504	186921	250207	219223	121576	1008298
>= 6 to < 7	8.1	14987	10629	17478	47281	85019	124476	105237	54297	459404
>= 7 to < 8	8.5	6716	4441	7411	20933	42906	66081	54071	26850	229409
>= 8 to < 9	8.9	2871	1720	2867	8707	21631	35041	27640	13161	113638
>= 9 to < 10	9.1	1221	647	1068	3518	11300	18785	14281	6558	57378
>= 10 to < 11	9.4	618	319	489	1749	6586	10864	8096	3648	32369
>= 11 to < 12	9.6	276	136	178	758	3629	5903	4270	1875	17025
>= 12 to < 13	9.8	149	72	92	434	2287	3608	2560	1100	10302
>= 13 to < 14	10.0	56	25	26	182	1260	1912	1312	544	5317
>= 14 to < 15	10.4	13	4	3	66	633	837	533	206	2295
>= 15 to < 16	10.5	11	4	3	52	439	614	397	157	1677
>= 16 to < 17	10.6	2	0	0	14	225	242	140	53	676
>= 17 to < 18	10.7	2	0	0	11	158	174	106	43	494
>= 18 to < 19	10.8	0	0	0	3	70	57	30	10	170
>= 19 to < 20	10.8	0	0	0	0	30	19	4	4	57
>= 20 to < 21	10.9	0	0	0	0	22	17	4	3	46
>= 21 to < 22	11.0	0	0	0	0	8	2	0	1	11
>= 22 to < 23	11.6	0	0	0	0	1	0	0	0	1
>= 23 to < 24	11.6	0	0	0	0	1	0	0	0	1
Totals		7516059	7067973	9464730	19474825	24744867	20667328	15920008	13982380	118838170

High waves are more easily formed in winter when both the water and atmosphere are unstable. During this season, the winds are predominately from the west, and not a favourable direction for wave/current interaction. During summer, the winds are more often from the south and southwest, but since the water is stratified and the atmospheric conditions are stable, it is much more difficult to generate high waves. Important factors to consider are how far and in what direction an episodic wave would travel should such an event occur. The distance an episodic wave can travel before losing its energy to internal friction and air resistance requires research. Should an episodic wave be formed from southerly or southerly winds through wind/wave interaction with a southerly

flowing opposing Labrador Current, the resulting wave would travel in a northerly or northeasterly direction, away from White Rose. Therefore, it would seem that there is minimal risk for such an event to affect the White Rose location even though White Rose is located close to the boundary of the Labrador Current.

5.0 Extreme Wind and Waves

Extreme wind and waves were calculated for the White Rose Field using the MSC50 hindcast data set. This data set was determined to be the most representative of the available data sets, as it provides a continuous 55-year period of 1 hourly data for the site. All extremes are specified for return periods of 1-yr, 10-yr, 50-yr, 100-yr, 1,000-yr and 10,000-yr. All wind speeds are referenced to the 10 m height.

5.1 The MSC50 Hindcast Approach

The extreme analysis was derived from the results of the 55-year continuous hindcast of the North Atlantic Ocean from 1954 to 2009 by Oceanweather Inc. This hindcast project was an update of the AES40 hindcast carried out by Oceanweather between 1997 and 1999. Swail et al. (2006) gives a description of the MSC50 hindcast which is incorporated in the following paragraphs.

The MSC50 hindcast incorporated new dynamic repositioning of marine data and allowed direct kinematic analysis of isotachs and/or streamlines within the toolset. One deficiency identified in the AES40 was in the use of 6-hourly analysis during rapidly developing winter storms off the U.S. New England coastline. These storms would intensify rapidly in the Gulf of Maine and then track over Canadian waters. In the MSC50 data, these systems were addressed with a 3-hourly analysis time-step to better capture these systems. Original 6-hourly NCEP/NCAR 10 m wind fields were time interpolated using a moving centers interpolation algorithm which maintains the spatial characteristics of a storm without "smearing" the solution. The moving centers were derived from the NCEP/NCAR sea level pressures with manual shifting of the centers to ensure a smooth track. These moving centers were also applied in the dynamic repositioning of off-hour data. This repositioning allows better use of the US and Canadian buoy arrays during storm periods and was also very useful for asynoptic fields such as scatterometer winds. Individual inputs such as buoys, ships, CMAN stations, scatterometer winds and tropical model output are shown as color coded wind barbs.

The MSC50 wave hindcast improved on the AES40 wave hindcast by applying a shallow water version of the OWI-3G on a 0.1 degree grid covering much of the Canadian Maritimes. The North Atlantic basin model was also upgraded to the OWI-3G shallow water model and run at a 0.5 degree resolution.

OWI-3G follows the formulation of the first 3G spectral wave model, WAM (WAMDI, 1988) with a few notable exceptions as noted below:

- The Spectral Resolution
- Propagation Scheme
- Spectral Growth/Dissipation Algorithms

Bathymetry for the model was supplied from two basic sources. The General Bathymetric Chart of the Oceans digital atlas (2003 edition) provided water depths for most of the basin wide hindcasting. This source data is a gridded product with resolution of 1-minute covering the global oceans. Depths were supplied from the Canadian Hydrographic Service 15-second archive (Swail et al. 2006).

5.2 Extremal Analysis Results

The extreme value analysis for wind speeds was carried out using the peak-over-threshold method. For the extreme wave analysis, two methods were used; the peak-over-threshold method and the joint probability method.

After considering four different distributions, the Gumbel distribution was chosen to be the most representative for the peak-over-threshold method as it provided the best fit to the data. Since extreme values can vary depending on how well the data fits the distribution, a sensitivity analysis was carried out to determine the number storms to use, whereby the number of storms, the 100-year extreme value, the correlation coefficient and storm threshold were all compared on an annual and monthly basis. Figure 5.1 and 5.2 show how the extreme values and Gumbel correlation coefficient varies according to the number of storms used in the analysis. The number of storms determined to provide the best fit annually and monthly for each grid point are presented in Table 5.1.

The annual extreme values for winds were calculated from 290 storms with a threshold wind speed above 21.5 m/s. The annual extreme values for waves were calculated from 239 events with a threshold significant wave height of 8.75 m.

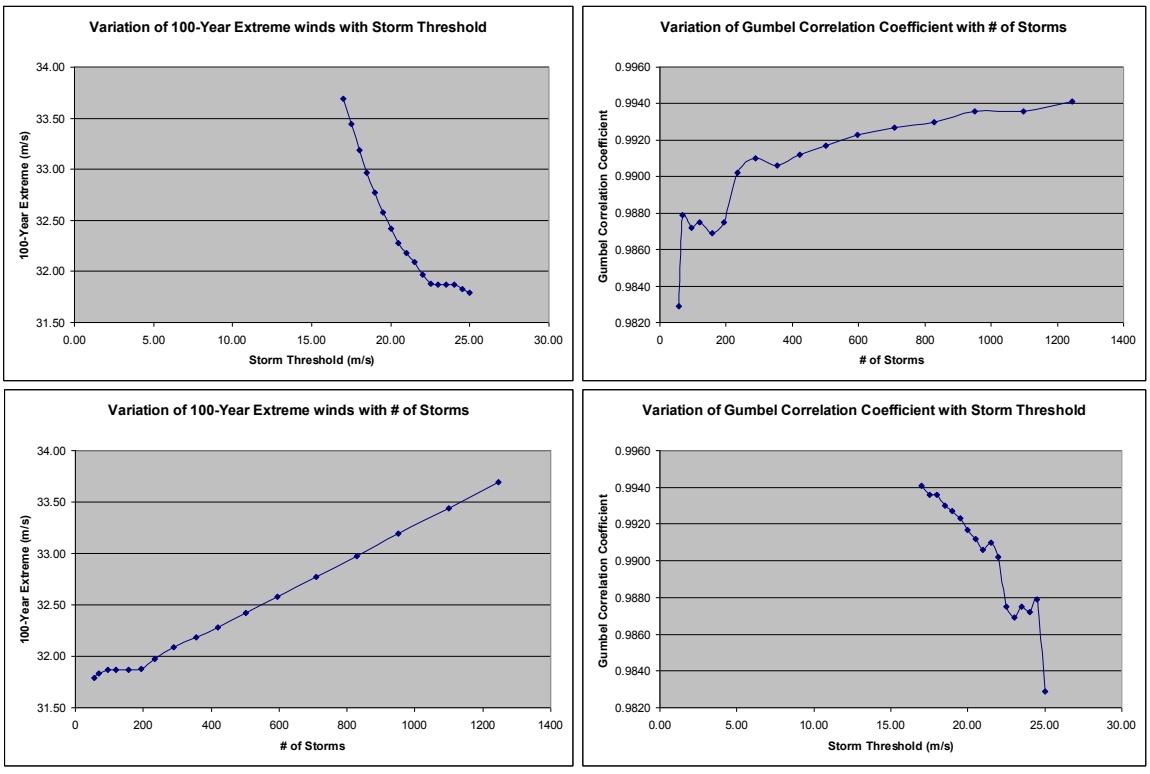

Figure 5.1 Sensitivity Analysis Plots for Extreme Wind Speeds

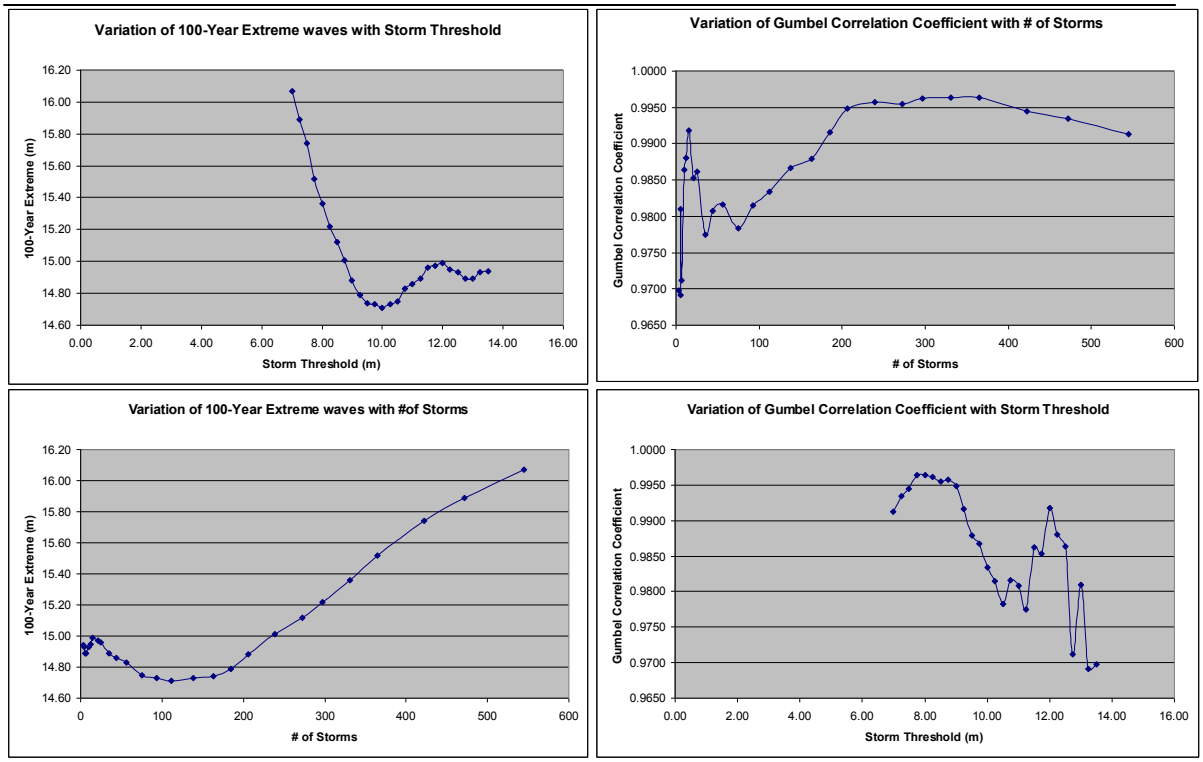

Figure 5.2 Sensitivity Analysis Plots for Extreme Wave Heights

Table 5.1 Number of Storms Providing Best Fit for Extreme Value Analysis of Winds and Waves

		Annually	Monthly
Grid Point 11034	Wind	290	110
	Wave	239	68

5.3 Extreme Value Estimates for Winds from the Gumbel Distribution

The extreme value estimates for wind were calculated using Oceanweather‟s Osmosis software program for the return periods of 1-year, 10-years, 25-years, 50-years, 100-years, 1,000-years and 10,000-years. The analysis used hourly wind values for the reference height of 10 m above sea level. These values were converted to 10-minute and 1-minute wind values using a constant ration of 1.06 and 1.22, respectively (U.S. Geological Survey, 1979).

A comparison of these values, with actual values measured by platforms in the project area was not possible. Logarithmic profiles for adjusting wind speeds from anemometer height to the surface are valid only in neutral or unstable conditions. Observations from platforms on the Grand Banks over the past ten years frequently show stable conditions in which the surface layer wind speed profiles are not valid. Using a logarithmic profile to

adjust wind speeds between the 10 m and anemometer level would therefore introduce an unnecessary source of error in the results.

The maximum individual wave heights were calculated within Oceanweather's OSMOSIS software by evaluating the Borgman integral (Borgman, 1973), which was derived from a Raleigh distribution function. The variant of this equation used in the software has the following form (Forristall, 1978):

$$\Pr\{H > h\} = \exp\left[-1.08311\left(\frac{h^2}{8M_0}\right)^{1.063}\right]; \quad T = \frac{M_0}{M_1}$$

where h is the significant wave height, T is the wave period, and M_0 and M_1 are the first and second spectral moments of the total spectrum. The associated peak periods are calculated by plotting the peak periods of the chosen storm peak values versus the corresponding significant wave heights. This plot is fitted to a power function ($y = ax^b$), and the resulting equation is used to calculate the peak periods associated with the extreme values of significant wave height.

The calculated annual and monthly values for 1-hour, 10-minutes and 1-minute are presented in Table 5.2 to Table 5.4. The annual 100-year extreme 1-hour wind speed was determined to be 32.1 m/s at Grid Point 11034. Monthly, the highest extreme winds occur during February with a 100-year extreme wind estimate of 31.5 m/s.

Table 5.2 1-hr Extreme Wind Speed Estimates (m/s) for Return Periods of 1, 10, 25, 50, 100, 1,000 and 10,000 Years

	Wind Speed 1-hr (m/s)						
Period	**1**	**10**	**25**	**50**	**100**	**1000**	**10000**
January	22.5	26.2	27.6	28.6	29.6	32.9	36.2
February	22.2	27.1	28.9	30.2	31.5	35.9	40.2
March	20.3	24.6	26.1	27.2	28.4	32.1	35.9
April	17.9	22.3	23.9	25.1	26.2	30.1	34.0
May	15.5	19.5	20.9	22.0	23.1	26.6	30.2
June	14.3	18.1	19.4	20.4	21.5	24.8	28.1
July	13.3	16.9	18.1	19.1	20.1	23.3	26.4
August	14.7	21.1	23.4	25.1	26.8	32.4	38.1
September	17.0	22.1	23.9	25.3	26.7	31.2	35.7
October	18.4	23.3	25.1	26.4	27.8	32.2	36.5
November	19.8	24.2	25.8	27.0	28.2	32.1	36.0
December	21.7	26.4	28.0	29.3	30.5	34.6	38.7
Annual	25.1	28.6	30.0	31.1	32.1	35.5	39.0

Table 5.3 10-minute Extreme Wind Speed Estimates (m/s) for Return Periods of 1, 10, 25, 50, 100, 1,000 and 10,000 Years

	Wind Speed 10-min (m/s)						
Period	**1**	**10**	**25**	**50**	**100**	**1000**	**10000**
January	23.8	27.8	29.2	30.3	31.4	34.9	38.4
February	23.5	28.7	30.6	32.0	33.4	38.0	42.6
March	21.5	26.0	27.6	28.9	30.1	34.0	38.0
April	19.0	23.7	25.3	26.6	27.8	31.9	36.0
May	16.4	20.7	22.2	23.3	24.5	28.2	32.0
June	15.2	19.2	20.6	21.7	22.7	26.3	29.8
July	14.0	17.9	19.2	20.3	21.3	24.6	28.0
August	15.6	22.3	24.8	26.6	28.4	34.4	40.4
September	18.0	23.4	25.4	26.8	28.2	33.0	37.8
October	19.5	24.7	26.6	28.0	29.4	34.1	38.7
November	20.9	25.7	27.3	28.6	29.9	34.0	38.2
December	23.0	28.0	29.7	31.0	32.3	36.7	41.0
Annual	26.6	30.4	31.8	32.9	34.0	37.7	41.3

Table 5.4 1-minute Extreme Wind Speed Estimates (m/s) for Return Periods of 1, 10, 25, 50, 100, 1,000 and 10,000 Years

	Wind Speed 1-min (m/s)						
Period	**1**	**10**	**25**	**50**	**100**	**1000**	**10000**
January	27.4	32.0	33.6	34.9	36.1	40.2	44.2
February	27.0	33.0	35.2	36.8	38.4	43.7	49.1
March	24.8	30.0	31.8	33.2	34.6	39.2	43.7
April	21.9	27.2	29.2	30.6	32.0	36.7	41.5
May	18.9	23.8	25.5	26.8	28.1	32.5	36.8
June	17.4	22.1	23.7	24.9	26.2	30.2	34.3
July	16.2	20.6	22.1	23.3	24.5	28.4	32.2
August	17.9	25.7	28.5	30.6	32.7	39.6	46.5
September	20.8	27.0	29.2	30.9	32.5	38.0	43.5
October	22.4	28.5	30.6	32.3	33.9	39.2	44.6
November	24.1	29.5	31.5	32.9	34.4	39.2	44.0
December	26.5	32.2	34.2	35.7	37.2	42.2	47.2
Annual	30.6	34.9	36.6	37.9	39.1	43.3	47.5

5.4 Extreme Value Estimates for Waves from a Gumbel Distribution

The annual and monthly extreme value estimates for significant wave height for return periods of 1-year, 10-years, 25-years, 50-years and 100-years, 1,000-years and 10,000-years are given in Table 5.5. The annual 100-year extreme significant wave height is 15.0 m for Grid Point 11034. Monthly, the highest extreme significant wave height occurs during the month of February with an extreme height of 15.1 m.

During a storm event on January 08, 2007 a maximum individual wave height of 22.6 m was recorded by a waverider in the Terra Nova field. This is greater than the January maximum 10-year return period estimate of 21.8 m for grid point 11034, but less than the 25-year return period estimate of 23.5 m. The significant wave height during this event was 9.72 m.

Table 5.5 Extreme Significant Wave Height Estimates (m) for Return Periods of 1, 10, 25, 50, 100, 1,000 and 10,000 Years

	Grid Point #11034						
Period	**1**	**10**	**25**	**50**	**100**	**1000**	**10000**
January	9.1	12.0	12.9	13.6	14.3	16.5	18.7
February	8.3	12.2	13.4	14.3	15.1	18.1	21.0
March	7.0	10.2	11.2	12.0	12.7	15.1	17.6
April	5.5	8.7	9.6	10.4	11.1	13.5	15.9
May	4.4	7.2	8.0	8.7	9.3	11.5	13.6
June	3.6	6.1	6.9	7.4	8.0	9.9	11.8
July	3.3	5.3	5.9	6.4	6.9	8.4	10.0
August	3.6	6.8	7.8	8.6	9.3	11.8	14.2
September	5.0	9.0	10.3	11.2	12.1	15.2	18.2
October	6.1	10.0	11.2	12.1	13.0	15.9	18.9
November	7.2	10.5	11.5	12.2	13.0	15.5	18.0
December	8.8	11.7	12.7	13.4	14.0	16.3	18.6
Annual	10.8	13.0	13.8	14.4	15.0	17.1	19.1

The maximum individual wave heights and extreme associated peak periods are presented in Table 5.6 and Table 5.7, respectively. Maximum individual wave heights and the extreme associated peak periods are highest during the month of February.

Table 5.6 Extreme Maximum Wave Height Estimates (m) for Return Periods of 1, 10, 25, 50, 100, 1,000 and 10,000 Years

	Grid Point #11034						
Period	**1**	**10**	**25**	**50**	**100**	**1000**	**10000**
January	16.6	21.8	23.5	24.7	25.9	29.9	33.9
February	15.4	22.4	24.7	26.3	27.9	33.3	38.7
March	12.8	18.6	20.4	21.8	23.1	27.5	32.0
April	10.2	15.8	17.6	18.9	20.2	24.6	28.9
May	8.2	13.2	14.7	15.9	17.1	20.9	24.7
June	6.8	11.4	12.9	13.9	15.0	18.5	22.0
July	6.2	9.8	11.0	11.9	12.7	15.5	18.4
August	6.8	12.5	14.2	15.6	16.9	21.2	25.5
September	9.3	16.3	18.4	20.1	21.7	27.0	32.4
October	11.4	18.2	20.4	22.0	23.6	28.8	34.1
November	13.2	19.2	21.0	22.4	23.8	28.4	33.0
December	16.1	21.5	23.2	24.4	25.7	29.8	34.0
Annual	19.8	23.7	25.2	26.3	27.5	31.2	34.9

Table 5.7 Associated Peak Period Estimates (s) for Return Periods of 1, 10, 25, 50, 100, 1,000 and 10,000 Years

	Grid Point #11034						
Period	**1**	**10**	**25**	**50**	**100**	**1000**	**10000**
January	12.7	14.4	14.9	15.3	15.6	16.7	17.7
February	12.1	14.4	15.1	15.5	16.0	17.4	18.6
March	11.8	13.3	13.7	14.0	14.2	15.1	15.8
April	10.7	12.3	12.7	13.0	13.2	14.0	14.7
May	9.9	11.8	12.3	12.7	13.0	14.0	14.9
June	8.6	10.9	11.6	12.0	12.4	13.7	14.8
July	8.3	10.7	11.3	11.8	12.2	13.6	14.9
August	8.8	11.9	12.7	13.2	13.7	15.3	16.7
September	10.6	13.3	14.0	14.4	14.9	16.3	17.5
October	11.3	13.4	13.9	14.3	14.7	15.7	16.7
November	12.0	13.4	13.7	14.0	14.2	15.0	15.6
December	12.7	14.2	14.7	15.0	15.3	16.2	17.1
Annual	13.7	15.0	15.4	15.7	16.0	17.0	18.0

5.5 Joint Probability of Extreme wave Heights and Spectral Peak Period

The extreme analysis was carried out on the 3-hourly data set. For comparison purposes with the previous report and since the equations involved in the methodology were originally developed for 6-hourly data, a 6-hourly data set was also analyzed. In order to examine the period ranges of storm events, an environmental contour plot was produced showing the probability of the joint occurrence of significant wave heights and the spectral peak periods using the methodology of Winterstein et al. (1993). The wave heights were fitted to a Weibull distribution and the peak periods to a lognormal distribution. The wave data was divided into bins of 1 m for significant wave heights and 1 second for peak periods. Since the lower wave values were having too much of an impact on the wave extremes, the wave heights below 2 m were modeled separately in a Weibull distribution. The two Weibull curves were combined near 2 m, the point where both functions had the same probability.

Three-parameter Weibull distributions were used with a scaling parameter α, shape parameter β, and location parameter γ. The three parameters were solved by using a least square method, the maximum log likelihood, and the method of moments. The following equation was minimized to get the coefficients:

$$LS(\alpha,\beta,\gamma) := \sum_{i=0}^{13}\left[\ln\left(-\ln\left(1-FP_i\right)\right) - \beta\cdot\ln\left[\frac{\left(h_i-\gamma\right)}{\alpha}\right]\right]^2$$

where h_i is the endpoint of the height bin (0.5, 1.5, …) and FP_i is the cumulative probability of the height bin. Using a minimizing function the three parameters α, β and γ were calculated.

A lognormal distribution was fitted to the spectral peak periods in each wave height bin. The coefficient of the lognormal distribution was then calculated. Using the coefficients and the two distribution functions, the joint wave height and period combinations were calculated for the various return periods.

3-hourly

A contour plot depicting these values for return periods of 1-year, 10-years, 25-years, 50-years, and 100-years for the 3-hour subset is presented in Figure 5.3. The same plot with the addition of 1,000-year and 10,000-year return periods is presented in Figure 5.4. The annual and monthly values for the significant wave height estimates and the associated spectral peak periods are given in Table 5.8 and Table 5.9, respectively. Monthly contour plots are presented in Appendix 3. The extreme wave height for all return periods was higher using the Weibull distribution when compared to the Gumbel distribution.

Table 5.8 Extreme Combined Significant Wave Height Estimates from a Weibull Distribution

Combined Significant Wave Height (m)													
Return Period (Years)	**Jan**	**Feb**	**Mar**	**Apr**	**May**	**Jun**	**Jul**	**Aug**	**Sep**	**Oct**	**Nov**	**Dec**	**Annual**
1.0	10.5	10.3	8.8	7.5	6.2	5.2	4.4	5.3	7.4	8.3	8.7	10.2	11.8
10.0	12.8	12.9	10.9	9.7	8.5	7.3	5.9	7.5	10.5	10.8	10.8	12.7	14.2
25.0	13.7	13.9	11.7	10.5	9.4	8.2	6.5	8.5	11.8	11.8	11.5	13.6	15.1
50.0	14.4	14.6	12.3	11.2	10.1	8.9	7.0	9.2	12.7	12.5	12.1	14.2	15.8
100.0	15.0	15.3	12.8	11.8	10.9	9.6	7.5	10.0	13.8	13.3	12.6	14.9	16.5
1000.0	17.0	17.6	14.6	13.9	13.3	12.0	9.2	12.5	17.2	15.7	14.3	16.9	18.8
10000.0	18.9	19.8	16.3	15.9	15.9	14.6	10.9	15.3	20.9	18.1	15.9	18.9	21.0

Table 5.9 Extreme Associated Spectral Peak Period Estimates from a Weibull Distribution

Associated Median Spectral Peak Period (s)													
Return Period (Years)	**Jan**	**Feb**	**Mar**	**Apr**	**May**	**Jun**	**Jul**	**Aug**	**Sep**	**Oct**	**Nov**	**Dec**	**Annual**
1.0	13.5	13.4	12.7	11.8	11.1	10.3	9.5	10.2	11.9	12.5	12.5	13.5	14.3
10.0	14.8	14.7	13.5	12.8	12.6	11.7	10.9	11.6	13.8	13.8	13.6	14.6	15.5
25.0	15.2	15.2	13.8	13.1	13.2	12.4	11.4	12.2	14.6	14.3	14.1	15.1	16.0
50.0	15.6	15.6	14.0	13.4	13.6	12.9	11.9	12.7	15.2	14.7	14.4	15.4	16.3
100.0	15.9	15.9	14.2	13.7	14.1	13.4	12.4	13.2	15.8	15.1	14.7	15.7	16.7
1000.0	17.0	17.0	14.8	14.6	15.8	15.2	14.3	14.9	18.1	16.4	15.7	16.7	17.8
10000.0	18.1	18.1	15.4	15.4	17.7	17.3	16.5	16.9	20.6	17.6	16.7	17.6	18.8

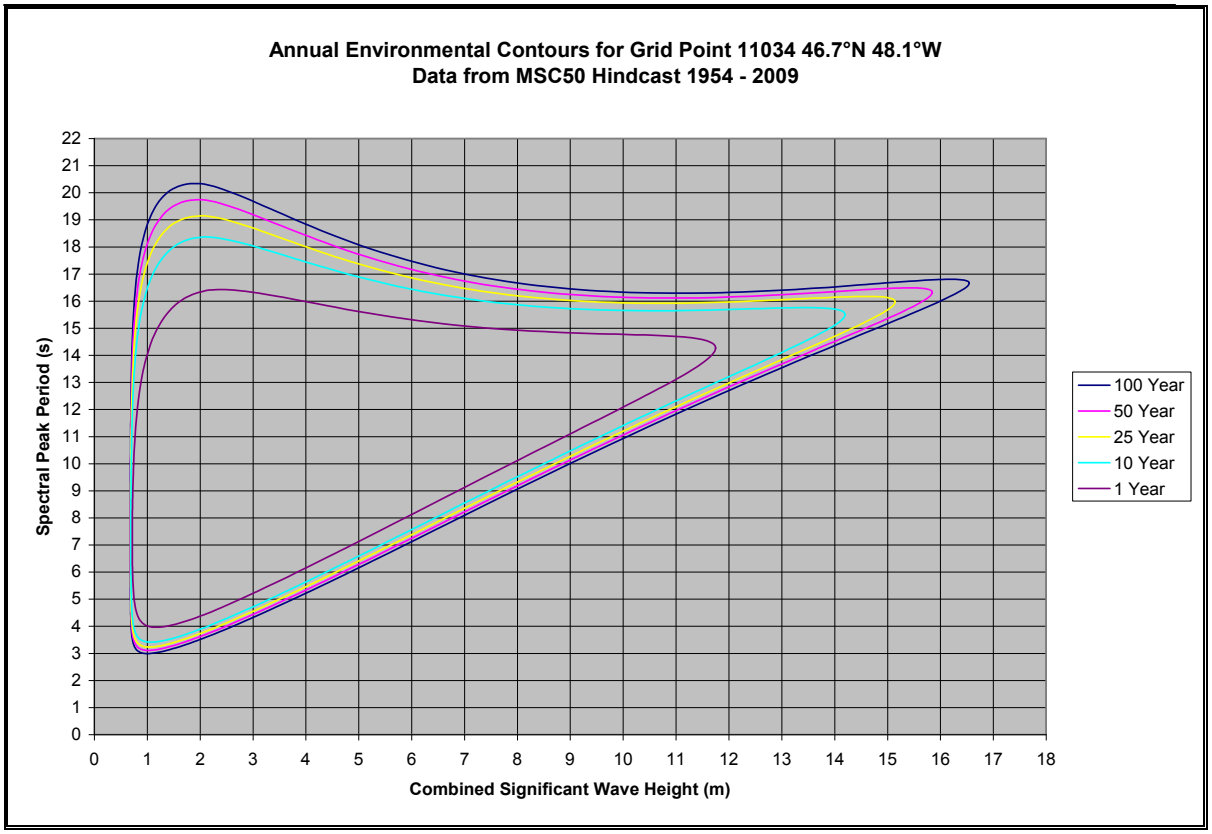

Figure 5.3 Environmental Contour Plot of 1, 10, 25, 50 and 100-year Return Periods for Grid Point 11034 located near 46.3°N; 48.0°W using a 3-hourly data set

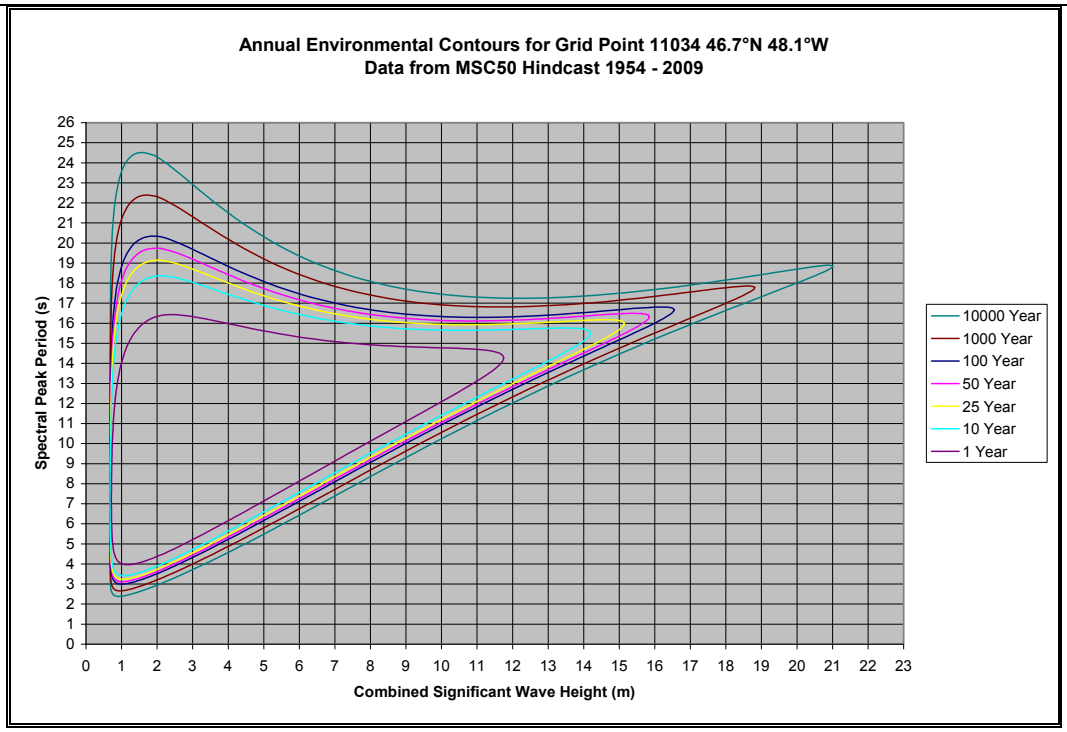

Figure 5.4 Environmental Contour Plot of 1, 10, 25, 50, 100, 1,000 and 10,000-year Return Periods for Grid Point 11034 located near 46.3°N; 48.0°W using a 3-hourly data set

6-hourly

A contour plot depicting these values for return periods of 1-year, 10-years, 25-years, 50-years, and 100-years for the 6-hourly data set is presented in Figure 5.5. The same plot with the addition of 1,000-year and 10,000-year return periods is presented in Figure 5.6. The annual values for the significant wave height estimates and the associated spectral peak periods are given in Table 5.10 for comparison purposes with the 3-hourly data set.

Table 5.10 Extreme Combined Significant Wave Height and Associated Spectral Peak Period Estimates from a Weibull Distribution

Return Period (Years)	Combined Significant Wave Height (m)	Associated Median Peak Spectral Period (s)
1.0	11.0	13.8
10.0	13.5	15.0
25.0	14.4	15.5
50.0	15.2	15.8
100.0	15.9	16.1
1000.0	18.2	17.2
10000.0	20.5	18.3

The AES40 data set for years 1958 to 1998 gave a 100-year extreme significant wave height of 15.0 m. The AES40 data set consisted of 6 hourly by data values. The MSC50 data set for years 1954 to 2009 gives a 100-year extreme significant wave height of 15.9 m using 6 hourly data values. The increased value is due to more intense storms in later years and a higher spatial resolution in the MSC50 model data. Since there is a tendency for 6 hourly data to miss some of the higher storm peaks, then MSC50 hindcast data set was developed using 3 hour intervals. The 3 hourly data gives a 100 year extreme significant wave height of 16.5 m.

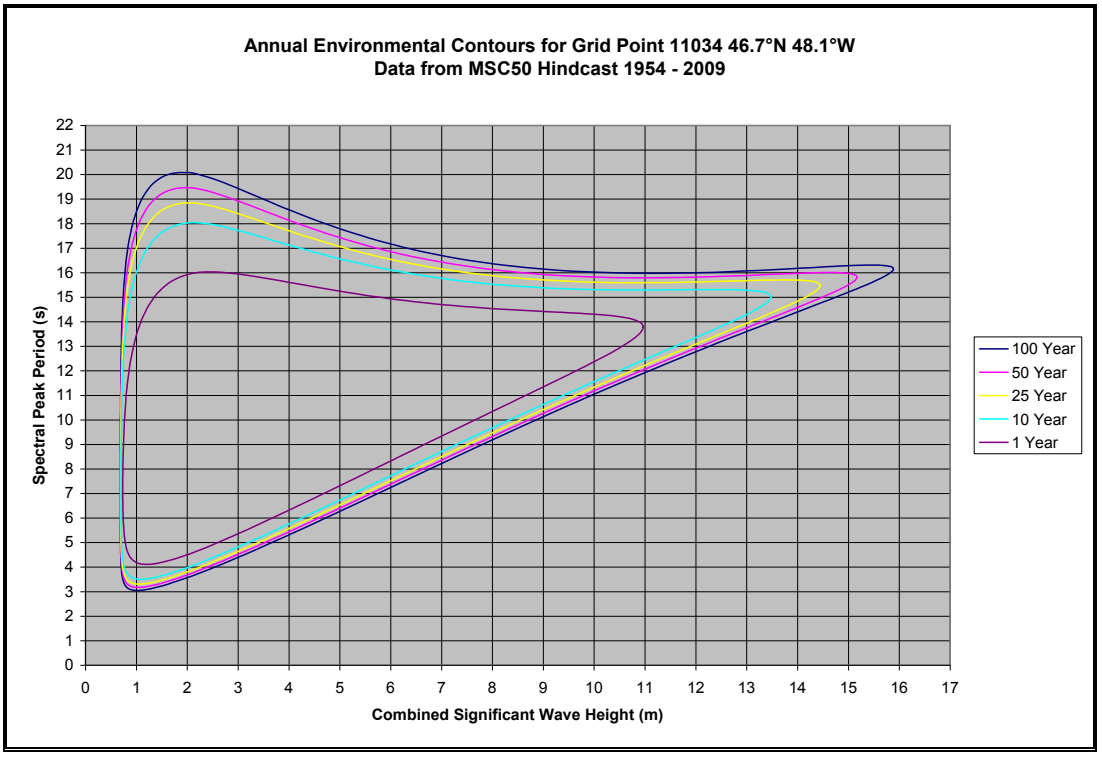

Figure 5.5 Environmental Contour Plot of 1, 10, 25, 50 and 100-year Return Periods for Grid Point 11034 located near 46.3°N; 48.0°W using a 6-hourly data set

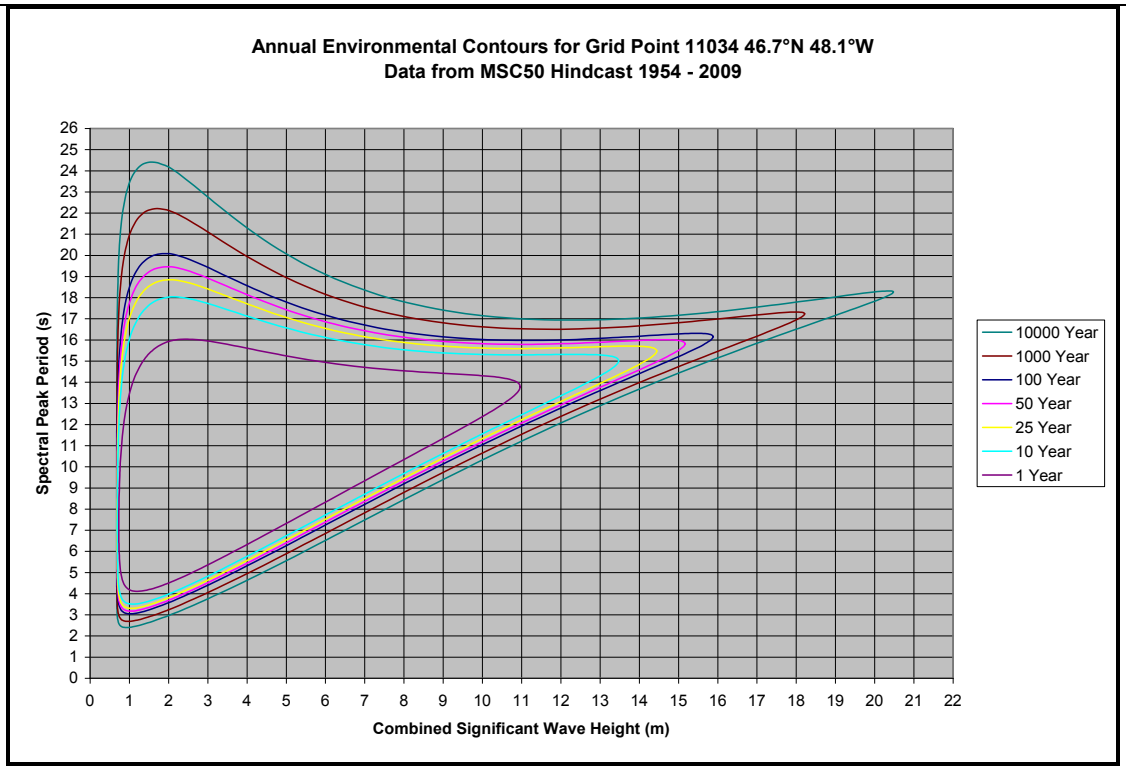

Figure 5.6 Environmental Contour Plot of 1, 10, 25, 50, 100, 1,000 and 10,000-year Return Periods for Grid Point 11034 located near 46.3°N; 48.0°W using a 6-hourly data set

6.0 Currents

6.1 General Circulation

The regional oceanic circulation on the Grand Banks and surrounding areas is governed by the bathymetric features of the continental shelf. A major characteristic of ocean currents is their tendency to follow local and regional underwater bathymetry.

The Grand Banks–Flemish Cap bathymetric features (Figure 1.1) exert a major influence on the regional oceanic circulation. The shape of the banks and channels steers the flow of the Labrador Current. The Labrador Current is comprised of two main streams; an inshore stream near the coast, and a more intense offshore stream over the shelf break between the 400 and 1200 m isobaths (Lazier and Wright 1993). There is some exchange between these two streams which occurs in the channels and saddles that separate the banks offshore Labrador and Newfoundland. The inshore branch of the Labrador Current flows through the Avalon Channel, while the offshore branch flows along the northern slope of the Grand Banks (Figure 6.1). This branch of the Labrador Current divides east of 48°W, resulting in part of the branch flowing to the east around Flemish Cap and the other flowing south around the eastern edge of the Grand Banks and through Flemish Pass.

The volume transport of the Labrador Current is variable from year to year. Han et al. (2010) found that the transport decreased by 6.3 Sv from the early to late 1990ʺs and increased by 3.2 Sv from the late 1990ʺs to the early 2000ʺs. They found that the multi-year changes in the Labrador Current transport appeared to be primarily barotopic and positively correlated with the North Atlantic Oscillation at zero lag implying a fast response of the regional circulation to the atmospheric forcing variability.

Another major current system is situated to the south of the Grand Banks. The Gulf Stream, a major western boundary current, departs the shelf break near Cape Hatteras, USA at approximately 75°W, flowing northeast. In the area of the Southeast Newfoundland Rise which runs from the Tail of the Grand Banks toward the mid-Atlantic Ridge, the Gulf Stream branches into two streams. The southern branch continues east at approximately 40°N. The northern branch, known as the North Atlantic Current, turns north and runs along the east side of the Grand Banks and Flemish Cap, and then turns east following approximately 50°N latitude across the Atlantic. Krauss (1990) found the North Atlantic Current to be approximately 300 km wide. Near the Tail of the Grand Banks, the North Atlantic Current comes into contact with the Continental Slope and follows it northeast around Flemish Cap (Figure 6.2). In this area, it also meets the Labrador Current flowing south. The entire area of the southeastern Grand Banks is a massive mixing area between two water masses with very different temperature and salinity characteristics. A secondary eastward current also flows inshore of the Atlantic Current along the Continental Slope, sometimes referred to as the Slope Current, with characteristics of Slope Water (McLellan, 1957). Slope Water is formed from Atlantic Current Water and Coastal Water. The North Atlantic Current and Slope Current transport warmer, high salinity water to the northeast along the southeast slope of the Grand Banks and Flemish Cap.

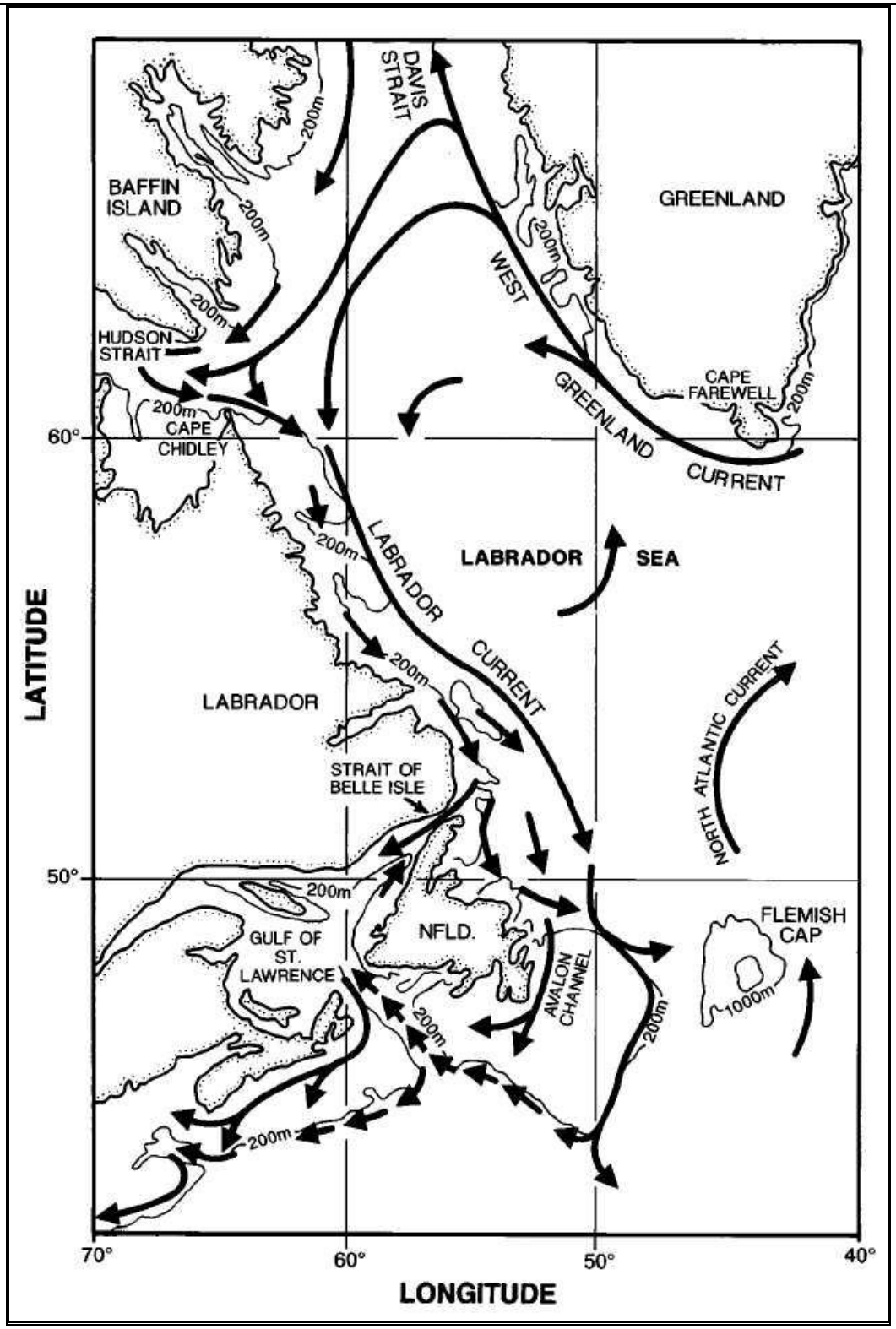

Figure 6.1 Major Ocean Circulation Features in the Northeast Atlantic (Colbourne et al., 1997)

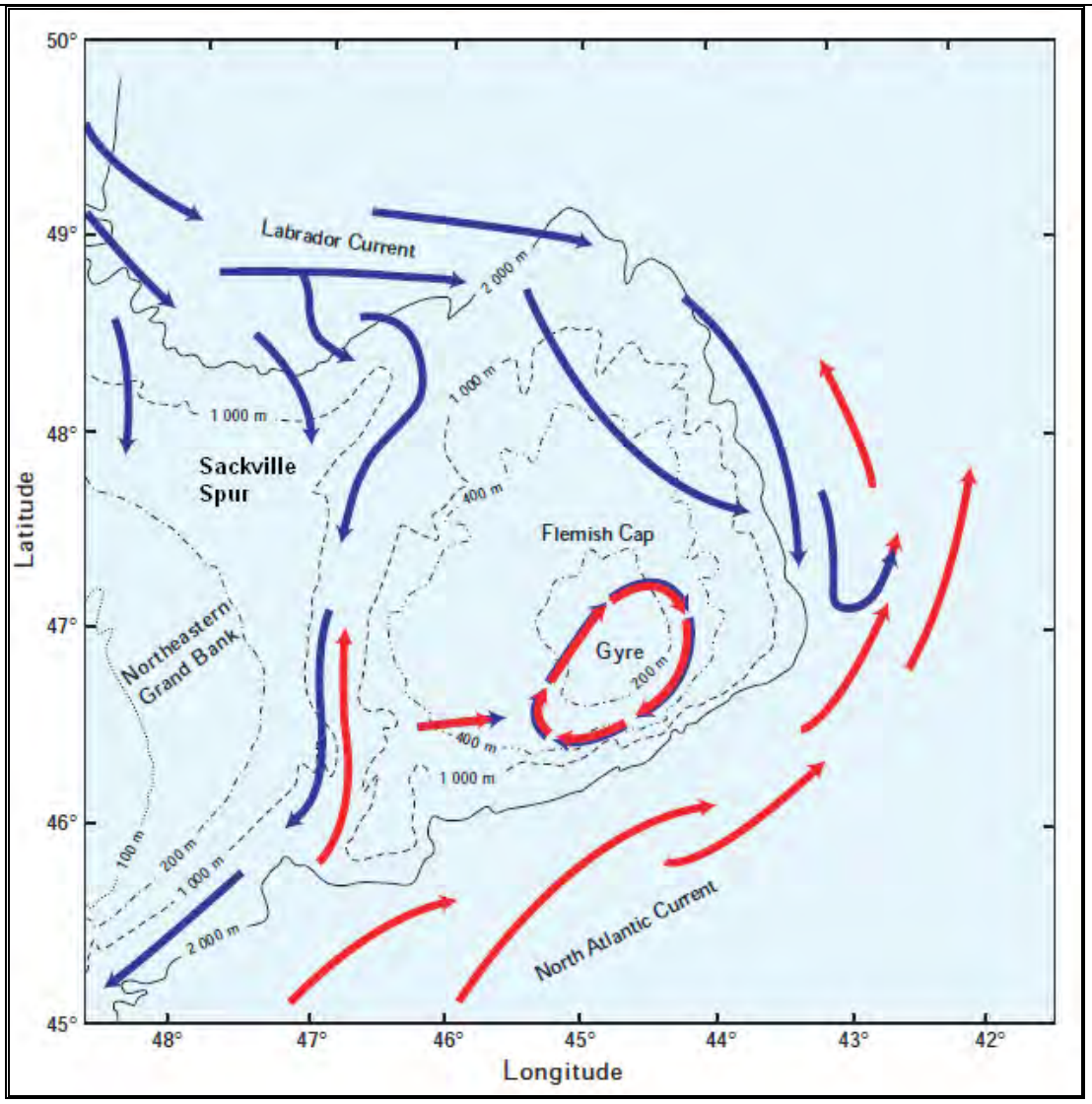

Figure 6.2 The Major Circulation Features around the Flemish Cap and Sackville Spur (modified from Colbourne & Foote, 2000)

White Rose is located at the northeast sector of the Grand Banks and is located in a water depth of approximately 120 m. In the immediate area, the bottom relief is relatively featureless, but steep slopes occur to the north and east at the edge of the Grand Banks. White Rose is located inshore of the Labrador Current, where most of the time the flow is weak, with variable mean flows, compared to the strength of the two major current systems in the vicinity. At times, the variabilities in the mixing and interactions created by these two major current systems can have an effect on the current flow at White Rose.

The general circulation and mean currents on the Grand Banks are well understood from geostrophic calculations, drifter data, current modeling, and direct measurements. The variabilites are becoming more understood as the quantity of data collected at White Rose increases.

6.2 Historical Data

6.2.1 Geostrophic Flow

Geostrophic calculations are an indirect means of deriving the velocity field from the internal pressure and density distribution of the water. The internal pressure and density distributions are determined from vertical profiles of temperature and salinity. This method was widely used by oceanographers to understand the general pattern of ocean currents before current meters became available. In the 1950s and 1960s, the International Ice Patrol (IIP) did routine surveys on the outer edge of the Grand Banks to assist with understanding iceberg drift. In later years, they relied more heavily on surface drifters. The dynamic topography of the sea surface calculated from temperature and salinity measurements collected between May 23 and June 4, 1951, is shown in Figure 6.3. This figure shows general features of the current pattern in the study area. The Labrador Current is flowing southward with a maximum geostrophic component of approximately 60 cm/sec east of White Rose on the West Side of Flemish Pass at location 47°15′W (Soule et al., 1951). Other interesting features include a clockwise circulation around Flemish Cap, an eastward flowing current in the vicinity of White Rose, and the influence of the North Atlantic Current as far north as 46°N in the area south of Flemish Cap. South of White Rose, the core of the North Atlantic current is at 45°N during this particular year. The north boundary of the North Atlantic Current is quite variable, but often seen further south and at times further north.

Recent geostrophic currents were calculated by Colbourne (2000) from the temperature and salinity measurements taken along the standard Flemish cap transit during summers in 1998 and 1999 (Figure 6.4). The geostrophic currents shown in the figure are the components perpendicular to the Flemish Cap transit. Colbourne (2000) found that during 1999 the offshore branch of the Labrador Current was narrower than usual (less than 100 km) and had higher current speeds than in 1998. In 1999, the southward component of the surface currents at the time of sampling was greater than approximately 20 cm/s. At the location of White Rose, the geostrophic currents were negligible.

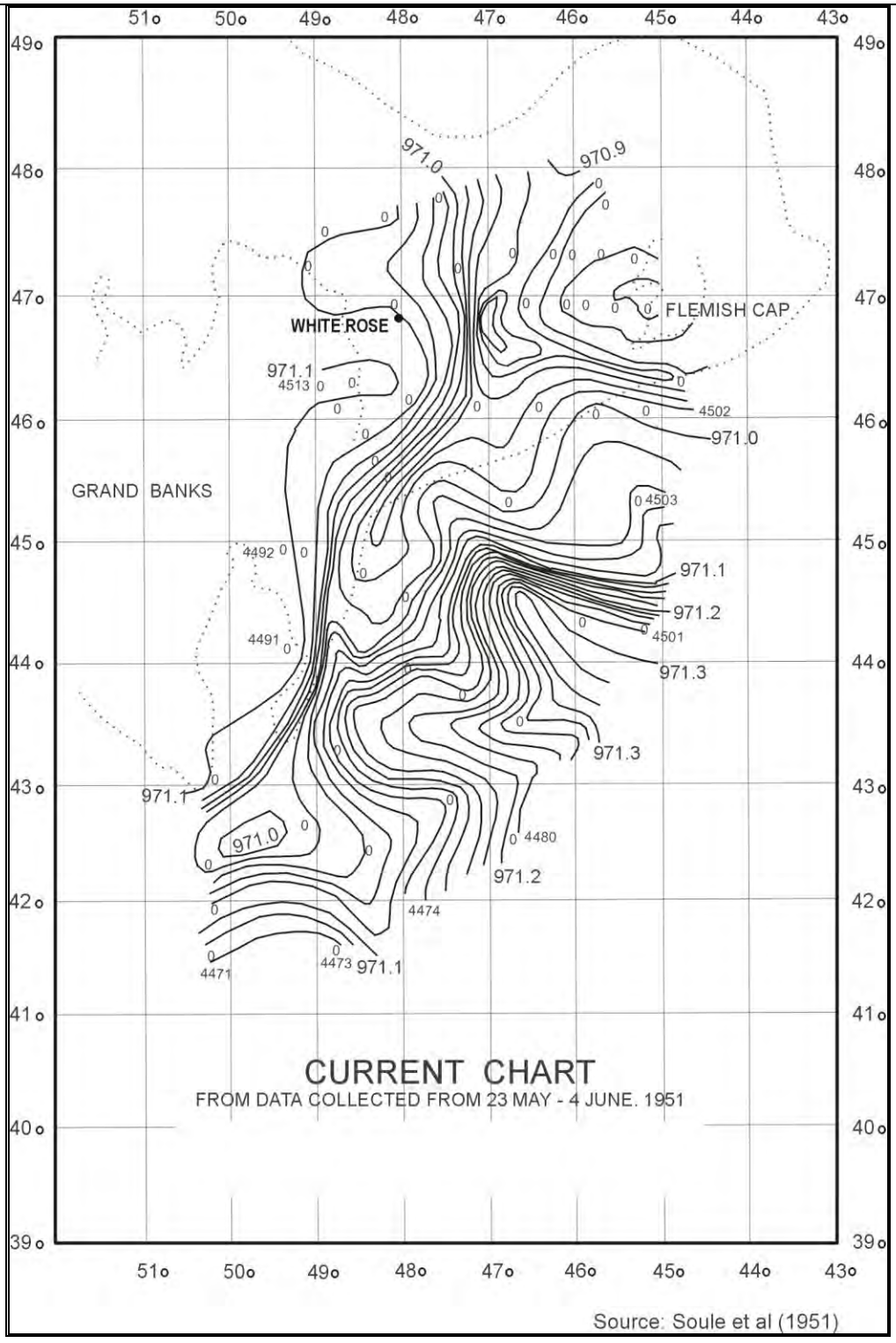

Figure 6.3 Dynamic Topography of the Sea Surface Relative to the 1,000 Decibar Surface Data Collected May 23 to June 4, 1951

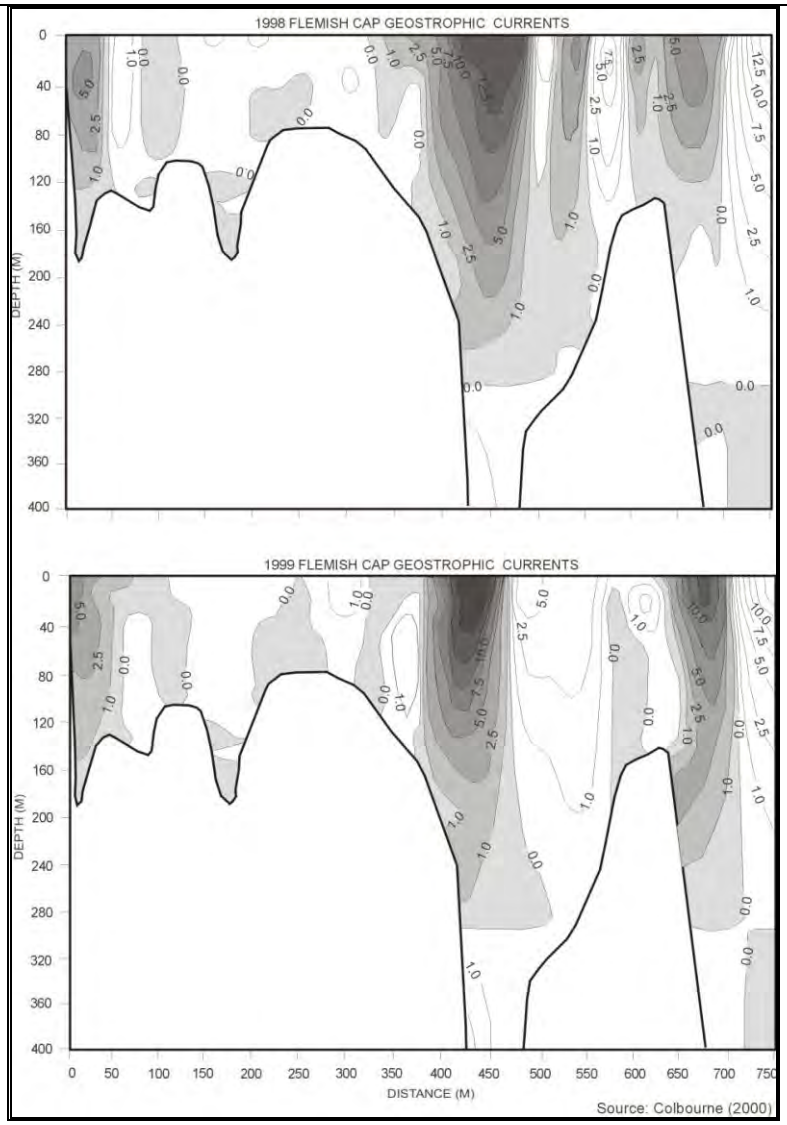

Figure 6.4 A Vertical Cross-Section of the Geostrophic Currents (cm/s) along the Standard Flemish Cap Transect for the Summer of 1998 and 1999

Note: Negative Southward Values are Shaded
Source: Colbourne (2000)

6.2.2 Surface Circulation from Drifter Buoys

During the last 25 years, satellite-tracked drifting buoys have been deployed in the Labrador Current to measure Lagrangian surface currents. The IIP has been operating a drifting buoy program since 1976 during the spring iceberg season. Additional surface drifters have been deployed by the Bedford Institute of Oceanography (Petrie and Isenor, 1984; Petrie and Warnell, 1988), and by the Northwest Atlantic Research Centre in support of northern cod research (Pepin and Helbig, 1997). A composite of 144 drifter tracks was compiled by Helbig and Brett (1995). The drifter track positions and their calculated mean velocity vectors are shown in Figure 6.5. Surface currents derived by

Murphy et al. (1991) and updated by Yao et al. (1992) are presented in Figure 6.6. These surface currents were derived from the IIP‟s drifting buoy data between 1976 and 1989 (Murphy et al., 1991) and updated by Yao et al. (1992) using two more years of drifter data and some current meter data.

The IIP‟s near-surface current map was compared with some moored current measurements made between 1980 and 1993 (Narayanan et al., 1996). Narayanan et al. (1996) found that the measurements were generally consistent with the IIP gridded surface current field, except that the currents were considered to be overestimated in some locations. This data set is periodically revised, as new observations become available, and is still the best source of surface current data available for the Grand Banks and surrounding regions.

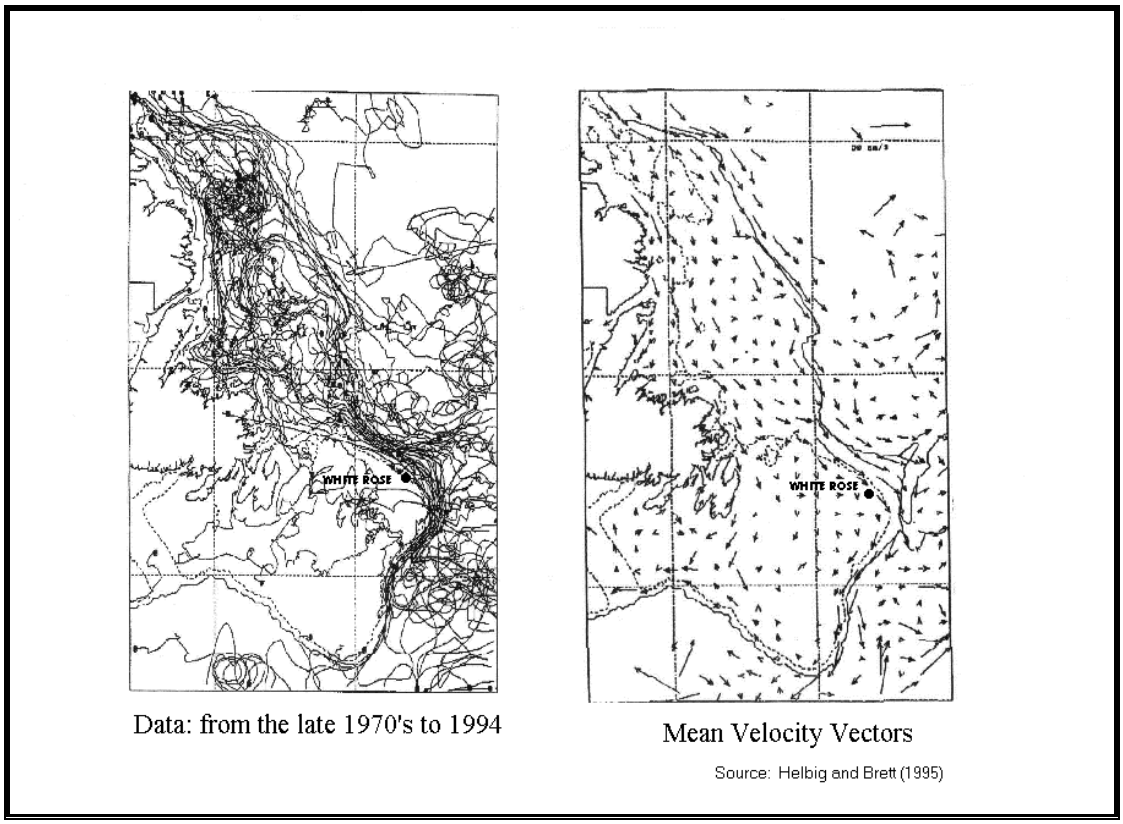

Figure 6.5 Computed Currents from Drifting Buoy Data

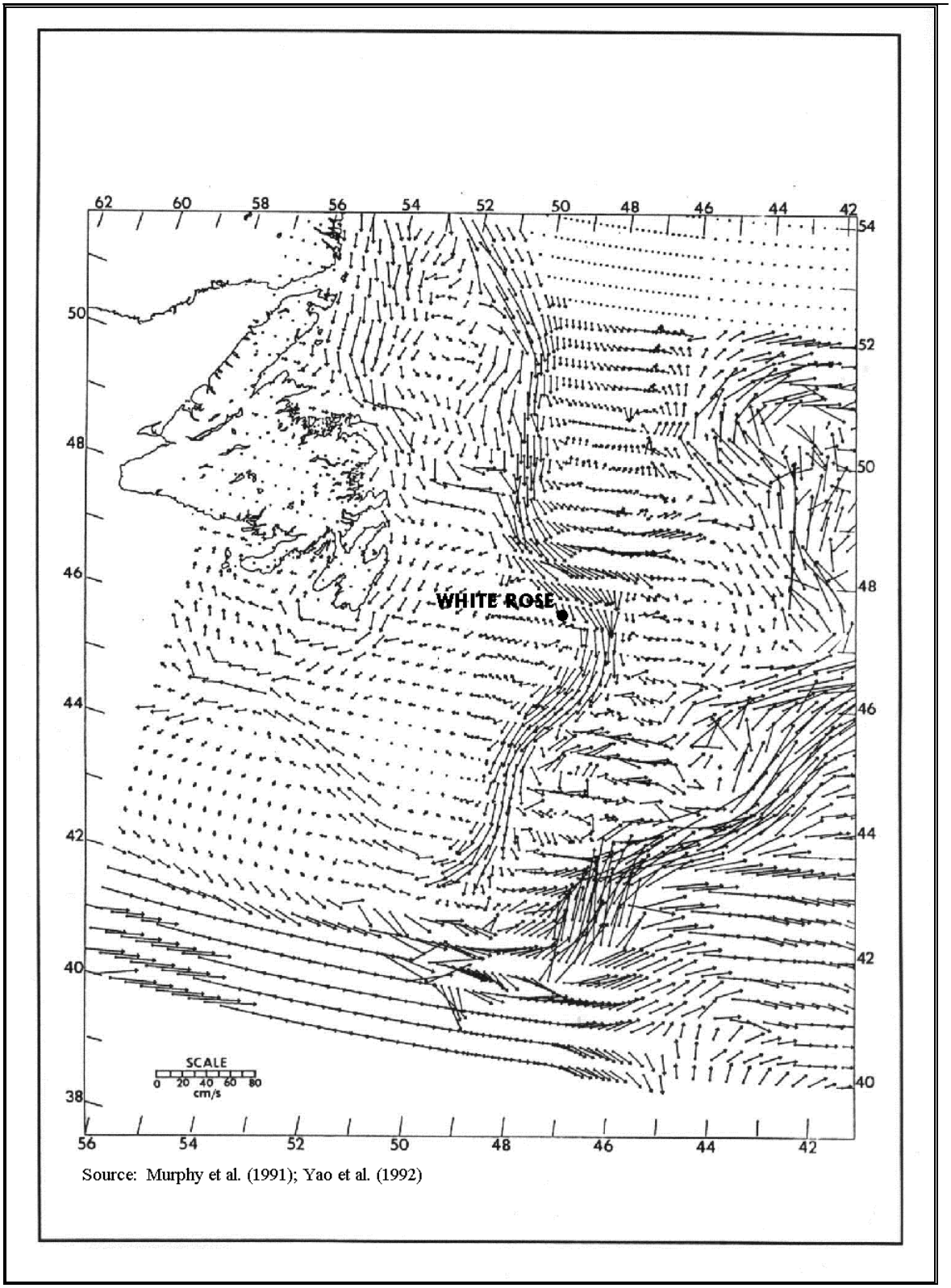

Figure 6.6 Composite Map of Mean Near-Surface Currents

6.2.3 Numerical Models

The results of numerical models have also contributed to the knowledge of the circulation on the Grand Banks. The numerical model developed by Greenberg and Petrie (1988) produced a detailed, high-resolution presentation of the barotrophic (vertically, uniform currents) mean circulation on the Grand Banks and surrounding areas. The 1988 model was a first step in modeling the mean circulation in the Newfoundland Shelf region and did not take into account the effects of stratification in the water column and the effects of wind stress, both important driving forces on the Newfoundland Shelf. The barotrophic model was driven by a sea surface slope at a northern boundary across Hamilton Bank and adjusted to give a specified inflow over different parts of the shelf and/or the shelf edge. A map of the currents on the Newfoundland Shelf, as calculated from the Greenberg and Petrie model is presented in Figure 6.7. The major characteristics of the circulation produced by their model were: 1) a strong topographical steering of the currents; 2) the splitting of the Labrador Current into two branches north of Flemish Pass; and 3) northwestward movement of water over the eastern part of the Grand Banks.

Narayanan et al. (1996) compared the current meter data sets obtained between 1980 and 1993 with the barotrophic model results of Greenberg and Petrie (1988), and found that the model predictions were more or less in agreement with observations made at the comparison mooring sites. The model underestimated the magnitude of the offshore branch of the Labrador Current along the northeast Newfoundland Shelf. It did not duplicate the clockwise circulation on Flemish Cap as indicated by drifter data (Ross, 1980) or the eddy like features in the slope region south of Flemish Pass. The intersection between the Labrador Current and the North Atlantic Current was not taken into consideration in the model. Since the development of the 1988 barotrophic model, modeling of currents on the Grand Banks has been an on-going process by Fisheries and Oceans Canada.

Hukuda et al. (1989) developed a three-dimensional model to estimate the mass exchange at different depths. Similar to the Greenberg and Petrie model (1988), their model was driven by specifying the sea level along a northern boundary. Similarly, their model reproduced the circulation pattern found by Greenberg and Petrie (1988). They examined the onshore-offshore mass exchange over the southeastern edge of the Grand Banks and found that the southward flowing Labrador Current along the shelf break leads to an onshore flux in the upper part of the water column and an offshore flux in the bottom Ekman layer.

Sheng and Thompson (1995) developed a model by using currents calculated from vertical density profiles across the northern boundary as input to their model. The currents, initially computed from vertical density profiles relative to fixed depth levels, were compared with observations. From the comparisons, optimal inflow boundary conditions were estimated, and used to drive the northern boundary of a limited area numerical model. This model agreed well with the Greenberg and Petrie (1988) model results and gave a high-resolution presentation of the strong topographically influenced flows of the inner and outer branches of the Labrador Current, and the anticyclonic (clockwise) gyre centered on the Flemish Cap.

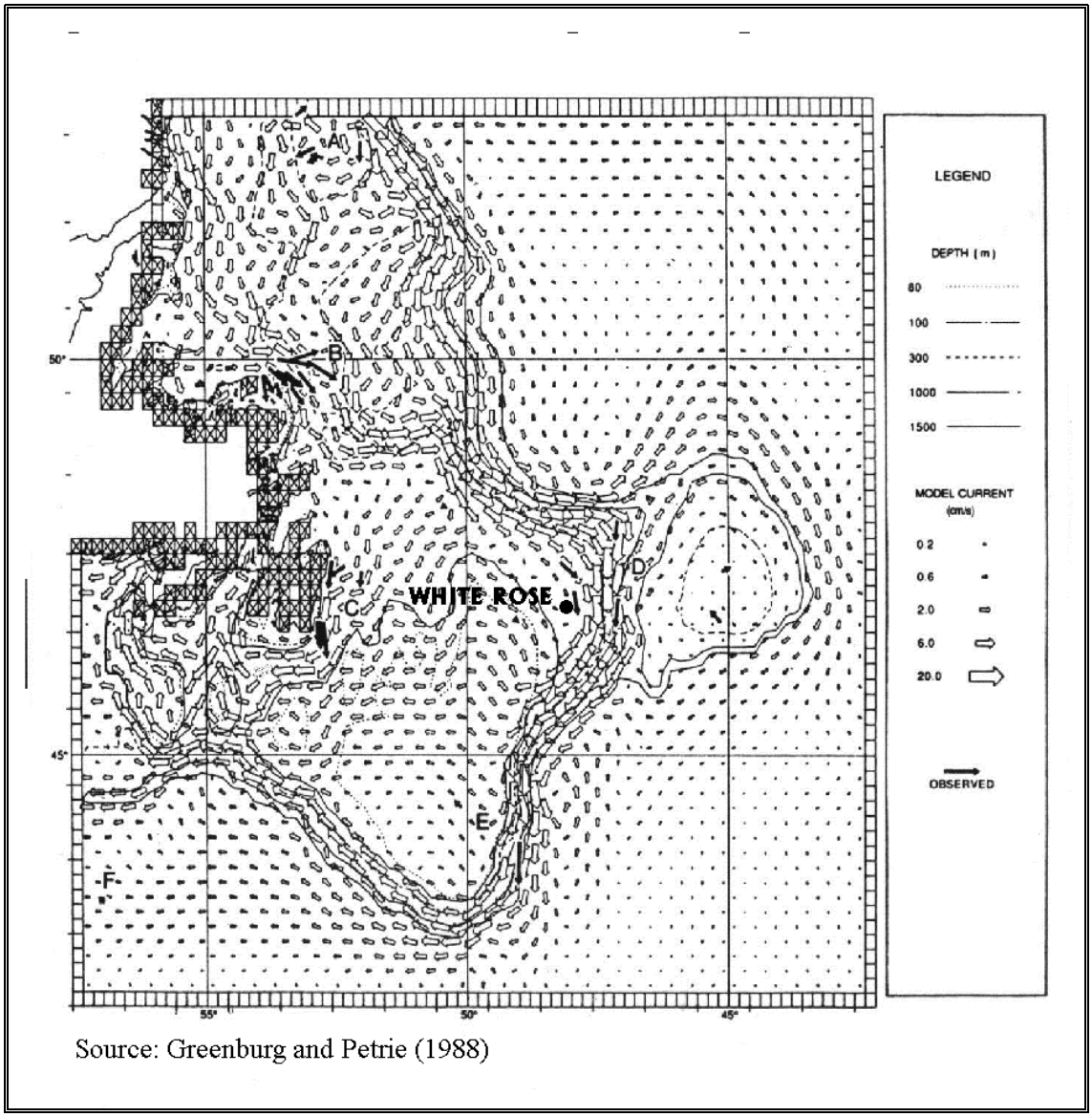

Source: Greenburg and Petrie (1988)

Figure 6.7 Model-Derived Depth-Averaged Currents

A recent modeling study by Han and Wang (2006), found that the circulation over the Newfoundland Shelf and its northeast slope is dominated by equator-ward flows associated with the inshore and offshore Labrador Current. Their model study supported a significant seasonal cycle in the current regime with strong flows during the fall/winter and weak flows in spring/summer. This is demonstrated in Figure 6.8 which shows the model currents near the surface (30 m) and near the bottom (20 m) above the ocean floor, for the months of May and November.

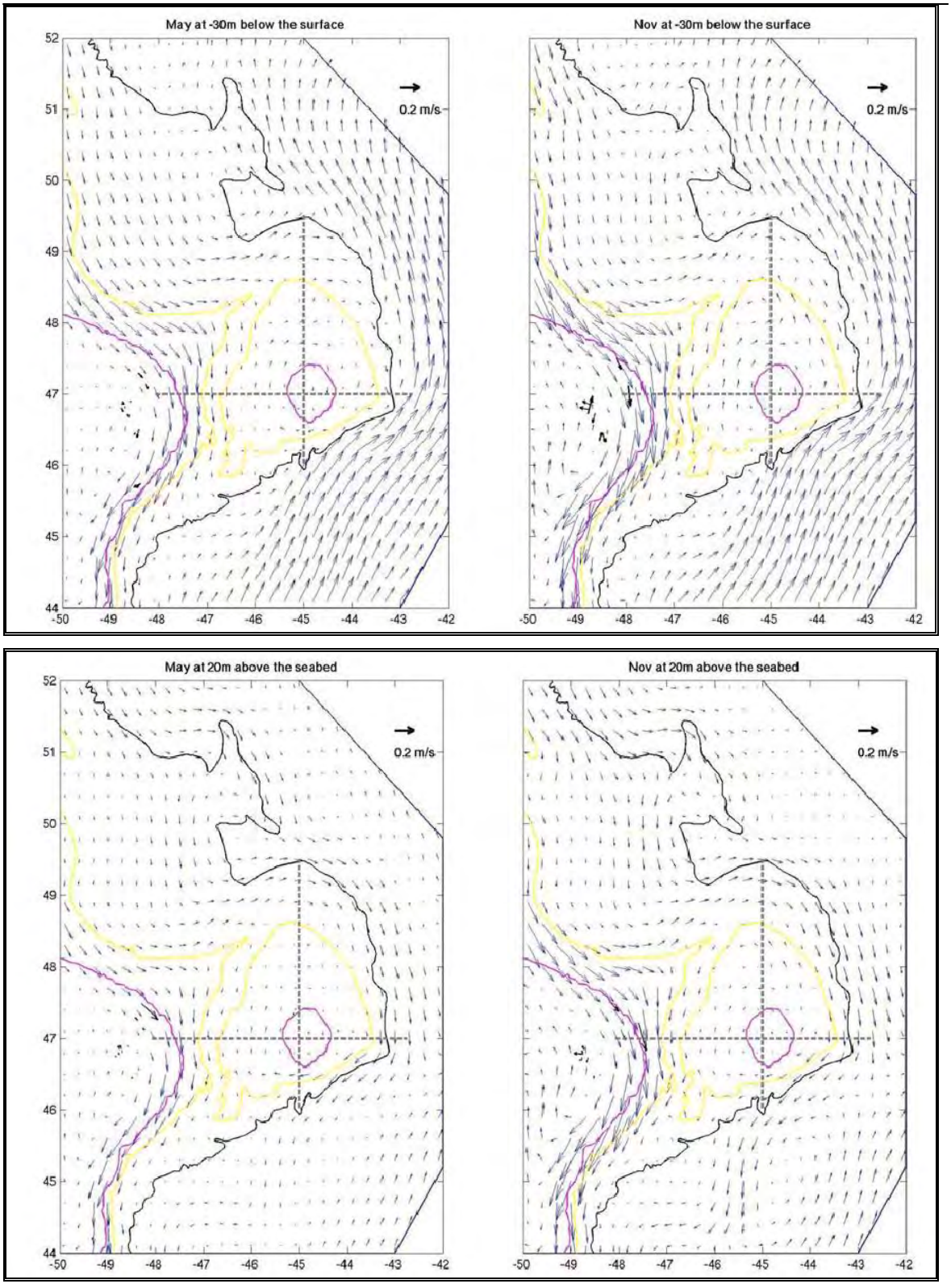

Figure 6.8 Modeled Currents at 30 m below the Surface (left) and 20 m above the Seabed (right) in May (above) and November (below). From Han and Wang (2006)

Table 6.1 Near-Surface Currents (Intermittent Data) at White Rose

Well Site	Period	Max. Speed (cm/s)	Mean Speed (cm/s)	Mean Velocity (cm/s)	Direction
Gros Morne C-17	Sept 4 – Sept 18, 2002	41.0	14.7	6.9	South
Trepassey J-91	Jul25 – Aug 27, 2002	33.0	11.7	6.8	South
White Rose H-20	May 15 – Jul 8, 2000	67.0	12.5	0.5	Southeast
White Rose N-30	Aug 19 – Sept 29, 1999	89.9	27.0	5.0	Southeast
White Rose A-17	Jun 23 – Aug 6, 1999	42.1	11.4	8.4	Northeast
White Rose L-08	Mar 31 – Jun 22, 1999	45.7	10.4	2.7	Northwest
White Rose E-09	May 14 – Jul 5, 1988	45.2	15.7	7.5	Southeast
White Rose J-49	Aug 10 – Nov 19, 1985	61.7	14.7	4.9	South
White Rose L-61	Dec 19 – Feb 15, 1986	36.0	13.0	6.4	Northeast
White Rose N-22	Jul 5 – Oct 16, 1984	82.0	19.6	19.0	Southwest
Trave E-87	Nov 15 – Jan 14, 1984	55.0	19.5	8.1	South
Trave E-87	Feb 1 – Mar 11, 1984	40.0	16.9	11.1	Southeast

6.3 Moored Current Meter Data

In the White Rose area, moored current meter data was collected over short intervals (few months per site) during the early exploration period between 1984 and 1988 for the period between 1999 and 2002. These data sets and statistical information are listed in Tables 6.1 to 6.3. At mid-depth and near-bottom, continuous data exists from August 2007 to December 2010. Since January 2008, there has been continuous near-surface current data measured at White Rose. There is current data for White Rose available for the period 2005 to August 2007, but it could not be used due to contamination from instrument movements. The ADCP was mounted looking downward from a buoy on the surface such that the measurements are a combination of the currents and the movements of the buoy from wave action.

Table 6.2 Currents (Intermittent Data) at Mid-Depth at White Rose

Well Site	Period	Max. Speed (cm/s)	Mean Speed (cm/s)	Mean Velocity (cm/s)	Direction
Gros Morne C-17	Sep 4 – Sep 18, 2002	24.0	11.4	2.6	South
Trepassey J-91	Jul 25 – Aug 27, 2002	31.0	9.0	3.0	South
White Rose H-20	May 15 – Jull 8, 2000	25.0	9.3	0.5	South
White Rose N-30	Aug 19 – Oct 14, 1999	40.8	11.2	10.6	Northeast
White Rose L-08	Mar 31 – Jun 22, 1999	29.4	12.1	3.8	South
White Rose A-90	Jul 13 – Aug 11, 1988	24.7	8.9	3.4	Southeast
White Rose E-09	May 14 – Jul 5, 1988	39.0	12.3	5.9	Southeast
White Rose E-09	Jan 19 – Feb 20, 1988	35.0	10.4	3.5	Southeast
Whites Rose E-09	Sept 01 – Oct 22, 1987	32.6	10.0	9.0	Southwest
White Rose J-49	Aug 10 – Nov 19, 1985	43.7	11.8	2.6	Southeast
White Rose N-22	Jul 5 – Nov 10, 1984	31.0	9.6	1.8	Southeast
Trave E-87	Feb 1 – Mar 12, 1984	31.0	12.2	7.5	South
Trave E-87	Nov 14 – Jan 15, 1984	46.0	13.7	5.0	Southeast

Table 6.3 Currents (Intermittent Data) Near-Bottom at White Rose

Well Site	Period	Max. Speed (cm/s)	Mean Speed (cm/s)	Mean Velocity (cm/s)	Direction
Gros Morn C-17	Sep 4 – Sep 18, 2002	30.0	10.2	1.2	Southwest
Trepassey J-91	Jul 25 – Aug 27, 2002	30.0	8.7	1.3	South
White Rose H-20	May 11 – Jul 8, 2000	25.0	9.1	1.8	Southeast
White Rose L-08	Mar 31 – Jun 22, 1999	27.6	9.5	2.8	Southeast
White Rose A-90	Jul 13 – Aug 11, 1988	25.2	8.9	4.1	Southeast
White Rose E-09	May 14 – Jul 5, 1988	32.6	10.8	3.7	Southeast
White Rose E-09	Jan 19 – Feb 20, 1988	34.5	13.0	3.7	Southeast
White Rose E-09	Sep 1 – Nov 19, 1987	36.2	10.9	2.7	Southeast
White Rose J-49	Aug 10 – Nov 19, 1985	50.6	10.7	2.0	Southeast
White Rose N-22	Jul 5 – Nov 10, 1984	18.0	5.9	-	No Direction
Trave E-87	Nov 14 – Jan 21, 1984	39.0	13.1	6.6	Southeast
Trave E-87	Feb 1 – Mar 11, 1984	32.0	10.1	5.9	Southeast

Statistics from the continuous data since August 2007 are listed in Tables 6.4 to 6.6. Current measurements at White Rose are now being measured on an-ongoing basis. Since January 2008, measurements are available in 4 m bins throughout the water column. The annual environmental data reports contain the processed data for the three traditional mooring depths. Table 6.1 to 6.6 lists the data collection periods, the maximum speeds, means speeds, and mean velocities. At 20 m (near surface), the maximum speed that was measured was 89.9 cm/s in September 1999 at White Rose N-30 (Table 6.1). During the same event, current speeds of 40.8 cm/s were measured at mid-depth. These strong currents were due to the passage of Hurricane Gert.

At mid depth, the maximum current speed of 55.6 cm/s (Table 6.5) occurred in December 2007 during a winter storm. During the same event the currents near bottom were 36.1 cm/s. On this occasion there were no near-surface current measurements because a 300 kHz ADCP was mounted on the bottom looking upward to test the range of the current meter configured in broadband mode. The current meter failed to measure the currents in the upper one-third of the water column.

The maximum speed near-bottom occurred in November 1985 at White Rose J-49 with a speed of 50.6 cm/s (Table 6.3). During the same event near-surface speed was 61.7 cm/s.

Table 6.4 Near-Surface Currents (Continuous Data) at White Rose (Jan 2008 -Dec 2010)

Year	Max Speed (cm/s)	Mean Speed (cm/s)	Mean Velocity (cm/s)	Direction
2008	60.7	15.3	3.2	South
2009	56.0	14.4	2.9	South
2010	52.8	13.5	1.9	Southwest

Table 6.5 Currents (Continuous Data) Mid-depth at White Rose (Aug 2007 - Dec 2010)

Year	Max Speed (cm/s)	Mean Speed (cm/s)	Mean Velocity (cm/s)	Direction
2007	55.6	13.4	1.7	Southeast
2008	39.3	10.7	1.5	Southeast
2009	37.8	11.8	1.6	South
2010	40.5	11.1	0.9	Southwest

Table 6.6 Currents (Continuous Data) Near-Bottom at White Rose (Aug 2007 - Dec 2010)

Year	Max Speed (cm/s)	Mean Speed (cm/s)	Mean Velocity (cm/s)	Direction
2007	36.1	11.9	2.6	Southeast
2008	36.4	11.7	1.5	Southeast
2009	34.5	11.4	1.6	Southeast
2010	41.6	11.2	1.1	Southeast

6.4 Current Variability

The most notable characteristic of the currents at White Rose is the amount of variability in the current flow. The residual flow over a year time period is in a southerly direction, anywhere from southwest to southeast. This is illustrated in Figure 6.9 which shows the progressive vector diagrams for 2010 at depths of 20 m, 64 m, and 112 m. The current at White Rose can flow in any direction for days at a time. This high degree of variability is illustrated in Figure 6.10 which presents progressive vector diagrams for February 2010 for the same three depths. The current direction during any month is also variable from year to year as illustrated in Figure 6.11 which shows the progressive vector diagrams at 20 m for the month of July for years 2008 to 2010.

There are many contributing factors to the variability in current flow at White Rose. The largest contributing factor is the sea surface slope produced by atmospheric pressure systems as they pass through the area. Other contributing factors to the variability at White Rose include the surface wind stress, tidal forces, buoyancy fluxes, and the large-scale circulation and interactions associated with the Labrador Current and the North Atlantic Current. Wind stress influences the flow in two time scales; synoptic periods of the order of 2 to 10 days assorted with severe storms, and the inertial period of 16.4 hours. Wind stress provides a major driving force of currents on the Continental Shelf, with a distinct annual cycle of comparatively strong winds in fall and winter, and weaker more variable winds in spring and summer.

An analysis of the measured currents prior to 2007 showed that tides accounted for approximately 20% of the variability at White Rose. Buoyancy fluxes associated with large freshwater inputs produce strong density gradients leading to pressure gradients that drive along-shore currents. The outer branch of the Labrador Current exhibits a distinct seasonal variation in flow speeds (Lazier and Wright, 1993) in which the mean flows from September to October are nearly twice as large as the mean flows in March and

April. The large variation in density on the shelf results from increased freshwater input from melting ice and freshwater run-off taking place upstream in the spring and summer.

Offshore eddies and rings have an important influence on the circulation over the Continental Slope. Interactions between the Labrador Current and eddies of the North Atlantic Current system will influence the flow along the southeastern section of the Grand Banks. When a Gulf Stream ring encounters a sloping bottom, it radiates low-frequency energy in the form of topographic Rossby waves with characteristic periods of 10 to 30 days (Louis et al., 1982). On approach to the shelf, the wave energy is strongly reflected by the Continental Slope and scattered into baroclinic modes trapped to the shelf edge such that little energy penetrates onto the shelf (Smith and Schwing, 1991). However, the resulting redistribution of the density field may have an influence on the currents near the shelf edge. Voorheis et al. (1973) have identified over 30 eddies on the central part of the Continental Slope along the eastern margin of the Grand Banks from an analysis of historical oceanographic data sets going back to the 1920s. The eddies were mostly counterclockwise, with typical speed of 25 to 30 cm/s and with an average size of 102 km in diameter. Meanders had typical lengths of 275 km in the along-stream direction, and about half this distance in the cross-stream direction.

White Rose is situated far enough north on the Grand Banks to avoid any direct effects from the eddies and meanders on the southern part of the banks. The years when the northern boundary of the North Atlantic Current is further north than usual there is a potential for some indirect effects.

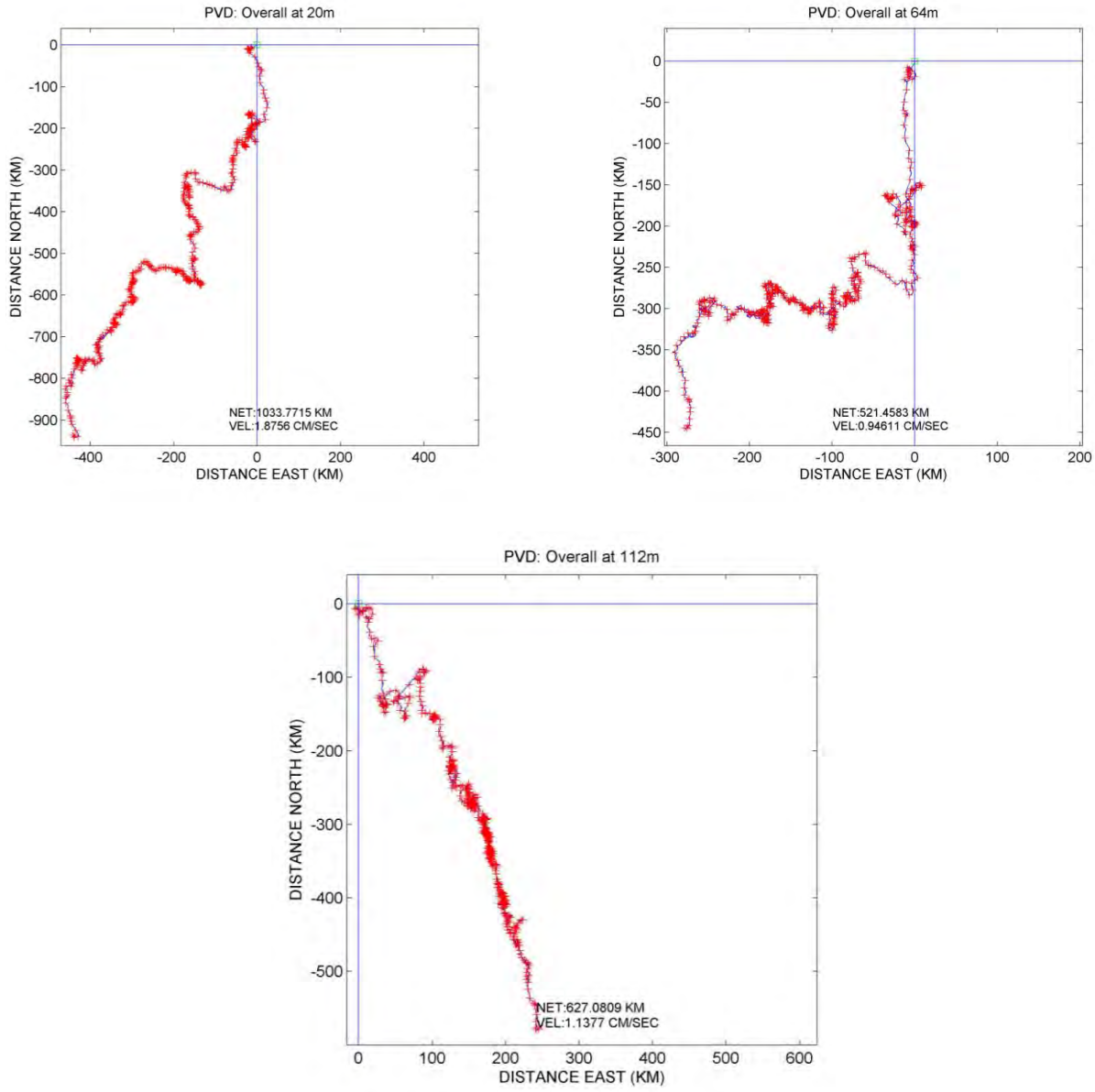

Figure 6.9 Annual Progressive Vector Diagrams for 2010 at depths of 20m, 64 m, and 112 m at White Rose

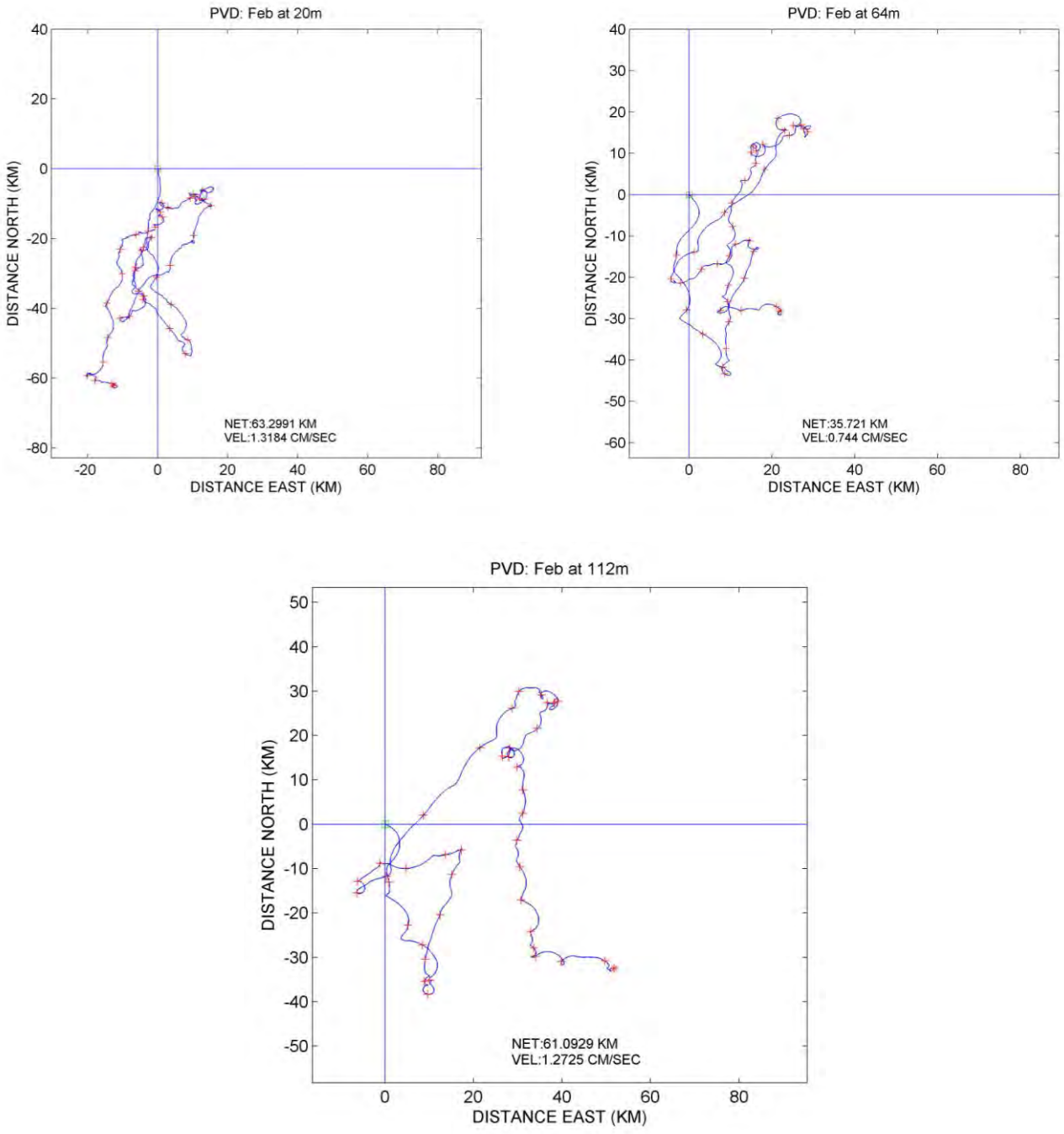

Figure 6.10 Progressive Vector Diagrams for February 2010 at depths of 20 m, 64 m, and 112 m at White Rose

2008

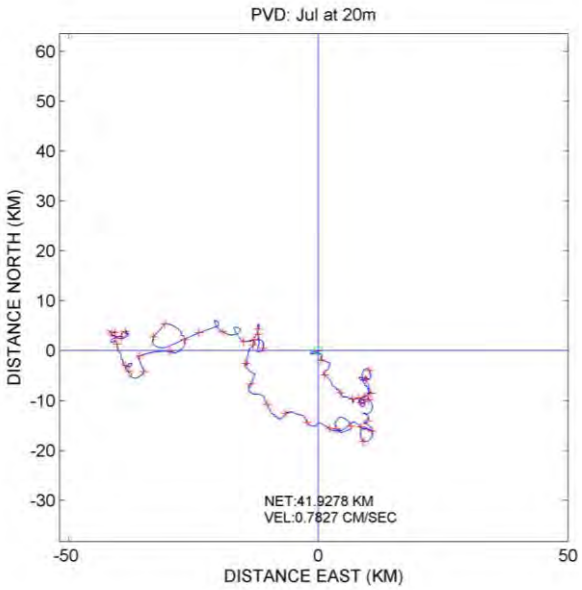

2009

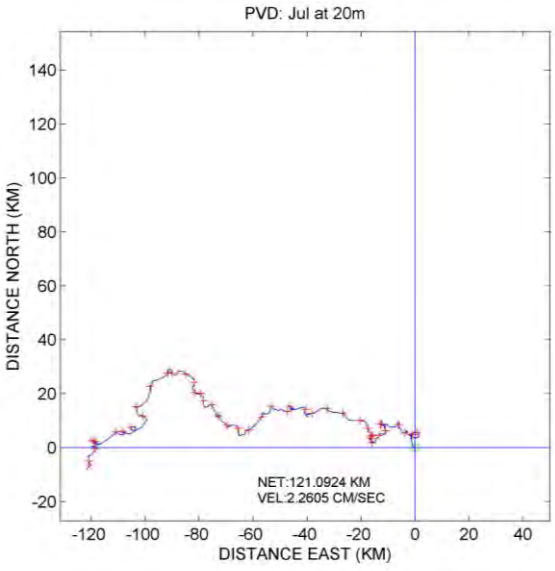

2010

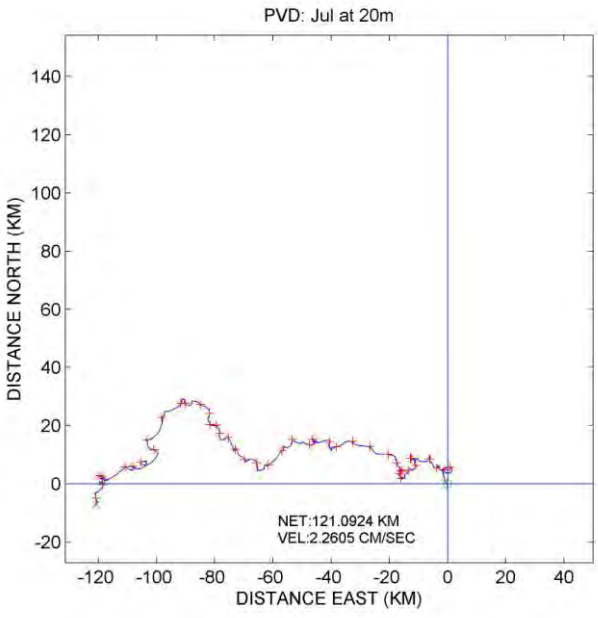

Figure 6.11 Progressive Vector Diagrams for July at 20 m, for years 2008 to 2010 at White Rose

6.5 Tidal Current

The major tidal constituents for the currents at White Rose are shown in Table 6.7. The tidal constituents were resolved from the current data collected at White Rose for years 2008 to 2010, using the standard analysis software programs (Foreman, 1978) used by Canadian oceanographers. M_2 and S_2 are the major semidiurnal (highs and lows twice daily) constituents and O_1 and K_1 are the major diurinal (highs and lows once daily) constituents. At White Rose, M_2 is the largest contributor to the tidal current followed by K_2, O_1, and S_2, respectively (Table 6.7). Since the tidal ellipses for all constituents are close to circular, the constituents can be added together to obtain the magnitude of the tidal current. Using constituent values in Table 6.7, the tidal current near-surface, mid-depth and near bottom are 12.3 cm/s, 14.1 cm/s and 14.7 cm/s, respectively.

Table 6.7 Tidal Constituents at White Rose resolved from Measured Currents 2008 to 2009

Depth	M_2	S_2	K_1	O_1
Near-Surface (20 m)	4.6	1.7	3.5	2.5
Mid-Depth	5.1	2.1	4.0	2.9
Near-Bottom	5.3	2.2	4.2	3.0

6.6 Wind Driven Currents

Wind driven currents are a dominant feature of the circulation on the Grand Banks. The episodes of stronger currents are usually associated with the passage of storms; hence currents tend to be stronger during fall and winter. Wind blowing over the ocean surface produces two different types of responses in ocean currents. The direct wind driven component in the surface waters has a magnitude of approximately 3% of the wind speed and in a direction of 20° to 45° to the right of the driving force of the wind. This wind driven current has a synoptic period of 2 to 10 days. The other wind effect is an ocean response through strong inertial motions to the passage of storms. Due to the Earth"s rotation, the current is always in a clockwise direction in the Northern Hemisphere. Over the northern Grand Banks, the inertial period is approximately 16.5 hours. The strong 80 cm/s currents found in September at White Rose in the near surface waters was the result of the passage of an autumn storm at a time when the water was still strongly stratified.

6.7 Currents near the Seabed

Near bottom currents have been measured at a height of 10 m above the seabed for consistency at all development and exploration sites on the Grand Banks. In spring 2002, currents were measured at a height of 3 m above the seabed in order to get current information in the bottom boundary layer at White Rose. The objective was to establish whether there was a difference in the current speed at 3 m above the seabed as compared with 10 m above the seabed. Two InterOcean S4 vector averaging current meters were moored close to White Rose L-08 at location 46°47'42"N; 48°01'33"W. The instrument at 3 m above the sea floor collected data between April 15 and August 22, 2002. The

other instrument was moored at 10 m above the sea floor collecting data between April 15 and June 18, 2002.

The study showed that the currents were slightly lower at 3 m above the seabed than at 10 m above the seabed. The statistics are presented in Table 6.8. A sample of a time series of the data is presented in Figure 6.12. Figure 6.12 show that the currents at 3 m above the bottom followed the current pattern at 10 m remarkably well. Overall, the mean difference between the two values was 2.2 cm/s.

Table 6.8 3m above the Seabed

Month	Mean Speed (cm/s)	Stand Deviation	Maximum Speed (cm/s)
April	9.30	4.66	23.60
May	6.81	3.39	19.32
June	6.22	3.19	22.11

Table 6.9 10 m above the Seabed

Month	Mean Speed (cm/s)	Stand Deviation	Maximum Speed (cm/s)
April	11.48	5.85	31.83
May	8.98	4.76	29.41
June	8.58	4.90	25.29

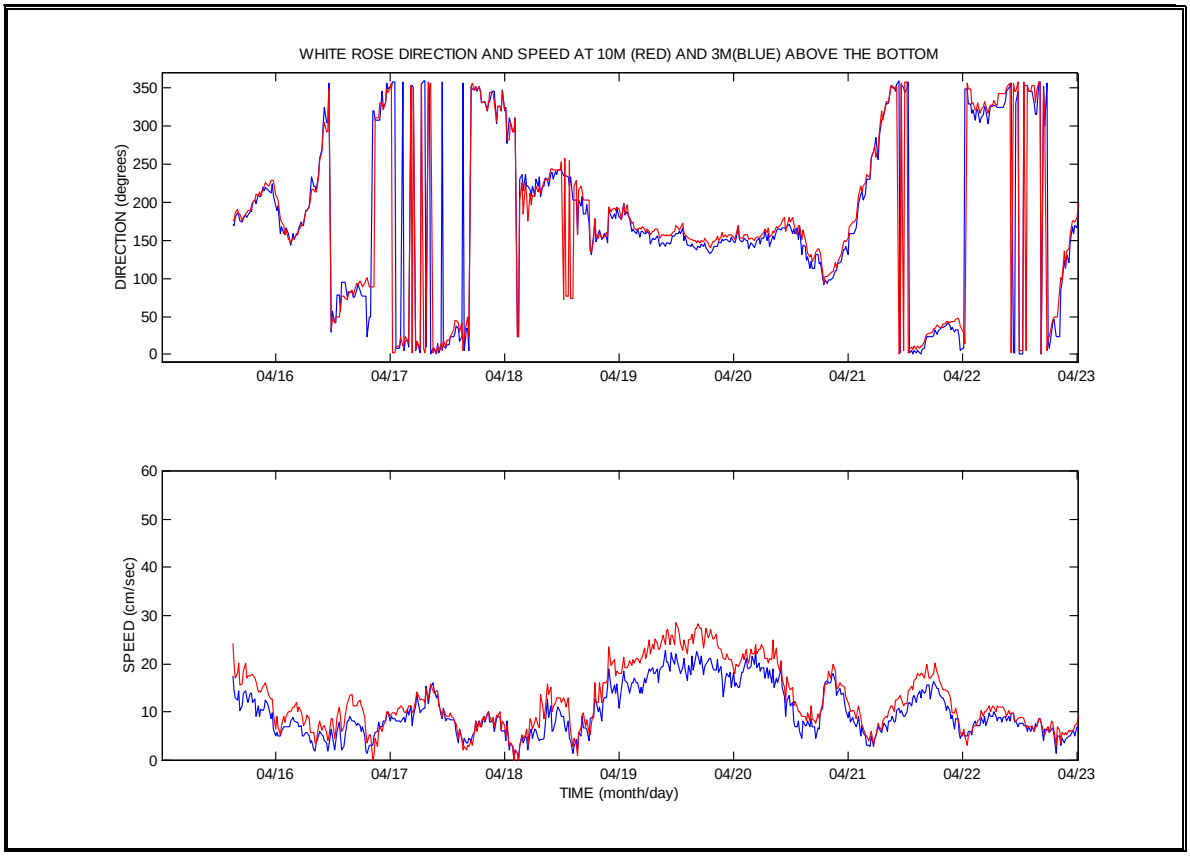

Figure 6.12 Comparison of Current Data between 3 m and 10 m above the Seabed

There was a strong signal between the higher currents at both 10 m and 3 m above the bottom, and the passage of weather systems. There was no direct relationship between the measured winds on the Grand banks and the current velocity near the bottom. For instance the strongest currents occurred on April 26 when both the waves and winds were low on the Grand Banks. Equivalent peaks in current occurred on May 4 and May 6. On May 4 there were high winds and on May 6 there was no wind. On May 6 there was a low pressure system with winds of 45 knots (23.15 m/s) over Newfoundland. On May 4, White Rose was situated between a high pressure system offshore Newfoundland and a low pressure system offshore Labrador. This information indicates that the higher currents measured near the bottom are directly related to the atmospheric pressure gradients over a larger area and not to the local weather conditions.

Upon examination of these phenomena, it was noted that every peak in the currents during the measurement period could be related to the atmospheric pressure gradients over the wider area. This indicates that the higher bottom currents are barotropic and related to the sea surface gradient.

The most prominent event took place on April 19 and 20. During this occasion there was an intense low pressure system in the North Atlantic, south of Greenland with a low pressure of 959 millibars. The winds offshore were in the order of 40 knots (20.56 m/s). There was also a high pressure system offshore Nova Scotia. During this occasion there

were high winds, 8 m waves, and a strong atmospheric pressure gradient. During this occasion the peak in bottom currents extended over a two day period. The current direction was southerly for the whole period with no tidal influence evident, due to the stronger pressure gradient force.

6.7.1 Differences in Current Speeds between the Two Water Depths

Using a second order polynomial regression, a fit was calculated to estimate the relationship between the difference in speed values between the two levels and the speed at 10 m above the bottom. Figure 6.13 shows the scatter plot with a trend line of the value pairs‟ distribution. The speed at 10 m is shown in the X axis. The Y axis shows the corresponding differences of speed (speed at 10 m to speed at 3 m).

The plot shows an unmistakable tendency to larger speed differences for higher 10 m speed values. The time series plots indicate that this relationship is mainly due to the tides being attenuated towards the bottom. The negative differences are occurring when the speeds at 10 m are negligible together with minor tidal phase shifts between the currents at the two levels.

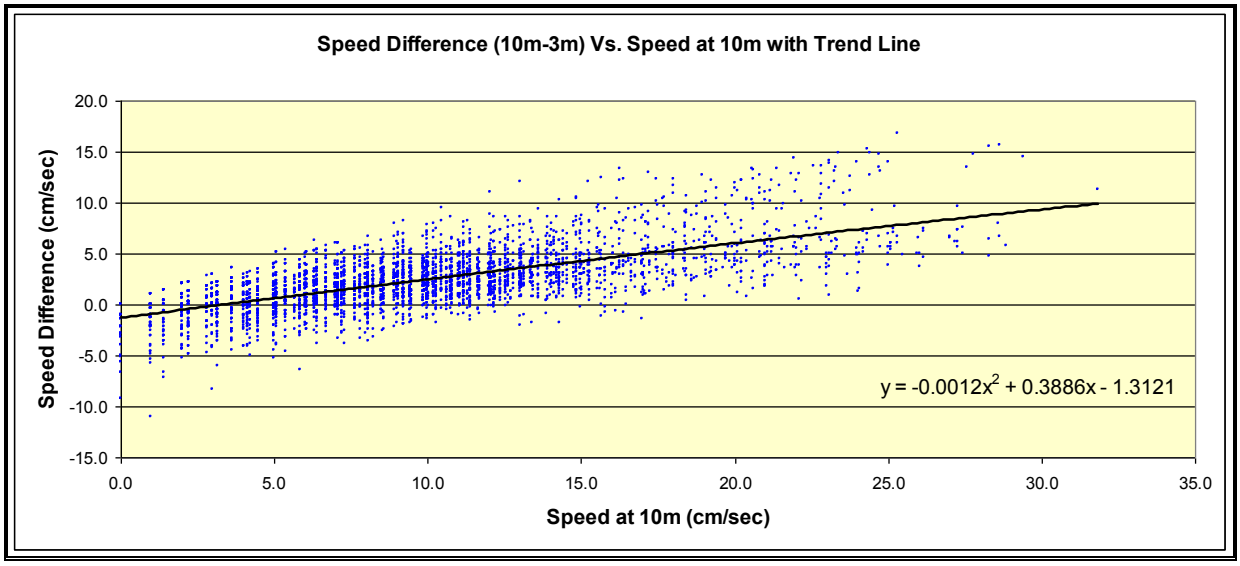

Figure 6.13 Speed Difference (10 m - 3 m) versus Speed at 10 m

6.7.2 Current Speed Profile above the Seabed

The monthly averaged values for the speed at 3 m above the bottom appear to be in reasonable agreement with the Prandtl's One-Seventh-Power Law for the velocity distribution in turbulent flows; however, the data obtained is not sufficient for coming to definite conclusions about the vertical structure of the speed in the immediate vicinity of the ocean floor below 3 m.

Figure 6.14 shows the theoretical one-seventh-power distribution together with the observed data calculated from the average speed at 10 m. For the classical problem of a turbulent flow in a pipe, the radius of the pipe was equaled to 10 m, thus assuming that at this level the friction with the bottom would be negligible. The blue line represents the theoretical decay of the current speed from its 10 m value according to the one-seventh-power law. The red star represents the overall averaged speed value for 3 m above the bottom and the green stars represent the monthly averaged values.

As can be appreciated in Figure 6.14, the overall average and almost all the monthly averages, fall below the theoretical one-seventh-power law curve for a distance of 3 m from the bottom. However in the month of April, the mean speed at this level is almost of the same magnitude as the average speed for 10 m and falls to the right of the theoretical curve.

To further investigate whether the one-seventh-power law holds for currents with speeds higher than the mean, a plot (Figure 6.15) was produced for the mean speed on April 19, and for maximum speeds on April 26 and May 6. In all three cases the speed at 3 m followed the one-seventh-power distribution.

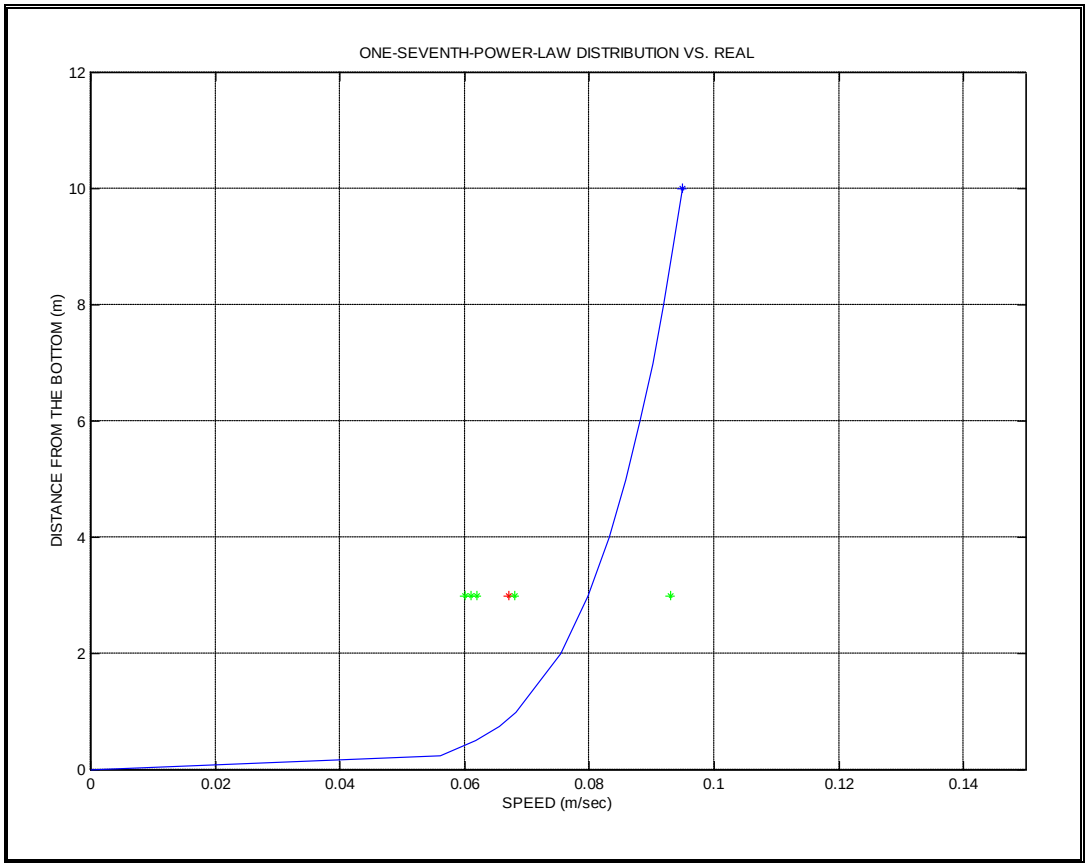

Figure 6.14 Vertical Distribution of Current Speed in Relation to the One-Seventh-Power Law

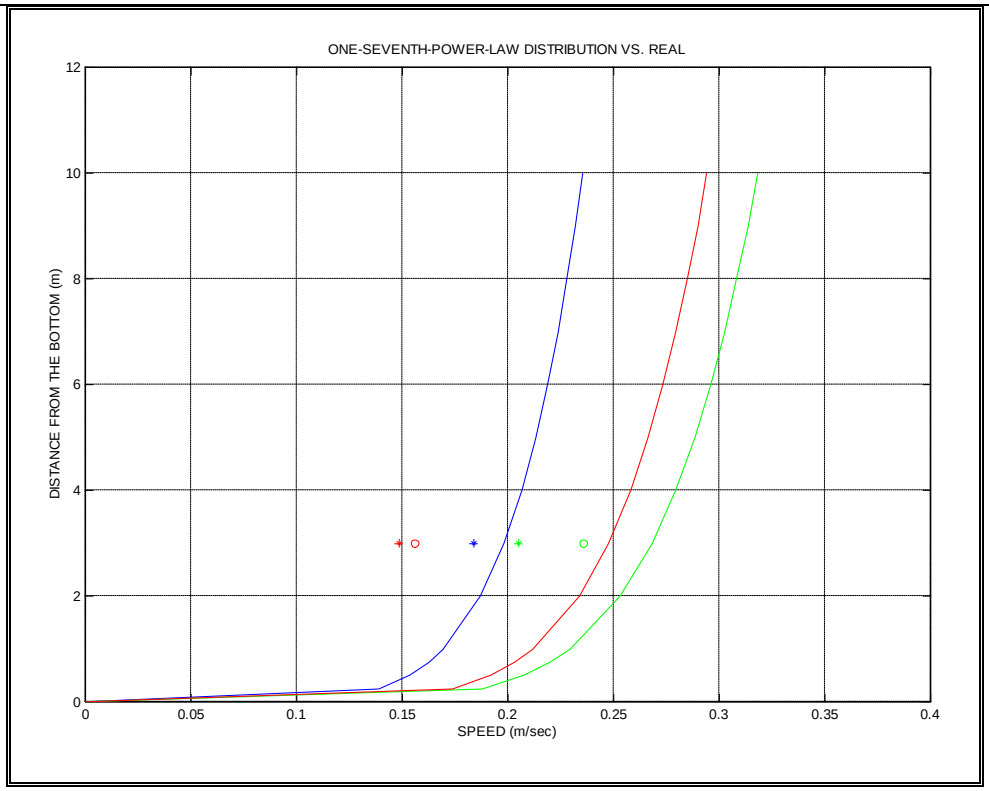

Figure 6.15 Vertical Distribution of Current Speed in Relation with Different One-Seventh-Power Law Distributions

Legend:

- One-seventh–power law decay from the average 10 m speed value for April 19.
- One-seventh–power law decay from the maximum 10 m speed value for April 26.
- One-seventh–power law decay from the maximum speed value for May 6.

Stars represent the speed value at 3 m at the moment of the maximum value at 10 m.

Circles represent the 3 m speed maximum closely related to the maximum at 10 m.

This maximum may be shifted in time from the maximum at 10 m.

6.7.3 Relationship between the Current at 3 m and 10 m above the Seabed

In order to look for the relationship between 3 m and 10 m, the daily maximum speed at 10 m was plotted against the daily maximum speed at 3 m. This scatter plot is shown in Figure 16. The regression curve fitted to the data, resulting in the following relationship:

$$Y = 0.0079X^2 + 0.2154X + 6.74$$

Where **Y** is the maximum daily current speed at 3 m and **X** is the maximum daily current speed at 10 m.

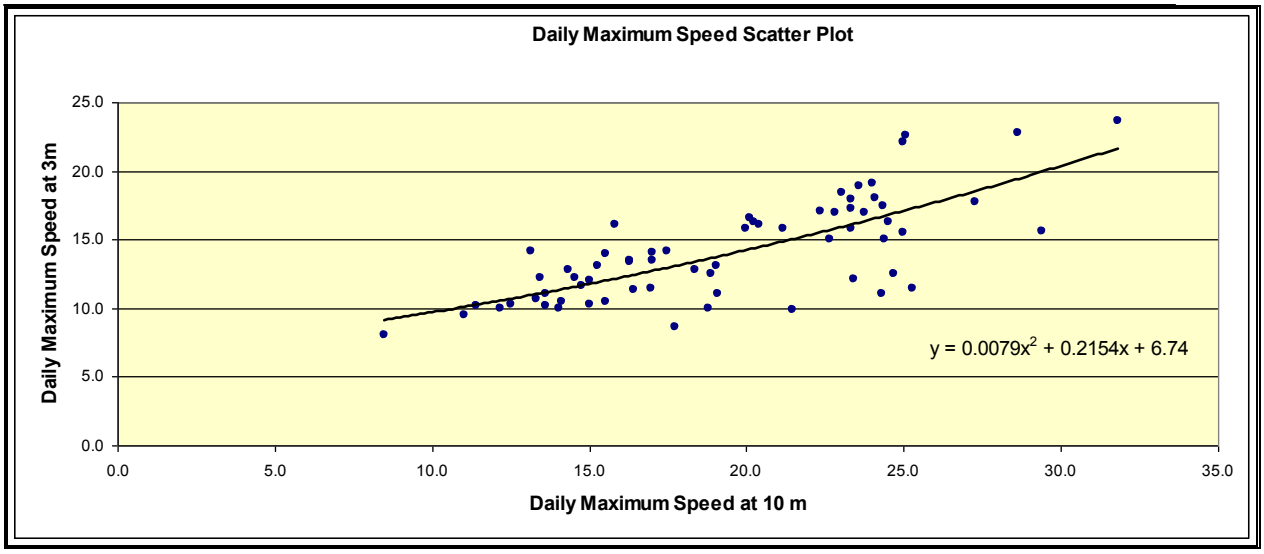

Figure 6.16 Daily Maximum Speed at 10 m versus 3 m above the Seabed

6.8 Tsunami Current

Tsunamis are long, surface gravity waves in the ocean produced by earthquakes, submarine landslides and volcanic island explosions. Tsunami amplitudes are usually less than one to two metres in height in the open ocean. Since the associated currents have nearly uniform speed from the water surface to bottom, they can induce large forces.

Not all earthquakes generate tsunamis since an earthquake must be of sufficient magnitude and accompanied by an appropriate deformation of the sea floor to produce tsunamis. Amplitude magnitudes depend primarily on the mass displaced, but also on the depth of submergence, the water depth, and other characteristics of the generation (Murty, 1977). Information from Japanese tsunamis shows that apart from rare exceptions, the limiting earthquake magnitude M for tsunamis producing earthquake is M = 6.3 + 0.0005D where D is the focal depth in kilometres. An alternate form for M and the one used by Terra Nova is M = 5.6 + 0.01D (Seaconsult, 1988). In the Terra Nova analysis D was taken as 0 so that M = 5.6 was a conservative estimate for the limiting magnitude to produce a tsunami. The tsunami of 1929 which occurred offshore southern Newfoundland has a Richter Scale magnitude of 7.2. This earthquake produced a tsunami which caused deaths and extensive property damage. The absence of a tsunami for the 1951 (A = 5.0) and the two in 1954 (M = 5.2 and 5.3) earthquakes in this area confirm the presence of a lower threshold (Seaconsult, 1988).

Abe (1979), related earthquake magnitude M, to tsunami amplitude A, where A is half the height between crest and trough through the following relationship.

$$M = log\ A + B$$

where A is the observed maximum amplitude in metres, and B is a constant that depends upon the source region and station (calibration constant). For Pacific tsunamis, Abe (1979) found B = 9.1 $\pm$ 0.3. Using only one earthquake for the Atlantic Ocean (Lisbon Earthquake of November 1, 1755) Abe (1979) found B = 8.5.

For the Terra Nova project the tsunami wave amplitudes on the Grand Banks were modeled based on the principle of transforming the recurrence relations for earthquake magnitude M into wave amplitudes accounting for far-field and near-field sources.

The magnitude recurrences success (Figure 6.17) proposed by Bashám and Adams (1983) and COGLA (1987) were adopted initially to give a conservative estimate of local earthquake magnitude.

The return period of a tsunami is expressed as

$$T_A = \left[\frac{1}{T_F} + \frac{1}{T_N} \right]^1$$

where T_F is the period of a tsunami in the far-field (occurring at a large distance away) and T_N is the period of a tsunamis in the near-field.

The current speed from a tsunami is expressed as

$$U = A\sqrt{g/h}$$

where g is the gravitational acceleration

A is the tsunami amplitude

and h is the water depth

Seaconsult (1988) used a Monte Carlo simulation for both the Bashám-Adams and COGLA M-recurrence relationships to calculate the mean amplitude for different return periods with the 95% confidence intervals (Tables 6.10). The expect extreme tsunamis amplitudes for different return periods together with the expected and upper limit current speeds for the Terra Nova project are shown in Table 6.11. Note that the 95% upper confidence limit in Table 6.10 is unrealistic at long return periods because an upper limit to earthquake magnitude was not imposed on the calculations. The values in Table 6.11 have been adjusted to bring them into better agreement with observations and model simulations. Placing a limit of approximately 2 m for the wave amplitude produces a corresponding limit in current speed of 0.70 m/s for the 100-year return period (Seaconsult, 1988).

Using equivalent extreme tsunami amplitudes for White Rose as was used at Terra Nova the resulting current speeds are shown in Table 6.12. The table shows that the 100-year extreme tsunami is not expected to exceed 63 cm/s.

In the Terra Nova Alliance (1997) document, the expected amplitude values for the different return periods were taken as the design values together with the mean current, and not the 95% upper confident limit current values for the expected tsunami amplitude. The same methodology has been used for White Rose.

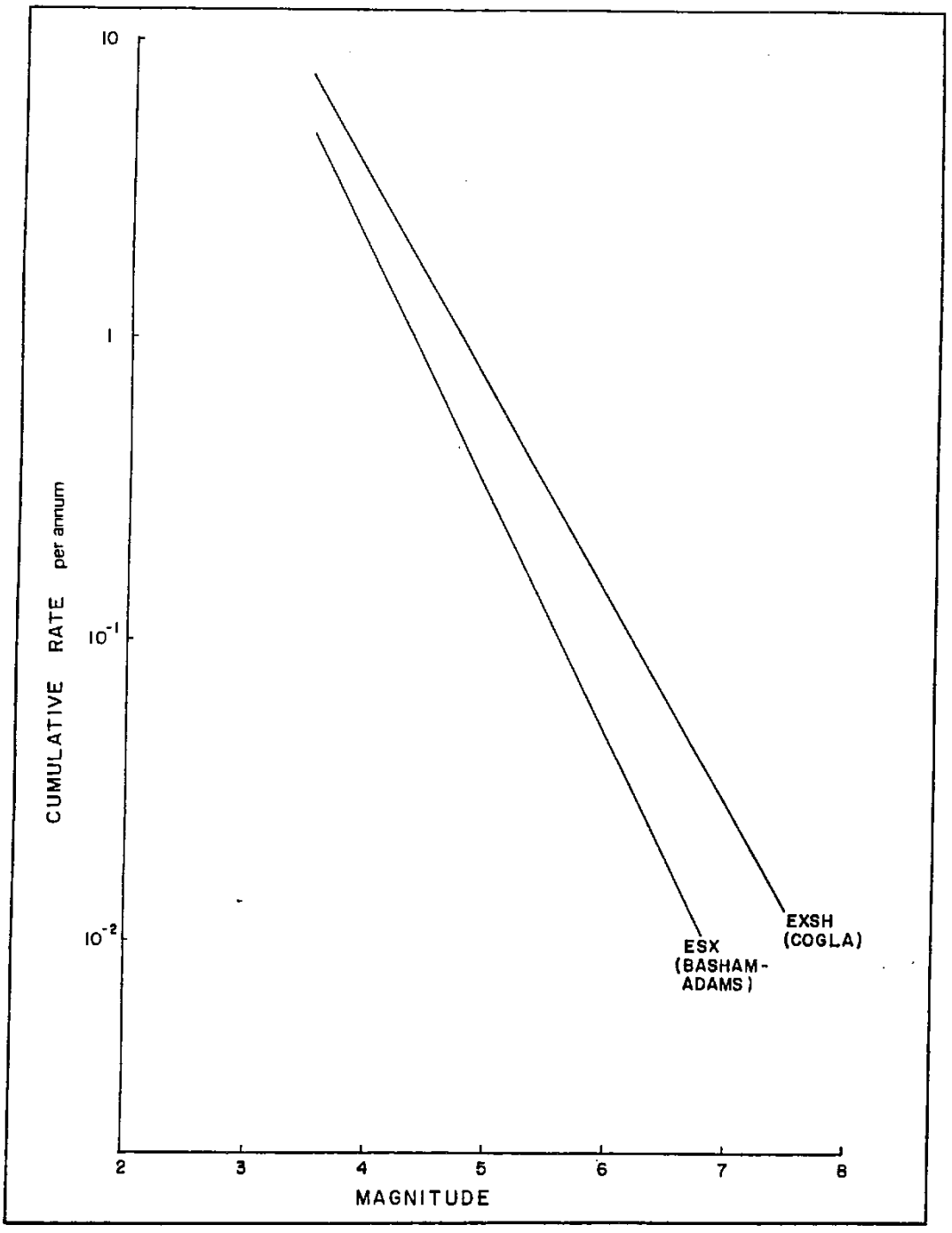

Figure 6.17 Magnitude Recurrence Relationships for Source Zone ESX (after Basham and Adams (1983) and COGLA 1987)

Table 6.10 Extreme Tsunami Amplitudes and 95 Percent Confidence Limits

	M-Recurrence Relation			
	Bashám-Adams		COGLA	
Return Period (years)	Mean Amplitude (m)	95% c.l. (m)	Mean Amplitude (m)	95% c.l. (m)
1	0.0012	<.001-.0075	0.0015	<.001-.0095
10	0.043	.011-.18	0.10	.03-.24
25	0.14	.040-.69	0.26	.10-.90
50	0.30	.095-1.7	0.54	.21-2.3+
100	0.70	.23-4.7+	1.2	.45-6.4+

+ These values exceed the hypothesized limit of 2 m discussed in the text.
Source: Seaconsult (1988)

Table 6.11 Extreme Tsunami Amplitudes and Current Speeds for Terra Nova

	Amplitude		Current Speed	
Return Period T_R (years)	Expected Value (m)	95% Upper Limit (m)	Expected Value (cm/s)	95% Upper Limit (cm/s)
1	negl.	negl.	negl.	negl.
10	0.10	0.24	negl.	negl.
25	0.26	0.90	8	26
50	0.54	2.0+	17	67
100	1.20	2.0+	35	70+

Note that to get to the current speeds quoted the amplitudes for 50-year return and 100-year return would be 2.1 m and 2.2 m, respectively.
Source: Seaconsult (1988)

Table 6.12 Extreme Tsunami Amplitudes and Current Speeds for White Rose

	Amplitude		Current Speed	
Return Period (years)	Expected Value (m)	95% Upper Limit (m)	Expected Value (cm/s)	95% Upper Limit (cm/s)
1	negl.	negl.	negl.	negl.
10	0.10	0.24	3	7
25	0.26	0.90	7	26
50	0.54	2.1	15	60
100	1.20	2.2	34	63

Note: The 95 percent upper limit values for tsunami amplitudes have been adjusted for consistency with observations and with the Terra Nova analysis results.

6.9 Extreme Currents

The data for the extreme current analysis came from 4 years of data. There were 3 continuous years of data at White Rose for 2008 to 2010, plus the one-year data set

complied from different exploration wells that were used for the previous calculated extremes before construction of the Sea Rose.

A Gumbel Extreme value analysis was carried out by fitting the higher values in the 4 year time series to a Gumbel distribution. The extreme current values for return periods of 1-year, 10-years, 25- years, 50-years, and 100-years are presented in Table 6.13. The values for both the 80% confidence limits and 95% confidence limits are included in Table 6.13.

Table 6.13 Gumbel Extreme Analysis

Near-Surface			
Return Periods	**Current Speeds (cm/s)**		
	Extreme Value	**Upper 80% Prediction Limit**	**Upper 95% Prediction Limit**
1 years	81	89	93
10 years	104	118	125
25 years	112	129	138
50 years	119	138	148
100 years	126	146	157
Mid-Depth			
Return Periods	**Current Speeds (cm/s)**		
	Extreme Value	**Upper 80% Prediction Limit**	**Upper 95% Prediction Limit**
1 years	43	44	45
10 years	47	50	51
25 years	49	52	54
50 years	50	54	56
100 years	51	56	58
Near-Bottom			
Return Periods	**Current Speeds (cm/s)**		
	Extreme Value	**Upper 80% Prediction Limit**	**Upper 95% Prediction Limit**
1 years	43	45	47
10 years	51	56	58
25 years	54	59	63
50 years	56	62	66
100 years	58	65	69

Note that at all three depths the maximum observed current was between the 1-year and 10-year extreme current estimates. The maximum current at White Rose is an indirect effect of storms and thus more likely to occur in the fall or winter seasons. For the extreme currents at mid-depth and near-bottom, both the 80% and 95% upper prediction limits give similar values indicating a higher level of confidence in the predictions than those in previous work. In the near surface waters, the difference in values between the two prediction limits only varies between 4 cm/s and 11 cm/s for the range of 1-year to 100-year return period.

It would be prudent to add on the maximum tidal current since it is conceivable that the tidal component could be in the same direction as the storm induced current. The tidal currents at White Rose are in the order of 15 cm/s. This is slightly lower than the tidal currents at Hibernia and Terra Nova where the water depth is less. Using the upper 95% prediction limits from the Gumbel distribution together with spring tides, gives the extreme value estimated presented in Table 6.14. Note that the tsunami currents have not been added to these values to be consistent with the methods of extreme currents for Terra Nova and Hibernia, and with previous work for White Rose.

Table 6.14 Extreme Current Estimates at White Rose

Return Period	Near-Surface (cm/s)	Mid-Depth (cm/s)	Near-Bottom (cm./s)
1 year	108	60	62
10 years	140	66	73
25 years	153	69	78
50 years	163	71	81
100 years	172	73	84

7.0 Water Levels

7.1 Tides

Astronomical tides are highly predictable. From an extended measurement at any selected site, the major astronomical constituents can be determined and used to accurately predict tidal heights. Over the Grand Banks, the largest tidal constituent is the lunar semidiurnal (M_2) with amplitude of approximately 40 cm. The other major semidiurnal (S_2) and diurnal constituents (0_1, K_1) are lower in amplitude; each constituent has a value of approximately 10 to 15 cm (Godin, 1980).

The tides on the Grand Banks are mixed, mainly semidiurnal with two high tides and two low tides occurring each day. The successive highs (and lows) are usually not the same height. A typical tidal range is 1 m.

7.1.1 Tidal Data Collected in the 1980's

Tidal information for the Grand Banks comes from a tidal study carried out by the Bedford Institute of Oceanography (BIO) in 1983-84, and tidal data collected by Husky Oil for two periods; August 6 to December 10, 1985; and December 28, 1985 to February 13, 1986. BIO collected data at eight sites over a period of six months on the Grand Banks, and along its edge (Petrie et al., 1987). From the BIO data, Petrie et al., (1987) prepared co-range and co-phase charts for the Grand Banks for constituents M_2, S_2, and K_1. These charts are presented in Figure 7.1. Co-range lines are lines of equal amplitude and co-phase lines are lines of equal phase. The co-range lines show that the M_2 constituent is of the order of 25 cm at White Rose and S_2 and K_1 are of the order of 10 cm and 17 cm, respectively.

Water levels from the White Rose data collected in 1985 and 1986 were analyzed to get the tidal constituents. These constituents are given in Table 7.1.

Table 7.1 Tidal Constituents for White Rose form Data Collect in 1985/86

Name	Frequency	Amplitude	Phase
Z0	0.00000000	0.7665	0.00
MM	0.00151215	0.0054	274.31
MSF	0.00282193	0.0052	19.69
ALP1	0.03439657	0.0022	28.13
2Q1	0.03570635	0.0022	288.90
Q1	0.03721850	0.0101	144.38
O1	0.03873065	0.0661	278.75
NO1	0.04026860	0.0083	162.56
K1	0.04178075	0.0652	255.20
J1	0.04329290	0.0040	307.73
OO1	0.04483084	0.0041	14.82
UPS1	0.04634299	0.0012	70.76

Name	Frequency	Amplitude	Phase
EPS2	0.07617731	0.0045	244.78
MU2	0.07768947	0.0125	11.65
N2	0.07899925	0.0395	80.83
M2	0.08051140	0.1802	194.04
L2	0.08202355	0.0048	63.58
S2	0.08333334	0.0968	17.35
ETA2	0.08507364	0.0007	74.93
MO3	0.11924206	0.0011	29.49
M3	0.12076710	0.0026	212.25
MK3	0.12229215	0.0006	276.69
SK3	0.12511408	0.0024	305.66
MN4	0.15951064	0.0028	102.81
M4	0.16102280	0.0044	238.55
SN4	0.16233258	0.0007	85.55
MS4	0.16384473	0.0020	142.34
S4	0.16666667	0.0008	90.24
2MK5	0.20280355	0.0002	175.71
2SK5	0.20844741	0.0003	279.69
2MN6	0.24002205	0.0035	302.32
M6	0.24153420	0.0059	80.53
2MS6	0.24435614	0.0054	343.24
2SM6	0.24717806	0.0006	187.95
3MK7	0.28331494	0.0004	52.17
M8	0.32204559	0.0005	19.21

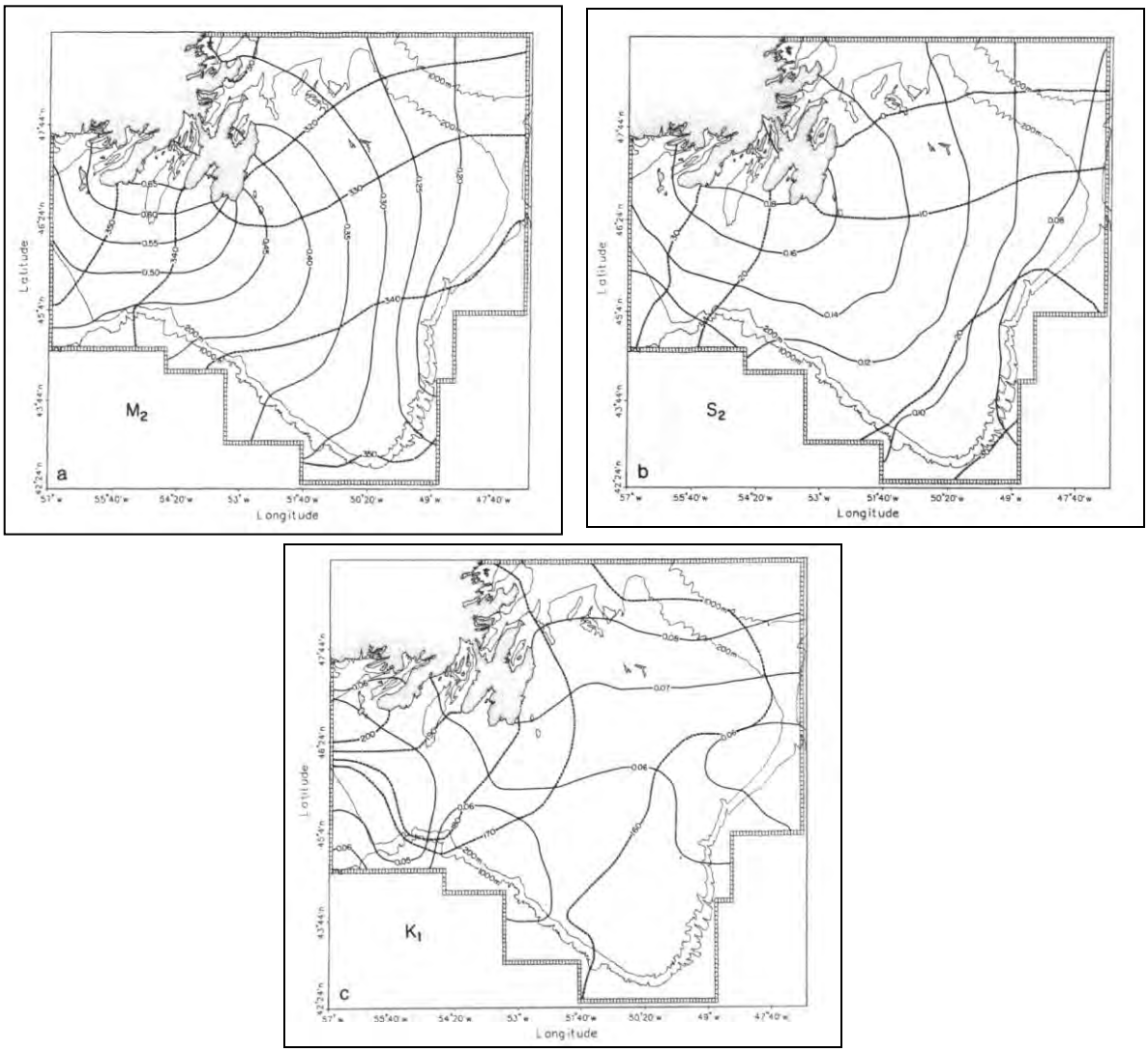

Figure 7.1 The Co-Range (solid line in metres) and Co-phase (broken line) Charts for the Grand Banks

(source: Petrie et al., 1987)

7.1.2 Tidal Data Collected in 2009

There was an uncertainty about whether the times were correct in the 1985/86 data set. Therefore, tidal data was collected between November 6, 2009 and February 28, 2010 on the White Rose field with an Aanderaa water level recorder. The water level difference between the lowest low water and highest high water was 1.44 m. The tidal constituents are presented in Table 7.2. The values for the largest constituents M_2, S_2, K_1, and O_1 are 0.177 m, 0.076 m, 0.073 m and 0.056 m, respectively. Note that these values represent one half of the tidal constituent amplitude. These values are slightly less than the constituent values calculated for the 1985/86 data set. The phases do not compare, confirming the problem with the previous data set.

Table 7.2 Tidal Constituents from Husky Water Level Data (Nov 2009- Feb 2010)

Name	Frequency (cph)	Amplitude (m)	Phase (o)
MM	0.001512	0.072224	144.2981
MSF	0.002822	0.034239	111.6555
ALP1	0.034397	0.011391	136.7266
2Q1	0.035706	0.007278	303.1457
Q1	0.037219	0.004892	87.79878
O1	0.038731	0.05575	127.3923
NO1	0.040269	0.010553	191.5029
K1	0.041781	0.072579	171.2435
J1	0.043293	0.010472	234.6508
OO1	0.044831	0.004553	196.534
UPS1	0.046343	0.006569	239.454
EPS2	0.076177	0.008509	341.3757
MU2	0.077689	0.010182	325.0568
N2	0.078999	0.038217	297.1987
M2	0.080511	0.177036	318.2682
L2	0.082024	0.002987	255.5125
S2	0.083333	0.076496	11.217
ETA2	0.085074	0.006589	296.0131
MO3	0.119242	0.008784	301.2988
M3	0.120767	0.004968	17.19392
MK3	0.122292	0.008286	97.04533
SK3	0.125114	0.00985	305.0364
MN4	0.159511	0.011279	110.979
M4	0.161023	0.013567	147.5201
SN4	0.162333	0.008624	331.5436
MS4	0.163845	0.007564	10.27288
S4	0.166667	0.006295	243.3306
2MK5	0.202804	0.008836	5.287672
2SK5	0.208447	0.007707	74.58054
2MN6	0.240022	0.011561	23.54241
M6	0.241534	0.013034	67.6537
2MS6	0.244356	0.010059	247.7408
2SM6	0.247178	0.008403	129.7494
3MK7	0.283315	0.007977	258.7407
M8	0.322046	0.006795	307.5446

7.2 Extreme Water Level Heights

A harmonic analysis was carried out on the tidal constituents resolved from the 2009/2010 tidal record at White Rose. Using the tidal constituents, a 20-year tidal prediction was carried out for White Rose. From the 20-year tidal prediction the maximum tidal height was 45 cm above mean sea level and the minimum tidal height was 38 cm below mean sea level for a total range of 83 cm.

Storm surges cause sea level to rise as a result of wind stress on the surface of the ocean. Severe storm surges can cause the ocean to rise by a few metres in coastal regions, but away from the coast the effect of wind stress is much smaller in the absence of a boundary. The extreme storm surge values for a site near Terra Nova were calculated by Seaconsult, 1988 using a Gaussican distribution. These values are given in Table 7.3.

Table 7.3 Extreme Storm Surge

		Surge Levels (cm)	
Return Period T_R (years)		**Expected**	**95% UPL**
1	z+ z^-	50 54	64 69
10	z+ z^-	61 66	75 81
25	z+ z^-	66 71	79 85
50	z+ z^-	70 75	83 89
100	z+ z^-	73 79	86 92

z+ is the elevation above MWL

z^- is the elevation below MWL

The water heights due to tsunami waves were discussed in Section 6.8 and the amplitudes of the return periods given in Table 6.10 and 6.11. The mean amplitude for 100-year return period was 1.2 m, but the 95% confidence level was unusually high at 6.4 m. The height of tsunamis in the open ocean is not expected to exceed 2 m.

Sea level heights can also change due to variations in the atmospheric pressure. Sea level rises as atmospheric pressure drops by 1 cm / 1 millibar. The minimum atmospheric pressure measured on the Grand Bank over the last 10 years was 952.0 millibars on February 20, 2007, and the maximum was 1046.6 millibars on January 27, 2003. The mean atmosphere pressure during winter is approximately 1008 millibars. These values would give a sea level rise of 56 cm and a drop in sea level of 37 cm.

The combined effects of astronomical tides, storm surges and atmospheric pressure changes would produce a maximum water level of 1.74 m above mean sea level and a minimum water level of 1.54 m below mean sea level. These values do not include sea level changes for a tsunami.

8.0 Water Properties

8.1 Description of Water Masses

The water characteristics at White Rose can be expected to show yearly variations depending on the strength and position of the North Atlantic Current. As previously explained in Section 6.1, the northern branch of the Gulf Stream, known as the North Atlantic Current, usually turns north along the east side of the Grand Banks and Flemish Cap, and then turns east at approximately 50°N. Krauss (1990) found that approximately two-thirds of the volume transport of the Gulf Stream continues as the North Atlantic Current. White Rose is located at approximately 47°N. Near the edge of the Grand Banks current flows southward along the edge of the Grand Banks, through Flemish pass and around Flemish Cap. Due to its position the water properties at White Rose are influenced by the water properties of the Labrador Current and often by the North Atlantic Current when its inshore boundary is in a northern position within the area of 43° and 46°N.

The water mass characteristics created by these two current systems are described below:

- cold (<4°C), low salinity water (<34 parts per thousand (‰)) originating on the continental shelf off Labrador and further north and transported into the area by the Labrador Current;
- further offshore, warm (7°C-18°C), high salinity (>35‰) Western North Atlantic Central water of the North Atlantic Current;
- mixed intermediate water formed when the warm and high salinity water of the North Atlantic Current comes into contact with the cold low salinity water of the Labrador Current on the southern and eastern slope of the Grand Banks; and
- Slope Water is formed south of the Grand Banks from Atlantic Current water and coastal water. Slope Water has characteristics similar to Atlantic Water but with a slightly lower salinity (Figure 8.1).

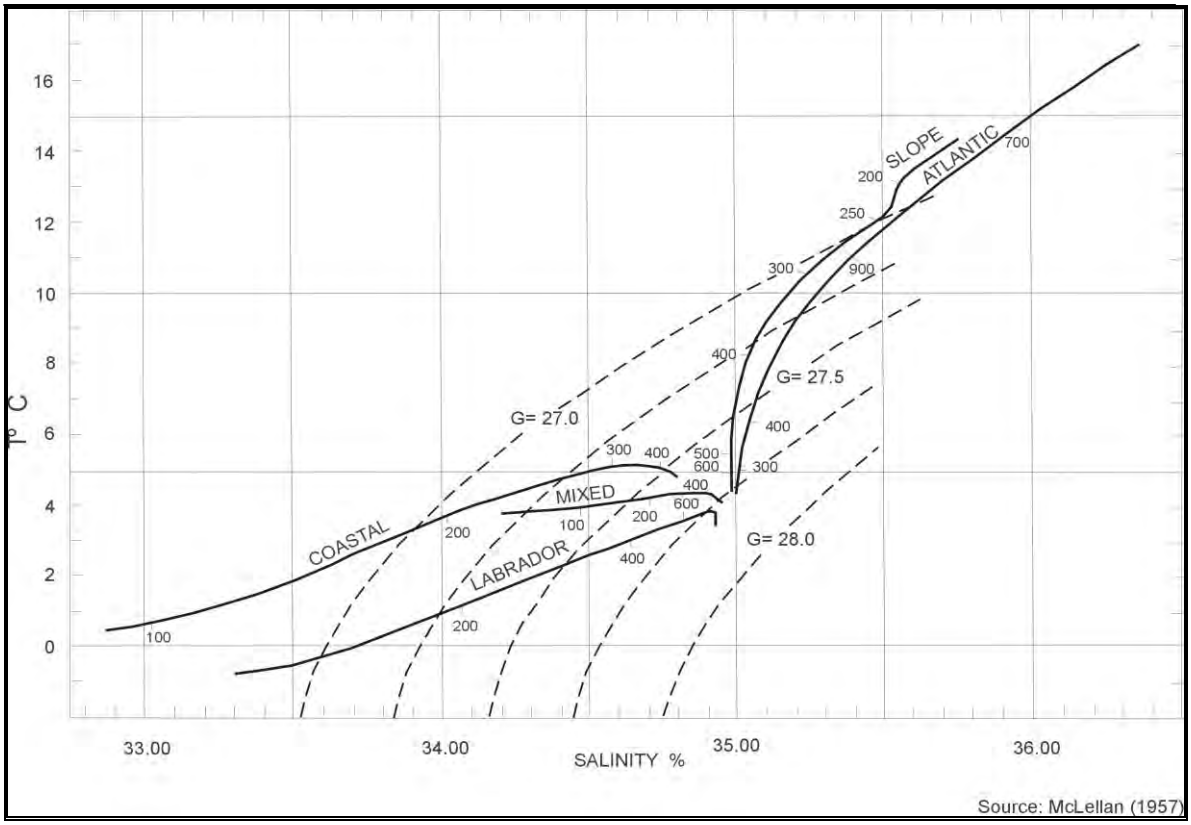

Figure 8.1 T-S Curves for Five Water Masses found between the Gulf Stream and the Continental Shelf West of 45° West

Source: McLellan(1957)

The water structure on the northeastern edge of the Grand Banks of Newfoundland is characterized by the presence of three identifiable features.

The first identifiable feature is the surface layer which is exposed to interaction with the atmosphere, and experiences temperature variations from sub zero values in January and February to above 15°C in summer and early fall. Salinity at this layer is strongly impacted by wave action and local precipitations. Considering that a water mass is a body of water which retains its well defined physical properties over a long time period, the surface layer of variable temperature and salinity is usually left out of a water mass analysis for a particular region. During the summer, the stratified surface layer can extend to a depth of 40 m or more. In winter, the stratification in the surface layer disappears and becomes well mixed due to atmospheric cooling and intense mixing processes from wave action.

A second element of the thermohaline structure on the Grand Banks is the Cold Intermediate Layer (Petrie et al., 1988). In areas where the water is deep enough, this layer of cold water is trapped during summer between the seasonally heated upper layer and warmer slope water near the seabed (Colbourne, 2002). Its temperatures range from less than -1.5°C to 0°C (Petrie and al., 1988; Colbourne et al., 1996)) and salinities vary within 32 and 33 psu. It can reach a maximum vertical extent of over 200 m (Colbourne,

2004). The Cold Intermediate Layer is the residual cold layer that occurs from late spring to fall and is composed of cold waters formed during the previous winter season. It becomes isolated from the sea surface by the formation of the warm surface layer during summer, and disappears again during late fall and winter due to the intense mixing processes that take place in the surface layer from strong winds, high waves and atmospheric cooling. In winter the two layer structure is replaced by a mixed cold body of water which occupies the entire water column.

Figure 8.2 shows average bottom temperature during the decade from 1991 to 2000. The figure shows that positive bottom temperatures are found south of 46°N. The blue area to the north of 46°N in Figure 8.2 corresponds to the average spread of the Cold Intermediate Layer. The variabilities in temperature and salinity in the area have been the subject of systematic research (Colbourne, 2004; Colbourne et al., 1997; Colbourne and Foote, 1994). These studies suggest that the water properties on the Grand Banks experience notable temporal variability. Colbourne (2004) explains that bottom temperatures ranged from near record lows during 1991 to very high values in the late 90‟s. The areal coverage of the Cold Intermediate Layer was highest on the Newfoundland Shelf during years 1972, 1984 and 1991 (Colbourne, 2004). Since 1991, the areal coverage of the Cold Intermediate Layer has been decreasing.

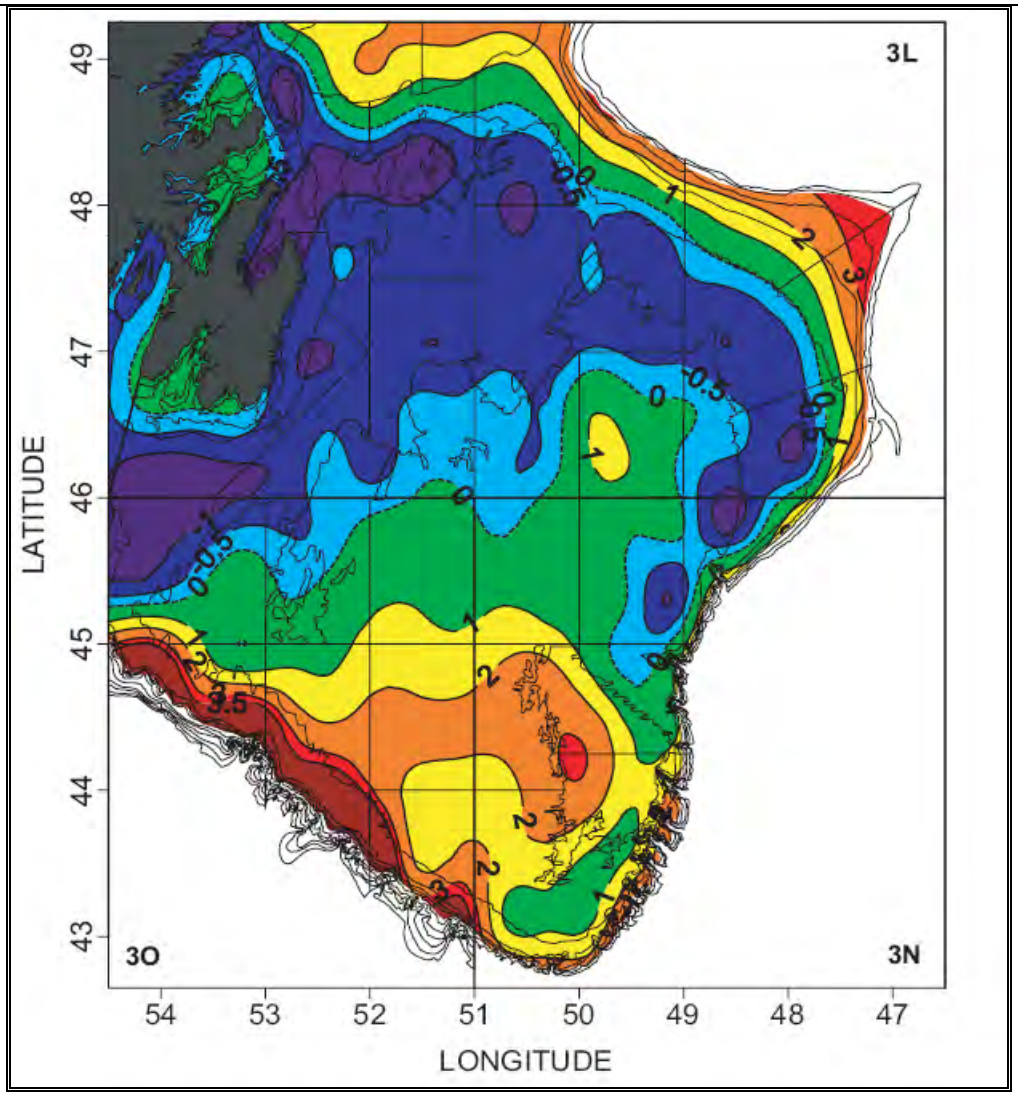

Figure 8.2 Average near Bottom Temperature during Spring from all Available Data for the Decade 1991-2000 (adapted from Colbourne, 2004)

A third element is the Labrador Sea water which is formed in the Labrador Sea as a result of the deep convection processes that take place during severe winters. The Labrador Sea has temperatures between 2°C to 4°C and salinities between 34.8 psu to 35 psu. The Labrador Sea water is separated from the Intermediate Cold Layer by a frontal region denoted by a strong temperature and salinity gradient near the edge of the continental shelf (Colbourne, 2004; Stein, 2007).

During the last 50 years there have been three warming periods in the Labrador Sea; 1960 to 1971, 1977 to 1983, and 1994 to present. In 1994, the Labrador Sea water filled the entire central part of the Labrador Sea basin within the depth range of 500-2400 m (Yashayaev and Clarke, 2006). The warming trend since 1994 has caused the water to become warmer, saltier, and more stratified; thus making it more difficult for winter renewal of Labrador Sea Water to take place. Unusual warming took place in 2004

believed to have originated from waters transported north and west by the North Atlantic Current and the Irminger Current (Yashayaev and Clarke, 2006).

8.2 Seasonal Variations

Figure 8.3 presents the sea surface temperatures in the study area which shows the geographic location and characteristics by season of the frontal region east of the Grand Banks. The seasonal variability of the characteristics by depth over the northeast Grand Banks near the White Rose location has been presented by Drinkwater and Trites (1986) for bottle data collected between 1910 and 1982. The seasonal variations show a pattern where the variability is largest at the surface and decreases with depth, similar to Station 27 (the reference station located east of Cape Spear Newfoundland). The least variability in both temperature and salinity is between 50 and 100 m. At the surface, the highest temperature is in August and the lowest is in March and April, while the highest salinity is in February and the lowest is in August and September (Figure 8.4).

The spatial distribution of water properties offshore Newfoundland at 20 and 75 m is presented for July and January in Figures 8.5 and 8.6, respectively (Colbourne and Foote, 1994). The warmer, high- salinity slope water is evident to the south and east of the Grand Banks at both 20 and 75 m depths. The large horizontal gradients mark the boundaries (oceanic fronts) between the cold low salinity water of the Labrador Current and coastal waters, and the warm high salinity Slope and Atlantic Current waters.

The spatial variability of temperature and salinity in the northeast sector of the Grand Banks is routinely sampled in each year by Fisheries and Oceans Canada. During 2010, this hydrographic section was sampled in April, July and December. Figures 8.7 to 8.9 show the temperature and salinity contours across the Flemish Cap section in 2010. The temperature distribution is characterized by an area of strong vertical gradients located above the Grand Banks in July (Figure 8.8). This vertical temperature structure breaks down during the winter season as seen by Figure 8.7 and 8.9. The salinity structure follows the same pattern as temperature being more stratified in July, but having a lower salinity in December and a higher salinity in March.

The most noticeable feature is the high horizontal gradients in the area over the shelf break that separates the relatively fresh low salinity waters of the Grand Banks from the warmer, higher salinity waters in Flemish Pass (Figure 8.8). The offshore branch of the Labrador Current flows along the shelf break in the region of the strong density gradients shown in Figures 8.7 to 8.9. The majority of the water in the offshore branch of the Labrador Current has been known to have temperatures between 3°C and 4°C and salinities of 34.88 psu to 34.92 psu (Lazier, 1982).

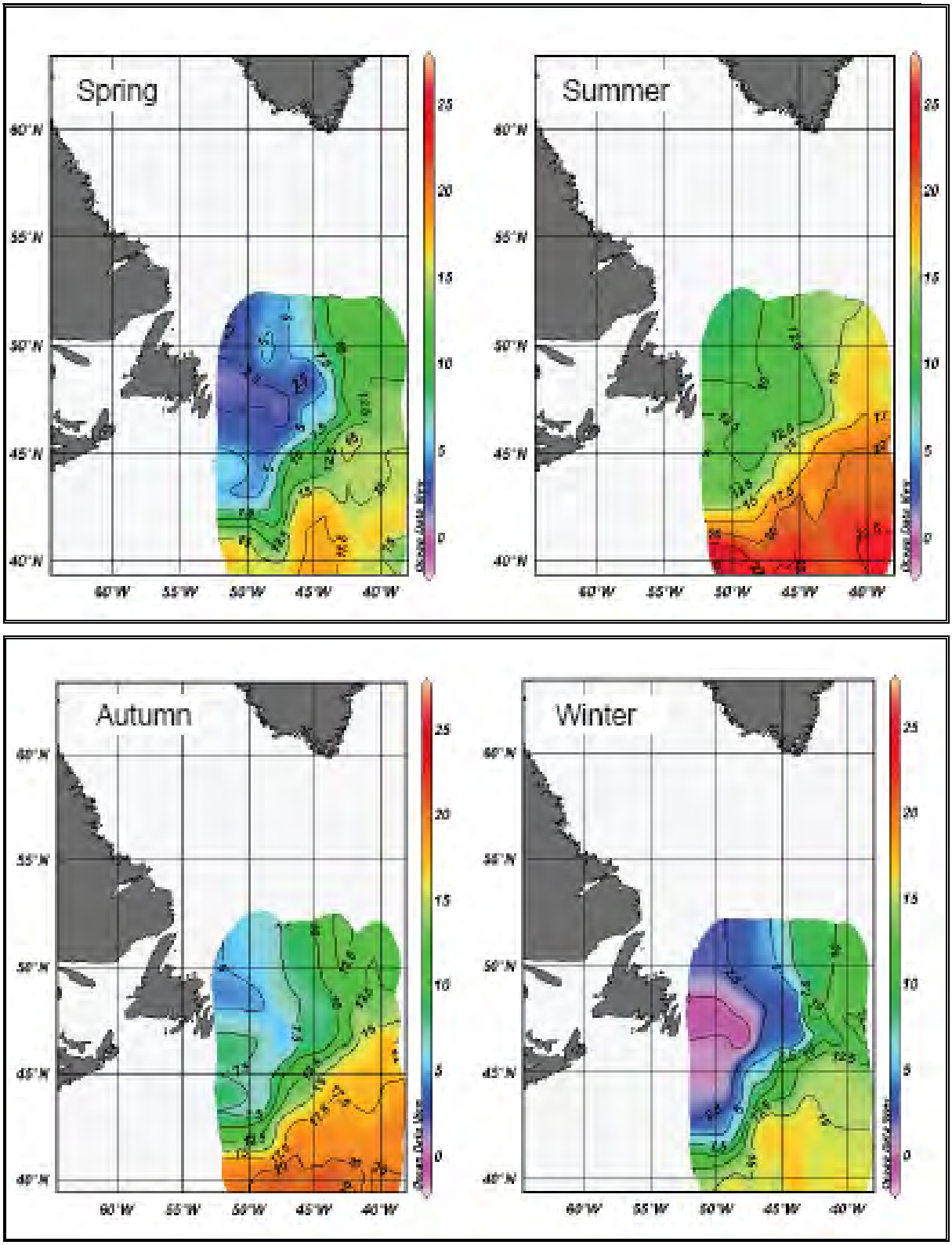

Figure 8.3 Sea Surface Temperatures as produced from the World Oceans Database 2001 for each Season (from Stein, 2007)

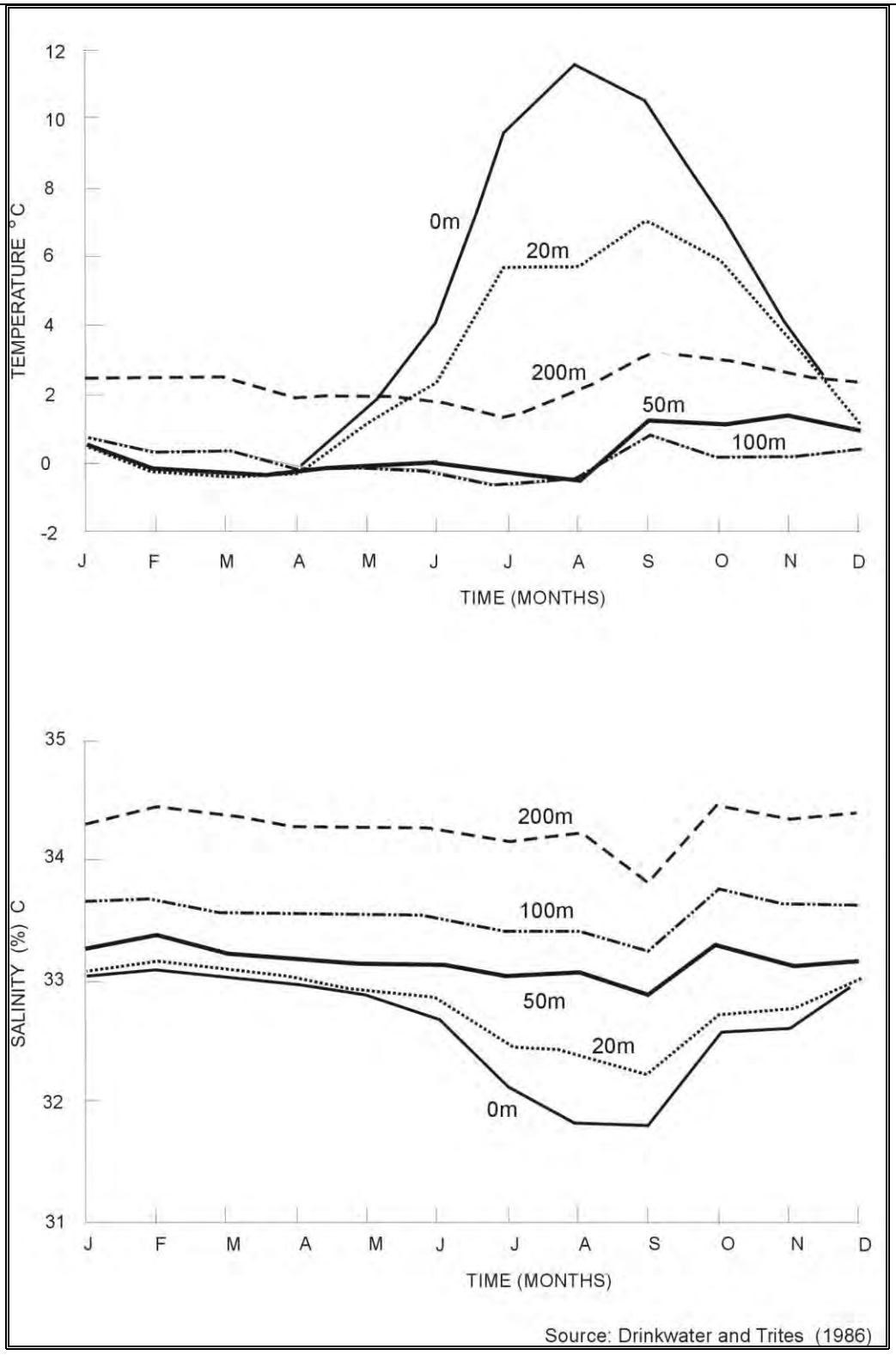

Figure 8.4 Seasonal Variation of the Monthly Mean Temperature and Salinity for the Northern Slope of the Grand Banks

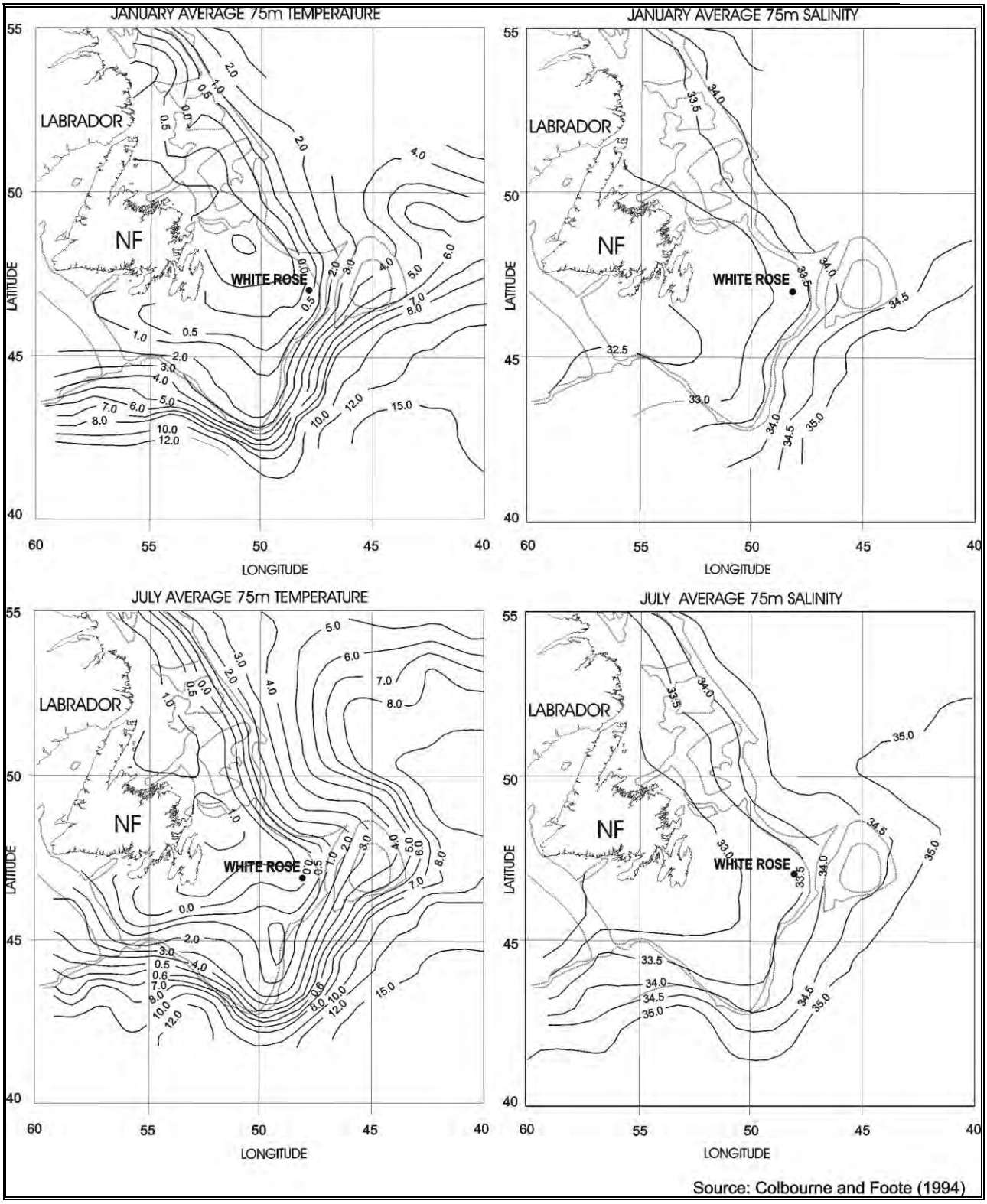

Figure 8.5 Average Spatial Distribution of Temperatures and Salinity at 75 m in January and July

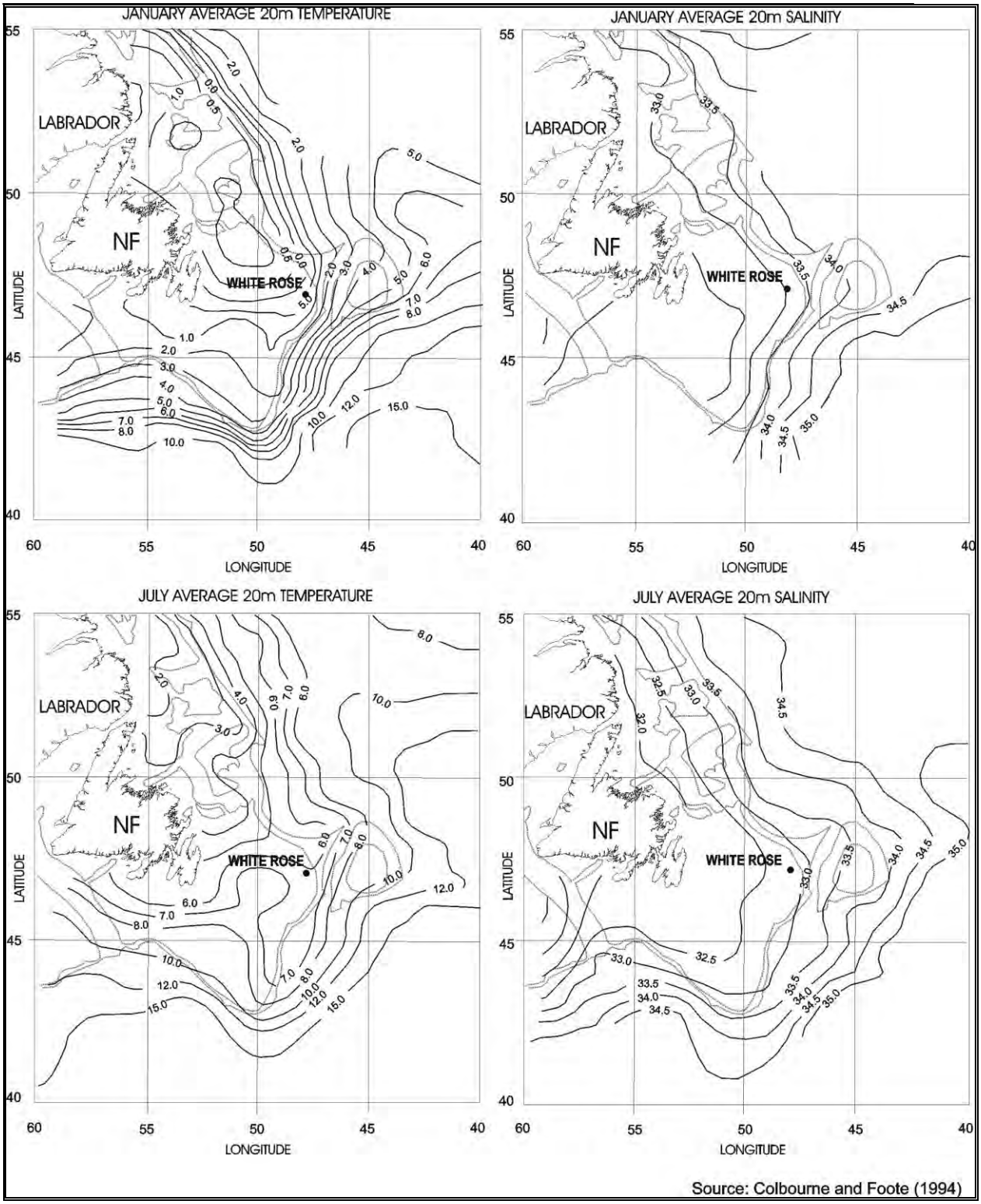

Figure 8.6 Average Spatial Distribution of Temperature and Salinity at 20 m in January and July

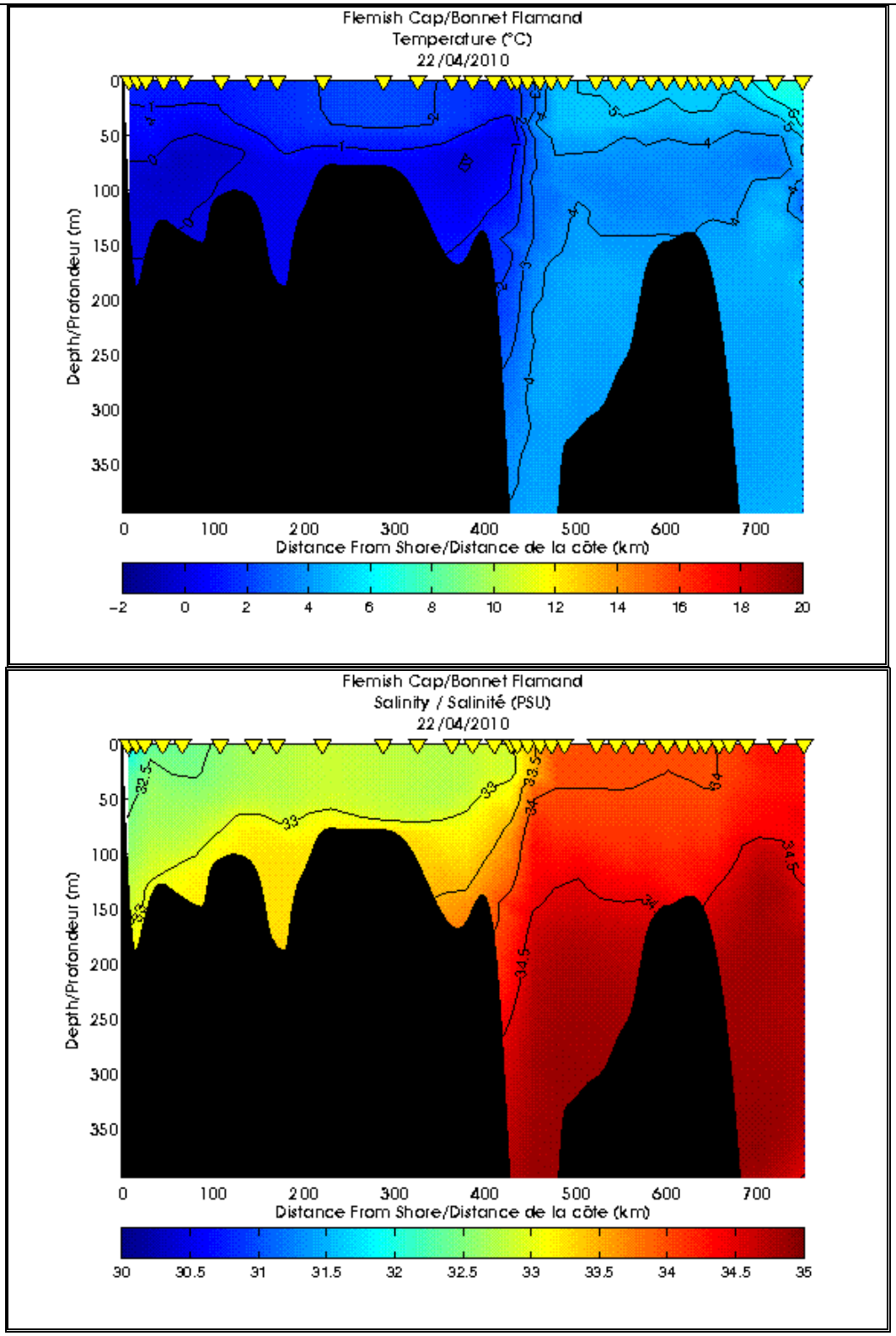

Figure 8.7 Hydrographic Contours across the Flemish Cap Section during April 2010 (from DFO Marine Environmental Data Service Website)

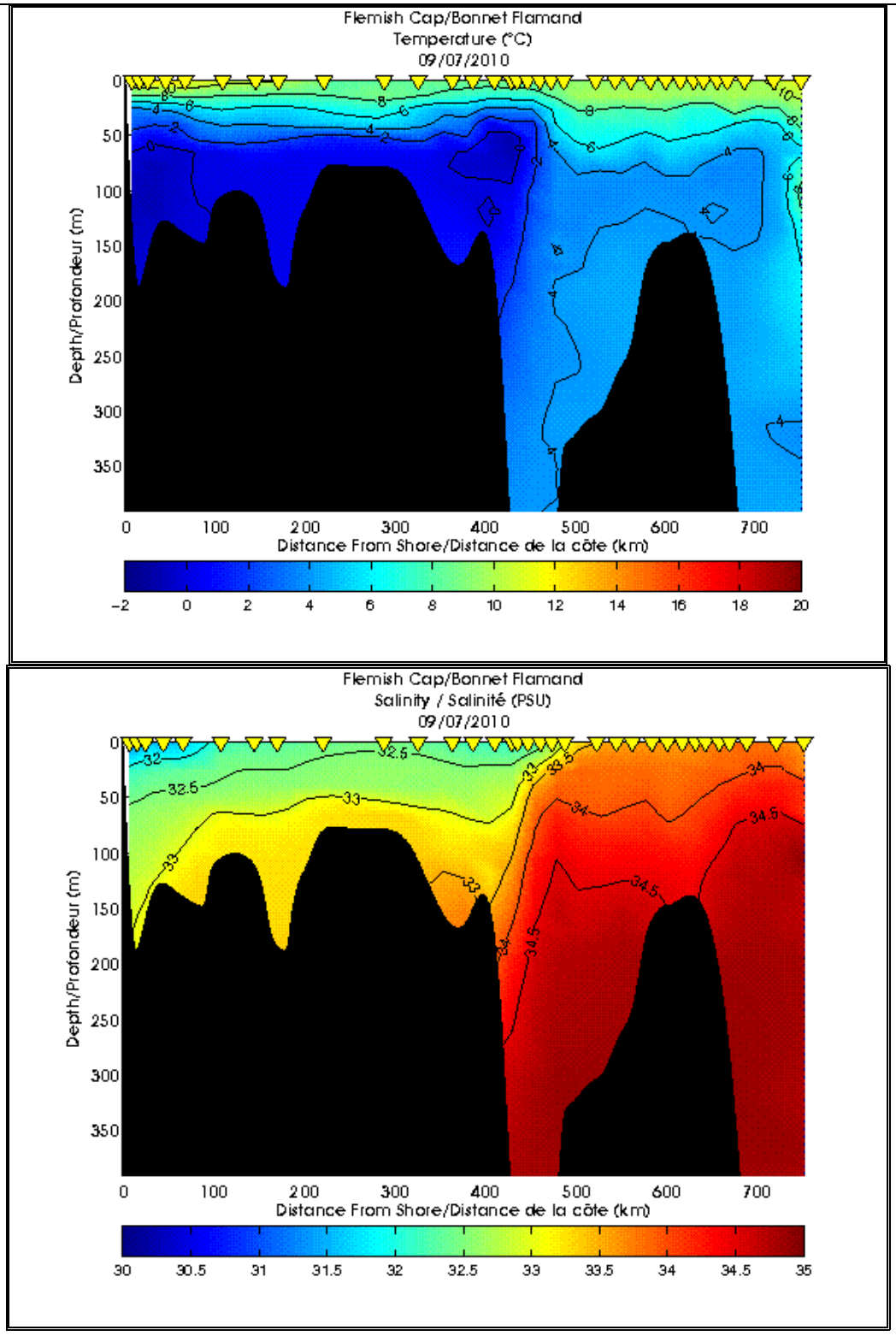

Figure 8.8 Hydrographic Contours across the Flemish Cap section during July 2010 (from DFO Marine Environmental Data Service Website)

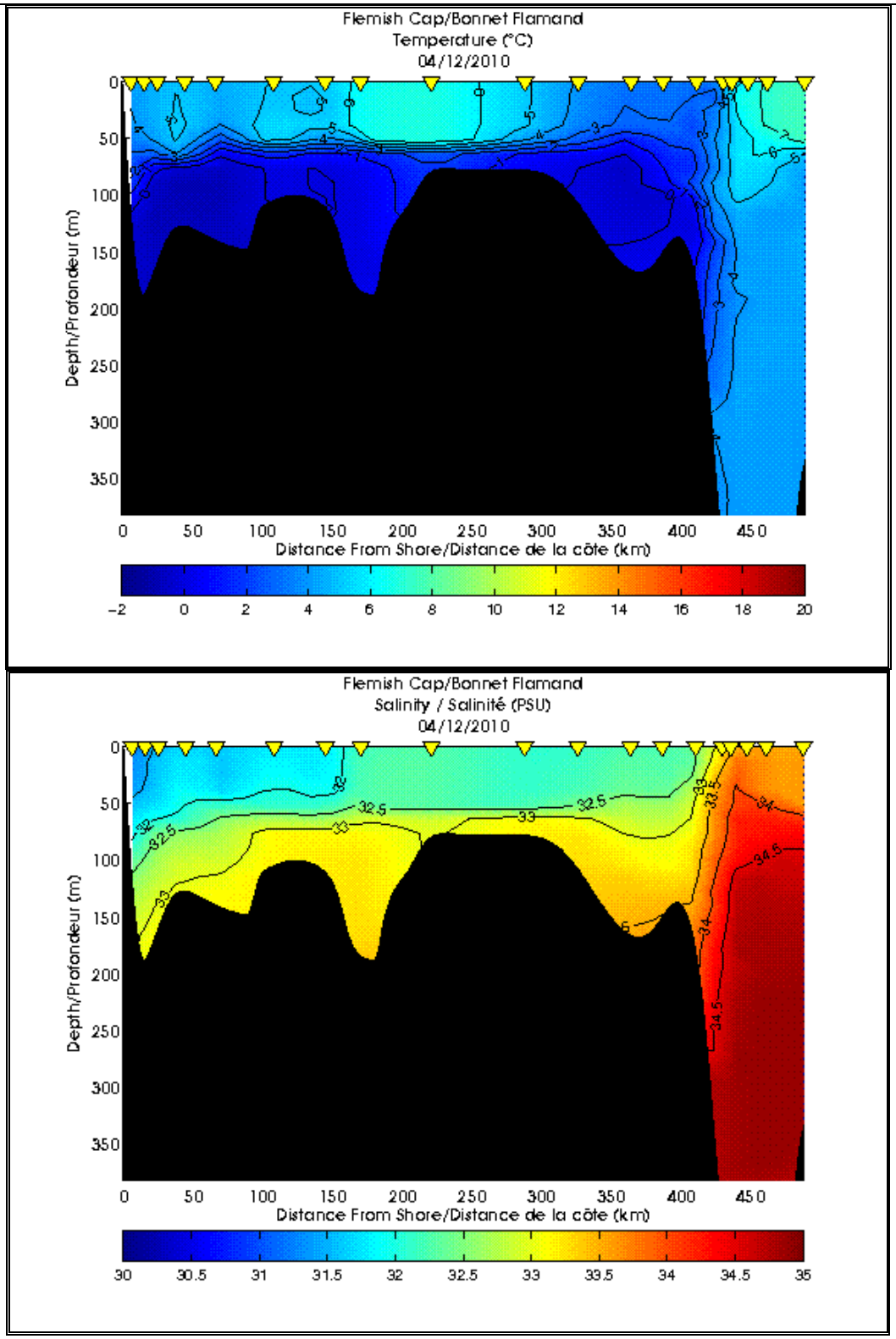

Figure 8.9 Hydrographic Contour across the Flemish Cap Section during December 2010 (from DFO Marine Environmental Data Service Website)

Historical CTD data were obtained from the Bedford Institute of Oceanography archives (BIO) for the area between 100 m and 200 m isobaths on the Northeast Grand Bank. Tables 8.1 and 8.2 present the temperature and salinity data by month at the surface and at 75 m. The information in the tables shows that the surface waters were warmest during the months of July to September with mean temperatures ranging from 9.08° to 11.28°C. The coldest temperatures were in February and March with mean temperatures of -0.61°C and -0.75°C, respectively. The main salinities ranged between 31.59 psu in August and 32.94 psu in February.

At a depth of 75 m, the mean temperatures were always negative, ranging between -1.50°C in August to -0.25°C in November. The mean salinities ranged between 32.94 psu in April and 33.18 psu in February.

The colder waters in this section indicate that the water in this area is experiencing advection from the north by the Labrador Current rather than by vertical mixing through local cooling.

The T-S diagrams in Figure 8.10 show two distinct water masses and the surface seasonally mixed layer. During summer and fall strong stratification occurs in the top 50 m which disappears to being a well mixed surface layer during winter and spring. The core of the Cold Intermediate Layer occurs between the 75 m and 100 m depths. Below 100 m the water is mixed with Labrador Sea water.

Table 8.1 Monthly Temperature and Salinity Statistics for the Surface Water from Historical CTD data for a Water Depth between 100 m and 200 m

Temperature surface (0 m) on the outer edge of the Grand Banks

MONTH	# Observations	Mean	Min	Max	STD
January	15	0.10	-1.40	1.40	0.90
February	23	-0.61	-1.81	0.55	0.80
March	33	-0.75	-1.77	0.50	0.78
April	235	-0.16	-1.50	2.53	0.77
May	303	1.52	-1.10	5.08	1.33
June	422	4.15	0.64	10.34	1.70
July	249	9.08	4.15	13.7	1.86
August	72	11.28	6.37	16.08	2.08
September	87	9.98	4.23	17.1	2.61
October	60	7.13	3.54	11.54	1.97
November	184	4.19	0.83	9.74	1.72
December	53	2.44	-1.00	6.06	1.37

Salinity surface (0 m) on the outer edge of the Grand Banks

MONTH	# Observations	Mean	Min	Max	STD
January	15	32.77	32.19	33.30	0.31
February	23	32.94	32.61	33.29	0.21
March	33	32.91	32.41	33.37	0.18
April	235	32.86	32.23	33.33	0.19
May	303	32.72	31.82	33.19	0.22
June	422	32.56	31.62	33.50	0.24
July	249	32.23	31.08	32.77	0.27

August	72	31.59	30.62	32.65	0.53
September	87	31.87	31.16	32.68	0.32
October	60	32.10	31.32	33.21	0.44
November	184	32.39	31.45	33.77	0.36
December	53	32.51	31.91	33.08	0.27

Table 8.2 Monthly Temperature and Salinity Statistic for 75 m Depth from Historical CTD Data for Water Depth between 100 m and 200 m

Temperature 75 m on the outer edge of the Grand Banks

MONTH	# Observations	Mean	Min	Max	STD
January	16	-0.38	-1.40	0.55	0.54
February	19	-0.71	-1.73	0.96	0.79
March	29	-0.88	-1.76	0.57	0.76
April	384	-1.11	-1.78	1.62	0.55
May	285	-0.88	-1.76	1.48	0.71
June	391	-0.99	-1.80	1.49	0.55
July	244	-0.84	-1.81	5.90	0.79
August	130	-1.50	-1.70	-0.21	0.31
September	71	-1.25	-1.68	-0.05	0.37
October	133	-1.01	-1.65	0.05	0.33
November	178	-0.25	-1.50	3.30	1.10
December	55	-0.27	-1.44	2.13	0.98

Salinity 75 m on the outer edge of the Grand Banks

MONTH	# Observations	Mean	Min	Max	STD
January	16	33.03	32.69	33.33	0.20
February	19	33.18	32.66	33.55	0.22
March	29	33.11	32.77	33.68	0.23
April	384	32.94	32.53	33.8	0.29
May	285	33.09	32.65	34.11	0.19
June	391	33.06	32.53	33.66	0.18
July	244	33.05	32.56	34.00	0.15
August	130	33.08	32.75	33.52	0.11
September	71	33.16	32.79	33.79	0.25
October	133	33.16	32.81	33.69	0.19
November	178	33.17	32.48	33.98	0.24
December	55	33.14	32.75	33.69	0.20

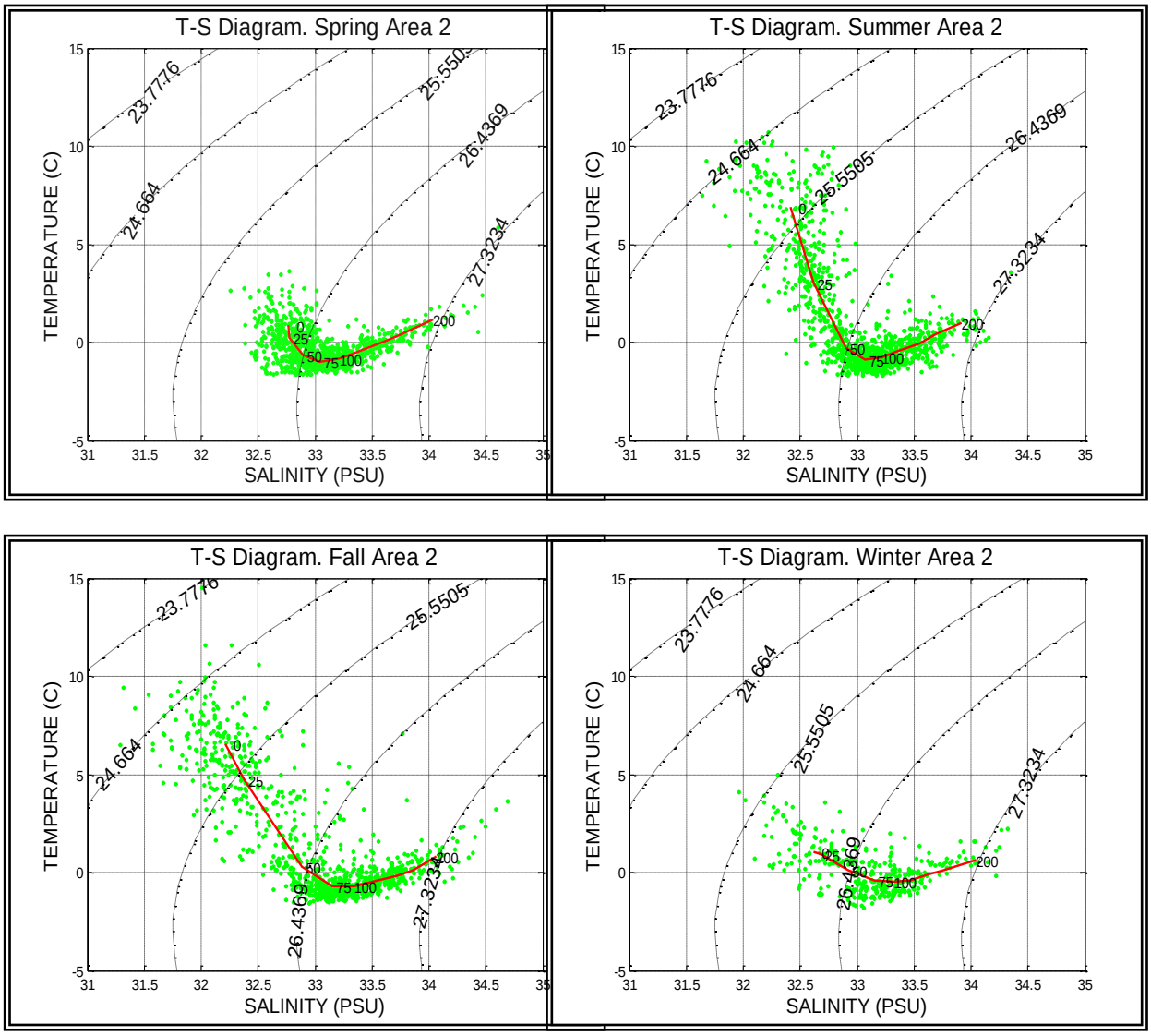

Figure 8.10 Seasonal T-S Diagrams for Sub-area 3 at Depths from 100 m – 200 m

Note: The red lines correspond to the average T-S curve for each area. The numbers on these curves represent the depth in metres.

8.3 Recent CTD Measurements at White Rose

8.3.1 Sippican Data

In recent years six CTD water structure profiles were conducted on the White Rose field using the Sippican CTD system. These profiles are presented in Figures 8.11 and 8.12. Three of the six profiles were carried out in the months of November for years 2008 to 2010. The temperature profiles in Figure 8.11 show that the surface waters (top 20 m) were approximately 5 degrees warmer in November 2008 and 2010 than in 2009. In 2008 and 2009, the water temperature reached approximately 0°C just below a depth of

40 m, but in 2010 the water did not reach 0°C until 100 m depth. This unusually warm water was probably due to the prevalent westward flowing currents between March and October transporting warmer water onto the shelf (Figure 8.13). The water salinity indicated that the source of the warmer water is from the north rather than the south.

The temperature and salinity profiles show that the water structure is practical isothermal during winter. During May, the 2008 profile shows an influx of colder water as compared to that which existed during winter between 45 m and 105 m depths. This is the Cold Intermediate Layer, characteristic of the water on the Grand Banks during the summer months.

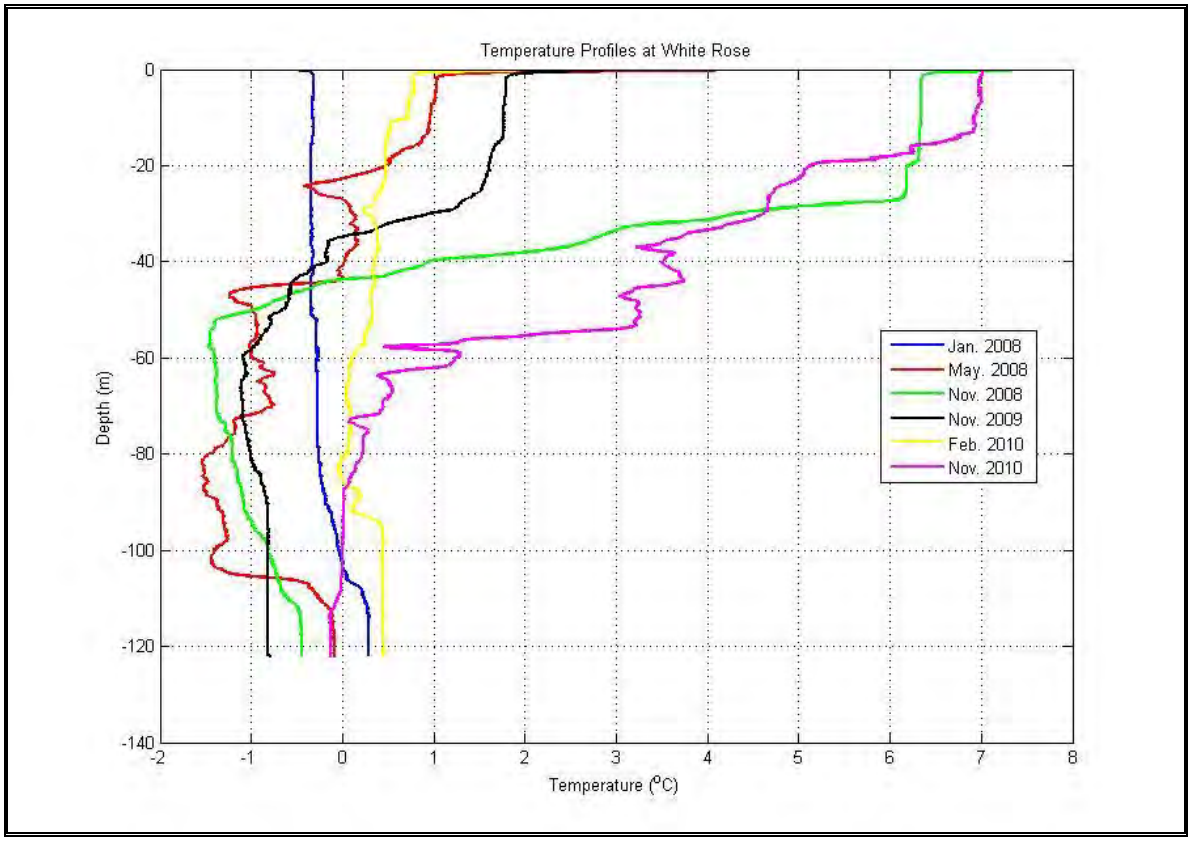

Figure 8.11 Temperature Profiles at White Rose

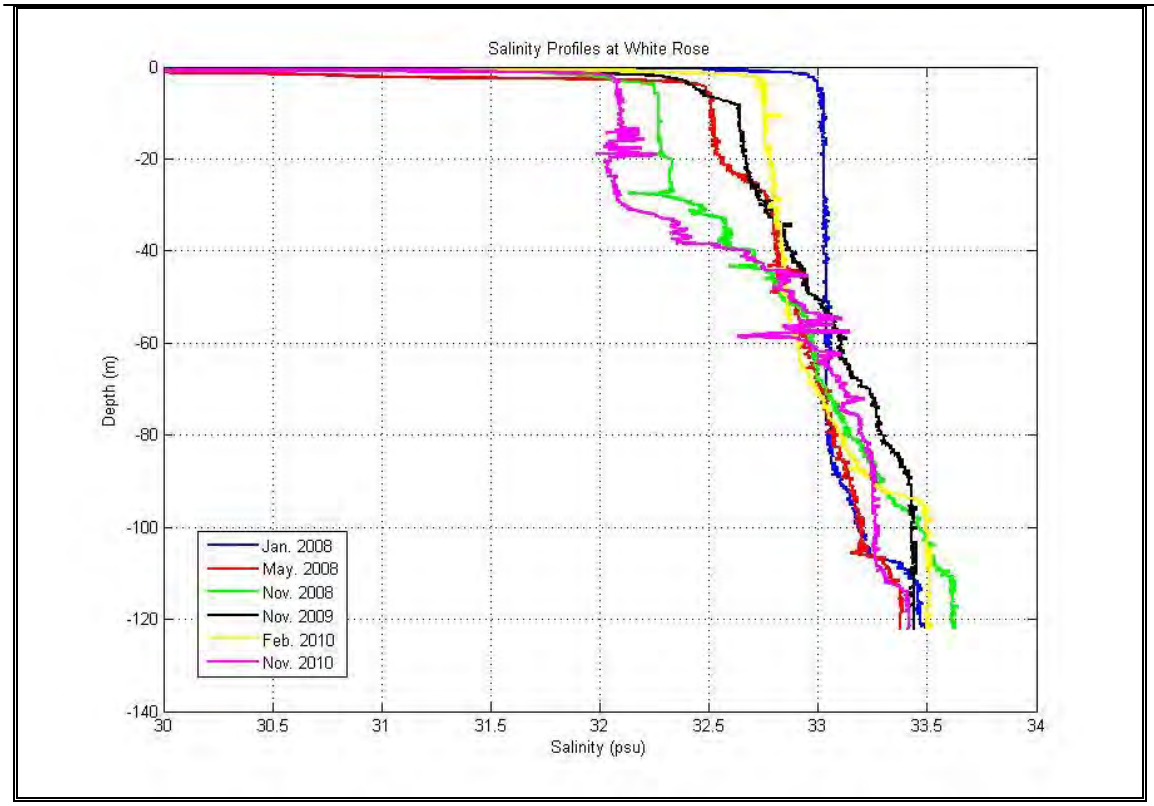

Figure 8.12 Salinity Profiles at White Rose

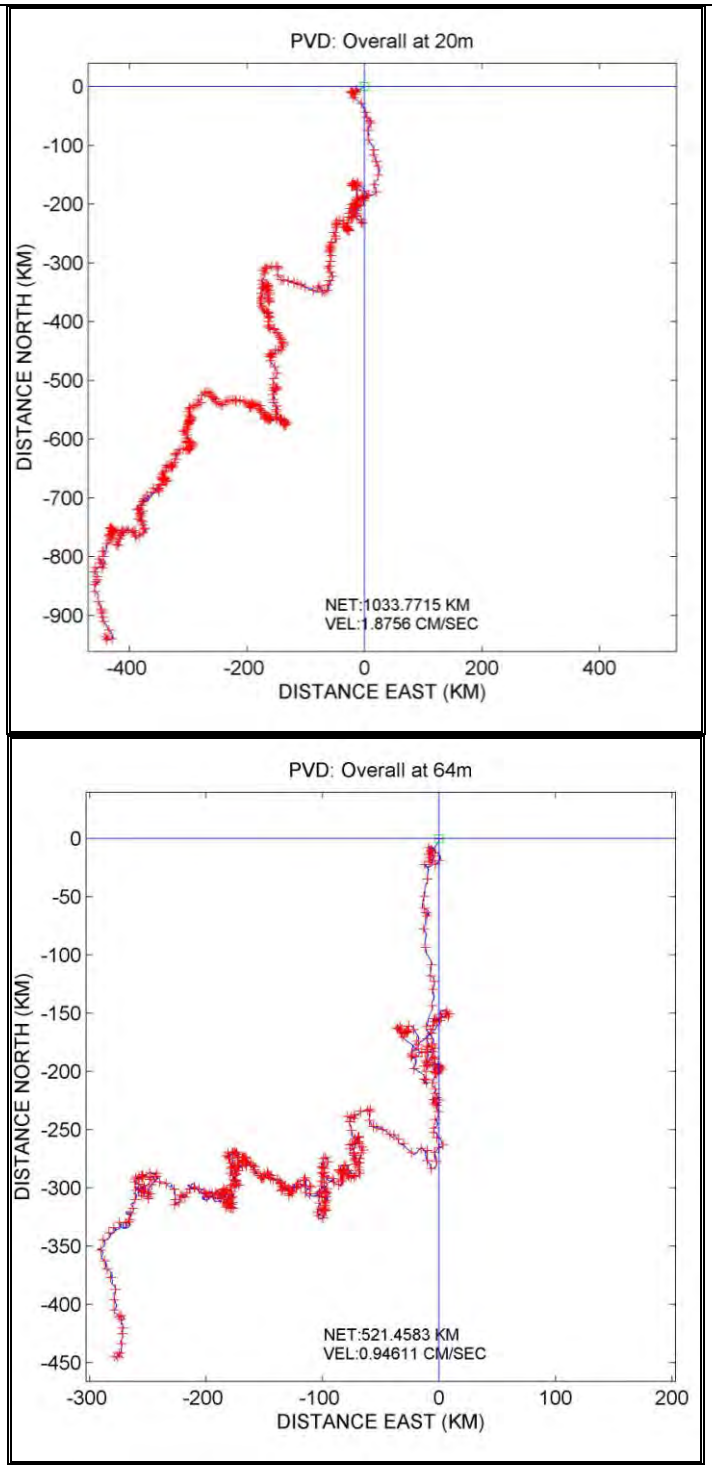

Figure 8.13 Progressive Vector Diagrams of Current Flow near the Surface and at Mid-depth during 2010 at White Rose

8.3.2 Seabird Microcat Data

Time series CTD data was also measured at White Rose from August 2007 to present. The time series data was collected at approximately 0.5 m below the surface, mid-depth, and at 4 m above bottom. The measurement depths were dependent upon where the Seabird instruments could be attached to the mooring configuration. Statistics on the data are presented in Table 8.3.

Table 8.3 Statistics of Temperature and Salinity in 2007

Near-Surface

AUGUST				
	mean	stdev	min	max
temp	10.55	2.13	1.54	14.00
sali	32.11	0.29	30.88	34.17
SEPTEMBER				
	mean	stdev	min	max
temp	10.50	3.15	0.61	14.28
sali	31.83	0.39	30.01	34.11
OCTOBER				
	mean	stdev	min	max
temp	7.92	2.70	-1.10	12.55
sali	31.98	0.31	30.73	34.06
NOVEMBER				
	mean	stdev	min	max
temp	6.15	1.08	0.75	8.65
sali	32.14	0.18	31.71	33.06
DECEMBER				
	mean	stdev	min	max
temp	2.15	1.90	0.38	6.44
sali	32.61	0.32	32.01	33.30
OVERALL				
	mean	stdev	min	max
Temp	6.00	4.42	-1.10	14.28
Sali	32.29	0.51	30.01	34.17

Mid-Depth

AUGUST				
	mean	stdev	min	max
temp	-0.91	0.67	-1.57	1.86
sali	33.28	0.06	33.08	33.56
SEPTEMBER				
	mean	stdev	min	max
temp	-1.15	0.31	-1.59	0.36
sali	33.28	0.07	33.14	33.55
OCTOBER				
	mean	stdev	min	max
temp	-1.19	0.20	-1.57	-0.22
sali	33.30	0.08	33.09	33.54
NOVEMBER				
	mean	stdev	min	max
temp	-0.99	0.27	-1.43	0.72
sali	33.32	0.06	33.07	33.52

DECEMBER				
	mean	stdev	min	max
temp	-0.61	0.43	-1.05	1.30
Sali	33.42	0.09	33.10	33.65
OVERALL				
	mean	stdev	min	max
temp	-1.02	0.41	-1.59	1.86
sali	33.31	0.08	33.07	33.65

Near-Bottom

AUGUST				
	mean	stdev	min	max
temp	-0.41	0.11	-0.60	-0.14
sali	33.36	0.03	33.25	33.47
SEPTEMBER				
	mean	stdev	min	max
temp	-0.51	0.16	-0.89	0.25
sali	33.34	0.08	33.19	33.74
OCTOBER				
	mean	stdev	min	max
temp	-0.39	0.26	-0.76	0.38
sali	33.42	0.15	33.17	33.83
NOVEMBER				
	mean	stdev	min	max
temp	-0.21	0.13	-0.72	0.07
sali	33.55	0.08	33.28	33.75
DECEMBER				
	mean	stdev	min	max
temp	0.05	0.41	-0.36	2.49
Sali	33.56	0.07	33.29	34.04
OVERALL				
	mean	stdev	min	max
temp	-0.21	0.36	-0.89	2.49
sali	33.46	0.13	33.17	34.09

Table 8.4 Statistics of Temperatures and Salinity in 2008

Near-Surface

JANUARY				
	mean	stdev	min	max
temp	0.00	0.11	-0.19	0.14
sali	33.00	0.03	32.94	33.05
FEBRUARY				
	mean	stdev	min	max
temp	-0.28	0.12	-0.54	0.11
sali	33.01	0.04	32.93	33.11
May				
	mean	stdev	min	max
temp	2.52	0.91	0.24	5.59
sali	32.45	0.04	32.34	32.82
JUNE				
	mean	stdev	min	max
temp	5.29	1.43	2.93	8.62
sali	32.46	0.08	32.29	32.77

JULY				
	mean	stdev	min	max
temp	10.90	1.68	7.60	14.39
sali	32.24	0.07	32.01	32.41
AUGUST				
	mean	stdev	min	max
temp	10.45	0.94	8.95	15.68
sali	32.27	0.08	31.88	32.37
SEPTEMBER				
	mean	stdev	min	max
temp	12.39	0.37	11.39	13.33
sali	32.10	0.14	31.83	32.41
OCTOBER				
	mean	stdev	min	max
temp	9.55	1.96	5.18	12.67
sali	32.04	0.13	31.78	32.37
NOVEMBER				
	mean	stdev	min	max
temp	6.94	0.48	5.90	8.68
sali	32.14	0.08	32.02	32.30
DECEMBER				
	mean	stdev	min	max
temp	4.35	1.98	1.33	7.44
sali	32.27	0.16	32.06	32.64

Mid-Depth

JANUARY				
	mean	stdev	min	max
temp	-0.11	0.04	-0.20	-0.05
sali	33.04	0.01	33.02	33.06
FEBRUARY				
	mean	stdev	min	max
temp	0.00	0.20	-0.44	0.68
sali	33.26	0.15	32.96	33.71
May				
	mean	stdev	min	max
temp	-1.19	0.27	-1.68	-0.31
sali	32.98	0.04	32.79	33.15
JUNE				
	mean	stdev	min	max
temp	-1.32	0.23	-1.68	-0.42
sali	33.10	0.08	32.90	33.39
JULY				
	mean	stdev	min	max
temp	-1.35	0.17	-1.62	-0.52
sali	33.11	0.06	32.88	33.36
AUGUST				
	mean	stdev	min	max
temp	-1.18	0.15	-1.49	0.24
sali	33.09	0.06	32.81	33.25
SEPTEMBER				
	mean	stdev	min	max
temp	-0.97	0.28	-1.48	1.07
sali	33.12	0.09	32.76	33.44
OCTOBER				
	mean	stdev	min	max

temp	-1.07	0.15	-1.34	-0.02
sali	33.13	0.08	32.84	33.44
NOVEMBER				
	mean	stdev	min	max
temp	-0.97	0.17	-1.45	-0.23
sali	33.11	0.09	32.79	33.42
DECEMBER				
	mean	stdev	min	max
temp	-0.41	0.74	-1.14	1.59
sali	33.04	0.18	32.55	33.32

Near-Bottom

JANUARY				
	mean	stdev	min	max
temp	0.34	0.25	0.22	1.11
sali	33.48	0.14	33.41	33.90
FEBRUARY				
	mean	stdev	min	max
temp	0.71	0.17	0.08	1.19
sali	33.69	0.09	33.39	33.93
MARCH				
	mean	stdev	min	max
temp	0.28	0.18	-0.08	0.72
sali	33.51	0.07	33.38	33.70
APRIL				
	mean	stdev	min	max
temp	0.08	0.15	-0.33	0.41
sali	33.43	0.04	33.35	33.55
MAY				
	mean	stdev	min	max
temp	0.09	0.05	-0.09	0.17
sali	33.41	0.01	33.38	33.43
JUNE				
	mean	stdev	min	max
temp	-0.36	0.20	-0.71	0.38
sali	33.43	0.10	33.26	33.76
JULY				
	mean	stdev	min	max
temp	-0.18	0.22	-0.74	0.30
sali	33.53	0.09	33.33	33.74
AUGUST				
	mean	stdev	min	max
temp	-0.28	0.16	-0.68	0.11
sali	33.55	0.07	33.31	33.67
SEPTEMBER				
	mean	stdev	min	max
temp	-0.28	0.13	-0.56	0.13
sali	33.60	0.07	33.40	33.79
OCTOBER				
	mean	stdev	min	max
temp	-0.40	0.11	-0.62	-0.07
sali	33.58	0.05	33.47	33.71
NOVEMBER				
	mean	stdev	min	max
temp	-0.51	0.09	-0.63	-0.24
sali	33.57	0.04	33.49	33.67

DECEMBER				
	mean	stdev	min	max
temp	-0.69	0.08	-0.86	-0.55
sali	33.44	0.08	33.28	33.56

Table 8.5 Statistics of Temperature and Salinity in 2009

Near-Surface

JANUARY				
	mean	stdev	min	max
temp	0.78	0.79	-0.62	2.66
sali	32.59	0.14	32.27	32.92
FEBRUARY				
	mean	stdev	min	max
temp	-0.50	0.12	-0.84	-0.21
sali	32.91	0.05	32.69	33.16
MARCH				
	mean	stdev	min	max
temp	-0.59	0.28	-1.27	0.00
sali	32.90	0.03	32.79	32.95
JUNE				
	mean	stdev	min	max
temp	5.31	1.72	2.90	8.57
sali	32.23	0.16	31.83	32.76
JULY				
	mean	stdev	min	max
temp	11.63	1.48	8.41	13.72
sali	31.99	0.09	31.78	32.43
AUGUST				
	mean	stdev	min	max
temp	12.94	1.67	8.13	14.96
sali	31.88	0.11	31.46	32.03
SEPTEMBER				
	mean	stdev	min	max
temp	10.04	0.61	8.65	11.05
sali	31.93	0.02	31.87	31.99

Mid-depth

JANUARY				
	mean	stdev	min	max
temp	0.21	0.52	-0.72	1.48
sali	32.82	0.13	32.54	33.24
FEBRUARY				
	mean	stdev	min	max
temp	-0.50	0.15	-0.83	0.30
sali	33.03	0.13	32.79	33.68
MARCH				
	mean	stdev	min	max
temp	-0.67	0.20	-1.34	-0.18
sali	32.93	0.04	32.74	33.11
APRIL				
	mean	stdev	min	max
temp	-1.25	0.31	-1.70	-0.60
sali	32.92	0.05	32.66	33.12

MAY				
	mean	stdev	min	max
temp	-1.25	0.29	-1.71	0.65
sali	32.90	0.07	32.51	33.14
JUNE				
	mean	stdev	min	max
temp	-1.58	0.08	-1.70	-1.20
sali	32.95	0.03	32.81	33.06
JULY				
	mean	stdev	min	max
temp	-1.56	0.08	-1.69	-1.25
sali	32.91	0.03	32.78	33.01
AUGUST				
	mean	stdev	min	max
temp	-1.59	0.06	-1.69	-1.30
sali	32.91	0.03	32.80	33.03
SEPTEMBER				
	mean	stdev	min	max
temp	-1.53	0.05	-1.66	-1.36
sali	32.91	0.04	32.76	33.02
NOVEMBER				
	mean	stdev	min	max
temp	1.46	0.42	-0.91	1.90
sali	32.94	0.11	32.66	33.26
DECEMBER				
	mean	stdev	min	max
temp	0.97	0.36	-0.15	1.91
sali	32.93	0.12	32.67	33.35

Near- Bottom

JANUARY				
	mean	stdev	min	max
temp	-0.58	0.15	-0.84	0.08
sali	33.24	0.06	33.07	33.46
FEBRUARY				
	mean	stdev	min	max
temp	-0.07	0.20	-0.41	0.62
sali	33.39	0.16	33.12	33.85
MARCH				
	mean	stdev	min	max
temp	-0.33	0.08	-0.48	-0.07
sali	33.27	0.05	33.15	33.36
APRIL				
	mean	stdev	min	max
temp	-0.61	0.14	-1.17	-0.40
sali	33.22	0.05	32.96	33.35
MAY				
	mean	stdev	min	max
temp	-0.78	0.07	-1.01	-0.63
sali	33.15	0.02	33.07	33.21
JUNE				
	mean	stdev	min	max
temp	-1.06	0.11	-1.30	-0.87
sali	33.16	0.03	33.12	33.26
JULY				

	mean	stdev	min	max
temp	-1.25	0.06	-1.34	-1.13
sali	33.10	0.02	33.07	33.15
AUGUST				
	mean	stdev	min	max
temp	-1.32	0.05	-1.47	-1.11
sali	33.07	0.03	33.02	33.26
SEPTEMBER				
	mean	stdev	min	max
temp	-1.36	0.03	-1.41	-1.31
sali	33.04	0.01	33.02	33.07
NOVEMBER				
	mean	stdev	min	max
temp	-0.53	0.22	-0.83	0.16
sali	33.50	0.04	33.39	33.62
DECEMBER				
	mean	stdev	min	max
temp	-0.27	0.52	-0.75	1.62
sali	33.46	0.13	33.24	33.97

Table 8.6 Statistics of Temperature and Salinity in 2010

Mid-depth

JANUARY				
	mean	stdev	min	max
temp	0.45	0.30	-0.02	0.93
sali	32.96	0.06	32.84	33.25
FEBRUARY				
	mean	stdev	min	max
temp	0.05	0.16	-0.29	0.44
sali	32.95	0.08	32.82	33.20
MARCH				
	mean	stdev	min	max
temp	0.25	0.23	-0.46	0.97
sali	32.96	0.12	32.79	33.57
APRIL				
	mean	stdev	min	max
temp	0.51	0.27	-0.16	.76
sali	32.88	0.09	32.52	33.27
MAY				
	mean	stdev	min	max
temp	0.50	0.27	-0.54	3.15
sali	32.88	0.09	32.50	33.61
JUNE				
	mean	stdev	min	max
temp	0.28	0.49	-0.39	4.67
sali	33.04	0.09	32.47	33.89
JULY				
	mean	stdev	min	max
temp	-0.12	0.43	-1.17	3.39
sali	32.66	0.51	31.00	33.43
AUGUST				
	mean	stdev	min	max
temp	-0.27	0.53	-1.22	2.96
sali	32.59	0.63	30.30	33.25

SEPTEMBER				
	mean	stdev	min	max
temp	-0.05	1.34	-1.28	7.13
sali	32.87	0.18	31.18	33.88
OCTOBER				
	mean	stdev	min	max
temp	1.59	1.22	-0.95	5.39
sali	32.66	0.22	31.52	34.10
NOVEMBER				
	mean	stdev	min	max
temp	2.56	1.34	-0.93	6.99
sali	32.60	0.28	31.40	33.78
OVERALL				
	mean	stdev	min	max
temp	0.44	1.02	-1.28	7.13
Sali	32.84	0.33	30.30	34.10

Near- Bottom

JANUARY				
	mean	stdev	min	max
temp	0.31	0.29	-0.42	0.95
sali	33.48	0.09	33.24	33.79
FEBRUARY				
	mean	stdev	min	max
temp	0.64	0.24	0.00	1.31
sali	33.56	0.09	33.33	33.87
MARCH				
	mean	stdev	min	max
temp	0.81	0.33	0.45	1.82
sali	33.61	0.15	33.40	34.09
APRIL				
	mean	stdev	min	max
temp	0.65	0.25	0.44	1.48
sali	33.46	0.13	33.34	33.92
MAY				
	mean	stdev	min	max
temp	0.63	0.10	0.46	0.82
sali	33.43	0.06	32.86	33.56
JUNE				
	mean	stdev	min	max
temp	0.69	0.08	0.48	0.80
sali	33.51	0.05	33.38	33.57
JULY				
	mean	stdev	min	max
temp	0.64	0.06	0.47	0.78
sali	33.51	0.03	33.44	33.58
AUGUST				
	mean	stdev	min	max
temp	0.52	0.05	0.35	0.63
sali	33.47	0.03	33.41	33.56
SEPTEMBER				
	mean	stdev	min	max
temp	0.29	0.20	-0.15	0.54
sali	33.44	0.05	33.32	33.54
OCTOBER				
	mean	stdev	min	max

temp	-0.06	0.10	-0.26	0.22
sali	33.33	0.03	33.29	33.41
NOVEMBER				
	mean	stdev	min	max
temp	0.00	0.55	-0.34	3.15
sali	33.40	0.13	33.24	34.06
OVERALL				
	mean	stdev	min	max
temp	0.48	0.36	-0.42	3.15
Sali	33.47	0.11	32.86	34.09

8.3.3 Extreme Values

The minimum temperatures at White Rose are a function of the freezing point of sea water that varies with salinity. Therefore, the minimum water temperature at White Rose would be approximately -1.8°C. The maximum temperatures were measured as 15.7°C, 7.1°C and 3.1°C at surface, mid-depth and near bottom, respectively. The maximum temperature for each month from 2008 to 2010 was fitted to a Gumbel distribution and the return periods calculated (Table 8.7).

Due to the wide variability in sea surface temperatures, the Gumbel distribution could not produce realistic maximum temperatures on only three years of data for near-surface waters at White Rose. The 1-year maximum of 22°C with a 95% prediction limit would be an extreme surface temperature for White Rose.

The salinity from surface to bottom can vary between 30.5% and 34.5%, and the density can vary between 1.023 kg/m^3 and 1.027 kg/m^3.

Table 8.7 Extreme Water Temperatures Estimates for White Rose

Near-Surface			
Return Periods	**Temperature (°C)**		
	Extreme Value	**Upper 80% Prediction Limit**	**Upper 95% Prediction Limit**
1 years	17	21	22
10 years	28	34	37
25 years	32	39	43
50 years	35	43	47
100 years	38	47	52

Note: These values are not realistic. Due to the wide variability in sea surface temperature, 3 years of data was not sufficient.

Mid-Depth			
Return Periods	**Temperature (°C)**		
	Extreme Value	**Upper 80% Prediction Limit**	**Upper 95% Prediction Limit**
1 years	4	5	6
10 years	8	10	11
25 years	10	12	13
50 years	11	13	15
100 years	12	15	16

Near-Bottom			
Return Periods	**Temperature (°C)**		
	Extreme Value	**Upper 80% Prediction Limit**	**Upper 95% Prediction Limit**
1 years	2	2	3
10 years	3	4	5
25 years	4	5	6
50 years	5	6	6
100 years	5	6	7

9.0 Sea Ice and Icebergs

The following section documents ice conditions at and around the White Rose development area. It has been produced to summarize ice conditions that could cause environmental loadings on any proposed production facility.

Sea ice and iceberg incursions at White Rose are not an annual event. However, the area has been subject to both sea ice and iceberg incursions every few years over the past forty years of records considered for this report.

This report provides descriptions of the various components of the ice regime and includes tables of mean, maximum and where applicable, extremes for each component.

9.1 Sea Ice

Sea ice in the area of White Rose can be classified as quite thins (30-70 cm) and is usually not continuous in terms of coverage. Floe sizes are typically from tens to hundred of metres in diameter. Sea ice is not an annual event but occurs every few years lasting from days to months.

White Rose is located near the edge of the Grand Banks and can be affected by the seasonal ice tongue created when sea ice is swept around the edge of the Grand Banks by the Labrador Current.

9.1.1 Terminology

Classification of ice commonly found in the waters along Canada‟s Eastern Seaboard according to internationally accepted terminology (Environment Canada, 2001).

Sea Ice

Any form of ice found at sea which has originated from the freezing of sea water.

A. Ages of Sea Ice

New Ice

A general term for recently formed ice which includes frazil ice, grease ice, slush and shuga. These types of ice are composed of ice crystals which are only weakly frozen together (if at all) and have a definite form only while they are afloat. In Canada, the term „new ice‟ is applied to all recently formed sea ice having thickness up to 10 cm. This includes ice rind, light nilas and dark nilas.

Frazil Ice – Fine spicules or plates of ice suspended in water.

Grease Ice – A later stage of freezing than Frazil Ice when crystals have coagulated to form a soupy layer on the surface. Grease ice reflects little light, giving the sea a matt appearance.

Slush – Snow which is saturated and mixed with water on land or ice surfaces, or as a viscous floating mass in water after a heavy snowfall.

Shuga – An accumulation of spongy white ice lumps, a few centimeters across; they are formed from grease ice or slush and sometimes from anchor ice rising to the surface.

Nilas

A thin elastic crust of ice, easily bending on the waves and swell and under pressure, thrusting in a pattern of interlocking „fingers" (finger rafting). Has a matt surface and may be subdivided into darl nilas and light nilas.

Dark Nilas – Nilas which is under 5 cm in thickness and is very dark in colour.

Light Nilas – Nilas which is more than 5 cm in thickness and rather lighter in colour than dark nilas.

Young Ice

Ice in the transition stage between nilas and first year ice, 10 -30 cm in thickness. May be subdivided into grey ice and grey-white ice.

Grey Ice

Young ice 10-15 cm thick. Less elastic than nilas and breaks in swell. Usually rafts under pressure.

Grey-white Ice

Young ice 15-30 cm thick. Under pressure is more likely to ridge than raft.

First-year Ice

Sea ice of not more than one winter"s growth, developing from young ice; thickness 30 cm to 2 m, and sometimes slightly more. May be subdivided into thin first-year ice/white ice, medium first-year ice and thick first-year ice.

Thin First-year Ice/white ice

First-year ice 30-70 cm thick. May be subdivided into thin first-year ice of the first stage 30-50 cm thick and thin first-year ice of the second stage 50-70 cm thick.

Medium First-year Ice

First-year ice 70-120 cm thick.

Thick First-year Ice

First-year ice over 120 cm thick.

Old Ice

Sea ice which has survived at least one summer"s melt. Most topographic features are smoother than first-year ice.

B. Concentration of Sea Ice

Concentration is the ratio expressed in tenths describing the amount of the sea surface covered by ice as a fraction of the whole area being considered. Total concentration includes all stages of development that are present, partial concentration may refer to the amount of a particular stage or a particular form of ice and represents only a part of the total. The following terms are used:

Compact Ice

Floating ice in which the concentration is 10/10 and no water is visible.

Consolidated Ice

Floating ice in which the concentration is 10/10 and the floes are frozen together.

Very Close Ice

Floating ice in which the concentration is 9/10 to less than 10/10.

Close Ice

Floating ice, in which the concentration is 7/10 to less than 8/10, composed of floes mostly in contact.

Open Ice

Floating ice in which the concentration is 4/10 to less than 6/10 with many leads and polynyas, and the floes are generally not in contact with one another.

Very Open Water

Floating ice in which the concentration is 1/10 to less than 3/10 and water preponderates over ice.

Open Water

A large area of freely navigable water in which sea ice is present in concentration less than 1/10. No ice of land origin is present.

Ice Free

No ice present.

Bergy Water

An area of freely navigable water in which ice of land origin is present in concentrations less than 1/10. There may be sea ice present, although the total concentration of all ice shall not exceed 1/10.

(Ice of land origin is defined as ice formed on land or in an ice shelf, found floating in water.)

C. *Forms of Sea Ice*

Ice Floe

Any relatively flat piece of sea ice 20 m or more across.

D. *Surface features of Sea Ice*

Rafted Ice

Type of deformed ice formed by one piece of ice overriding another.

Ridge

A line or wall of broken ice forced up by pressure. May be fresh or weathered. The submerged volume of broken ice under a ridge, forced downwards by pressure is termed an ***ice keel***.

9.1.2 Data Sources

There is a limited amount of data on pack ice characteristics for the Grand Banks. This applies to features such as: thickness, floe size, and the presence of ridge fragments and rafted ice. Most statistical data for ice conditions at White Rose have been derived from Canadian Ice Services (CIS) weekly ice charts and several early studies conducted to support development applications for both Hibernia and Terra Nova.

The CIS weekly data is now available in digital format but the data does not include floe size data. The data covers the years 1969 to 2010. Data points are spaced at 0.25 degrees latitude and longitude. In the tables and figures in this section of the report, plots with a value of 0.2 represents Bergy Water, 0.3 represents Open Water and a value of 9.7 represents an ice concentration of 9+ (tenths). Bergy water and Open water are taken as having trace amounts of ice.

The data points are shown in Table 9.1 and on the map in Figure 9.1.

Table 9.1 CIS Data Points

		Bearing from	Distance from
Latitude	Longitude	White Rose (° T)	White Rose (nm)
46.75N	48.00W	157.5	1.3
46.75N	47.75W	096.1	10.9
47.00N	48.25W	325.0	17.0
47.00N	48.00W	002.0	13.9
47.00N	47.75W	037.7	17.6

The PAL Ice Status Reports (produced daily in heavy ice/iceberg conditions) give a general sea ice drift direction from the CIS Sea Ice Drift Model. These are predictions only and not actual tracks.

Figure 9.1 Location of Data Points relative to the White Rose Field

9.1.3 Seasonal Ice Coverage

Yearly ice coverage around the White Rose Field is shown in Figure 9.2 from the CIS digital data base data. In the period 1980/81 to 1994/95, ice above trace amounts at all the data points occurred during twelve years. For the period 1995/96 to 2009/10 ice above trace amounts at all the data points occurred during four years. When ice did occur the maximum amount was between 2/10s and 9+/10s. At the point nearest the White Rose field for the period 1995/96 to 2009/10 ice above trace amounts occurred only once.

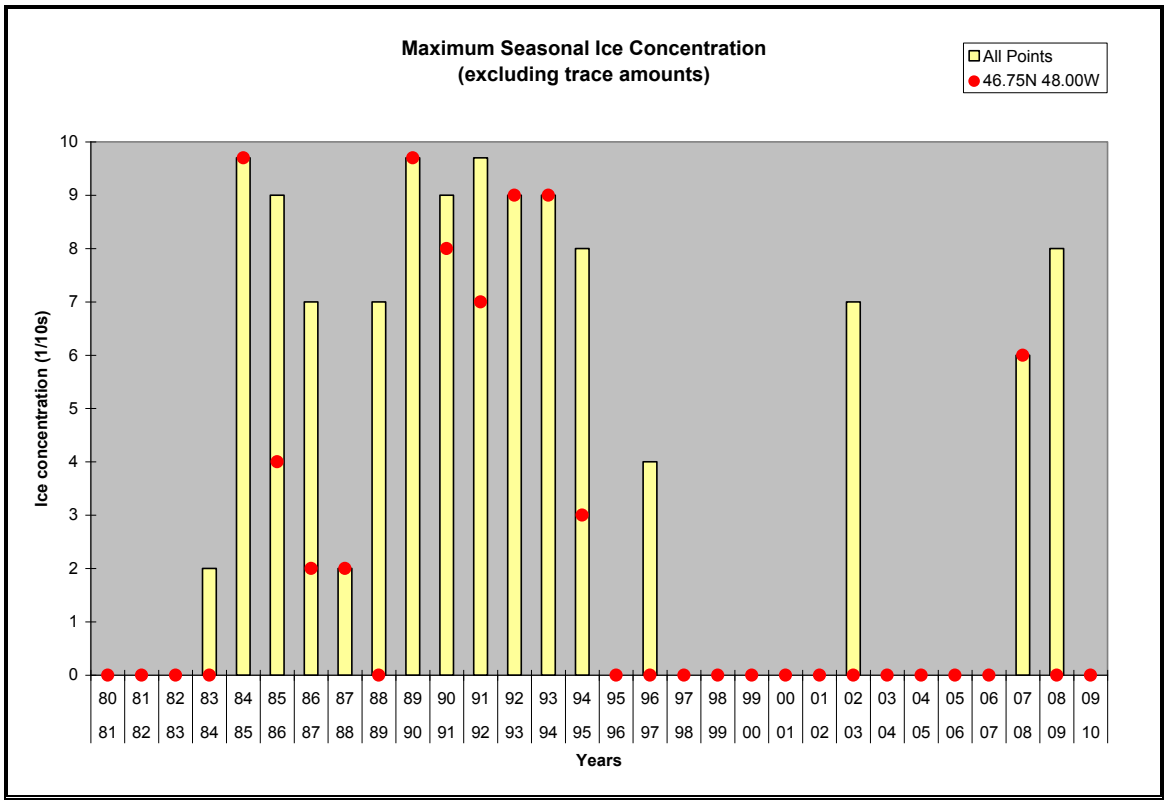

Figure 9.2 Seasonal Incursions of Sea Ice

9.1.4 Duration of Sea Ice Coverage near White Rose

Figure 9.3 shows the maximum weekly ice concentration at the data points from the CIS digital data base data. The first ice (above trace amounts) is reported in the chart issued in the week of the 15 January. The last reported ice is in the chart issued in the week of April 16th. Ice was reported in all the weeks in between these dates accept for the week starting January 29th. The longest period of continuous ice cover (above trace amounts) is 7 weeks reported at point 47.00°N;48.25°W for the season of 1984/85. The longest period from the first reported ice (above trace amounts) and the last reported ice is 14 weeks reported at point 47.00°N; 47.75°W for the season of 1992/93. Ice occurred for 7 of the weeks during the 14 week period.

Figure 9.4 to Figure 9.8 give the complete breakdown of sea ice at each of the data points using the data from the CIS digital data base. For the seasons 1980/81 to 2009/10 ice (above trace amounts) was reported at the data point closest to the White Rose field for eleven out of the thirty years. Out of those eleven years with ice, four of the years recorded maximum ice concentrations of 9/10s or more.

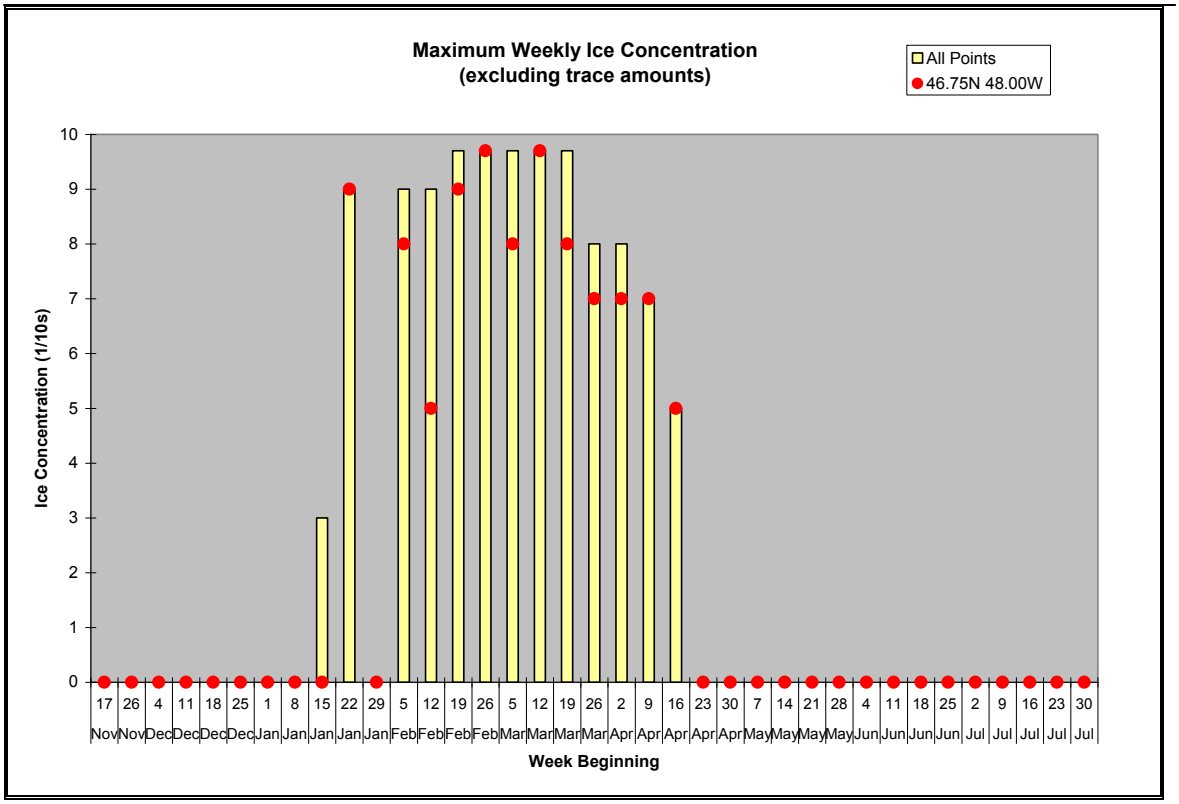

Figure 9.3 Weekly Incursions of Sea Ice

Figure 9.9 to Figure 9.18 show the 30-Year Frequency of Presence of Sea Ice for various weeks for the period of 1971 to 2000 and the period 1981 to 2010. The charts are taken from the Environment Canada Sea Ice Climatic Atlas"s produced by CIS. In the White Rose area the Frequency of Presence of Sea Ice is 1-15% for each week for each 30 year period, except for the week of March 19. For the week of March 19th the Presence of Sea Ice is 16-33% for the period 1971 to 2000 and 1 to 15% for the period 1981 to 2010.

The sea ice duration and concentration at White Rose is summarized in Tables 9.2 and 9.3. The mean sea ice duration was only 1.7 weeks over the 30 year period. On the average, sea ice occurs at White Rose in one out of every two years. Considering only the years when ice is present, the mean duration is 3.4 weeks.

Table 9.2 Sea Ice Duration at White Rose (all data points 1980-2010)

Mean	Maximum	Extreme
1.7 weeks	7 weeks	11 weeks

Table 9.3 Sea Ice Concentration at White Rose (all data points 1980-2010)

Mean	Maximum	Extreme
65 percent	95 percent	100 percent

	Season	1980 1981	1981 1982	1982 1983	1983 1984	1984 1985	1985 1986	1986 1987	1987 1988	1988 1989	1989 1990	1990 1991	1991 1992	1992 1993	1993 1994	1994 1995	1995 1996	1996 1997	1997 1998	1998 1999	1999 2000	2000 2001	2001 2002	2002 2003	2003 2004	2004 2005	2005 2006	2006 2007	2007 2008	2008 2009	2009 2010
Nov	17													0.2																	
Nov	26							0.2						0.2																	
Dec	4							0.2						0.2																	
Dec	11					0.2	0.2	0.2						0.2																	
Dec	18			0.3		0.2	0.2	0.2						0.2																	
Dec	25					0.2	0.2	0.2						0.2																	
Jan	1			0.2		0.2		0.2						0.2																	
Jan	8			0.2		0.2		0.2						0.2																	
Jan	15		0.3	0.2	0.2	0.2		0.2						0.2				0.2													
Jan	22			0.2	0.2	0.2	0.2	0.2						9																	
Jan	29		0.3	0.2		0.2	0.2	0.2				0.3		0.2					0.2												
Feb	5					8	0.2	0.2				0.2		6	0.3	0.2			0.2												
Feb	12		0.3	0.2		3		0.2		0.2	0.2	0.2	0.2	0.2	5	0.2			0.3												
Feb	19			0.2	0.3	0.2	0.3	0.2		0.2	7	0.2	0.2	0.2	9	0.2			0.2												
Feb	26			0.2		9.7	0.2	0.2		0.2	8	0.2	0.2	0.2	8	0.2		0.2	0.2				0.2								
Mar	5			0.2		8	0.2	3		0.2	0.2	0.3	7	0.2	0.2	0.2		0.2	0.2				0.2								
Mar	12			0.2		4				0.2	9.7	8	0.2	0.2	0.2	0.2		0.2	0.2		0.2	0.2	0.2	0.2						0.2	
Mar	19			0.2		0.2	4			0.2	8	3	0.2	0.2	3			0.2	0.2		0.2		0.2	0.2						0.2	
Mar	26				0.2	0.2	0.2			0.2	7	0.2	0.2	0.2	0.2	0.2		0.2	0.2		0.2		0.2	0.2					0.2	0.2	
Apr	2				0.2	7	0.2		2	0.2	7	0.2	0.2	2	0.2	0.2		0.2			0.2	0.2	0.2	0.2					6	0.2	
Apr	9		0.2	0.2	0.2	0.2	0.2		0.2	0.2	0.2	0.2	0.2	7	0.2	0.2	0.2	0.2			0.2		0.2	0.2	0.2				0.2	0.2	
Apr	16		0.2	0.2	0.2	0.2	0.2	0.2	0.2	0.2	0.2	0.2	0.2	5	0.2	0.2	0.2	0.2	0.2		0.2	0.2	0.2	0.2					0.2	0.2	
Apr	23		0.2	0.2	0.2	0.2	0.2	0.2	0.2	0.2	0.2	0.2	0.2	0.2	0.2	0.2	0.2	0.2	0.2		0.2		0.2	0.2	0.2				0.2	0.2	
Apr	30		0.2	0.2	0.2	0.2	0.2	0.2	0.2	0.2	0.2	0.2	0.2	0.2	0.2	0.2	0.2	0.2	0.2		0.2		0.2	0.2	0.2				0.2	0.2	
May	7		0.2	0.2	0.2	0.2	0.2	0.2	0.2	0.2	0.2	0.2	0.2	0.2	0.2	0.2	0.2	0.2	0.2		0.2	0.2	0.2	0.2	0.2				0.2	0.2	
May	14		0.3	0.2	0.2	0.2	0.2	0.2	0.2	0.2	0.2	0.2	0.2	0.2	0.2	0.2	0.2	0.2	0.2		0.2		0.2	0.2	0.2			0.2	0.2	0.2	
May	21		0.3	0.3	0.2	0.2	0.2	0.2	0.2	0.2	0.2	0.2	0.2	0.2	0.2	0.2	0.2	0.2	0.2		0.2	0.2	0.2	0.2				0.2	0.2	0.2	
May	28		0.2	0.2	0.2	0.2	0.2	0.2	0.2	0.2	0.2	0.2	0.2	0.2	0.2	0.2	0.2	0.2	0.2		0.2		0.2	0.2	0.2			0.2	0.2	0.2	
Jun	4			0.2	0.2	0.2	0.2	0.2	0.2	0.2	0.2	0.2	0.2	0.2	0.2	0.2	0.2	0.2	0.2		0.2		0.2	0.2	0.2			0.2	0.2	0.2	
Jun	11		0.2	0.2	0.2	0.2	0.2	0.2	0.2		0.2	0.2	0.2	0.2	0.2	0.2	0.2	0.2	0.2		0.2		0.2	0.2	0.2			0.2	0.2	0.2	
Jun	18		0.2	0.2	0.2	0.2			0.2		0.2	0.2	0.2	0.2	0.2	0.2	0.2		0.2		0.2		0.2	0.2	0.2			0.2	0.2	0.2	
Jun	25			0.2	0.2	0.2					0.2	0.2	0.2		0.2	0.2					0.2		0.2					0.2		0.2	
Jul	2			0.2	0.2	0.2					0.2	0.2	0.2								0.2	0.2	0.2					0.2		0.2	
Jul	9			0.2		0.2						0.2	0.2									0.2						0.2		0.2	
Jul	16					0.2						0.2	0.2															0.2			
Jul	23											0.2	0.2																		
Jul	30											0.2																			

Figure 9.4 Incursions of Sea Ice at Point 46.75N 48.00W

	Season	1980 1981	1981 1982	1982 1983	1983 1984	1984 1985	1985 1986	1986 1987	1987 1988	1988 1989	1989 1990	1990 1991	1991 1992	1992 1993	1993 1994	1994 1995	1995 1996	1996 1997	1997 1998	1998 1999	1999 2000	2000 2001	2001 2002	2002 2003	2003 2004	2004 2005	2005 2006	2006 2007	2007 2008	2008 2009	2009 2010
Nov	17													0.2																	
Nov	26							0.2						0.2																	
Dec	4							0.2						0.2																	
Dec	11					0.2	0.2	0.2						0.2																	
Dec	18			0.3		0.2	0.2	0.2						0.2																	
Dec	25					0.2	0.2	0.2						0.2																	
Jan	1			0.2		0.2		0.2						0.2																	
Jan	8			0.2		0.2								0.2																	
Jan	15		0.3	0.2	0.2	0.2		0.2						0.2																	
Jan	22			0.2	0.2	0.2	0.2	0.2						9																	
Jan	29		0.3	0.2		0.2	0.2	0.2				0.3		0.2					0.2												
Feb	5					8	0.2	0.2				9		6	0.3	0.2			0.2												
Feb	12		0.3	0.2		3		0.2		0.2	0.2	0.2	0.2	0.2	7	0.2			0.3												
Feb	19			0.2	0.3	0.2	0.3	0.2		0.2	0.2	0.2	0.2	0.2	9	0.2			0.2												
Feb	26			0.2	0.3	9.7	0.2	7		0.2	8	3	0.2	0.2	8	0.2		0.2	0.2												
Mar	5			0.2		8	0.2	0.2		0.2	0.2	0.3	7	0.2	8	0.2		0.2	0.2				0.2								
Mar	12			0.2		9				7	9.7	8	0.2	0.2	0.2			4	0.2		0.2	0.2	0.2	0.2						0.2	
Mar	19			0.2		0.2	9			0.2	8	3	0.2	0.2	0.2	3		0.2	0.2		0.2		0.2	7						0.2	
Mar	26				0.2	0.2	0.2			0.2	7	0.2	0.2	0.2	0.2	0.2		0.2	0.2		0.2		0.2	0.2					0.2	2	
Apr	2			0.2	0.2	7	0.2		2	0.2	7	0.2	0.2	8	0.2	0.2		0.2			0.2	0.2	0.2	0.2					6	0.2	
Apr	9		0.2	0.2	0.2	0.2	0.2		0.2	0.2	0.2	0.2	0.2	7	0.2	0.2	0.2	0.2			0.2		0.2	0.2	0.2				2	0.2	
Apr	16		0.2	0.2	0.2	0.2	0.2	0.2	0.2	0.2	0.2	0.2	0.2	5	0.2	0.2	0.2	0.2	0.2		0.2	0.2	0.2	0.2					0.2	0.2	
Apr	23		0.2	0.2	0.2	0.2	0.2	0.2	0.2	0.2	0.2	0.2	0.2	0.2	0.2	0.2	0.2	0.2	0.2		0.2		0.2	0.2	0.2				0.2	0.2	
Apr	30		0.2	0.2	0.2	0.2	0.2	0.2	0.2	0.2	0.2	0.2	0.2	0.2	0.2	0.2	0.2	0.2	0.2		0.2		0.2	0.2	0.2				0.2	0.2	
May	7		0.2	0.2	0.2	0.2	0.2	0.2	0.2	0.2	0.2	0.2	0.2	0.2	0.2	0.2	0.2	0.2	0.2		0.2	0.2	0.2	0.2	0.2				0.2	0.2	
May	14		0.3	0.2	0.2	0.2	0.2	0.2	0.2	0.2	0.2	0.2	0.2	0.2	0.2	0.2	0.2	0.2	0.2		0.2		0.2	0.2	0.2				0.2	0.2	
May	21		0.3	0.3	0.2	0.2	0.2	0.2	0.2	0.2	0.2	0.2	0.2	0.2	0.2	0.2	0.2	0.2	0.2		0.2	0.2	0.2	0.2				0.2	0.2	0.2	
May	28		0.2	0.2	0.2	0.2	0.2	0.2	0.2	0.2	0.2	0.2	0.2	0.2	0.2	0.2	0.2	0.2	0.2		0.2		0.2	0.2	0.2			0.2	0.2	0.2	
Jun	4			0.2	0.2	0.2	0.2	0.2	0.2	0.2	0.2	0.2	0.2	0.2	0.2	0.2	0.2	0.2	0.2		0.2		0.2	0.2	0.2				0.2	0.2	
Jun	11		0.2	0.2	0.2	0.2	0.2	0.2	0.2		0.2	0.2	0.2	0.2	0.2	0.2	0.2	0.2	0.2		0.2		0.2	0.2	0.2			0.2	0.2	0.2	
Jun	18		0.2	0.2	0.2	0.2			0.2		0.2	0.2	0.2	0.2	0.2	0.2	0.2		0.2		0.2		0.2	0.2	0.2			0.2	0.2	0.2	
Jun	25			0.2	0.2	0.2					0.2	0.2	0.2		0.2	0.2					0.2		0.2					0.2		0.2	
Jul	2			0.2	0.2	0.2					0.2	0.2	0.2								0.2	0.2	0.2					0.2		0.2	
Jul	9			0.2		0.2						0.2	0.2									0.2						0.2		0.2	
Jul	16					0.2						0.2	0.2															0.2			
Jul	23											0.2	0.2																		
Jul	30											0.2																			

Figure 9.5 Incursions of Sea Ice at Point 46.75N 47.75W

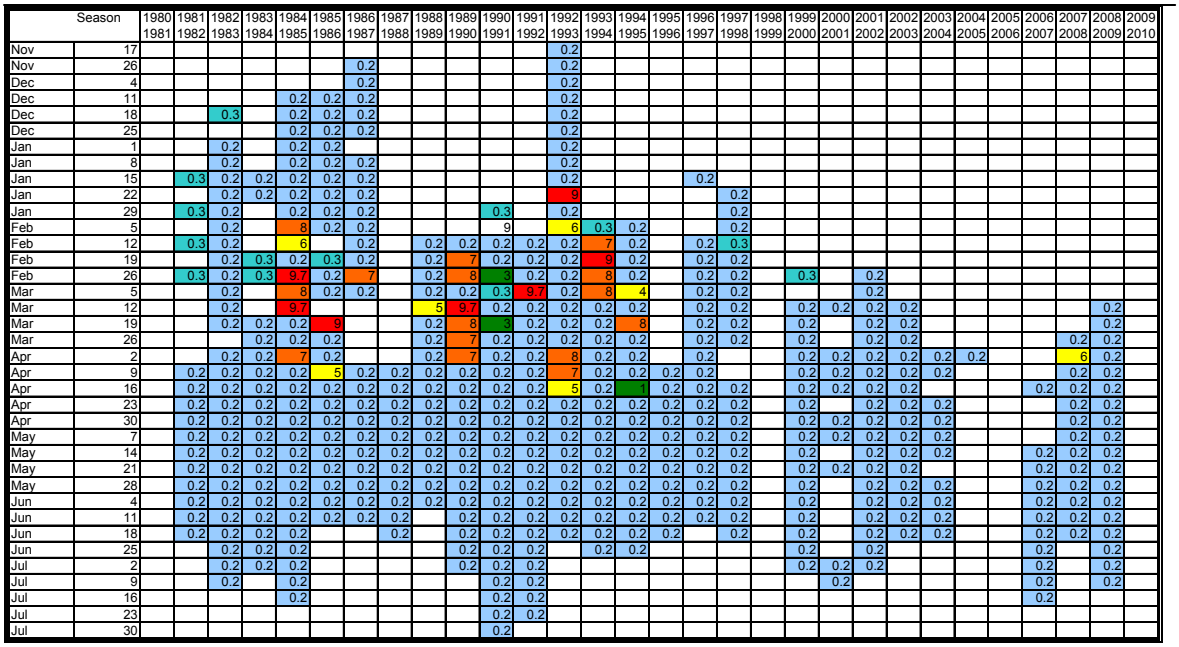

	Season	1980 1981	1981 1982	1982 1983	1983 1984	1984 1985	1985 1986	1986 1987	1987 1988	1988 1989	1989 1990	1990 1991	1991 1992	1992 1993	1993 1994	1994 1995	1995 1996	1996 1997	1997 1998	1998 1999	1999 2000	2000 2001	2001 2002	2002 2003	2003 2004	2004 2005	2005 2006	2006 2007	2007 2008	2008 2009	2009 2010
Nov	17													0.2																	
Nov	26							0.2						0.2																	
Dec	4							0.2						0.2																	
Dec	11					0.2	0.2	0.2						0.2																	
Dec	18			0.3		0.2	0.2	0.2						0.2																	
Dec	25					0.2	0.2	0.2						0.2																	
Jan	1			0.2		0.2	0.2							0.2																	
Jan	8			0.2		0.2	0.2	0.2						0.2																	
Jan	15		0.3	0.2	0.2	0.2	0.2	0.2						0.2				0.2													
Jan	22			0.2	0.2	0.2	0.2	0.2						9					0.2												
Jan	29		0.3	0.2		0.2	0.2	0.2				0.3		0.2					0.2												
Feb	5			0.2		8	0.2	0.2				9		6	0.3	0.2			0.2												
Feb	12		0.3	0.2		6		0.2		0.2	0.2	0.2	0.2	0.2	7	0.2		0.2	0.3												
Feb	19			0.2	0.3	0.2	0.3	0.2		0.2	7	0.2	0.2	0.2	9	0.2		0.2	0.2												
Feb	26		0.3	0.2	0.3	9.7	0.2	7		0.2	8	9	0.2	0.2	8	0.2		0.2	0.2		0.3		0.2								
Mar	5			0.2		8	0.2	0.2		0.2	0.2	0.3	9.7	0.2	8	4		0.2	0.2				0.2								
Mar	12			0.2		9.7				5	9.7	0.2	0.2	0.2	0.2	0.2		0.2	0.2		0.2	0.2	0.2	0.2					0.2	
Mar	19			0.2	0.2	0.2	9			0.2	8	9	0.2	0.2	0.2	8		0.2	0.2		0.2		0.2	0.2						0.2	
Mar	26				0.2	0.2	0.2			0.2	7	0.2	0.2	0.2	0.2	0.2		0.2	0.2		0.2		0.2	0.2					0.2	0.2	
Apr	2			0.2	0.2	7	0.2			0.2	7	0.2	0.2	8	0.2	0.2		0.2			0.2	0.2	0.2	0.2	0.2	0.2			6	0.2	
Apr	9	0.2	0.2	0.2	0.2	5	0.2	0.2	0.2	0.2	0.2	0.2	0.2	7	0.2	0.2	0.2	0.2			0.2	0.2	0.2	0.2	0.2				0.2	0.2	
Apr	16	0.2	0.2	0.2	0.2	0.2	0.2	0.2	0.2	0.2	0.2	0.2	0.2	5	0.2	1	0.2	0.2	0.2		0.2	0.2	0.2	0.2				0.2	0.2	0.2	
Apr	23	0.2	0.2	0.2	0.2	0.2	0.2	0.2	0.2	0.2	0.2	0.2	0.2	0.2	0.2	0.2	0.2	0.2	0.2		0.2		0.2	0.2	0.2				0.2	0.2	
Apr	30	0.2	0.2	0.2	0.2	0.2	0.2	0.2	0.2	0.2	0.2	0.2	0.2	0.2	0.2	0.2	0.2	0.2	0.2		0.2	0.2	0.2	0.2	0.2				0.2	0.2	
May	7	0.2	0.2	0.2	0.2	0.2	0.2	0.2	0.2	0.2	0.2	0.2	0.2	0.2	0.2	0.2	0.2	0.2	0.2		0.2	0.2	0.2	0.2	0.2				0.2	0.2	
May	14	0.2	0.2	0.2	0.2	0.2	0.2	0.2	0.2	0.2	0.2	0.2	0.2	0.2	0.2	0.2	0.2	0.2	0.2		0.2		0.2	0.2	0.2			0.2	0.2	0.2	
May	21	0.2	0.2	0.2	0.2	0.2	0.2	0.2	0.2	0.2	0.2	0.2	0.2	0.2	0.2	0.2	0.2	0.2	0.2		0.2	0.2	0.2	0.2				0.2	0.2	0.2	
May	28	0.2	0.2	0.2	0.2	0.2	0.2	0.2	0.2	0.2	0.2	0.2	0.2	0.2	0.2	0.2	0.2	0.2	0.2		0.2		0.2	0.2	0.2			0.2	0.2	0.2	
Jun	4	0.2	0.2	0.2	0.2	0.2	0.2	0.2	0.2	0.2	0.2	0.2	0.2	0.2	0.2	0.2	0.2	0.2	0.2		0.2		0.2	0.2	0.2			0.2	0.2	0.2	
Jun	11	0.2	0.2	0.2	0.2	0.2	0.2	0.2	0.2		0.2	0.2	0.2	0.2	0.2	0.2	0.2	0.2	0.2		0.2		0.2	0.2	0.2			0.2	0.2	0.2	
Jun	18	0.2	0.2	0.2	0.2			0.2		0.2	0.2	0.2	0.2	0.2	0.2	0.2		0.2			0.2		0.2	0.2	0.2			0.2	0.2	0.2	
Jun	25		0.2	0.2	0.2					0.2	0.2	0.2	0.2		0.2	0.2					0.2		0.2					0.2		0.2	
Jul	2		0.2	0.2	0.2					0.2	0.2	0.2									0.2	0.2	0.2					0.2		0.2	
Jul	9		0.2		0.2							0.2	0.2									0.2						0.2		0.2	
Jul	16				0.2							0.2	0.2															0.2			
Jul	23											0.2	0.2																		
Jul	30											0.2																			

Figure 9.6 Incursions of Sea Ice at Point 47.00N 48.00W

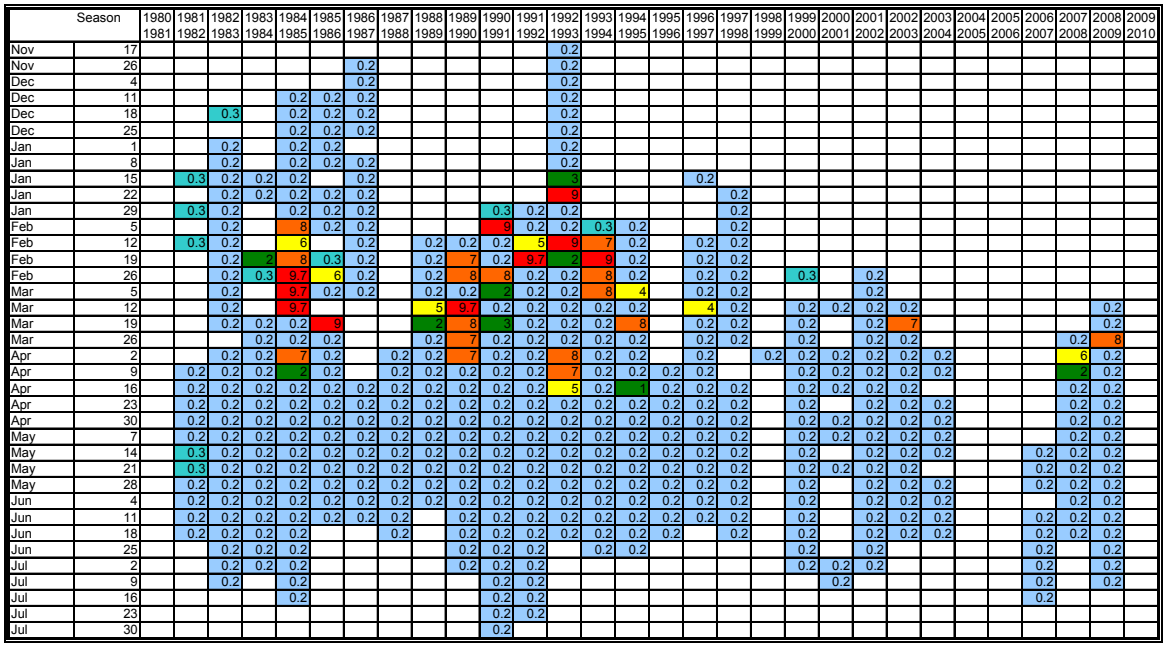

	Season	1980 1981	1981 1982	1982 1983	1983 1984	1984 1985	1985 1986	1986 1987	1987 1988	1988 1989	1989 1990	1990 1991	1991 1992	1992 1993	1993 1994	1994 1995	1995 1996	1996 1997	1997 1998	1998 1999	1999 2000	2000 2001	2001 2002	2002 2003	2003 2004	2004 2005	2005 2006	2006 2007	2007 2008	2008 2009	2009 2010
Nov	17													0.2																	
Nov	26							0.2						0.2																	
Dec	4							0.2						0.2																	
Dec	11					0.2	0.2	0.2						0.2																	
Dec	18			0.3		0.2	0.2	0.2						0.2																	
Dec	25					0.2	0.2	0.2						0.2																	
Jan	1			0.2		0.2	0.2							0.2																	
Jan	8			0.2		0.2	0.2	0.2						0.2																	
Jan	15		0.3	0.2	0.2	0.2		0.2						3				0.2													
Jan	22			0.2	0.2	0.2	0.2	0.2						9					0.2												
Jan	29		0.3	0.2		0.2	0.2	0.2				0.3	0.2	0.2					0.2												
Feb	5			0.2		8	0.2	0.2				9	0.2	0.2	0.3	0.2			0.2												
Feb	12		0.3	0.2		6		0.2		0.2	0.2	0.2	5	9	7	0.2		0.2	0.2												
Feb	19			0.2	2	8	0.3	0.2		0.2	7	0.2	9.7	2	9	0.2		0.2	0.2												
Feb	26			0.2	0.3	9.7	6	0.2		0.2	8	8	0.2	0.2	8	0.2		0.2	0.2		0.3		0.2								
Mar	5			0.2		9.7	0.2	0.2		0.2	0.2	2	0.2	0.2	8	4		0.2	0.2				0.2								
Mar	12			0.2		9.7				5	9.7	0.2	0.2	0.2	0.2	0.2		4	0.2		0.2	0.2	0.2	0.2					0.2	
Mar	19			0.2	0.2	0.2	9			2	8	9	0.2	0.2	0.2	8		0.2	0.2		0.2		0.2	7						0.2	
Mar	26				0.2	0.2	0.2			0.2	7	0.2	0.2	0.2	0.2	0.2		0.2	0.2		0.2		0.2	0.2					0.2	8	
Apr	2			0.2	0.2	7	0.2		0.2	0.2	7	0.2	0.2	8	0.2	0.2		0.2		0.2	0.2	0.2	0.2	0.2	0.2				6	0.2	
Apr	9	0.2	0.2	0.2	2	0.2		0.2	0.2	0.2	0.2	0.2	0.2	7	0.2	0.2	0.2	0.2			0.2	0.2	0.2	0.2	0.2				2	0.2	
Apr	16	0.2	0.2	0.2	0.2	0.2	0.2	0.2	0.2	0.2	0.2	0.2	0.2	5	0.2	1	0.2	0.2	0.2		0.2	0.2	0.2	0.2				0.2	0.2	0.2	
Apr	23	0.2	0.2	0.2	0.2	0.2	0.2	0.2	0.2	0.2	0.2	0.2	0.2	0.2	0.2	0.2	0.2	0.2	0.2		0.2		0.2	0.2	0.2				0.2	0.2	
Apr	30	0.2	0.2	0.2	0.2	0.2	0.2	0.2	0.2	0.2	0.2	0.2	0.2	0.2	0.2	0.2	0.2	0.2	0.2		0.2	0.2	0.2	0.2	0.2				0.2	0.2	
May	7	0.2	0.2	0.2	0.2	0.2	0.2	0.2	0.2	0.2	0.2	0.2	0.2	0.2	0.2	0.2	0.2	0.2	0.2		0.2	0.2	0.2	0.2	0.2				0.2	0.2	
May	14	0.3	0.2	0.2	0.2	0.2	0.2	0.2	0.2	0.2	0.2	0.2	0.2	0.2	0.2	0.2	0.2	0.2	0.2		0.2		0.2	0.2	0.2		0.2	0.2	0.2	0.2	
May	21	0.3	0.2	0.2	0.2	0.2	0.2	0.2	0.2	0.2	0.2	0.2	0.2	0.2	0.2	0.2	0.2	0.2	0.2		0.2	0.2	0.2	0.2			0.2	0.2	0.2	0.2	
May	28	0.2	0.2	0.2	0.2	0.2	0.2	0.2	0.2	0.2	0.2	0.2	0.2	0.2	0.2	0.2	0.2	0.2	0.2		0.2		0.2	0.2	0.2		0.2	0.2	0.2	0.2	
Jun	4	0.2	0.2	0.2	0.2	0.2	0.2	0.2	0.2	0.2	0.2	0.2	0.2	0.2	0.2	0.2	0.2	0.2	0.2		0.2		0.2	0.2	0.2				0.2	0.2	
Jun	11	0.2	0.2	0.2	0.2	0.2	0.2	0.2		0.2	0.2	0.2	0.2	0.2	0.2	0.2	0.2	0.2	0.2		0.2		0.2	0.2	0.2		0.2	0.2	0.2	0.2	
Jun	18	0.2	0.2	0.2	0.2			0.2		0.2	0.2	0.2	0.2	0.2	0.2	0.2	0.2		0.2		0.2		0.2	0.2	0.2		0.2	0.2	0.2		
Jun	25		0.2	0.2	0.2					0.2	0.2	0.2	0.2		0.2	0.2					0.2		0.2					0.2		0.2	
Jul	2		0.2	0.2	0.2					0.2	0.2	0.2									0.2	0.2	0.2					0.2		0.2	
Jul	9		0.2		0.2							0.2	0.2									0.2						0.2		0.2	
Jul	16				0.2							0.2	0.2															0.2			
Jul	23											0.2	0.2																		
Jul	30											0.2																			

Figure 9.7 Incursions of Sea Ice at Point 47.00N 47.75W

	Season	1980 1981	1981 1982	1982 1983	1983 1984	1984 1985	1985 1986	1986 1987	1987 1988	1988 1989	1989 1990	1990 1991	1991 1992	1992 1993	1993 1994	1994 1995	1995 1996	1996 1997	1997 1998	1998 1999	1999 2000	2000 2001	2001 2002	2002 2003	2003 2004	2004 2005	2005 2006	2006 2007	2007 2008	2008 2009	2009 2010
Nov	17													0.2																	
Nov	26							0.2						0.2																	
Dec	4							0.2						0.2																	
Dec	11					0.2	0.2	0.2						0.2																	
Dec	18			0.3		0.2	0.2	0.2						0.2																	
Dec	25					0.2	0.2	0.2						0.2																	
Jan	1			0.2		0.2	0.2							0.2																	
Jan	8			0.2		0.2	0.2	0.2						0.2																	
Jan	15		0.3	0.2	0.2	0.2	0.2	0.2						0.2				0.2													
Jan	22			0.2	0.2	0.2	0.2	0.2						9					0.2												
Jan	29		0.3	0.2		0.2	0.2	0.2				0.3		0.2					0.2												
Feb	5			0.2		8	0.2	0.2			0.3	0.2		6	0.3	0.2			0.2												
Feb	12		0.3	0.2		6		0.2		0.2	0.2	0.2	0.2	0.2	7	0.2		0.2	0.3												
Feb	19			0.2	0.3	2	0.3	0.2		0.2	7	0.2	0.2	0.2	9	0.2		0.2	0.2												
Feb	26		0.3	0.2	0.3	9.7	0.2	0.2		0.2	8	0.2	0.2	0.2	8	0.2		0.2	0.2		0.3		0.2								
Mar	5			0.2		8	0.2	2		0.2	0.2	2	7	0.2	8	4		0.2	0.2				0.2								
Mar	12			0.2		4		0.2		7	9.7	0.2	0.2	0.2	0.2	0.2		0.2	0.2		0.2	0.2	0.2	0.2						0.2	
Mar	19			0.2	0.2	9.7	4			0.2	8	3	0.2	0.2	0.2	8		0.2	0.2		0.2		0.2	0.2		0.2				0.2	
Mar	26				0.2	0.2	0.2			0.2	7	0.2	0.2	0.2	0.2	0.2		0.2	0.2		0.2	0.2	0.2	0.2					0.2	0.2	
Apr	2			0.2	0.2	7	0.2		2	0.2	7	0.2	0.2	2	0.2	1		0.2			0.2	0.2	0.2	0.2	0.2	0.2			0.2	0.2	
Apr	9		0.2	0.2	0.2	0.2	5	0.2	0.2	0.2	0.2	0.2	0.2	7	0.2	0.2	0.2	0.2			0.2	0.2	0.2	0.2	0.2				0.2	0.2	
Apr	16		0.2	0.2	0.2	0.2	0.2	0.2	0.2	0.2	0.2	0.2	0.2	5	0.2	0.2	0.2	0.2	0.2		0.2	0.2	0.2	0.2				0.2	0.2	0.2	
Apr	23		0.2	0.2	0.2	0.2	0.2	0.2	0.2	0.2	0.2	0.2	0.2	0.2	0.2	0.2	0.2	0.2	0.2		0.2		0.2	0.2	0.2				0.2	0.2	
Apr	30		0.2	0.2	0.2	0.2	0.2	0.2	0.2	0.2	0.2	0.2	0.2	0.2	0.2	0.2	0.2	0.2	0.2		0.2	0.2	0.2	0.2	0.2				0.2	0.2	
May	7		0.2	0.2	0.2	0.2	0.2	0.2	0.2	0.2	0.2	0.2	0.2	0.2	0.2	0.2	0.2	0.2	0.2		0.2	0.2	0.2	0.2	0.2				0.2	0.2	
May	14		0.3	0.2	0.2	0.2	0.2	0.2	0.2	0.2	0.2	0.2	0.2	0.2	0.2	0.2	0.2	0.2	0.2		0.2	0.2	0.2	0.2	0.2			0.2	0.2	0.2	
May	21		0.3	0.3	0.2	0.2	0.2	0.2	0.2	0.2	0.2	0.2	0.2	0.2	0.2	0.2	0.2	0.2	0.2		0.2	0.2	0.2	0.2	0.2			0.2	0.2	0.2	
May	28		0.2	0.2	0.2	0.2	0.2	0.2	0.2	0.2	0.2	0.2	0.2	0.2	0.2	0.2	0.2	0.2	0.2		0.2		0.2	0.2	0.2			0.2	0.2	0.2	
Jun	4		0.2	0.2	0.2	0.2	0.2	0.2	0.2	0.2	0.2	0.2	0.2	0.2	0.2	0.2	0.2	0.2	0.2		0.2		0.2	0.2	0.2			0.2	0.2	0.2	
Jun	11		0.2	0.2	0.2	0.2	0.2	0.2	0.2		0.2	0.2	0.2	0.2	0.2	0.2	0.2	0.2	0.2		0.2		0.2	0.2	0.2			0.2	0.2	0.2	
Jun	18		0.2	0.2	0.2	0.2			0.2		0.2	0.2	0.2	0.2	0.2	0.2	0.2		0.2		0.2		0.2	0.2	0.2			0.2	0.2	0.2	
Jun	25			0.2	0.2	0.2					0.2	0.2	0.2		0.2	0.2					0.2		0.2					0.2		0.2	
Jul	2			0.2	0.2	0.2					0.2	0.2	0.2								0.2	0.2	0.2					0.2		0.2	
Jul	9			0.2		0.2						0.2	0.2									0.2						0.2		0.2	
Jul	16					0.2						0.2	0.2															0.2			
Jul	23											0.2	0.2																		
Jul	30											0.2																			

Figure 9.8 Incursions of Sea Ice at Point 47.00N 48.25W

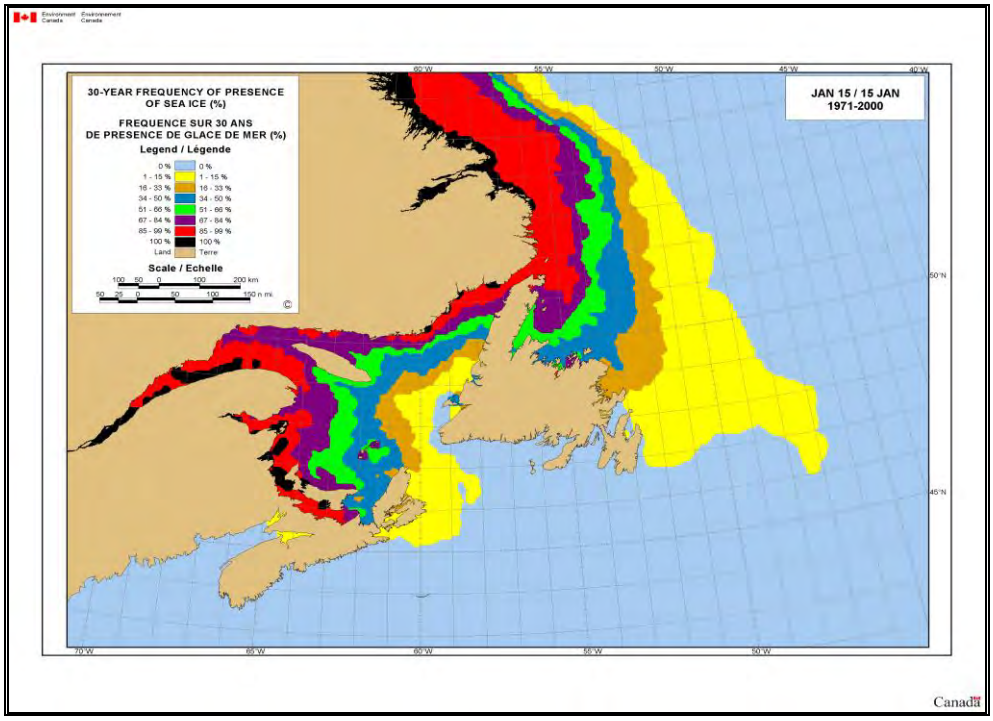

Figure 9.9 30-Year Frequency of Presence of Sea Ice (%) (January 15, 1971 - 2000)

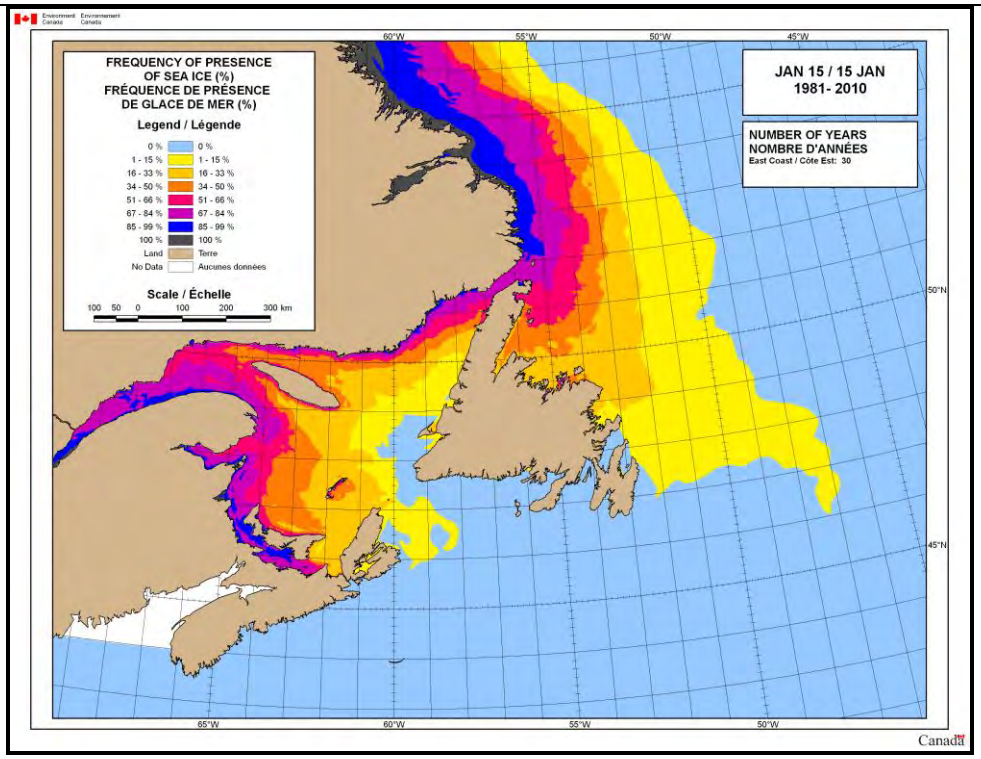

Figure 9.10 30-Year Frequency of Presence of Sea Ice (%) (January 15, 1981 - 2010)

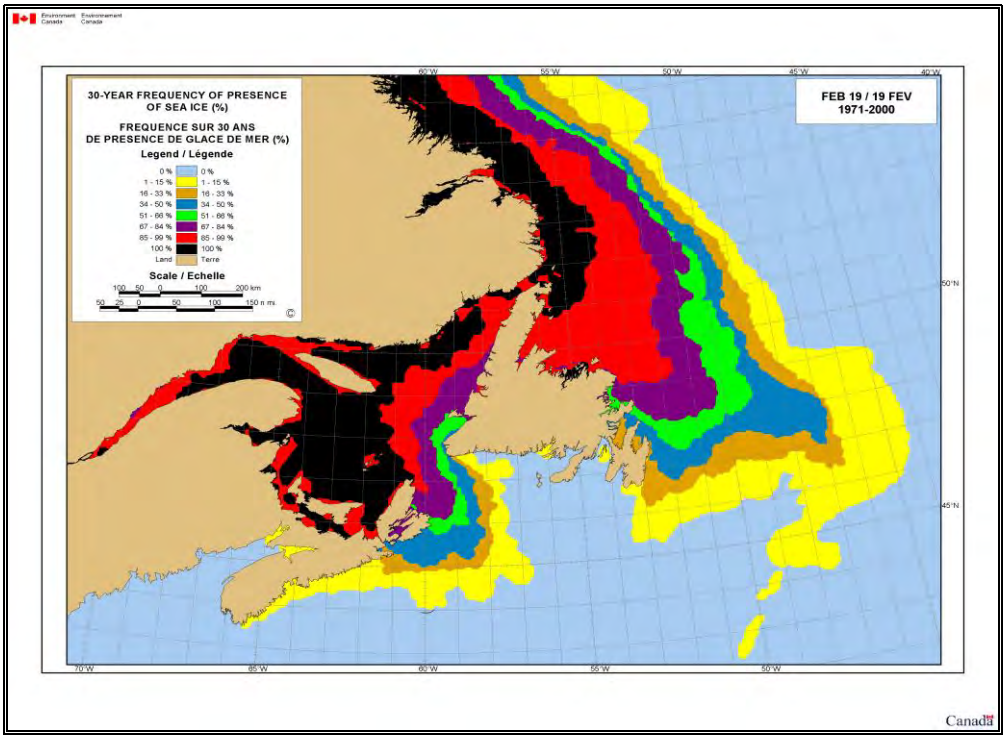

Figure 9.11 30-Year Frequency of Presence of Sea Ice (%) (February 19, 1971 - 2000)

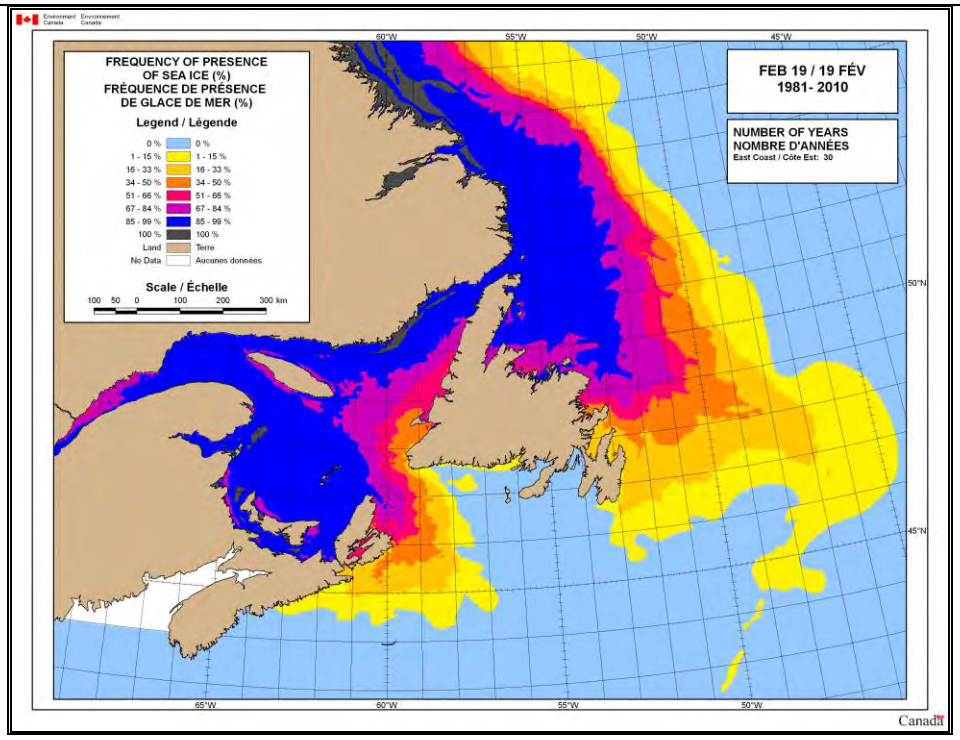

Figure 9.12 30-Year Frequency of Presence of Sea Ice (%) (February 19, 1981 - 2010)

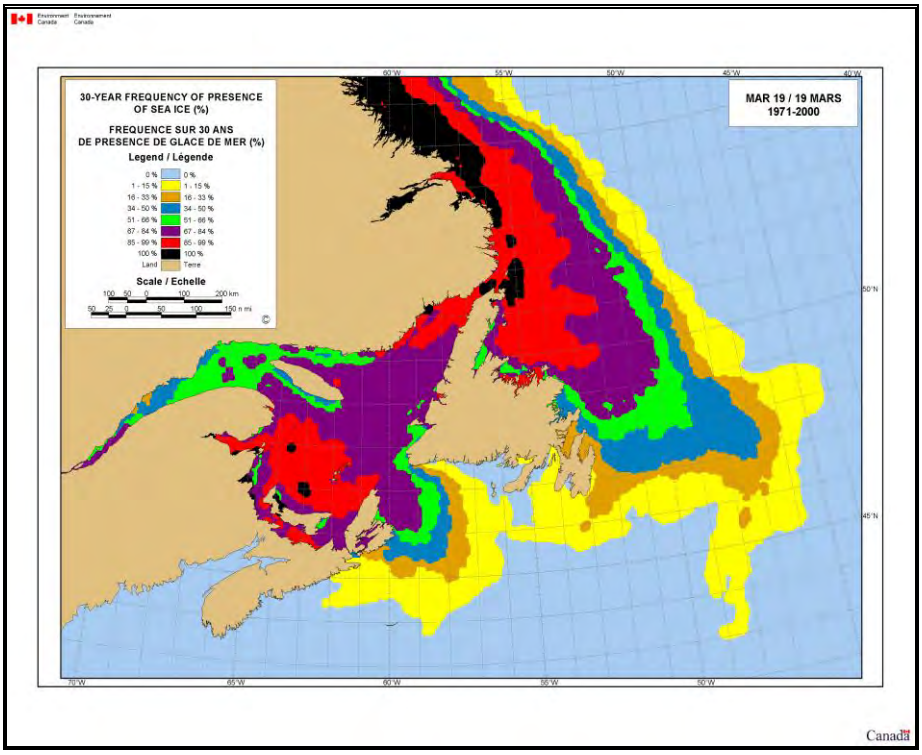

Figure 9.13 30-Year Frequency of Presence of Sea Ice (%) (March 19, 1971 - 2000)

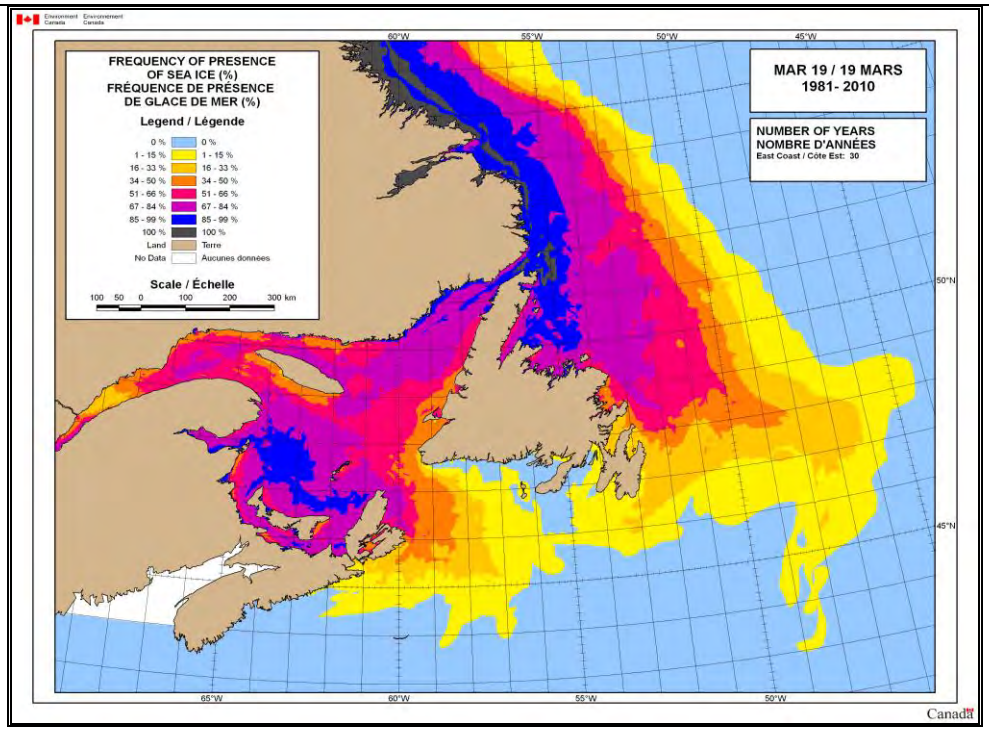

Figure 9.14 30-Year Frequency of Presence of Sea Ice (%) (March 19, 1981 - 2010)

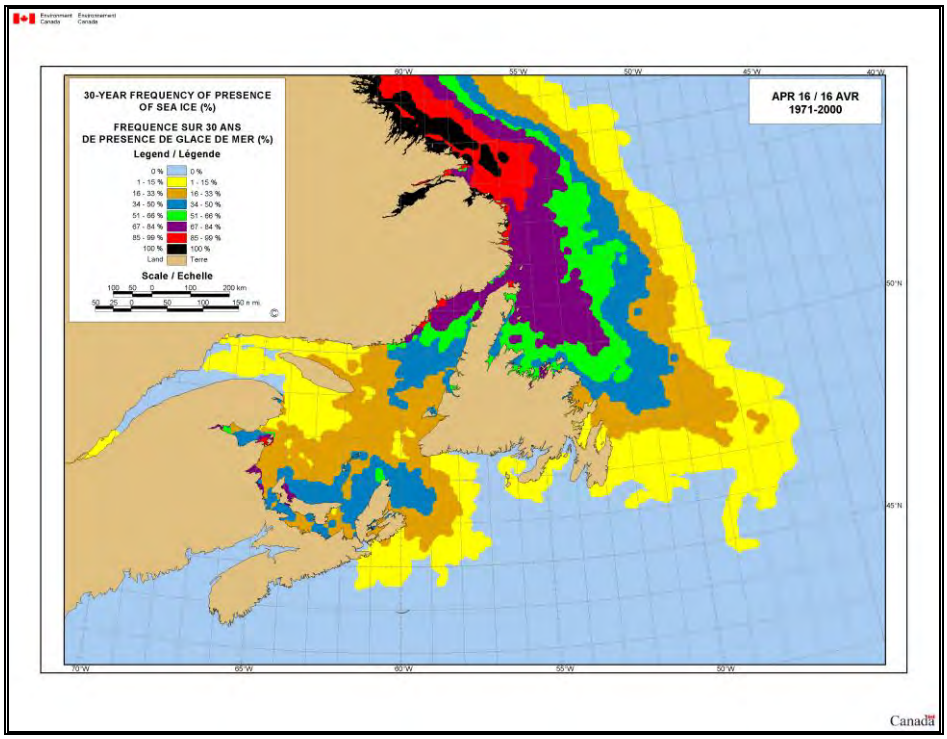

Figure 9.15 30-Year Frequency of Presence of Sea Ice (%) (April 16, 1971 - 2000)

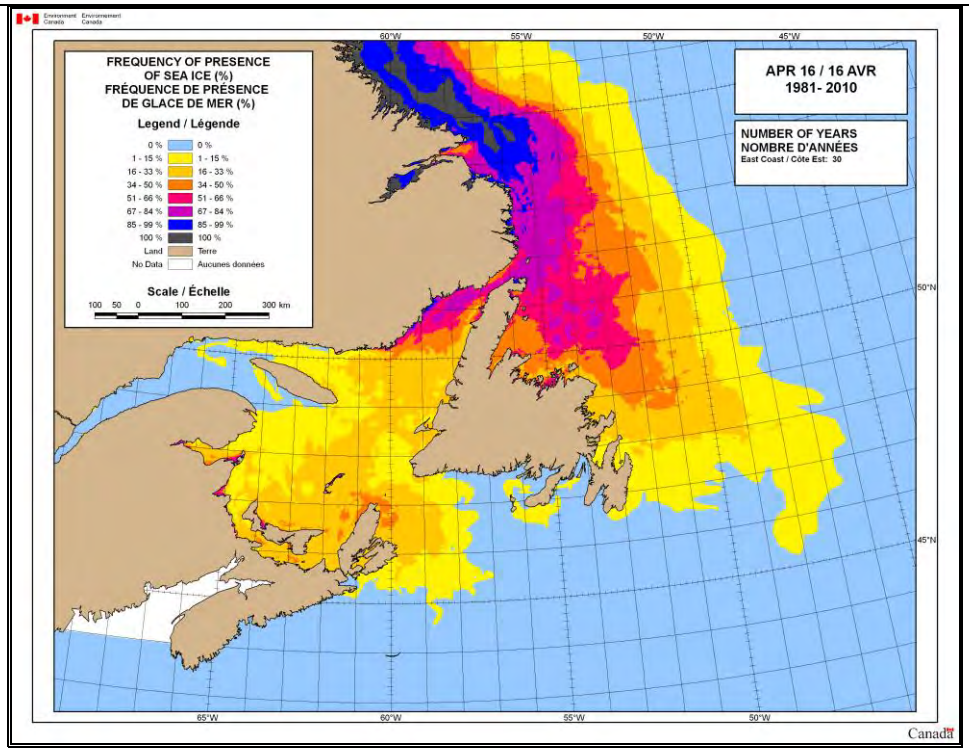

Figure 9.16 30-Year Frequency of Presence of Sea Ice (%) (April 16, 1981 - 2010)

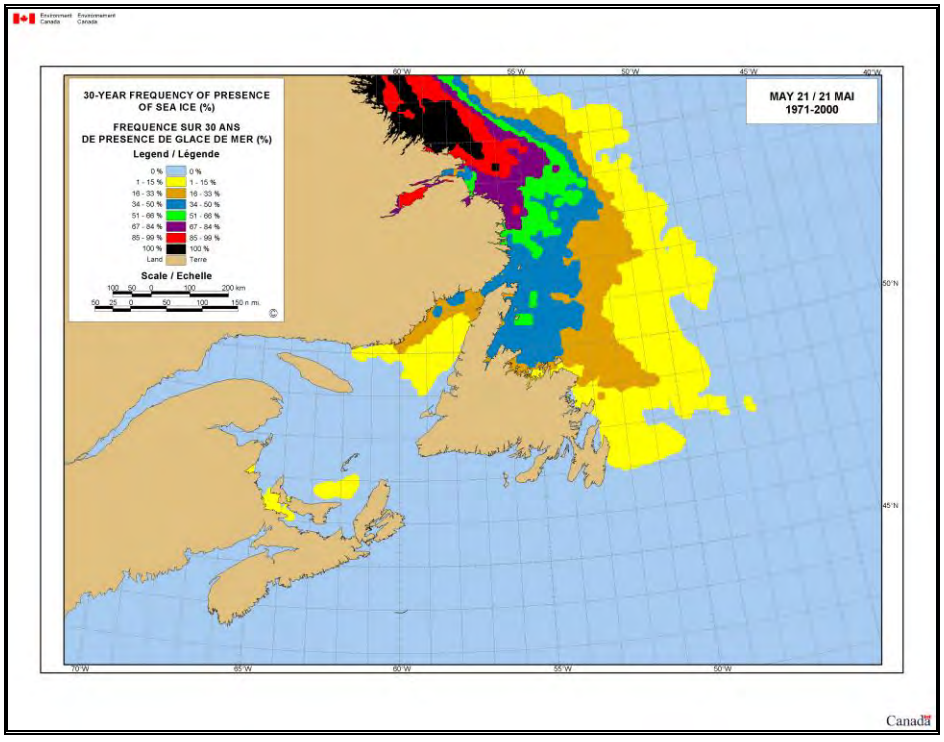

Figure 9.17 30-Year Frequency of Presence of Sea Ice (%) (May 21, 1971 - 2000)

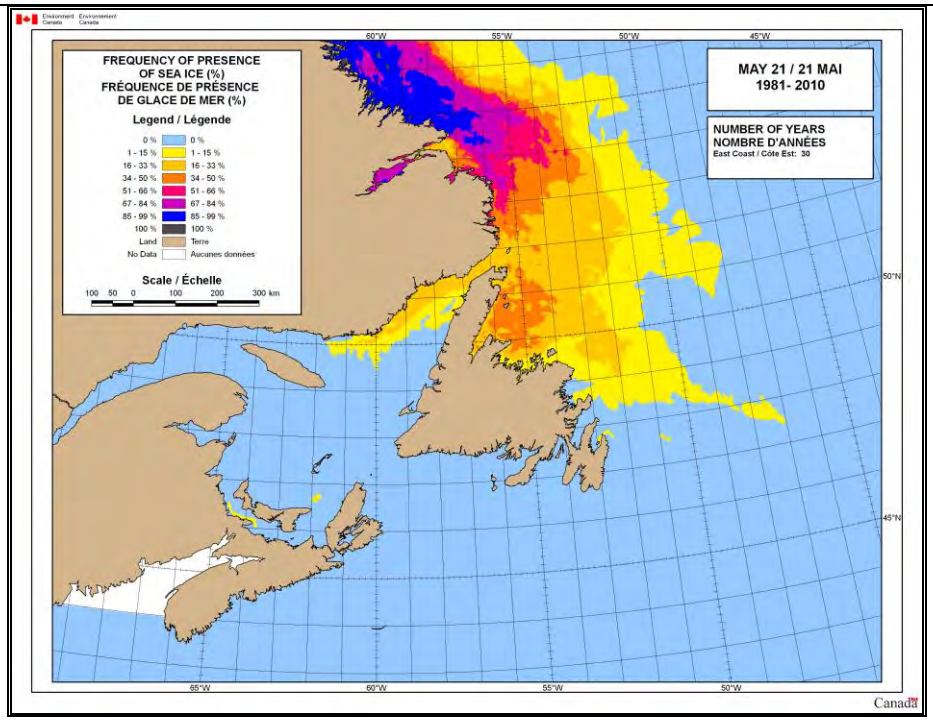

Figure 9.18 30-Year Frequency of Presence of Sea Ice (%) (May 21, 1981 - 2010)

9.1.5 Age and Thickness of Ice

Most of the sea ice found on the Grand Banks is formed in upstream areas and increases in thickness during subsequent southward drift during the ice season.

There is very little actual sea ice measurement data for the White Rose area. Ice thickness statistics can only be extracted in terms of ice classifications based on CIS weekly ice charts. The most common thickness coded for the White Rose area are grey/white and thin first-year ice with the occasional thick first-year ice (120-200 cm).

Table 9.4 gives the ages and thickness of sea ice at the point closest to the White Rose field (using data from the CIS digital data base). A trace of old ice was reported on three weekly charts in 1993 (5th, 12th, and 19th April) and on the charts for 20th March 1995 and 7th April 2008. Estimates of extreme ice thickness are given in Table 9.5.

Table 9.4 Age and Thickness of Ice at point 46.75N 48.00W (1980 to 2010)

		Mean	Maximum	Thickness	(cm)
		(1/10s)	(1/10s)	Min	Max
All First Year Ice		3.1	8		
	Thin	1.9	8	30	70
	Medium	1.1	4	70	120
	Thick	0.2	2	> 120	

All Young Ice		2.5	9		
	Grey	0.6	5	10	15
	Grey-White	1.9	6	15	30
All New Ice		0.6	7		< 10
All Old Ice			Trace		

Table 9.5 Sea Ice Thickness (undeformed) at White Rose (all data points 1980-2010)

Mean	Maximum	Extreme
70 cm	200 cm	>200 cm

9.1.6 Maximum Sea Ice Thickness

Maximum sea ice thickness in the area around White Rose is associated with deformed sea ice. Few quantitative data are available on ice deformation for the Grand Banks region, in part because linear ridge formations of the type commonly observed in Arctic areas are rare for this area. Instead, the deformed pack ice consists of fields of confused jumbles of uplifted and broken floes (Petro-Canada, 1995.). Observation indicates that maximum sail heights are approximately 2 m (Dobrocky Seatech, 1985). Nolte and Trethart (1971) calculated average ridge heights of approximately 1 m. Based on a keel to sail ratio of 3:1 mean ridge thickness in the order of 3 to 5 m and extremes of 15 m are suggested.

According to one of the senior forecasters at CIS, "ridging and rafting do of course have an influence on the thickness of ice; however, in the Grand Banks area this is not of major concern. Ridging and rafting tend to occur closer to shore along the Gulf, Labrador, and Newfoundland coasts. There can certainly be instances of this ice making its way to the Grand Banks but again, this should not be of major concern for the area."

In summary, there is the possible presence of ridge fragments several metres in thickness but the area extent of these fragments should be small. There is also a small possibility of old ice remnants embedded in the pack. Old ice is denser and hence harder than regular sea ice because it has been re-frozen many times and much of its brine has leached out. In practical terms, old ice and ridge fragments pose the same threat to vessels as growler- and bergy bit-sized iceberg fragments. Table 9.6 gives a summary of the maximum sea ice thickness.

Table 9.6 Sea Ice Deformation at White Rose

Mean	Maximum	Extreme
3 metres	5 metres	15 metres

9.1.7 Floe Size

AES composite ice chart data for 1964 to 1987 indicate that, within 50 km of White Rose, floes larger than 100 m are present only 10 % of the time. The ice chart reporting code is limited to reporting floe sizes for predominate ice types present. The "small floe" category (20-100 m) is the most commonly reported at the White Rose area. This category is somewhat broad and encompasses both the mean and extreme floe sizes for the area.

Floe estimates made in several studies (Blenkarn and Knapp, 1969; Nolte and Trethart, 1971; LeDrew and Culshaw, 1977; Dobrocky Seatech, 1985) indicate that mean floe diameters in offshore areas south of 49°N are less than 30 m. Only a few floes with diameters larger than 60 m were observed.

Mean and maximum floe diameters decreased from 8 m and 37 m, respectively, at 49°N, 51°W to 1 m and 3 m in the vicinity of White Rose (Seaconsult, 1988). Mean and maximum diameters may exceed these values by an order of magnitude or more when the ice extent is close to its seasonal maximum in years of exceptionally severe ice conditions.

According to CIS concerning the Grand Banks, "with respect to floe sizes, our senior ice forecaster said that typically floes will be in the range of 20 to 100 m (floe size "3") or smaller (including "strips and patches") with instances of larger floes from time-to-time."

In summary, based on the weekly ice charts the mean floe diameters are less than 30 m and it is extremely rare for a floe diameter to exceed 100 m (Table 9.7).

Table 9.7 Sea Ice Floe Size at White Rose

Mean	Maximum	Extreme
< 30 metres	60 metres	> 100 metres

9.1.8 Drift Speeds

When present, the pack ice at White Rose is made up of non-continuous, mobile ice. Because of the loose concentrations and the lack of restraint, pack ice in the White Rose area is not subject to pressure. However, this does not mean that any proposed facility will not experience ice loads that may be caused by the pack building up against the facility under the influence of currents, waves, and winds.

The amount of ice build-up (if any) will depend on the orientation of the facility to the ice drift, the speed of ice movement, and any ice management employed.

Drift speed calculated from the PAL Ice Status Reports for April 6, 2008 to April 9, 2008 give speeds in the range of 0.144 m/s to 0.185 m/s.

Pack ice drift rates on the Grand Banks virtually mirror the surface currents. Between 1984 and 1987 Petro-Canada conducted a series of studies using satellite tracked ice drifters. The resulting ice drift patterns and velocities were characteristic of currents on the slope region of the Grand Banks, and related closely to ice drift conditions at the

White Rose location. Eighty percent of the measured drift speeds were less than 0.6 m/sec with a preferred direction towards the southeast. Mean drift speeds were shown to be 0.25 m/sec and extremes of 0.75 to 1.0 m/sec (Table 9.8).

Table 9.8 Sea Ice Drift Speeds at White Rose

Mean	Maximum	Extreme
0.25 m/sec	0.6 m/sec	1.0 m/sec

Drift speeds calculated from the Pal Ice Status Reports for April 6, 2008 to April 9, 2008 give speeds in the range of 0.144 to 0.185 m/s.

9.1.9 Trend

Looking at the 30 year climatology there has been a lot more ice in the first 15 years of the period than in the last 15 years. To help identify a pattern the data for the grid point closest to White Rose for the period of 1968 to 1980 has been examined. The complete data is presented in Table 9.9. Data from 1968 to 2010 plotted in Figure 9.19 may suggest more of a cyclical pattern rather than an increasing or decreasing trend in sea ice at the data point.

Table 9.9 Presence of Sea Ice on the White Rose Field

Season	1968 1969	1969 1970	1970 1971	1971 1972	1972 1973	1973 1974	1974 1975	1975 1976	1976 1977	1977 1978	1978 1979	1979 1980
Nov 17												
Nov 26												
Dec 04												
Dec 11												
Dec 18												
Dec 25												
Jan 01		0.3										
Jan 08												
Jan 15					0.3							
Jan 22					8							
Jan 29					0.2	0.3						
Feb 05					0.2	0.3			0.2			
Feb 12					0.2	0.3			0.2		0.2	
Feb 19				0.3	0.2	0.3	0.2	0.2	0.2		0.3	
Feb 26			0.3	0.2	0.2	0.3	9	0.2	0.2		0.3	0.3
Mar 05			0.3	0.2	1	0.3	9	0.2	0.2		0.2	0.3
Mar 12			0.2	0.2	7	0.3	4	0.2	0.2		0.2	0.3
Mar 19			0.2	4	0.2	0.3	1	3	0.2			
Mar 26			0.2	0.2	2	0.2	3	0.2	0.2		0.2	
Apr 02			0.2	0.2	9	0.2	0.2	0.2	9	0.2	0.2	
Apr 09			0.2	0.2	0.2	0.2	0.2	0.2	0.2		0.2	

Apr 16			0.2	0.2	6	0.2	0.2		0.2	0.2	0.2	
Apr 23			0.2	0.2	9	0.2	0.2	0.2			0.2	
Apr 30			0.2	0.2	0.2	0.2	0.2	0.2			0.2	
May 07			0.2	0.2	0.2	0.2	0.2	0.2			0.2	
May 14				0.2	0.2	0.2	0.2	0.2				
May 21				0.2	0.2	0.2	0.2	0.2		0.2		
May 28	0.2			0.2	0.2	0.2	0.2	0.2		0.2		
Jun 04		0.2	0.2	0.2	0.2	0.2	0.2	0.2		0.2		
Jun 11		0.2		0.2	0.2	0.2	0.2			0.2		
Jun 18				0.2	0.3	0.2				0.2		
Jun 25				0.2		0.2				0.2		
Jul 02				0.2		0.2	0.2					
Jul 09				0.2		0.2						
Jul 16		0.2										
Jul 23												
Jul 30												

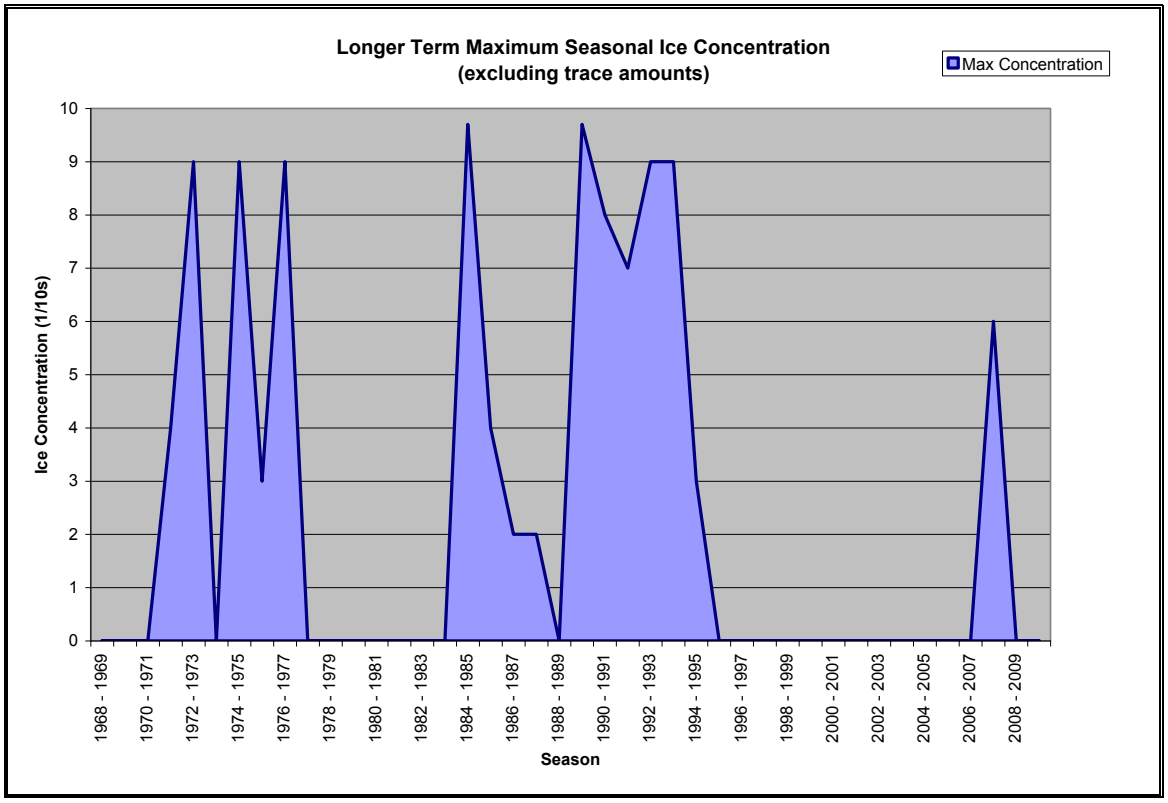

Figure 9.19 Maximum Seasonal Ice Concentrations

9.2 Icebergs

Glacial ice is formed from the accumulation of snow, which gradually changes form as it is compressed into a solid mass of large granular ice. This process produces a structure quite different from pack ice. The principal origins of the icebergs that reach the White

Rose location are the 100 tidewater glaciers of West Greenland. Between 10,000 and 15,000 icebergs are calved each year, primarily from 20 major glaciers between the Jacobshaven and Humboldt glaciers. These glaciers account for 85% of the icebergs that reach the Grand Banks. Of the remaining icebergs, 10% come from the East Greenland glaciers and 5% from the glaciers and ice shelves of Ellesmere Island.

The International Ice Patrol Iceberg Sightings Data Base from 1974-2009 was used as the primary data source in this analysis, (NSIDC 2009). This data was supplemented with the 2003 to 2010 PAL Environmental Services Division annual ice reports for the Grand Banks Joint Operators (Petro-Canada/Suncor, Hibernia Management and Development Company Ltd., and Husky Energy) as well as profile data obtained by Oceans Ltd.

9.2.1 Iceberg Sightings

Overall there is a good distribution of iceberg sightings in the Jean d"Arc Basin ranging from 987 in 1994 to only one in some years (Figure 9.20). Duplicate sightings of the same iceberg were eliminated from the data set so that only the initial sighting was counted.

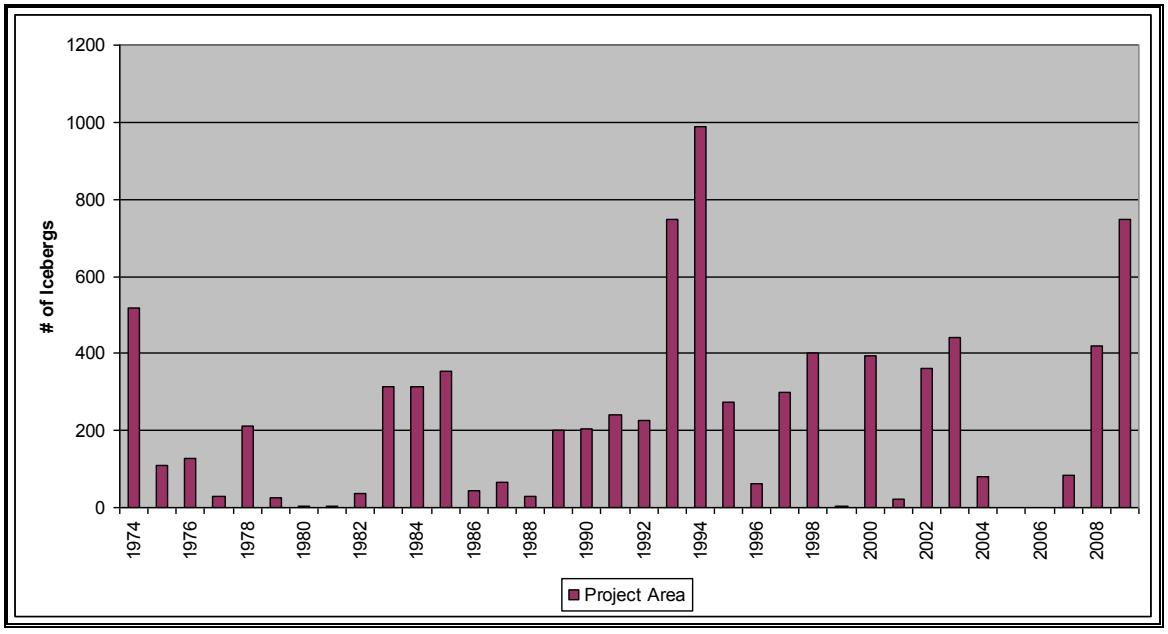

Figure 9.20 Number of Iceberg Sightings (Source: IIP)

Figure 9.21 shows the positions of all icebergs within the region from 1974-2009. Over the 35 years studied, 10,083 out of 23,570 icebergs in total have been sighted inside the area. Environmental factors such as iceberg concentration, ocean currents and wind determine how icebergs drift through the area. Statistics on the iceberg distribution are presented in Table 9.10.

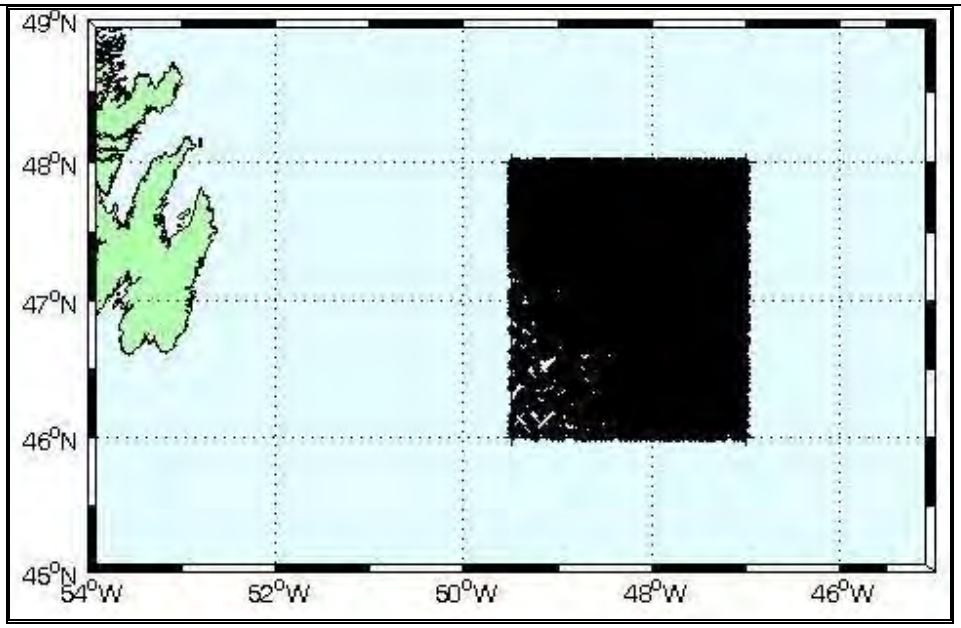

Figure 9.21 Locations of Iceberg sightings for 1974 – 2009 (from IPP data)

White Rose Field

An analysis of a 1 degree grid centered on the White Rose Field found that there were a total of 1924 icebergs from 1974 to 2009. The highest number of icebergs on the field occurred in 2008 when there were 215 icebergs sighted. Statistics on the iceberg distribution on the White Rose Field are also presented in Table 9.10.

Table 9.10 Iceberg Distribution at White Rose (from IPP data)

Area	Mean	Maximum	Extreme
Shaded area	233	987	987
1 Degree Grid	60	215	215

9.2.2 Iceberg Size and Shape

Icebergs are categorized by size, as defined in Table 9.11. These general size classifications have been in use for the past 30 years. However, the accuracy of size distributions extracted from the various databases is questionable, because most data are based on visual estimations and unspecified selection criteria.

Table 9.11 Iceberg Size

Category	Height (m)	Length (m)	Approx. Mass (T)
Very Large	> 75	>200	<10 Million
Large	46 -75	121 - 200	2 - 10 Million
Medium	16 - 45	61 - 120	100,000 - < 2 Million
Small	5 - 15	15 - 60	100,000

Bergy Bit	1.0 - < 5	5 - <15	10,000
Growler	< 1.0	< 5	1,000
Source: MANICE (June 2005)			

A monthly analysis (Table 9.12 and Figure 9.22) shows that icebergs have been spotted within the region from December to August and they are most prominent during the month of April. The most prominent icebergs are small, accounting for 27.7% of observed icebergs within the region. Large icebergs occur 10.4% of the time.

Table 9.12 Iceberg Size by month (source:IIP)

	Jan	Feb	Mar	Apr	May	Jun	Jul	Aug	Sep	Oct	Nov	Dec	Year
General	12	72	302	607	832	288	55	2	0	0	0	0	2170
Unidentified Target	11	85	114	24	63	29	7	2	0	2	0	2	339
Growler	1	12	78	155	187	34	25	0	0	0	0	0	492
Bergy Bit	5	4	66	110	77	23	5	0	0	0	0	0	290
Small	27	242	721	933	684	139	48	1	0	0	0	0	2795
Medium	12	112	596	886	752	240	62	2	0	0	0	1	2663
Large	2	22	202	370	280	151	20	0	0	0	0	0	1047
Very Large	0	1	18	34	15	3	3	0	0	0	0	0	74
Randomized	0	0	0	0	0	0	0	0	0	0	0	0	0
Total Monthly	70	552	2125	3171	2993	924	236	7	0	2	0	3	10083

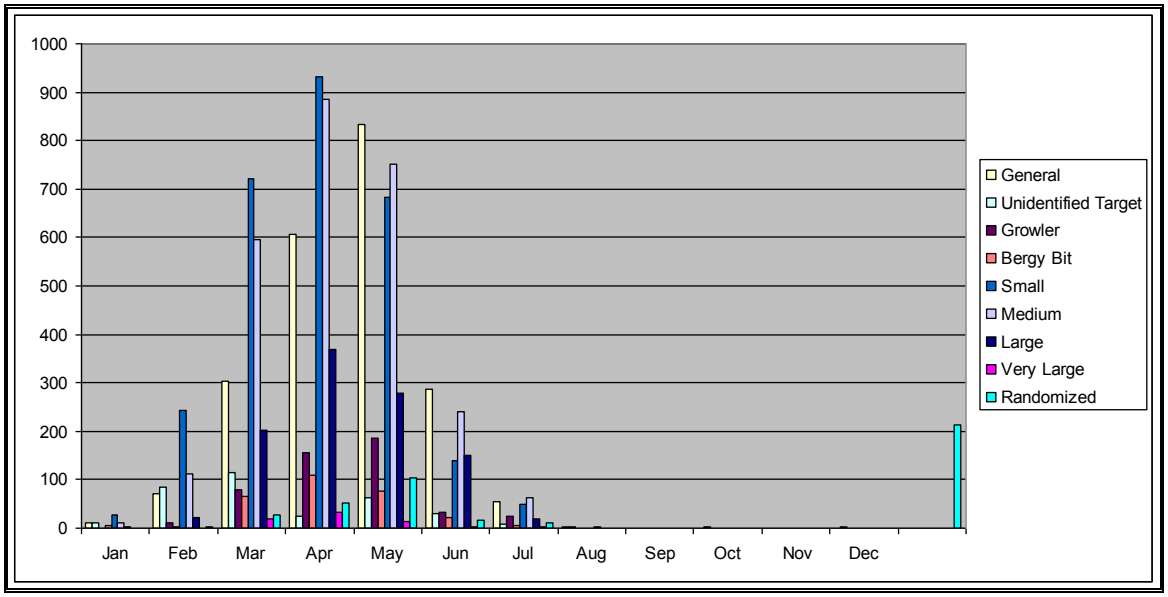

Figure 9.22 Iceberg Size by Month (source:IIP)

Statistics on iceberg size and shape for the Grand Banks were derived from Annual Ice Season reports prepared by PAL Environmental Services for the Grand Banks operators

from 2003 to 2010. During this period, 616 icebergs entered the area; however there were no icebergs on the field in 2006 and 2010. A summary of iceberg size for each year is provided in Table 9.13 and a chart of the percentage of icebergs by size is presented in Figure 9.23. Data was extracted from the PAL Environmental Services database for icebergs within a 60 nautical mile radius of White Rose. Figure 9.23 shows that for the White Rose area 65% of measured icebergs fall into the small or lower category, while 25% were medium and 10% were large. The 120 m water depth at White Rose will place a limit on the extreme iceberg size for most iceberg shapes. The exception is tabular icebergs. The IIP data base has a very large iceberg of approximately 25 nm from White Rose in 2009. PAL estimated this iceberg to have a mass of 5.92 million tonnes. This iceberg was located east of White Rose on the Continental Slope where the water depth was greater than at White Rose but since it was a tabular iceberg it is possible for this iceberg to reach White Rose. Oceans Ltd. measured a tabular iceberg in 2004 and calculated the mass to be 3.2 million tonnes (large iceberg). This was the second largest iceberg in the PAL data set and estimated to be 4.2 million tonnes.

Table 9.13 Iceberg Size (Data Source: PAL Environmental Services)

	Size					
	Very Large	Large	Medium	Small	Bergy Bit/ Growler	Unknown
2003	0	41	70	88	34	21
2004	0	2	5	11	2	0
2005	0	0	1	0	0	0
2006	0	0	0	0	0	0
2007	0	1	0	11	2	0
2008	0	4	11	51	8	8
2009	3	11	65	126	30	3
2010	0	0	0	0	0	0

Table 9.14 Iceberg Size Distribution at White Rose (Data Source: PAL Environmental Services)

Mean	Maximum	Extreme
Small	Large	Very Large

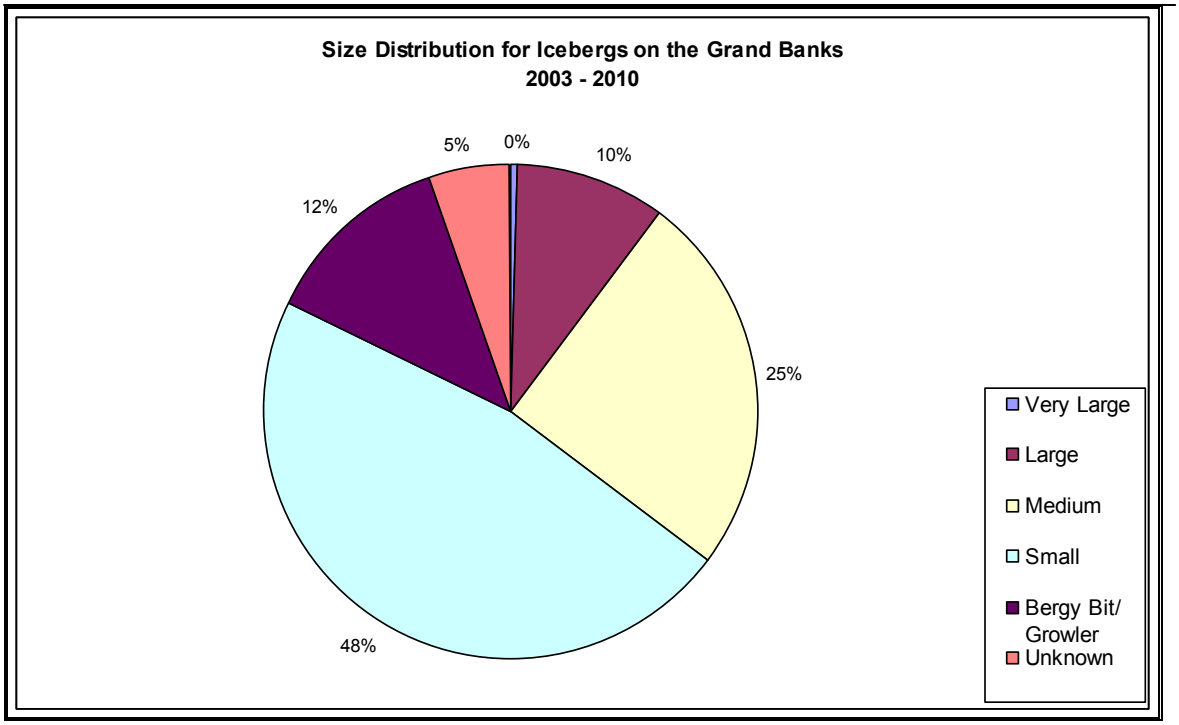

Figure 9.23 Size Distribution of Icebergs on the Grand Banks (Data Source: PAL Environmental Services)

The PAL Environmental Services division also records statistics on iceberg shape. The shapes of the Icebergs in the PAL data set are summarized in Table 9.15.

Table 9.15 Shape Distribution of Icebergs on the Grand Banks (Data Source: PAL Environmental Services)

	Shape						
	Tabular	Wedge	Dry Dock	Pinnacle	Dome	Blocky	Unknown
2003	74	20	76	21	32	2	29
2004	4	0	8	4	4	0	0
2005	0	0	1	0	0	0	0
2006	0	0	0	0	0	0	0
2007	0	0	5	4	3	0	2
2008	8	8	26	5	21	4	10
2009	33	19	73	37	41	23	12
2010	0	0	0	0	0	0	0

9.2.3 Iceberg Mass

Using the PAL data base for the 2003 to 2010 seasons, the mass of the icebergs on the Grand Banks have been calculated. The overall mass of an iceberg can be calculated based on the following equation:

M = 7.12 x Va

where 7.12 = a constant derived from $(\rho_i)(\rho_w) / (\rho_w - \rho_i)$

where Va = above water volume {L (m) x W (m) x H (m)} in (cubic metres)

ρ_i = density of ice

ρ_w = density of water

However, since no iceberg is cubical, a factor must be introduced to account for deviation from a cubical shape. This factor is known as the shape factor and can be defined as the ratio of the actual above water volume of an iceberg to the volume of a cube with the same length, width and height. Thus the above water volume of an iceberg is:

VA = (LWH) **S** where: ***S*** =shape factor. (Possible shape factors are:)

- Tabular and Blocky 0.50
- Pinnacle and wedge 0.25
- Dry-dock 0.15
- Dome 0.41

The final formula is expressed as: M= 7.12 x L x W x H x ***S.*** It should be kept in mind that the calculation is only an approximation of the iceberg's true mass.

Iceberg mass calculations for the Grand Banks (iceberg 2009-126) area range from less than 1,000 tonnes to a maximum of 5.9 million tonnes, with an average of 186,253 tonnes. Of the observations, 66.3% have a calculated mass below 50,000 tonnes while 4% have masses exceeding 1 million tonnes.

Since 2002, Oceans Ltd has been profiling icebergs on the Grand Banks for the Grand Banks Joint operators. During this period of 2002 to 2008, a total of 59 icebergs have been profiled and measurements of length, width, height and volume have been recorded. The mass is then determined from the volume using a porosity of 4% for iceberg ice.

The calculated mass, based on the formula above was also determined and compared with the mass determined from the iceberg profiling. Iceberg shape was not recorded in 2002 and therefore, the calculated mass cannot be determined for this year. Statistics for the 59 icebergs profiled by Oceans Ltd are presented in Table 9.16.

Table 9.16 Iceberg Dimensions (Data Source: Oceans Data Base)

Year	Iceberg #	Length	Width	Height	Draft	Volume	Shape	Mass	Formula Mass	% Difference
2002	OCEANS1	74.8	46.3	18.0	38.9	96305		84779		
	OCEANS2	26.9	25.4	6.4	31.9	12918	N/A	11372		
	OCEANS3	56.8	56.1	16.7	86.1	145792	N/A	128343		
	OCEANS4	57.1	51.1	12.3	83.0	148749	N/A	130946		
	OCEANS5	96.2	74.1	29.1	100.4	471541	N/A	415107		
	OCEANS6	104.2	91.8	14.7	82.5	444402	N/A	391216		
	OCEANS7	133.6	112.0	37.5	92.6	969562	N/A	853525		
	OCEANS8	78.1	60.2	9.2	77.1	204233	N/A	179790		
	OCEANS9	47.3	41.8	7.7	56.5	59103	N/A	52030		
	OCEANS10	60.9	56.3	20.6	64.1	138553	N/A	121971		
	OCEANS11	58.6	56.1	16.7	84.6	184480	N/A	162401		
	OCEANS12	46.2	45.4	15.1	82.7	88816	N/A	78187		
	OCEANS13	25.5	17.1	5.8	43.5	9242	N/A	8136		
	OCEANS14	33.7	31.4	9.1	89.0	40146	N/A	35342		
	OCEANS15	33.3	26.4	8.6	43.5	25323	N/A	22293		
	OCEANS16	250.5	196.8	9.1	68.9	2140834	N/A	1884619		
	OCEANS17	345.0	299.0	11.3	94.7	6368290	N/A	5606133		
	OCEANS18	43.9	42.8	11.2	48.3	40203	N/A	35391		
	OCEANS19	86.4	76.3	25.5	84.6	373524	N/A	328734		
	OCEANS20	112.7	87.3	16.8	102.1	518373	N/A	456334		
2003	HG03-011	39.2	34.4	6.8	44.9	25370	Small Dome	22334	26768	19.9
	HG03-012	131.4	124.0	18.3	98.7	443176	Large Pinnacle	390137	530748	36.0
	HG03-015	301.0	237.0	9.2	62.8	1147022	Large Tabular	1009747	2336429	131.4
	HG03-027	178.7	125.4	16.5	95.1	799966	Large Tabular	704224	1316303	86.9
	HG03-040	188.4	145.6	7.5	75.4	428407	Medium Tabular	377135	732409	94.2
	HG03-046	151.0	113.5	8.7	85.1	348043	Large Tabular	306389	530814	73.2
	HG03-109	89.7	70.9	9.6	91.1	258545	Medium Tabular	227602	217350	4.5
	HG03-132	87.0	77.4	18.5	93.9	344500	Medium Dry dock	303270	133046	56.1
	HG03-149	104.6	96.5	19.0	91.0	267350	Large Pinnacle	235354	341376	45.0
	HG03-149B	129.0	106.1	27.7	77.7	351951	Large Pinnacle	309830	674846	117.8
	HG03-149 C_2	99.6	82.9	23.5	95.8	318739	Medium Pinnacle	280592	345384	23.1
	HG03-160	100.2	81.2	21.5	61.1	154592	Medium Pinnacle	136090	311374	128.9
	HG03-160A	88.9	73.9	16.4	49.4	83036	Medium Dry Dock	73098	115070	57.4
	HG03-161	126.2	101.8	22.3	80.6	331313	Medium Wedge	291662	509955	74.8
	HG03-162	118.9	101.3	22.9	67.4	183967	Medium Pinnacle	161950	490961	203.1
	HG03-162A	62.4	57.2	13.0	47.3	47513	Medium Dry Dock	41827	49556	18.5
	HG03-164	51.9	45.3	12.2	48.3	40596	Small Pinnacle	35737	51056	42.9
	HG03-166	57.8	45.4	7.4	33.2	25362	Medium Dome	22327	56686	153.9
	HG03-167	59.2	52.1	14.7	45.2	52272	Small Dry Dock	46016	48423	5.2
	HG03-168	93.7	86.5	7.7	44.5	69752	Medium Dome	61404	182184	196.7
	HG03-168A	83.9	63.9	13.8	45.4	86196	Medium Wedge	75880	131693	73.6
2004	GB04-010	83.1	57.6	15.1	38.9	104513	Dry Dock	92005	77192	16.1
	GB04-011	430.9	286.0	8.8	48.9	3671475	Large Tabular	3232073	3860781	19.5
	GB04-012	95.9	50.7	15.0			Blocky		259638	

	GB04-013	34.1	16.8	6.7			Small Dry Dock		4099	
	GB04-014	75.9	33.3	9.1			Small Dry Dock		24429	
2007	2007-003	77.0	58.0	24.0			Pinnacle		190788	
	2007-005	40.0	32.0	10.0			Dry Dock		13670	
	2007-004	104.0	86.0	34.0	88.0	445945	Dry Dock	392571	324775	17.3
	2007-010	72.0	60.0	22.0			Dry Dock		101503	
	2007-009	77.0	62.0	22.0			Dry Dock		112170	
2008	RD001-1	58.0	48.2	22.2	59.6	225872.0	Dry Dock	198839.0	66172	66.7
	RD001-2	69.8	65.7	21.7	65.7	206078.0	Dry Dock	181415.0	106252	41.4
	RD001-3	70.8	56.2	18.1	56.7	167149.0	Dry Dock	147145.0	76778	47.8
	RD001-4	66.3	48.6	13.4	58.2	151571.0	Dry Dock	133431.0	46011	65.5
	RD001-5	66.0	63.9	24.0	57.1	225323.0	Wedge	198356.0	179651	9.4
	RD001-6	66.5	62.4	20.9	57.8	143519.0	Dry Dock	126343.0	92562	26.7
	RD001-7	69.5	52.5	23.3	64.1	196943.0	Wedge	173373.0	151306	12.7
	TN08-076	93.0	64.0	30.5			Dry Dock		193864	

Iceberg mass estimates for the White Rose area were extracted from the PAL data base of estimated iceberg masses. Iceberg mass distributions within 60 nautical miles of the White Rose area range from less than 1,000 tonnes to a maximum of 5.9 million tonnes, with an average of 168,532 tonnes. Sixty-seven percent of the icebergs have a calculated mass below 50,000 tonnes which only 4% have masses that exceed 1 million tonnes. These mass distributions are presented in Figure 9.24. Iceberg mass distribution was also calculated for the area within 25 nautical miles of the White Rose area. The percentage of icebergs with a mass below 50,000 tonnes increased to 73% while the mean and maximum decreased to 131,164 tonnes and 3.2 tonnes respectively. Iceberg mass distributions within 25 nautical miles of the White Rose area are presented in Figure 9.25.

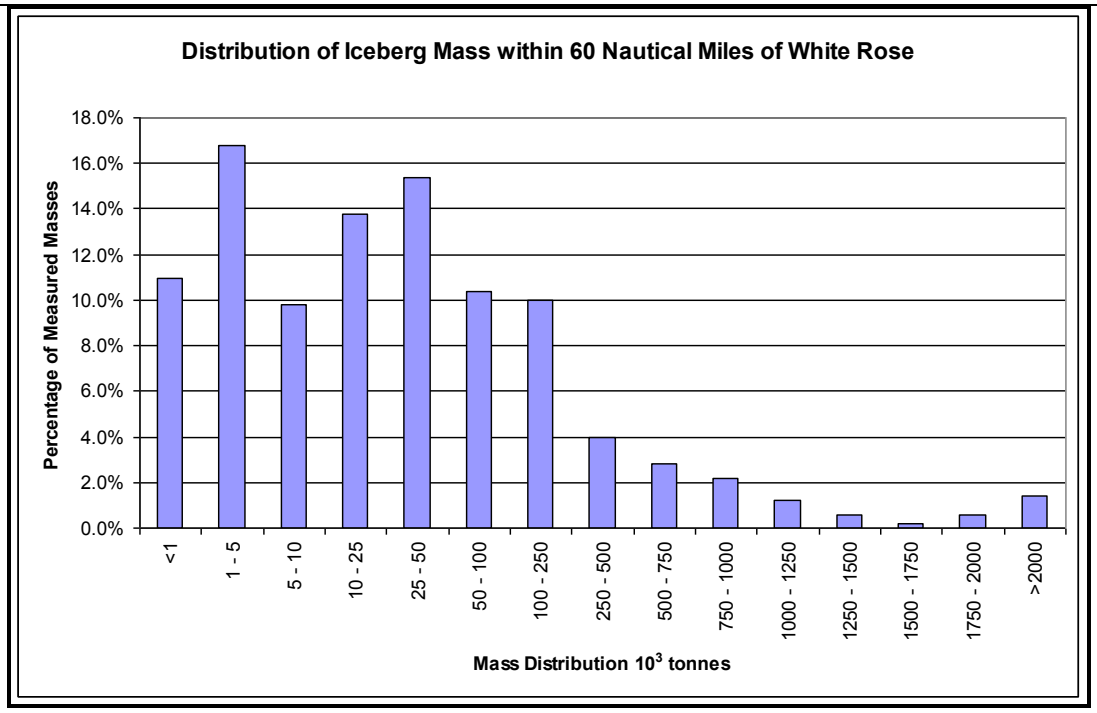

Figure 9.24 Distribution of Iceberg Mass within 60 nm of White Rose (from PAL data base)

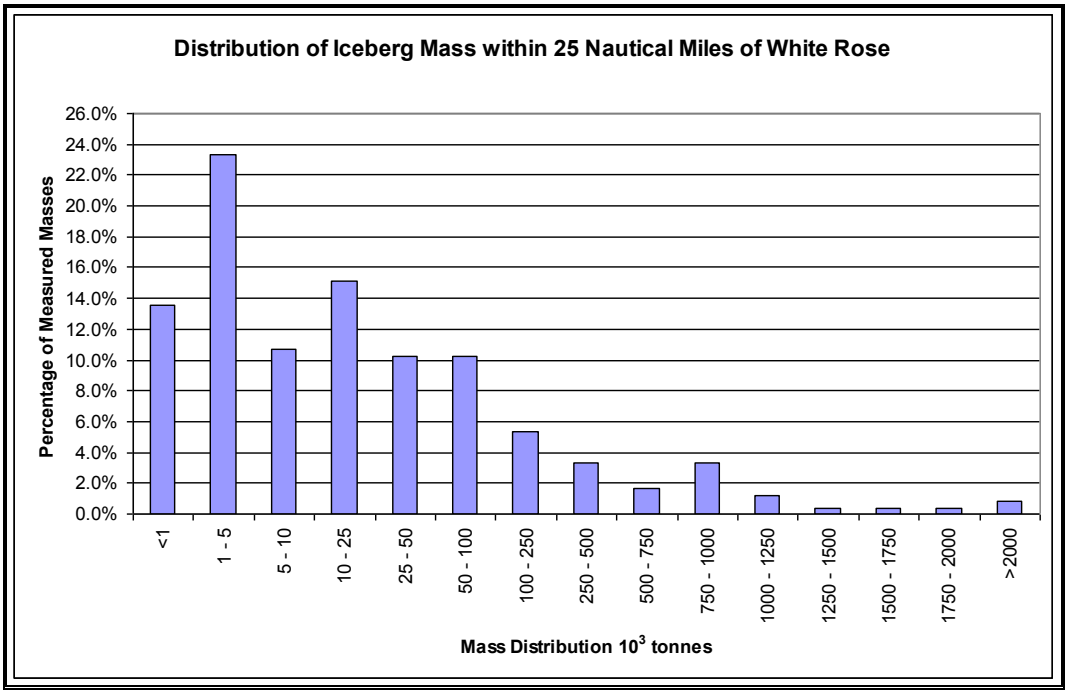

Figure 9.25 Distribution of Iceberg Mass within 25 nm of White Rose (from PAL data base)

Table 9.17 Iceberg Mass Distribution at White Rose (Data Source: PAL data base)

	Mean	Maximum	Extreme
60 nm	168,532 tonnes	5.9 Million tonnes	5.9 Million tonnes
25 nm	131,164 tonnes	32. Million tonnes	5.9 Million tonnes

9.2.4 Iceberg Drift Speeds

Iceberg drift speeds in the White Rose area show a correlation with the sub-surface currents.

Over the 2000 ice season, 1370 measurements of iceberg drift were calculated from position data. Due to insufficient data, drift statistics could not be determined from the 2005, 2006 and 2010 data. Speeds ranged from 0 to 1.3 m/sec and again the mean drift speed was 0.3 m/sec. Both of these observations agree with other studies conducted over the 1980"s, which had established a mean iceberg drift speed of 0.26 m/sec.

Over the 2003 to 2010 ice seasons, iceberg drift speeds were observed on 10,718 occasions. Speeds ranged from 0.0 m/s to 1.8 m/s and a mean drift speed of 0.57 m/s. Iceberg drift speeds from the PAL data base are presented in Tables 9.18 and 9.19.

Table 9.18 Iceberg Drift (Data Source: PAL Environmental Services)

	Drift (m/s)				
	Mean Speed	Minimum	Maximum	Number of Observations	Direction (Drift speed > 0.38 m/s)
2003	0.30	0.05	1.80	3648	SSW
2004	0.34	0.05	0.93	370	S
2005					
2006					
2007	0.26	0.03	0.93	371	SE
2008	0.30	0.02	1.18	1234	S
2009	0.26		1.54	5095	SE
2010					
Total	0.29			10718	

Table 9.19 Iceberg Drift Speed (m/s) Distributions at White Rose (Data Source: PAL Environmental Services)

Mean	Maximum	Extreme
0.26	1.8	1.8

9.3 Superstructure Icing

9.3.1 Freezing Precipitation

Freezing precipitation occurs when rain or drizzle aloft enters negative air temperatures near the surface and becomes super-cooled so that the droplets freeze upon impact with the surface. This situation typically arises ahead of a warm front extending from low pressure systems passing west of the area.

The percentage of occurrences of freezing precipitation (Table 3.7) was calculated using the ICOADS data set. Since negative air temperatures are required for freezing precipitation, statistics show the frequency of freezing precipitation occurs only during the months winter and spring months with winter having a slightly higher percentage occurrence than spring. On a monthly basis, the month of March has the highest frequency of freezing precipitation; however it occurs less than 1% of the time.

9.3.2 Sea Spray Vessel Icing

Spray icing can accumulate on vessels and shore structures when air temperatures are below the freezing temperature of water and there is potential for spray generation. In addition to air temperature, icing severity depends on water temperature, water salinity, wave conditions, and wind speed which influence the amount of spray and the cooling rate of droplets. A review of the spray icing hazard is provided by Minsk (1977). The frequency of potential icing conditions and its severity was estimated from the algorithm proposed by Overland et al. (1986) and subsequently updated by Overland (1990). These algorithms are based primarily on reports from vessels that were 20 to 75 m in length. Here is the algorithm presented by Overland (1990).

$$PPR = \frac{V_a\ (T_f - T_a)}{1 + 0.3(T_w - T_f)}$$

PPR = Icing Predictor ($m°Cs^{-1}$)
Va = Wind Speed (ms^{-1})
Tf = Freezing point of seawater (usually -1.7°C or -1.8°C)
Ta = Air Temperature (°C)
Tw = Sea temperature (°C)

The algorithm generates an icing predictor based on air temperature, wind speed, and sea surface temperature which was empirically related to observed icing rates of fishing vessels in the Gulf of Alaska. This method will provide conservative estimates of icing severity in the study region as winter sea surface temperatures are colder and wave conditions are lower in the study area compared to the Gulf of Alaska where the algorithm was calibrated (Makkonen et al., 1991). Based on the above algorithm the terminology and associated vessel icing rates for freezing spray forecasts are shown in Table 9.20. These rates and terminology are used when forecasting freezing spray on the Grand Banks.

Table 9.20 Intensity of Freezing Spray

Intensity Term	Icing Rate (centimeters (cm) per hour)
Light	less than 0.7 cm/hr
Moderate	0.7 to 2.0 cm/hr inclusive
Heavy	2.0 – 4.0 cm/hr
Extreme	greater than 4.0 cm/hr

Potential icing rates were computed using wind speed and air sea surface temperature observations from the MANMAR data set. A total of 67197 observations were used to calculate the percentage frequency of icing occurrence and severity for area. Monthly, seasonal, and annual summaries are presented in Table 9.21 and Figure 9.26.

Potential sea spray icing conditions start during the month of November with a frequency of icing potential of just 0.2%. As temperatures cool throughout the winter, the frequency of icing potential increases to a maximum of 26.7% of the time in February. Extreme sea spray icing conditions were calculated to occur 0.9% of the time during February. Icing potential decreases rapidly after February in response to warming air and sea surface temperatures, and by May the frequency of icing conditions is only 0.1%.

Table 9.21 Frequency of Occurrence of Potential Spray Icing Conditions

	None (0cm/hr)	Light (<0.7cm/hr)	Moderate (0.7-2.0cm/hr)	Heavy (2.0-4.0cm/hr)	Extreme (>4.0cm/hr)
January	77.7	16.2	4.8	1.1	0.2
February	73.3	18.3	6.2	1.3	0.9
March	82.6	12.8	3.6	0.7	0.4
April	94.8	4.5	0.6	0.1	0.0
May	99.9	0.1	0.0	0.0	0.0
June	100.0	0.0	0.0	0.0	0.0
July	100.0	0.0	0.0	0.0	0.0
August	100.0	0.0	0.0	0.0	0.0
September	100.0	0.0	0.0	0.0	0.0
October	100.0	0.0	0.0	0.0	0.0
November	99.8	0.2	0.0	0.0	0.0
December	91.6	7.6	0.8	0.0	0.0
Winter	80.9	14.0	3.9	0.8	0.3
Spring	92.4	5.8	1.4	0.3	0.1
Summer	100.0	0.0	0.0	0.0	0.0
Autumn	99.9	0.1	0.0	0.0	0.0
Annual	93.3	5.0	1.3	0.3	0.1

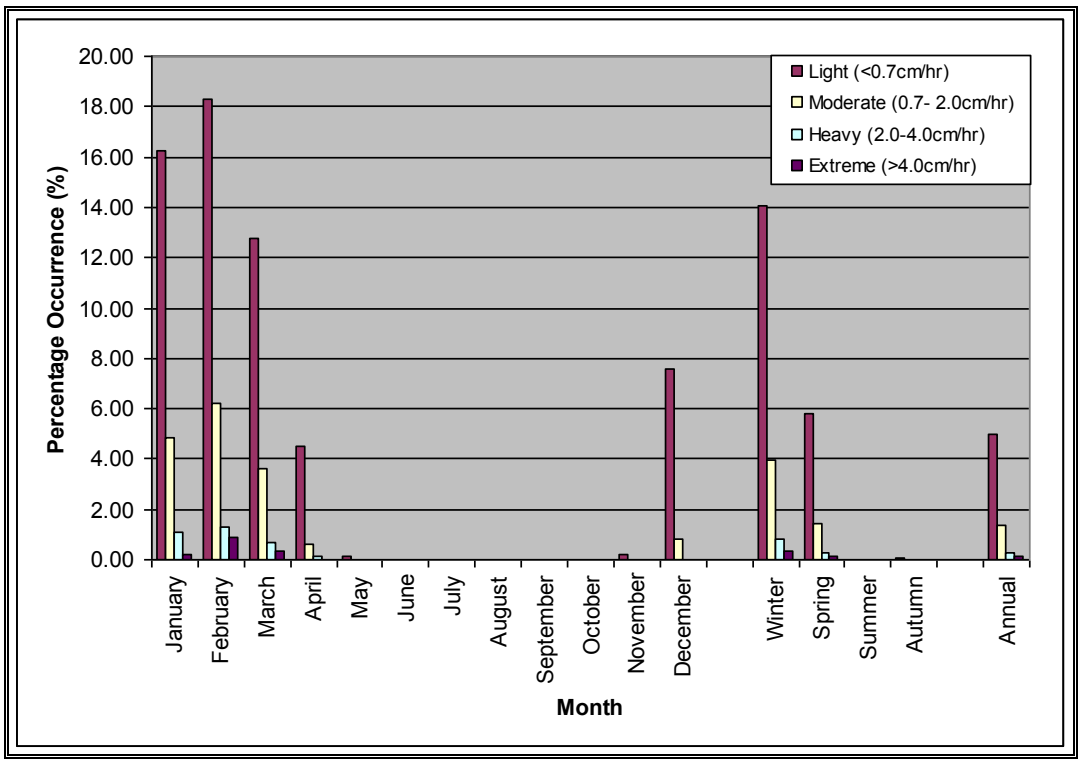

Figure 9.26 Frequency of Occurrence of Potential Spray Icing Conditions

9.3.3 Icing Load Design Guidelines

Oceans Ltd. has identified four sets of guidelines/regulations from research results that should be considered when establishing the design load criteria for offshore platforms. These guidelines/regulations are presented below.

Stability of Fishing Vessels - IMCO Recommendations

The recommendations on Intact Stability of Fishing Vessels of the Inter-Governmental Maritime Consultative Organization (IMCO), which is a subsidiary organ of the International Maritime Organization (IMO), lays down the following minimum ice allowance in calculating a vessel"s stability:

a. 30kg/m^2 (3.5 cm thickness) on exposed weather decks and gangways,

b. 7.5 kg/m^2 (0.9 cm thickness) for the projected lateral area of each side of the vessel above the water plane.

Note: The recommendations also recommend that the above values be doubled the further north one goes.

Large Fishing Vessel Inspection Regulations – Canada Shipping Act

The Canada Shipping Act defines a Large Fishing Vessel as being 24.4 m in length or 150 tons, gross tonnage.

With respect to stability inspection pertaining to ice loading the following Canada Shipping Act regulations pertain to vessels operating in northern or eastern waters of Canada. The Act states that on completion or near completion of a vessel, an inclining experiment shall be conducted in the presence of and to the satisfaction of a steamship inspector.

The results obtained from an inclining experiment shall be developed to indicate the stability of the vessel in the following conditions:

1) worst operating condition with accumulated ice on topsides and rigging; and

2) port after discharge of cargo with 10 per cent of fuel, fresh water and stores remaining and accumulated ice on topsides and rigging.

In developing the results of an inclining experiment to indicate the stability of a vessel in conditions described in paragraphs 1) and 2), accumulated ice shall be deemed to weigh:

a) 54 kg/m^2 (6.3 cm thick) of total deck area, including the superstructure and deckhouse tops that are exposed to the weather;

b) 37 kg/m^2 (4.3 cm thick) of area exposed to the weather in the case of the superstructure and deckhouse fronts, and the deckhouse sides and bulwarks including the area of the deckhouse sides and bulwarks on both sides of the vessel except that only the inboard surfaces shall be included in computing the bulwark areas

c) 78 kg/m^2 (9.0 cm thick) of area, taking into consideration overall block dimensions, in the case of the guardrails and stanchions, hatch coamings, companionways and ship fittings exposed to the weather; and

d) 48 kilograms per running metre (5.6 cm thick) in the case of rigging, masts, derricks and similar high objects measured to a height of 6.1 m above the main weatherdeck.

Stability Criteria for Offshore Supply Vessels - Transport Canada Marine Safety Directorate

For vessels operating in areas where severe ice accretion may be expected - the areas North of latitude 43°N bounded in the West by the North American Coast and the East by the rhumb line running from latitude 43°N longitude 48°W to latitude 63°N longitude 28°W and hence along longitude 28°W - the following ice accretion loads are to be used in the stability calculations:

1. 54 kg/m^2 (6.3 cm thick) of total deck area, including the superstructure and deckhouse tops that are exposed to the weather;
2. 37 kg/m^2 (4.3 cm thick) of area exposed to the weather in the case of the superstructure and deckhouse fronts, and the deckhouse sides and bulwarks including the area of the deckhouse sides and bulwarks on both sides of the vessel except that only the inboard surfaces shall be included in computing the bulwark areas;

3. 78 kg/m^2 (9.0 cm thick) of area, taking into consideration overall block dimensions, in the case of the guardrails and stanchions, hatch coamings, companionways and ship fittings exposed to the weather; and
4. 48 kg/m^2 (5.6 cm thick) in the case of rigging, masts, derricks and similar high objects measured to a height of 6.1 m above the main weatherdeck.
5. Relevant conditions should be clearly marked „ice accretion".

For vessels operating in the "north" – all sea areas north of the North American continent, west of the area defined above – a reduced ice accretion load may be considered by the Board where the owner demonstrates that lesser loads are encountered.

Norwegian Petroleum Directorate (NPD) Guidelines

Table 9.23 presents the NPD guidelines relating to loads and load effects to regulations relating to loadbearing structures in petroleum activities issued by the Norwegian Petroleum Directorate 7 February 1992 and last amended 8 March 1995 and 22 March 1996.

Table 9.22 NPD - Ice Loading Guidelines

Height above Sea level	Loadcase 1			Loadcase 2	
	Ice Caused by spray			Ice caused by rain / snow	
	56^{0}N to 68^0 N	North of 68^{0}N	Density	Thickness	Density
5 m – 10 m	**8.0 cm thick**	**15.0 cm thick**	**850 kg/m^3**	**10 mm**	**900 kg/m^3**
10 m – 25 m	Linear Reduction From 8.0 cm to 0	Linear Reduction From 15.0 cm to 0	Linear reduction from 850 kg/m^3 to 500 kg/m^3	10 mm	900 kg/m^3
Above 25 m	0	0		10 mm	900 kg/m^3
Ice loads with annual probability of exceedance 10^{-2}					

When referring to Table 9.22 one should consider the climate of the White Rose field in terms of air temperature, sea temperature and wind speed and how it compares to the two areas identified in the NPD guidelines.

A review of the U.S. Navy Marine Climatic Atlas of the World – Volume I North Atlantic Ocean (Revised 1974) by J.M. Meserve showed the White Rose climate to be more in line with the area north of 68°N than the southern area. In comparing the climate of the White Rose field to the area north of 68°N off Norway, the information showed that mean air temperatures off Norway during November and December were slightly colder than at the White Rose field. During January and February mean air temperatures at the White Rose field are colder than off Norway and for the months of March and April the mean air temperatures are comparable. In reviewing the mean sea temperatures for both areas it was found that the mean sea temperature at White Rose is colder than the northern region off Norway during the months of December through to April. With respect to wind conditions the monthly percent frequency of gales for the months

November through to April were reviewed and percent frequencies of gale force winds were found to be comparable.

9.3.4 Duration of Potential Icing Conditions

In order to look at duration of potential icing events on the Grand Banks a review was carried out on a drilling rig data set for the Grand Banks. The data set consisted of a time-series of Grand Banks rig observations from 1983 to 1989 and from 1999 to 2010. Three of the longer potential events where conditions were favorable for icing intensities of moderate or greater based on the Overland (1990) algorithm are discussed here.

Case 1: December 26 to 29, 1984, Near 47.1^{0}N 48.2^{0}W

Near midday on December 26 the air temperature was -5°C, the sea temperature was 0.5°C and the winds at anemometer height were westerly at 37 knots. This condition was favorable for moderate icing intensity. By mid day on the 27th the air temperature had fallen to -11 and the sea temperature to -1.7 with the winds out the west-northwest at 45 knots at anemometer height. This condition was favorable for extreme icing intensity. By mid day on the 28th the temperature had risen to -6, the sea temperature was near -1.8 and the winds were out of the west-northwest at 28 knots. These conditions were still favorable for moderate icing. By the morning of the 29th conditions had dropped out such that only light freezing spray potential existed. In this instance the potential of moderate or greater freezing spray lasted in the order of 60 hours with heavy to extreme being possible for 24 hours duration.

Case 2: March 9 to 12, 1986, Near 46.8^{0}N 48.1^{0}W

Near midnight on March 9th the air temperature was -5°C, the sea temperature was -1.4°C and the winds at anemometer height were west-southwest at 30 knots. This condition was favorable for moderate icing intensity. By the evening of the 10th the air temperature had fallen to -17 and the sea temperature to -1.8 with the winds out the northwest at 42 knots at anemometer height. This condition was favorable for extreme icing intensity. By mid day on the 11th the temperature had risen to -8, the sea temperature was near -1.8 and the winds were out of the west at 14 knots. These conditions were still favorable for moderate icing. By midnight on the 11th the temperature rose to -3, the sea temperature remained near -1.8 and the winds had increased to 43 knots out of the southeast. This condition was still favorable for moderate icing. Following this the temperature rose to where conditions were not favorable for freezing spray. In this case the potential for freezing spray of at least moderate intensity lasted for 48 hours of which 24 hours had the potential for heavy to extreme icing.

Case 3: March 07 to 08, 2003, Near 46.4N 48.4W

At 12Z, March 07 the air temperature dropped to -4.2°C, the sea temperature was -0.5°C and the winds at anemometer height were westerly at 27 knots. This condition was favorable for moderate icing intensity. As winds continued to increase, and temperatures drop, icing intensity increased, becoming heavy 3 hours later, and Extreme after another 3 hours. Extreme icing conditions peaked at 06Z, March 08 when temperatures dipped to -8°C and wind speeds increased to 60kts from the west. Conditions began to improve

after this and by 18Z, icing conditions were back to moderate. In this event, extreme icing conditions persisted over the area for a period of 18 or more hours.

10.0 Earthquakes

The earthquakes which have occurred within 500 km of White Rose over the last 22 years are shown in Figure 10.1. The list of these earthquakes is shown in Table 10.1. Table 10.1 shows that the largest earthquake in this time period had a magnitude of 4.2. This magnitude is too low to produce a tsunami.

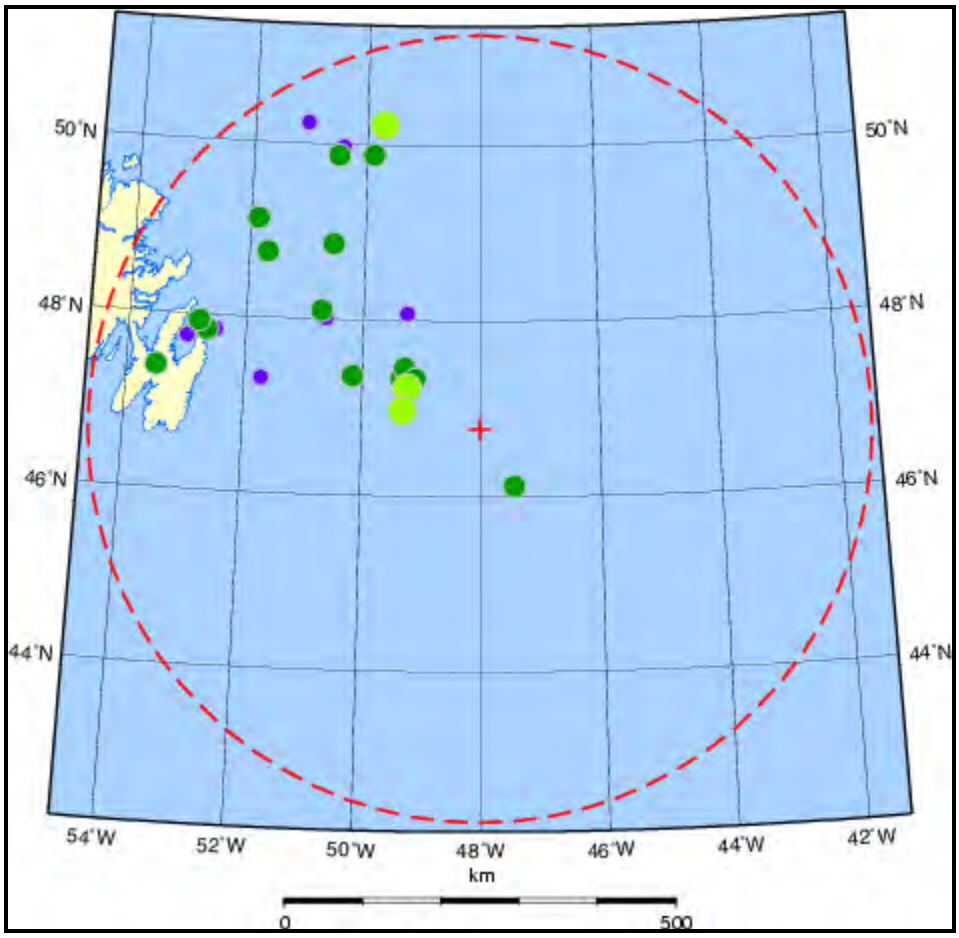

Figure 10.1 Earthquakes which have occurred between 1988 and 2010

Table 10.1 List of Earthquakes within 500 km of White Rose since 1988

Date	Time(UT)	Lat	Long	Depth	Mag	Region and Comment
2010/12/01	03:35:32	48.86	-50.55	18.0g	3.3ML	190 km E from Bonavista
2010/01/12	22:47:18	48.01	-50.65	18.0g	2.7MN	164 km E from St. John's
2009/04/29	01:26:03	47.40	-53.50	18.0g	3.3MN	28 km SW from Bay Roberts
2008/12/17	07:20:22	47.93	-52.81	18.0g	3.2MN	37 km NE from Carbonear
2008/11/18	00:15:29	50.23	-49.70	18.0g	4.2ML	Offshore Newfoundland.
2008/10/30	05:34:37	49.97	-50.42	18.0g	2.9ML	245 km NE from Bonavista
2008/06/12	12:34:51	48.10	-50.72	18.0g	3.1MN	162 km E from St. John's
2007/02/06	01:27:51	48.08	-49.25	18.0g	2.9MN	Grand Banks

2005/04/05	15:07:13	49.87	-50.50	18.0g	3.3ML	234 km NE from Bonavista
2003/04/20	10:30:25	50.24	-51.06	18.0g	2.6MN	320 km N from St. John's
2002/03/02	07:37:39	49.13	-51.87	18.0g	3.1MN	185 km N from St. John's
2001/04/06	21:09:48	48.75	-51.69	18.0g	3.1MN	150 km NE from St. John's
1996/03/13	23:55:07	47.75	-53.00	18.0g	2.4MN	Conception Bay
1995/01/22	06:46:20	47.84	-52.52	18.0g	2.4MN	34 km NE from St. John's
1994/12/01	09:32:25	47.31	-51.72	18.0g	2.6MN	Offshore Newfoundland
1994/08/11	18:13:49	47.83	-52.67	0.0g	3.1MN	St. John's Newfoundland
1992/08/10	11:31:52	47.34	-49.11	18.0g	3.4MN	Grand Banks
1992/07/17	04:20:22	46.12	-47.44	18.0g	3.9MN	Eastern Margin of Grand Banks
1992/07/06	16:58:16	47.33	-49.35	18.0g	3.0ML	Grand Banks
1992/01/13	06:07:28	47.24	-49.24	18.0g	4.0MN	Southern Grand Banks
1991/07/23	11:23:01	47.36	-50.17	18.0g	3.2MN	Grand Banks
1989/12/03	05:15:40	46.98	-49.32	18.0g	4.2ML	Offshore Newfoundland
1988/08/09	00:16:45	47.46	-49.29	18.0g	3.1ML	Grand Banks
1988/01/09	07:15:43	49.88	-49.88	18.0g	3.5ML	Offshore Newfoundland

The present earthquakes risk at White Rose is not expected to differ from the risk previously assessed for White Rose and Terra Nova. Hence, the information presented here has been extracted from the documentation provided to the Terra Nova project by Seaconsult Ltd. (1988).

The most active portion of the continental slope off the east coast occurs at the mouth of the Laurentian Channel where the magnitude 7.2 Grand Banks earthquake of 1929 occurred. The aftershocks which followed had the magnitudes as high as 6. Earthquakes in the same area, of the order of magnitude 5 occurred in 1951, 1954, and 1987 (Basham and Adams, 1982).

Figure 10.2 show the location of offshore earthquakes determined by Wahlstrom and Adams (Seaconsult 1988). This work represents a substantial improvement over earlier catalogued earthquake epicenters. Dots with a plus sign in Figure 10.2 are earthquakes found by searching the Corner Brook seismograms that do not appear in any catalogue. Magnitudes of the earthquakes are not distinguished in the figure. The box marked LSP encloses the many earthquakes on the Laurentian Slope near the epicenter of the 1929 Grand Bank"s earthquake.

Calculations of seismic risk for the Grand Banks were made by the Geophysics Division, Geological Survey of Canada (Energy, Mines and Resources Canada) using the Connell-McGuire method described by Basham et. al. (1982). The calculations were made for five locations at four different probabilities of exceedance as shown in Table 10.2. Location No. 5 is situated close to White Rose. The table presents peak horizontal ground accelerations and peak horizontal ground velocities. The earthquake source zones used by the Geophysics Division are shown in Figure 10.3. Basham et al. (1983) demonstrated that alternate offshore source models produce seismic ground motions that differ significantly from that given by the seismic zoning maps in Figure 10.3 that are used for the National Building Code of Canada (NBCC). The NBCC source zones and alternative source zones as proposed by Basham et al. (1983) for the eastern Canadian

offshore, together with the resulting contours of peak horizontal ground velocity having a probability of exceedance of 10% in 50 years are shown in Figure 10.4. The magnitude recurrence relation for zone ESX is shown in Figure 10.2. The contours in Figure 10.4 indicate that at Hibernia, Terra Nova, and White Rose a peak horizontal velocity of 8 cm/sec is expected using the Basham et al. (1983) source zone model.

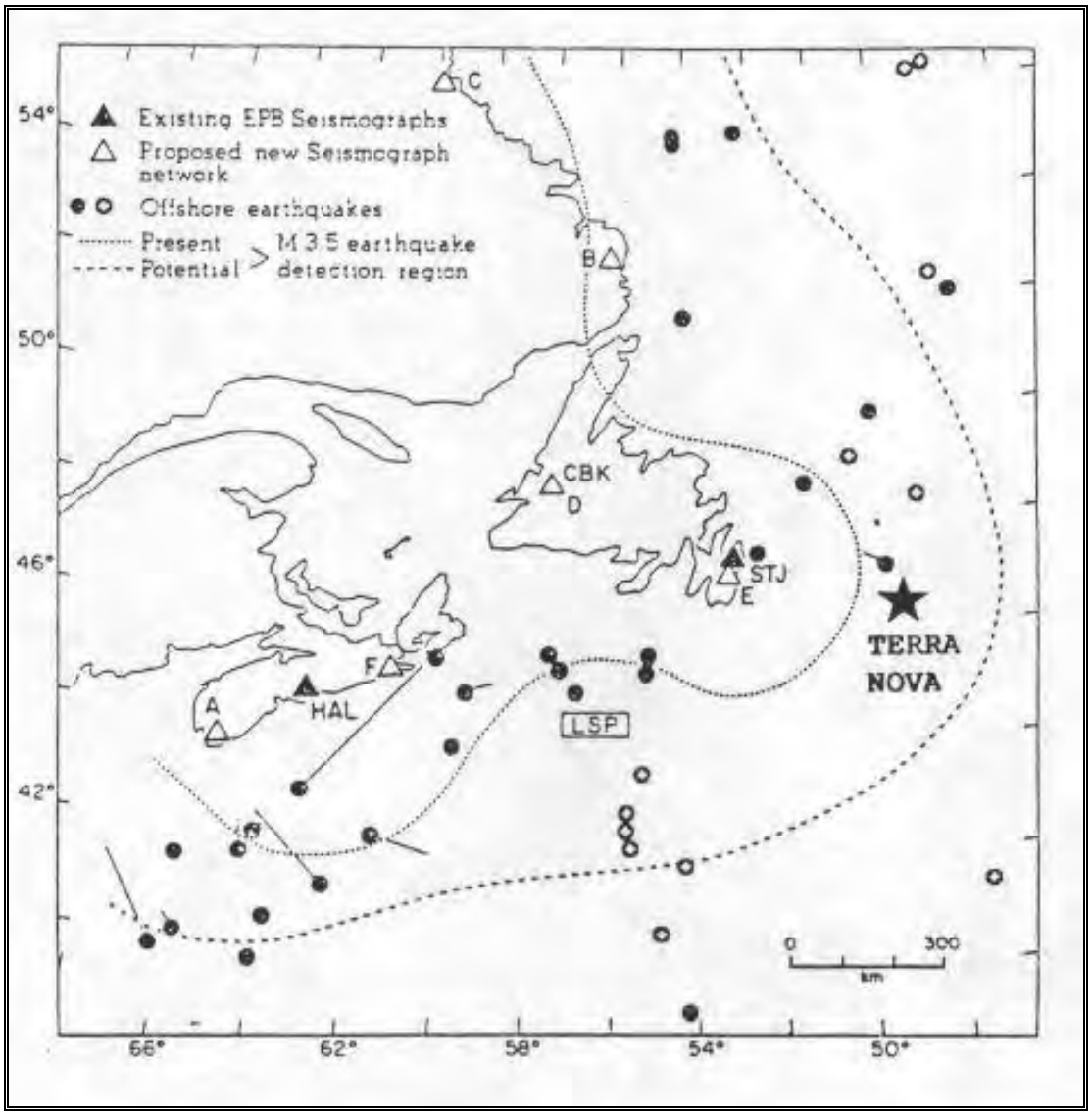

Figure 10.2 Map of Earthquakes off Canada's Southeastern Margin

whereas the NBCC source zone model has a value just under 4 cm/sec at these sites (Seaconsult 1988).

Table 10.2 Seismic Ground Motion Estimates for the Grand Banks

Location No.	Location	Probability of Exceedance per Annum	Peak Horizontal Ground Acceleration PHA (g)	Peak Horizontal Ground Velocity PHV (cm/sec)
1	46.5ºN 48.5ºW	0.01 0.005 0.0021 0.001	0.014 0.021 0.033 0.046	0.9 1.7 3.5 5.6
2	46.5ºN 48.11ºW	0.01 0.005 0.0021 0.001	0.013 0.020 0.032 0.044	0.9 1.7 3.4 5.4
3	46.5ºN 48.89ºW	0.01 0.005 0.0021 0.001	0.014 0.022 0.034 0.049	0.9 1.8 3.6 5.9
4	46.25ºN 48.5ºW	0.01 0.005 0.0021 0.001	0.013 0.021 0.033 0.047	0.9 1.7 3.5 5.7
5	46.77ºN 48.5ºW	0.01 0.005 0.0021 0.001	0.014 0.021 0.033 0.046	0.9 1.7 3.5 5.6

The earthquake source zone used in the COGLA (1987) study is shown in Figure 10.5. Figure 10.6 is comparison of the COGLA (1987) source zone with those of Basham e. al. (1983). The Terra Nova and White Rose sites are located in the Atlantic source zone regions; however, the seismic hazard is assumed to be the same as that for the adjacent shelf zone. The COGLA study calculated pseudo response velocity (PSRV) 5% dampled, at probabilities of exceedance of 10^{-2} and 10^{-4} per annum for frequencies 0.2 H_Z, 2.0 H_Z, and 10 H_Z. The PSRV values for the Terra Nova site are shown in Table 10.3.

Table 10.3 Response Velocities

Probability of Exceedance (per annum)	PSRV 10 H_z cm/sec	5% Damped 2 to 02 H_z
10^{-2}	0.5	1
10^{-4}	10	20

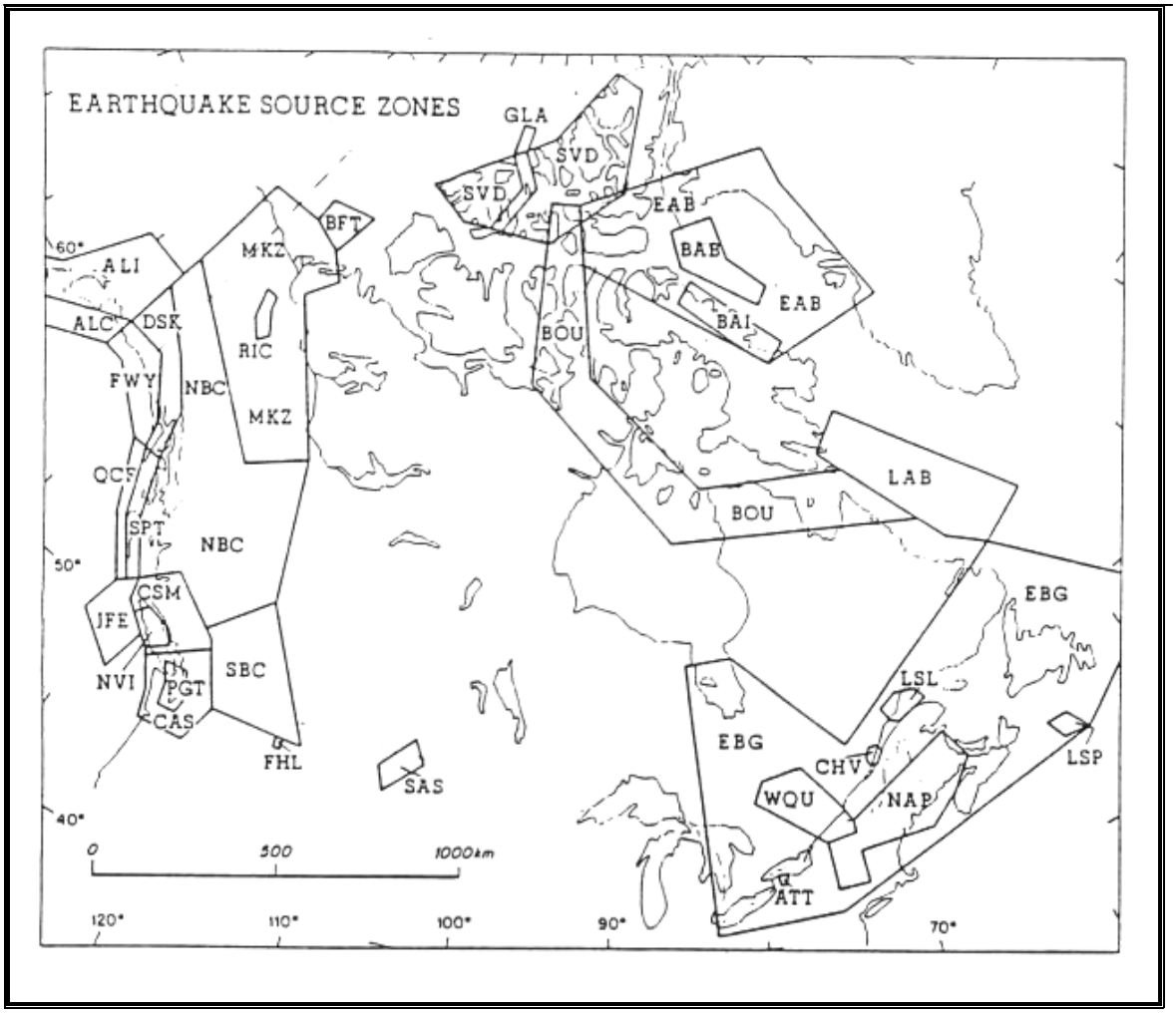

Figure 10.3 Earthquake Source Zones (from Seaconsult, 1988)

From Basham et al. 1983

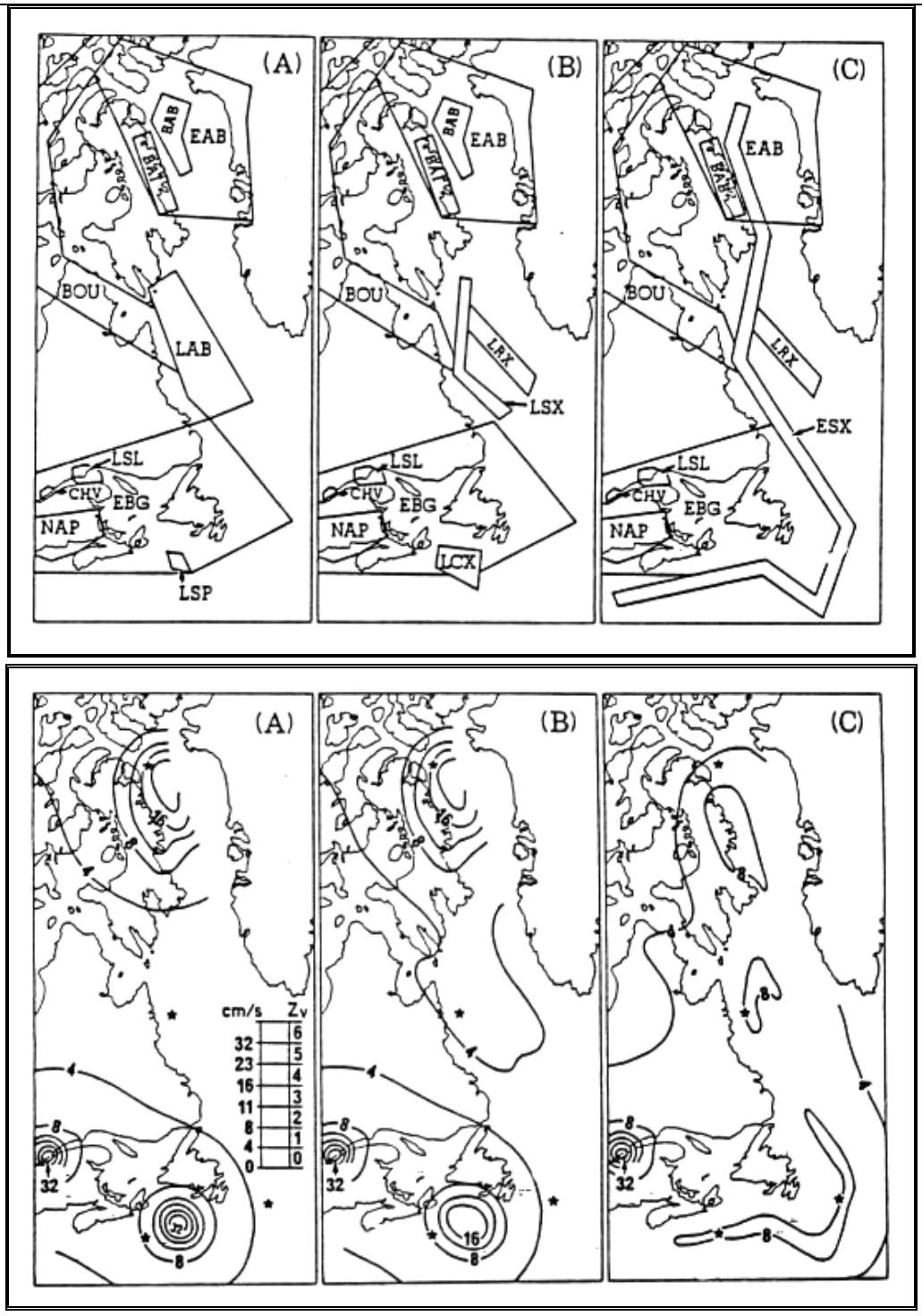

Figure 10.4 Alternate Earthquake Source Zone and Peak Horizontal Velocities

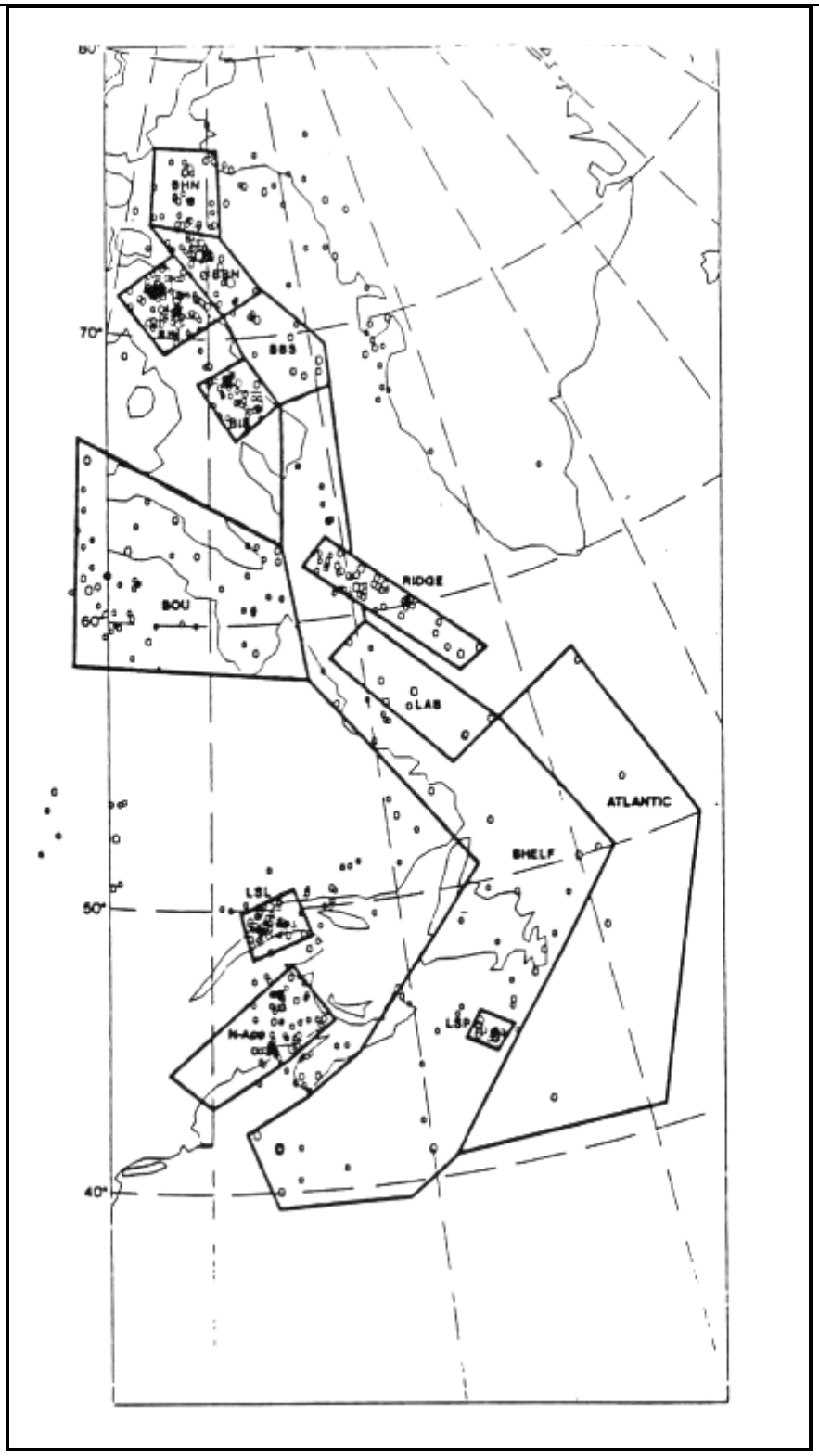

Figure 10.5 Eastern Canadian Offshore Earthquakes of M>3 through 1985 and Seismic Source Zones (Cogla, 1987)

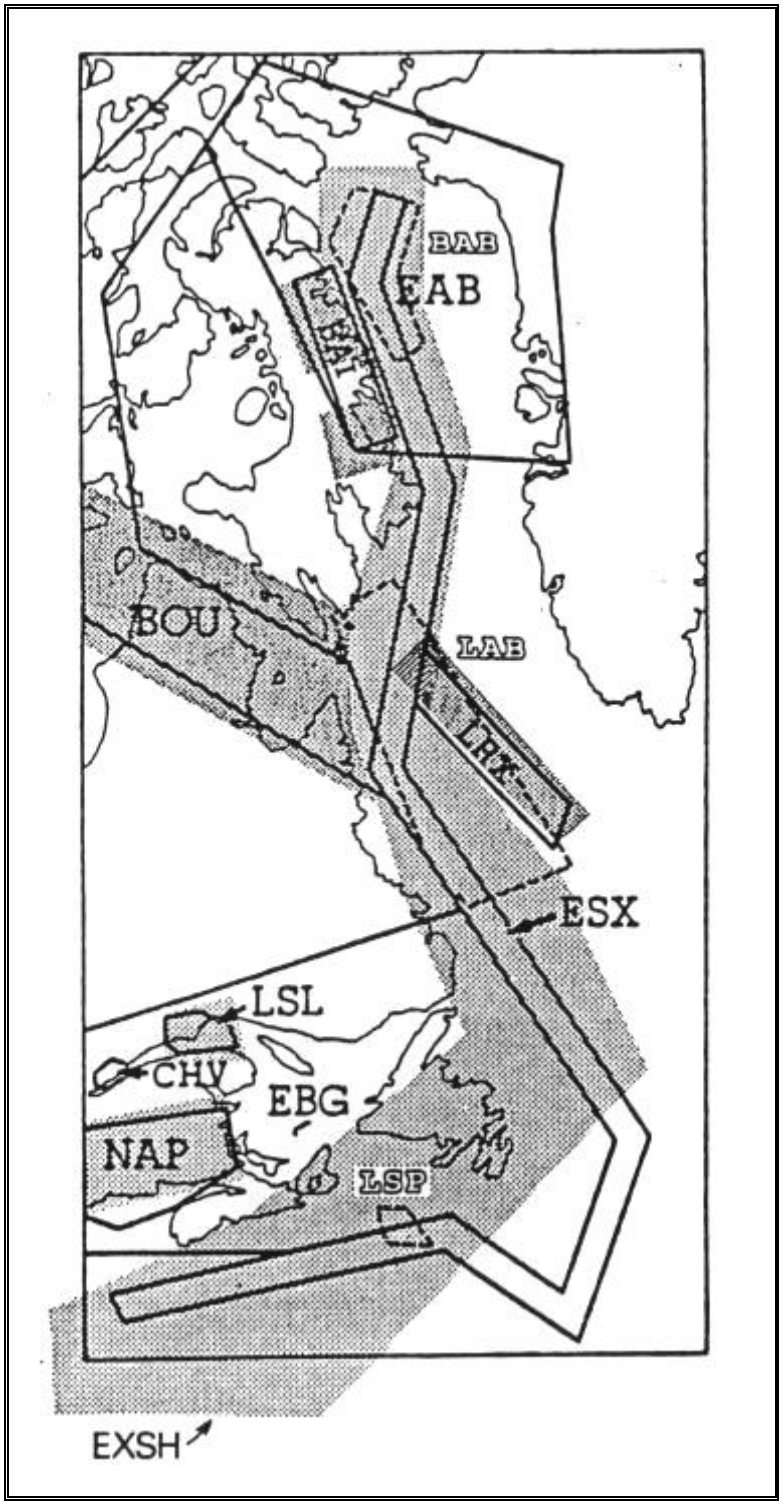

Figure 10.6 Comparison of COGLA (1987) and Basham et al. (1983)

The peak horizontal ground velocities were estimated for the Terra Nova site using the National Building code approved for probabilities of exceedances ranging from 10^{-2} to 10^{-3}. These peak ground velocities are shown in Figure 10.7. The peak ground velocities estimated for the Hibernia site which are similar are also shown.

The detailed seismicity studies undertaken for the Hibernia site resulted in site-specific design spectra for;

1. the level of earthquake ground motion that can normally be expected during the life of the structure and was assumed to have a return period between 100 and 400 years (OLE).
2. the maximum level of earthquake ground motion that can reasonably be expected to occur at the site (SLE).

From the Hibernia studies a peak ground acceleration of 0.05 g and a velocity value of 2 cm/sec were considered appropriate for the estimation of earthquake loads. The final site-specific design spectra recommended for the OLE is shown in Figure 10.8. Foo and Crouse (1986) suggested that a 200-year return period was appropriate for the offshore industry. For this return period, the peak ground acceleration and velocity were given as 0.03 g and 3.0 cm/sec, respectively.

On the basis of the seismicity of the region, Nolan-Ertec Ltd. (1981) selected the SLE according to the following criteria:

1. a magnitude 5.5 event close (around 20 km) to the site (near-field event), and
2. a magnitude 7.25 event on the Glooceap – Newfoundland Fracture Zone at a closest approach distance of 520 km from the site (far-field event).

The design spectra for the near-field and far-field events are presented in Figures 10.9 and 10.10.

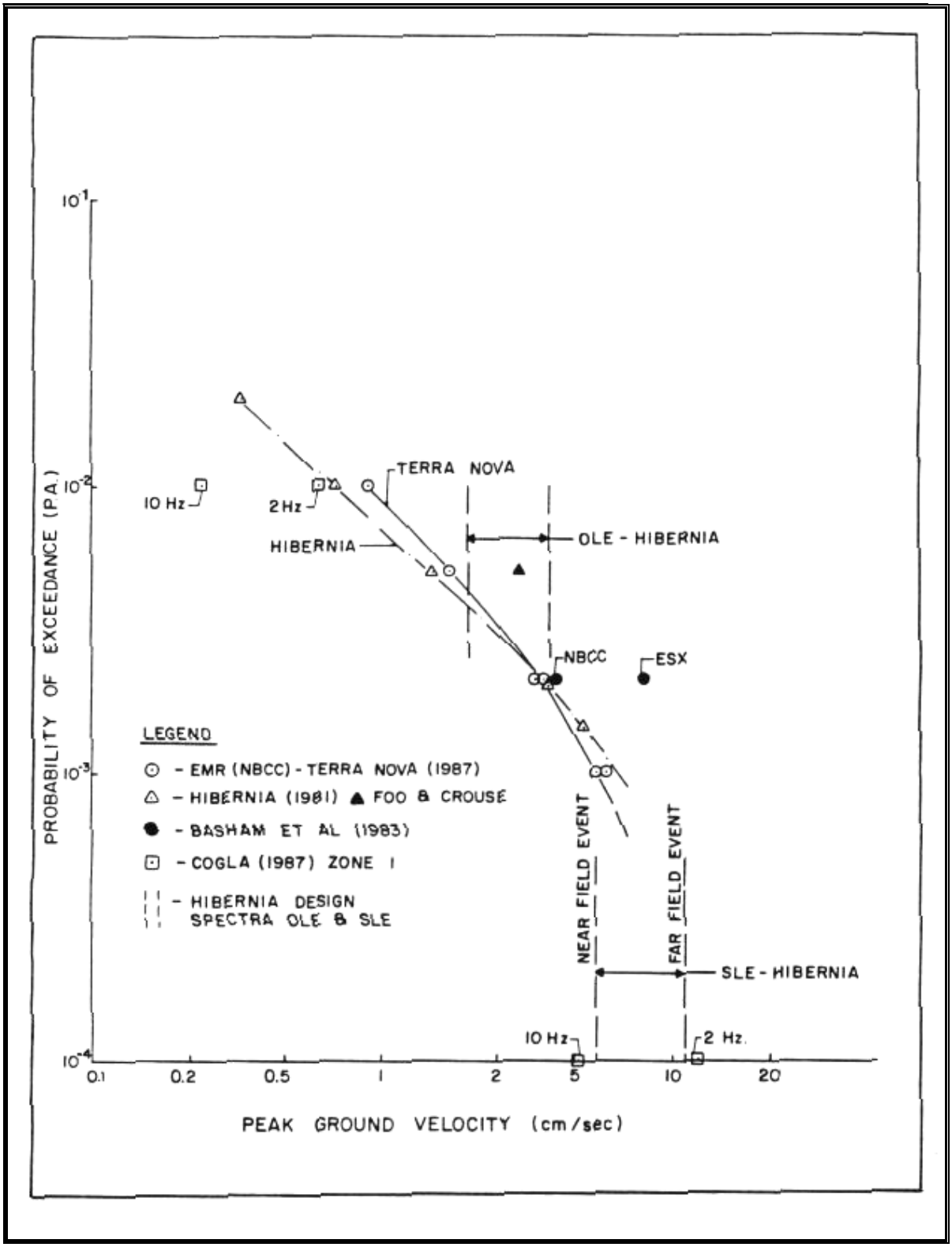

Figure 10.7 Peak Ground Velocity versus Probability of Exceedance for Terra Nova and Hibernia Sites

Source: Seaconsult (1984)

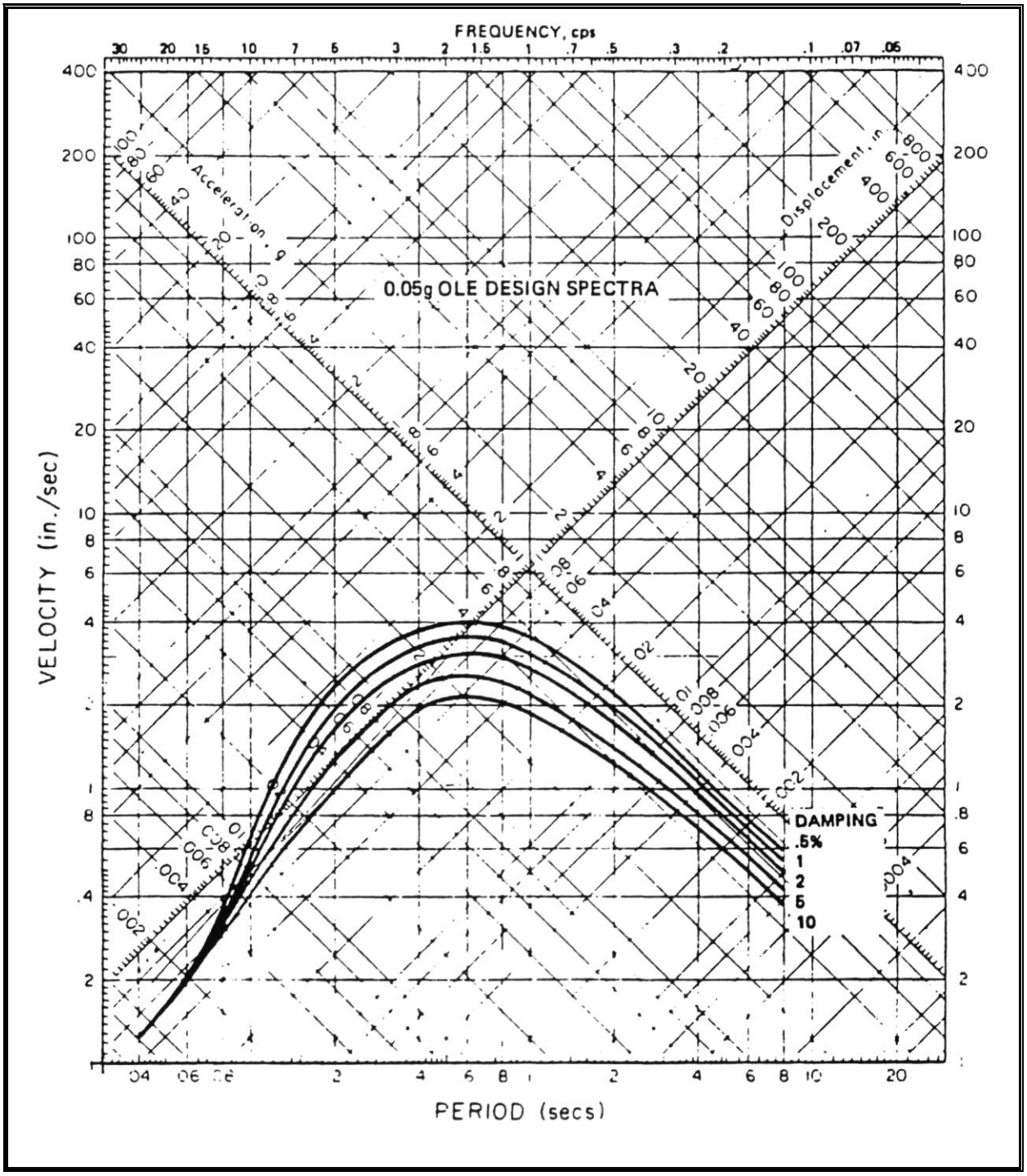

Figure 10.8 Site-Specific Design Spectra Recommended for OLE - Horizontal Component

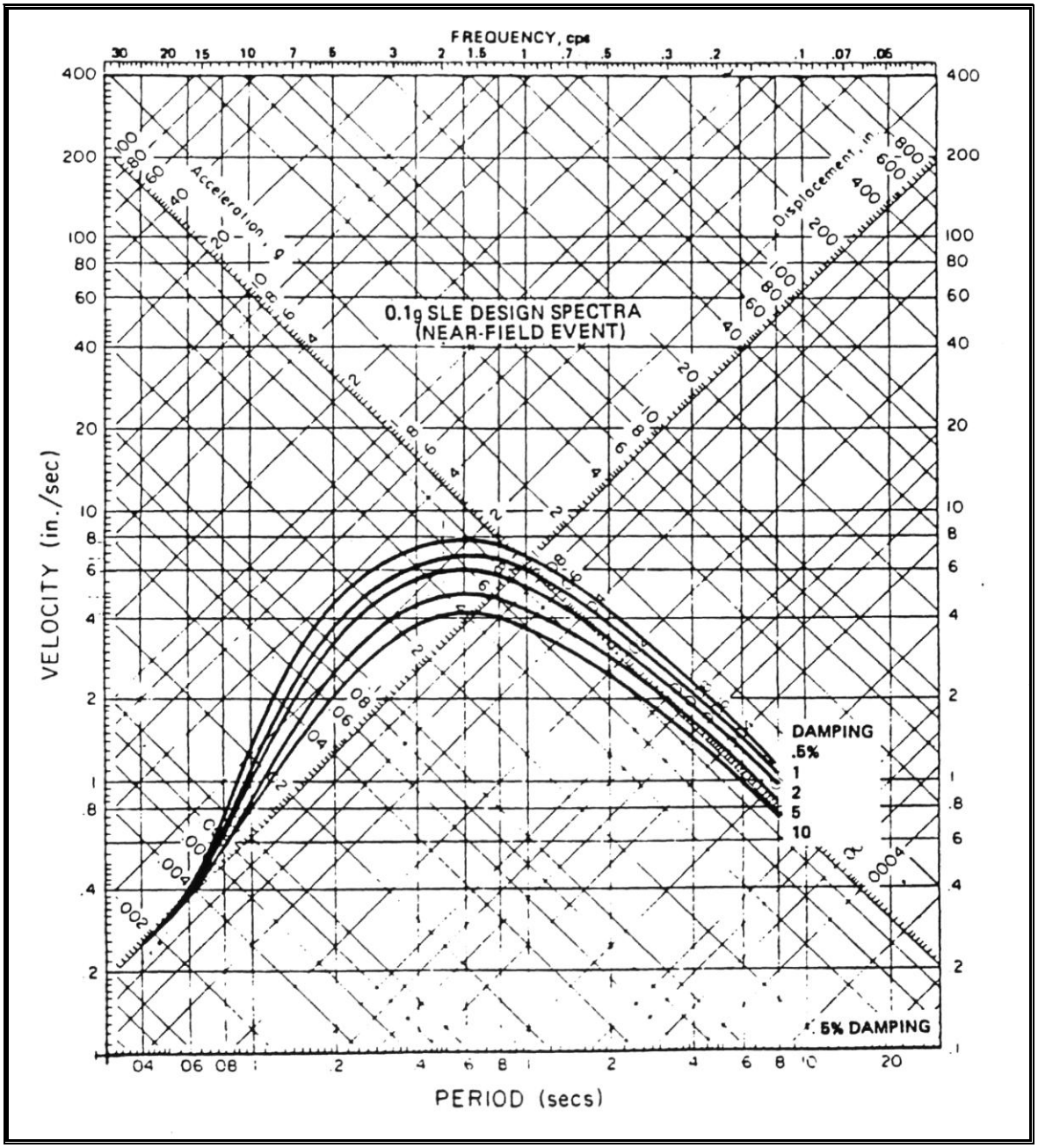

Figure 10.9 Site-Specific Design Spectra Recommended for Near-Field SLE Event - Horizontal Component

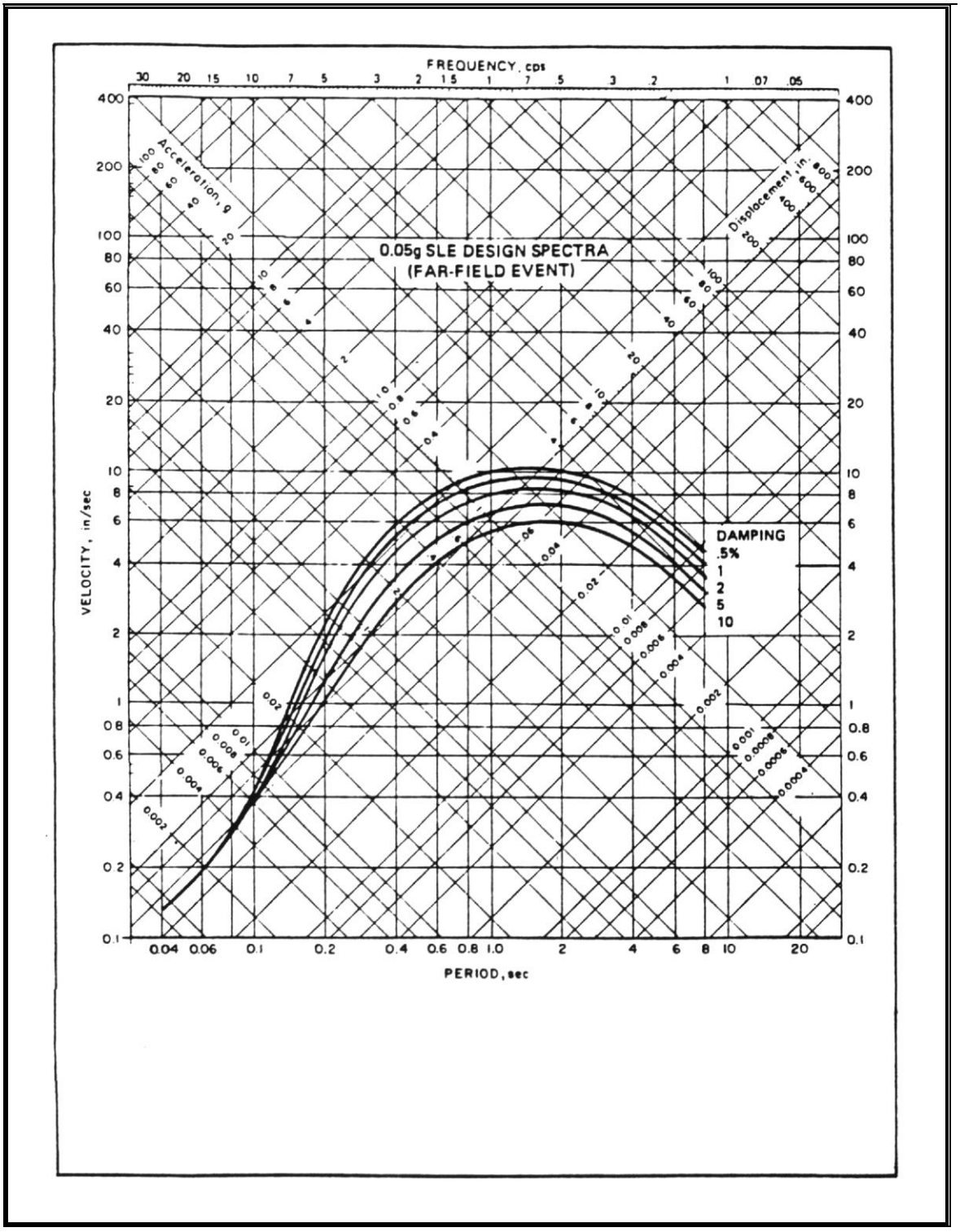

Figure 10.10 Site-Specific Design Spectra Recommended for Far-Field SLE Event - Horizontal Component

11.0 Climate Variability

Climate is naturally variable and can change over a range of time scales from the very short term, to seasonally, and to longer time periods in response to small and large-scale changes of atmospheric circulation patterns. Short-term meteorological variations are largely a consequence of the passage of synoptic scale weather systems: low pressure systems, high pressure systems, troughs and ridges. The energetics of these features varies seasonally in accordance with the changes in the strength of the mean tropical - polar temperature gradient. Long-term changes occur in response to small and large-scale changes of atmospheric circulation patterns in the Northern Hemisphere that are related to changes in the North Atlantic Oscillation (NAO). While the NAO still has an effect on climate patterns, there is a general consensus amongst the scientific community that Greenhouse Gas emissions have played a significant role in the climate during the last 50 years. However, the high degree of climate variation naturally experienced makes it difficult to identify, with any degree of certainty, trends that are a direct result of climate change (Environment Canada, 1997).

The dominate features of the mean sea level pressure pattern in the North Atlantic ocean are the semi-permanent area of relatively low pressure in the vicinity of Iceland and the sub-tropical high pressure region near the Azores. The relative strengths of these two systems control the strength and direction of westerly winds and storm tracks in the North Atlantic and therefore play a significant role in the climate of the North Atlantic. The long term fluctuating pressure difference between these two features is known as the North Atlantic Oscillation (NAO).

A measure of the North Atlantic Oscillation is the NAO Index, which is the normalized difference in pressure between the Icelandic low and the Azores high. A large difference in pressure results in a positive NAO Index and can be the result of a stronger than normal subtropical high, a deeper than normal sub-polar low, or a combination of both. The positive phase of the NAO index results in more and stronger winter storms crossing the North Atlantic on a more northerly track, and cold dry winters in Northern Canada and Greenland, while the negative phase results in fewer and weaker storms crossing on a more west-east track. A time-series of the Winter (Dec, Jan, Feb) North Atlantic Oscillation Index during the period of 1950 to 2011 is presented in Figure 11.1.

The negative phase of the NAO dominated from the mid to late 1950‟s until the early 1970‟s. There was a 5-year period of positive phase in the 1970‟s, then another shift back to a negative phase for three years from 1977 to 1979. From 1979/80 until the late 2000‟s the NAO index remained in a generally positive mode, with only six deviations into the negative mode during this 29 year period. For the past three years, the NAO has been in a negative phase with 2010 being the strongest negative phase sine 1950. It is uncertain how long this recent negative trend will persist.

11.1 Air and Sea Surface Temperature

The mean air temperature from the ICOADS data set was calculated for each winter season from 1950 to 2011 and the difference about the mean over the entire period plotted against the NAO index. This data is also presented in Figure 11.1. The plot

shows that the mean winter air temperature anomaly on the White Rose field is positive during the strong negative phase from the winter of 1963 to the winter of 1971 and negative during the strong positive phase from 1980 through 1995. This is conducive with the results mentioned previously where a positive phase of the NAO index results in colder winter, and a negative phase resulting in warmer winters.

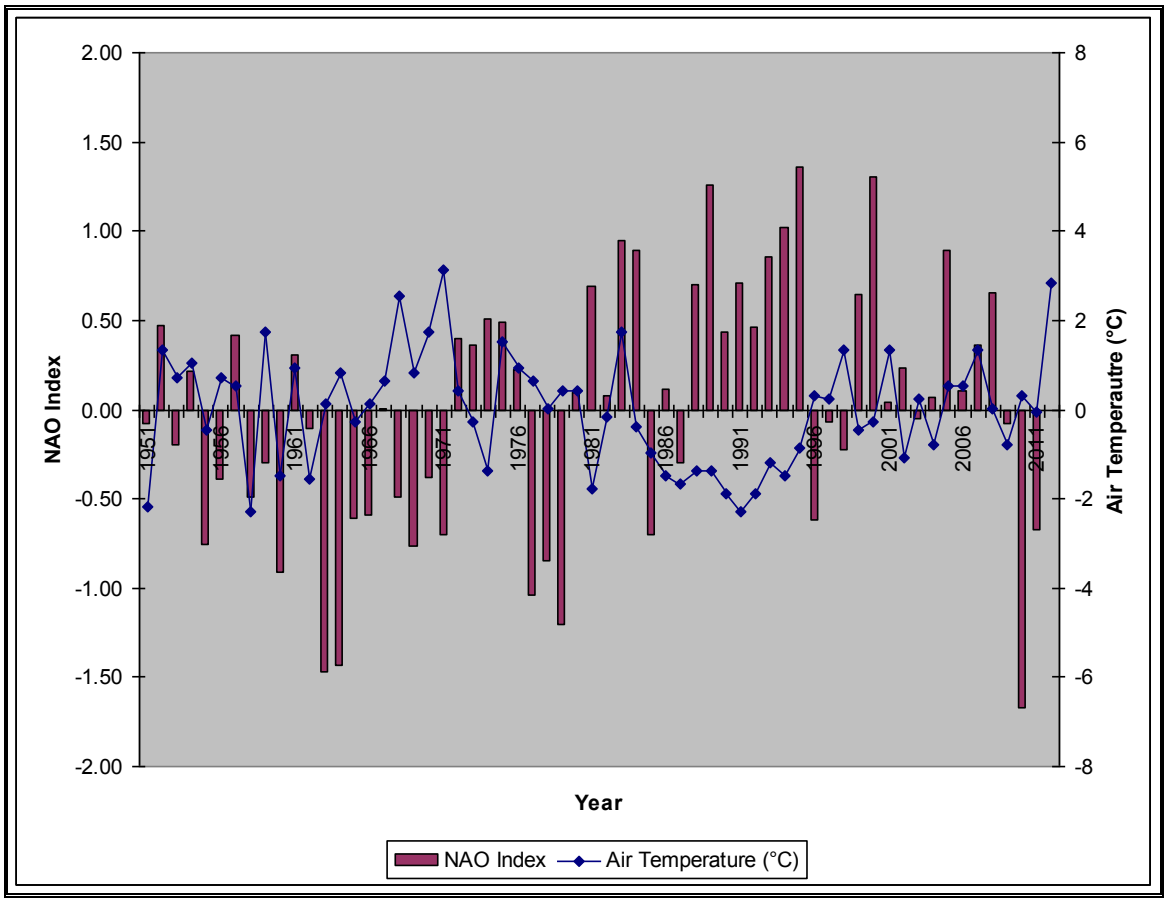

Figure 11.1 Winter North Atlantic Oscillation Index (1950 - 2011)

11.2 Storm Frequency and Intensity

The mean location of extratropical cyclones is referred to as the storm track, the location of which is determined by troughs and ridges in the upper atmosphere. Low pressure systems tend to form in the regions of maximum jet stream located downstream of the upper troughs, and once formed they follow the jet axes. As a result, areas immediately downstream of an upper trough typically experience more cyclones. A study by Reitan (1974) found that the highest frequency of storms occur between 40° to 50°N, with one of the most active areas being over the Gulf Stream off the United States Eastern Seaboard. Changes in the location of the jet stream and altitude can result in changes in the frequency and intensities of storm systems.

A number of studies have been done recently to assess whether climate change and global warming would have an effect on storm tracks, frequency and intensity. Archer and Caldeira (2008) found that during the period of 1979 to 2001, there was a poleward shift in the jet stream of 0.17 to 0.19 degrees/decade and a significant pressure decrease which would imply an increase in jet stream altitude in the Northern Hemisphere. These results were consistent with an increase in mean temperature from equator to pole. Changes in jet-stream latitude, altitude and strength, have the potential to affect the formation and evolution of storms in the mid-latitudes and of hurricanes in the sub-tropical regions. These results are consistent with a study by McCabe et al. (2001) which showed that from the period of 1959 to 1997, there has been a significant decrease in mid-latitude cyclone frequency and a significant increase in high-latitude cyclone frequency consistent with increases in winter Northern Hemisphere temperatures.

During the summer months, the NAO index has a less direct effect on the climate of Eastern Canada. However, studies have shown that the NAO has an effect on the track of hurricanes in the North Atlantic. During seasons with a negative NAO index, hurricanes tend to favour a track that parallels lines of latitude often ending up in the Gulf of Mexico and the Caribbean (Elsner, 2003), while during seasons with a positive NAO index, hurricanes tend to curve northward (Elsner & Bosak, 2004) along the United States Eastern Seaboard. An analysis of the number of tropical storms entering the Canadian Hurricane Centre Response Zone shows no correlation between Tropical cyclone frequency and the NAO Index.

11.3 Sea Ice and Icebergs

The thickness and extent of ice in the Arctic has long been considered to be a sensitive indicator of climate change. Studies in the past (McLaren 1989; McLaren et al., 1992; Wadhams, 1990) have shown that sea ice thickness has been decreasing and it was surmised that sea ice thickness would continue to decrease throughout the 1990s. Several recent studies however (Winsor, 2001; Laxon et al, 2003) have shown that this is not the case and that sea ice thickness has remained relatively constant during the 1990s. Winsor (2001) further surmised that the thickness of sea ice cover has remained on a near constant level during the period of 1986 to 1997. This is supported by Wadhams and Davis (2000) who concluded that a substantial part of the thinning in the previous studies took place during the late 1970s and early 1980s.

Interannual Arctic winter sea ice variability has been linked to large scale sea level pressure and surface air temperature changes associated with the North Atlantic Oscillation (Deser et al., 2000). The study by Deser et al. examined sea ice concentration anomalies in the Arctic during 1958 to 1997 and its association with surface air temperature and sea level pressure. The study found that when wintertime sea level pressure (SLP) is lower than normal over the North Atlantic (positive phase of the NAO), the Labrador Sea ice boundary extends further south in the spring.

A concern that often arises with global warming is whether or not there would be an increase in the number of icebergs off Newfoundland and Labrador due to an increase in calving at tidal glaciers. A study by Marko et al (1994) observed the inter-annual and seasonal variations in the numbers of icebergs passing south of 48°N off eastern North

America. This study showed that the number of icebergs off Newfoundland and Labrador is relatively insensitive to iceberg production rates and highly dependent on the Labrador spring ice extent, with higher numbers of icebergs occurring when the sea ice extent is greatest. The spring sea ice ensures iceberg survival by preventing them from grounding and subsequently melting on shallow continental shelves, suppressing sea surface temperatures.

11.4 Plausible Future Climate Scenarios

In an effort to understand how the world"s climate will react to anthropogenic influences the Intergovernmental Panel on Climate Change (IPCC) has developed numerous plausible scenarios of future climate situations. These scenarios are used in Global Climate Models to simulate the type of climate that might exist in the future. In this report, two of the five main climate models: the CGCM2 and HADCM3 are used to predict future temperature and precipitation trends for the Grand Banks.

Climate changes over Canada will not be distributed evenly. While some areas of the country may experience a general increasing trend in temperature and precipitation, other areas may not notice any trends. Furthermore, increases may not occur evenly throughout the year.

While year-to-year fluctuations in temperature exist the CGCM2 and HadCM3 climate models running the SRES B2 climate scenario predict a generally steady though slight increase in annual mean temperature trend. The predicted increase is 0.007°C/year for the CGCM2 model and an increase of 0.030°C/year for the HadCM3 model during the next 100 years for the Grand Banks of Newfoundland (Figure 11.2). These trends are also observed in the Grand Banks model seasonal data with the CGCM2 data showing a winter trend of 0.009°C/year, a spring trend of 0.010°C/year, a summer trend of 0.065°C/year, and an autumn trend of 0.003°C/year. The HadCM3 model shows positive trends during winter (0.020°C/year), spring (0.013°C/year), summer (0.049°/year) and autumn (0.041°C/year).

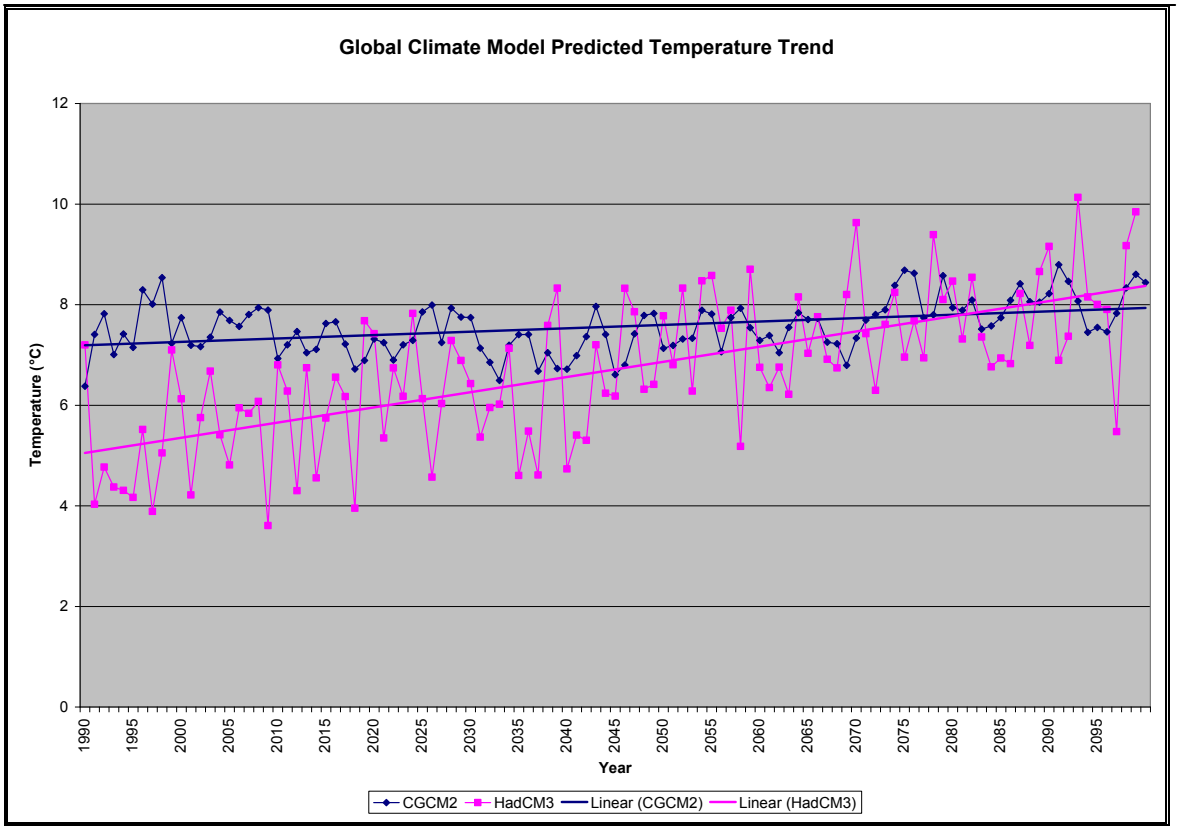

Figure 11.2 CGCM2 and HadCM3 Global Climate Models predicted Temperature Trend from 1990 – 2100

An analysis of daily averaged precipitation trends from both of these models shows only slight long-term trends in precipitation over the next 100 years for the Grand Banks of Newfoundland (Figure 11.3), with the CGCM2 model predicting a negative trend of 0.0007mm/year and the HadCM3 showing a slight increase of 0.0011mm/year. A seasonal analysis of the CGCM2 data shows that there is a decreasing trend in precipitation throughout most of the year, with the exception of winter which shows a slightly positive trend. The HadCM3 model has a positive precipitation trend for the winter and spring months, but no observable trend during the summer and autumn months.

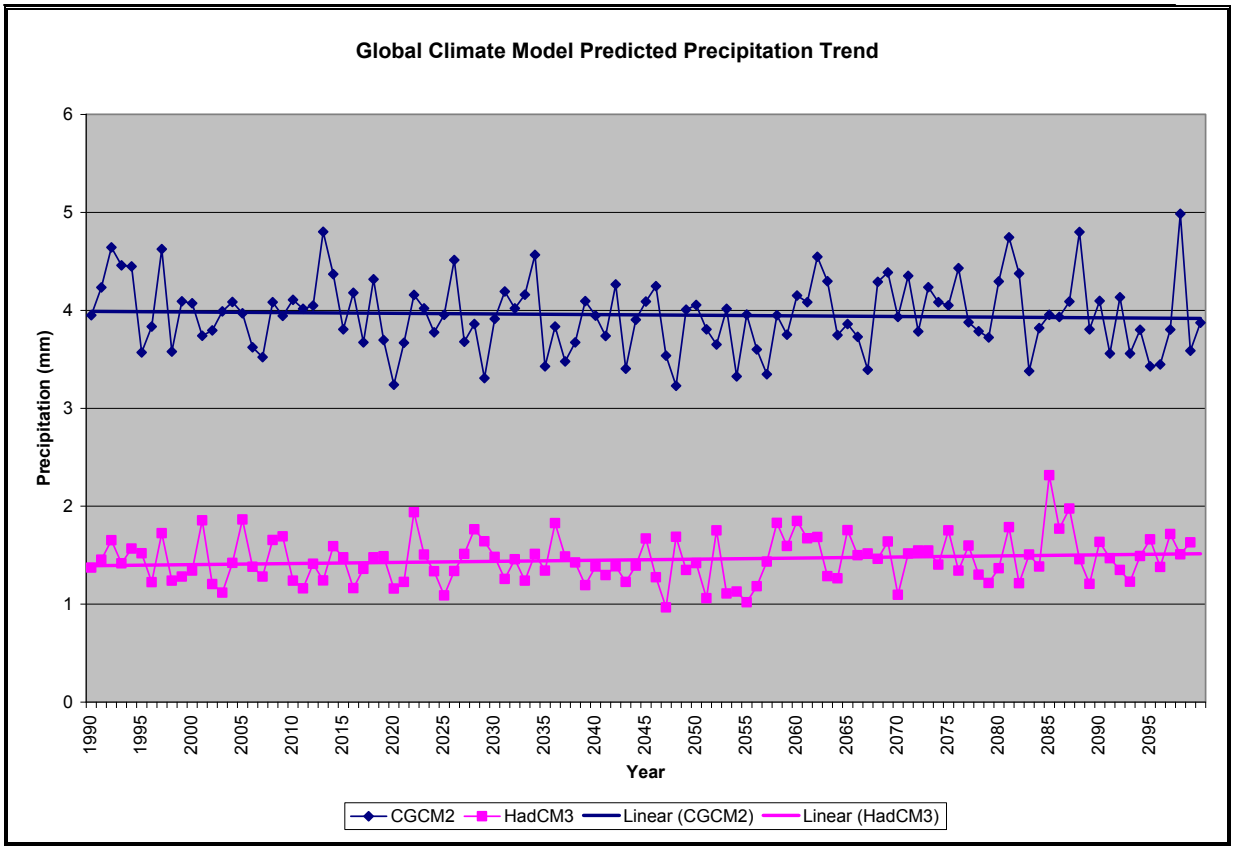

Figure 11.3 CGCM2 and HadCM3 Global Climate Model predicted Daily Averaged Precipitation Trend from 1990 – 2100

When referring to future climate change scenarios, it is customary amongst the scientific community to refer to three periods: the 2020‟s (2010 to 2039), the 2050‟s (2040 to 2049) and the 2080‟s (2070 to 2099). A monthly, seasonal and annual analysis of these three periods is presented in Table 11.1. Values presented in this table are predicted model changes from the 1980‟s base period (1971-2000). The table shows that temperature increases are generally expected in all three periods on an annual, seasonal, and monthly basis. One exception exists during the month of February in the HadCM3 model, where a decrease in mean temperature is predicted for the 2020‟s. This decrease is compensated for in the 2050‟s with a 0.89°C increase from the 1980‟s base period.

The models differ in their estimated precipitation predictions with the HadCM3 model predicting drier conditions than the CGCM2 model. The HadCM3 model predicts an annual increase in precipitation of 0.11% from the base period for the 2080‟s, while the CGCM2 model shows a decrease of 0.03% by the 2080‟s.

Table 11.1 Projected HadCM3 and CGCM2 Changes for Temperature and Precipitation

	Temperature (°C)						Precipitation (%)					
	HadCM3			CGCM2			HadCM3			CGCM2		
Month	2020's	2050's	2080's	2020's	2050's	2080's	2020's	2050's	2080's	2020's	2050's	2080's
January	0.42	0.73	1.58	0.73	1.60	3.67	0.18	0.13	0.60	0.28	0.01	0.26
February	-0.10	0.89	1.18	0.90	2.10	4.49	-0.11	-0.21	-0.81	-0.04	-0.14	0.15
March	0.73	1.66	2.16	3.17	3.10	3.83	-0.15	-0.07	0.50	0.13	0.15	0.02
April	0.74	1.75	2.40	2.94	3.31	3.39	-0.14	0.05	0.27	0.01	0.43	0.13
May	0.46	1.22	1.93	1.97	2.34	3.41	-0.58	-0.14	-0.31	-0.60	0.31	-0.45
June	0.65	1.35	2.32	1.64	1.76	3.43	-0.01	-0.11	-0.30	-0.08	0.93	0.36
July	0.83	1.68	2.52	1.54	2.01	3.61	0.01	0.52	0.37	-0.42	-0.53	-0.86
August	1.25	2.28	2.95	2.53	2.35	3.84	0.03	0.01	-0.22	0.00	0.15	-0.28
September	1.06	2.43	2.94	0.86	1.82	3.00	0.35	0.10	0.43	-0.25	-0.31	-0.27
October	0.76	1.81	2.14	1.07	2.23	2.44	-0.28	0.08	-0.17	0.29	0.28	0.28
November	0.55	1.03	1.51	1.88	2.28	3.27	0.20	0.12	0.36	0.11	0.30	0.32
December	0.77	0.93	1.34	0.12	2.10	2.28	0.30	0.20	0.62	0.01	-0.03	0.04
Winter	0.36	0.85	1.37	0.58	1.93	3.48	0.12	0.04	0.14	0.08	-0.05	0.15
Spring	0.64	1.54	2.16	2.69	2.92	3.54	-0.29	-0.05	0.15	-0.15	0.30	-0.10
Summer	0.91	1.77	2.60	1.90	2.04	3.63	0.01	0.14	-0.05	-0.17	0.18	-0.26
Autumn	0.79	1.76	2.20	1.27	2.11	2.90	0.09	0.10	0.21	0.05	0.09	0.11
Annual	0.68	1.48	2.08	1.61	2.25	3.39	-0.02	0.06	0.11	-0.05	0.13	-0.03

12.0 Comparison of Physical Environmental Data Assembled in 2001 and 2011

In 2001 a report was prepared on the physical environmental data which would impact production systems at White Rose. At that time there was less site specific data available. The data was largely intermittent with the exception of the AES40 data set which consisted of wind and wave modeling data produced in 6-hour time steps by Oceanweather Inc. The environmental data was collected during exploration drilling as a result of the CNLOPB Physical Environmental Guidelines for data collection during drilling periods. This data was biased towards the summer season, and very little data existed for the spring season due to sea ice coverage.

The same data sources were used for the 2011 report but due to production drilling there is more data available. The AES40 data set has been replaced with the MSC50 data set which consists of wind and wave modeling data results produced on 3-hour time steps. The current data is still lacking in quantity but the data set now consists of an additional three years of almost continuous current data for years 2008 to 2010.

12.1 Wind Speeds

The highest wind speed in the AES40 data set used in the previous report for the White Rose location was 29 m/s. The Hibernia 9-year time series from rigs during exploration drilling on the Grand Banks between 1980 and 1988 had a maximum wind speed of 42 m/s at anenometer height. During the "Ocean Ranger" storm of February 1982, the Sedco 706 reported winds of 40 m/s gusting to 47 m/s at anenometer height. Assuming a neutral atmosphere and adjusting this value to the 10 m reference height would give a value of approximately 32.4 m/s.

The wind speeds are higher in the present report due to the severe storm of February 11, 2003 and because there is more continuous observations from the Grand Banks. The MSC50 data has a maximum wind speed of 32 m/s as compared with 29 m/s from the AES40. In general, the MSC50 data set has higher wind speed values due to the time steps in the model changing from 6 hours to 3 hours.

During the February 11, 2003 storm, the Henry Goodrich reported a wind speed of 52.5 m/s and Hibernia reported 49.4 m/s, with gusts going off scale on the anemometers. These wind speeds are at anenometer height, and hence stronger than the winds would be at the 10 m reference height. The Terra Nova FPSO was not reporting and there were no platforms on the White Rose field during this event.

12.2 Waves

The highest significant wave height in the data used in the previous report from the AES40 data set and rig observations was 13.7 m. For the present analysis, the MSC50 data set had a maximum significant wave height of 14. 8 m for February 1982. Note that this value is due to a re-analysis of the data for the MSC50 data set and was not previously present in the AES40 data set. The February 1982 maximum significant wave

height was 12.1 m in the AES40 data set. During the February 11, 2003 storm, the significant wave height at Terra Nova measured 14. 6 m.

12.3 Extreme Wind and Waves

A comparison of the 1-hour, 10-minute and 1- minute winds between the previous work and the present report is shown in Table 12.1 for return periods of 1-year, 10-years, 25-years, 50-years and 100-years. Both sets of results were produced from an extremal analysis using a Gumbel distribution.

Table 12.1 Comparison of Extreme Winds between the 2001 Report and 2011 Report

Return Period	1-hr Winds (m/s)		10 Min (m/s)		1-sec (m/s)	
	2001	2011	2001	2011	2001	2011
1-year	24.3	25.1	25.7	26.6	29.6	30.6
10-years	27.5	28.6	29.2	30.4	33.6	34.5
25-years	28.8	30.0	30.5	31.8	35.1	36.6
50-years	29.7	31.1	31.4	32.9	36.2	37.9
100-years	30.6	32.1	32.4	34.0	37.3	39.1

Using a Gumbel distribution the extreme significant wave heights were calculated for the same return periods. A comparison of the results is shown in Table 12.2.

Table 12.2 Comparison of Extreme Waves between the 2001 Report and 2011 Report

Return Period	Significant Wave Height (m)		Associated Peak Period (s)	
	2001	2011	2001	2011
1-year	10.5	10.8	13.6	13.7
10-years	12.7	13.0	14.9	15.0
25-years	13.5	13.8	15.4	15.4
50-years	14.1	14.4	15.7	15.7
100-years	14.7	15.0	16.0	16.0

The extreme significant wave heights used in the basis of design for White Rose were derived from environmental contour plots of significant wave heights versus spectral peak periods for the various return periods. The significant wave heights were from a Weibull distribution and the spectral peak periods were from a lognormal distribution. The previous work was based on the AES40 data set in 6-hour time steps. The 100-year significant wave height was 15.0 m in the previous work whereas the 100-year significant wave height is 15.9 m from the present work using the MSC50 data set in 6-hour time steps and 16.5 m using the MSC50 data set in 3-hour time steps. The difference between 15.0 m and 15.9 m is partially due to values for the maximum significant wave heights changing to 14.8 m for February 1982 in the MSC50 data set as compared with 12.1 m in the AES40 data set. A comparison of the significant wave heights and spectral peak periods between the two data sets for 6-hour time steps is presented in Table 12.3. Table

12.4 presents the significant wave heights and spectral peak periods from the MSC50 data for 3-hour time steps.

Table 12.3 Comparison of Significant Wave Heights and Spectral Peak Periods between AES40 and MSC50 Data

	Significant Wave Height (m)		Spectral Peak Periods (s)	
Return Period	**2001**	**2011**	**2001**	2011
1-year	10.4	11.0	13.8	13.8
10-years	12.8	13.5	14.9	15.0
25-years	13.7	14.4	15.3	15.5
50-years	14.4	15.2	15.6	15.8
100-years	15.0	15.9	15.8	16.1

Table 12.4 Significant Wave Heights and Spectral Peak Periods from the Environmental Contour Plots using MSC50 Data in 3-hour Time Steps

Return Periods	Significant Wave Heights (m)	Spectral Peak Periods (s)
1-year	11.8	14.3
10-years	14.2	15.5
25-years	15.1	16.0
50-years	15.8	16.3
100-years	16.5	16.7

12.4 Extreme Air Temperatures

The coldest recorded temperature occurred on the Grand Bank on March 10, 1986 with a value of -17.3°C. This was an unusual event due to winds from the northwest and extensive sea ice coverage. The 100-year minimum extreme temperature was calculated as -18.5°C from a Gumbel distribution as compared to -19.2°C in the 2001 report when there was less data available. The 100-year maximum extreme temperature was calculated as 25.1°C as compared to the previous value of 24.8°C.

12.5 Currents

The maximum measured current in the previous work was 89.0 cm/s, 46.0 cm/s, and 50.6 cm/s for near-surface, mid-depth, and near-bottom, respectively. During the last three years, the maximum measured currents were 60.7 cm/s, 55.6 cm/s, and 41.6 cm/s for near surface, mid-depth, and near-bottom, respectively. The extreme analysis was carried out using a Gumbel distribution on 4-years of data in the present work and on 1-year of data previously. A comparison of the extreme values is presented in Table 12.5 and the upper 95% confidence limit values in Table 12.6.

Table 12.5 Extreme Current Speeds using 1-year and 4-years of Data

	Current Speed (cm/s) Near Surface		Current Speed (cm/s) Mid-depth		Current Speed (cm/s) Near-bottom	
Return Period	**2001**	**2011**	**2001**	**2011**	**2001**	**2011**
1-year	73	81	44	43	43	43
10-years	101	104	56	47	57	51
25-years	112	112	61	49	62	54
50-years	120	119	64	50	66	56
100-years	128	126	68	51	70	58

Table 12.6 Comparison of the Extreme Current Speeds with a Upper 95% Confidence Limit

	Current Speed (cm/s) Near Surface		Current Speed (cm/s) Mid-depth		Current Speed (cm/s) Near-bottom	
Return Period	**2001**	**2011**	**2001**	**2011**	**2001**	**2011**
1-year	93	93	53	45	53	47
10-years	136	125	71	51	73	58
25-years	153	138	78	54	82	63
50-years	166	148	84	56	88	66
100-years	180	157	89	58	94	69

In general, the increase in the amount of data resulted in a decrease in the extreme current speed values.

The maximum tidal current is approximately 15 cm/s. Therefore, this value is added to the extreme current speeds using the upper 95% confidence limit values in the basis for design values. The 100-year design values for White Rose was based on the upper 80% confidence limit and had values of 170 cm/s, 90 cm/s, and 94 cm/s for near-surface, mid-depth, and near-bottom, respectively. By being more conservative and using the 95% confidence limits plus adding the maximum tidal currents gives a 100-year extreme value of 172 cm/s, 73 cm/s, and 84 cm/s for near-surface, mid-depth, and near-bottom, respectively.

12.6 Tides

The tides were measured at White Rose between November 6, 2009 and February 28, 2010, from which the tidal constituents were calculated and a 20-year tidal prediction was carried out. From this analysis, the astronomical tidal range was found to be 83 cm as compared to 1.04 cm used previously from tidal heights measured at Terra Nova.

12.7 Sea Ice

The analysis of sea ice for the period 1980 – 2010 gave similar results to the information in the previous report. A comparison of the results for the two periods is presented in Table 12. 7.

Table 12.7 Comparison of Sea Ice Results

	1960 – 2000			1980 - 2010		
	Mean	**Maximum**	**Extreme**	**Mean**	**Maximum**	**Extreme**
Duration	3.9 weeks	7 weeks	11 weeks	3.4 weeks	7 weeks	11 weeks
Concentration	50%	90%	100%	65%	95%	100%
Thickness	70 cm	100 cm	200 cm	70 cm	200 cm	>200cm
Floe Size	< 30 m	60 m	>100 m	< 30 m	60 m	> 100 m
Drift Speeds	0.25 m/s	0.6 m/s	1.0 m/s	0.25 m/s	0.6 m/s	1.0 m/s

12.8 Icebergs

The mean number of iceberg in a 60 nautical mile radius of White Rose has changed only slightly from 47 to 60 per year. The maximum size of icebergs has increased due to the presence of a large tabular iceberg in 2004 which was measured and the mass calculated to be 3.2 million tonnes, and the observations of a very large iceberg in 2009 which PAL estimated to have a mass of 5.9 million tones. The comparison information is presented in Table 12.8.

Table 12.8 Comparison of Iceberg Results

	1988-2000		1974-2009	
	Mean	**Maximum**	**Mean**	**Maximum**
Distribution (1° grid)	47	217	60	215
Mass (tonnes)				
60 nm	215,350	3.9 million	168,532	5.9 million
25 nm	186,000	2.2 million	131,164	3.2 million
Drift Speeds	0.3 m/s	1.3 m/s	0.26 m/s	1.8 m/s

References

Archer, C.L., and K. Caldeira, 2000. Historical trends in the jet streams, *Geophys. Res. Lett.*, V.35, L08803, doi:10.1029/2008GL033614.

Archer, C.L., and K. Caldeira, 2008. Historical trends in the jet streams, *Geophys. Res. Lett.*, V.35, L08803.

Basham, P.W., D.H. Weichart, F.M. Anglin and M.J. Berry, 1982. New Probabilities Strong Seismic Ground Motion Maps of Canada. A compilation of Earthquake Source Zones, Methods and Results. Earth Physics Branch, Open File No. 82/33, Ottawa.

Basham, P.W. and J. Adams. 1982. Earthquake Hazards to Offshore Development on the Eastern Canadian Continental Shelves. Second Canadian Conference on

Basham, P.W., J. Adams and F.M. Anglin, 1983. Earthquake Source Models for Estimating Seismic Risk on the Eastern Canadian Continental Margin. Proceedings, Fourth Canadian Conference on Marine Geotechnical Engineering, p.495-508.

Basham, P.W., and J. Adams, 1983. Earthquakes of the Continental Margin of Eastern Canada. Need for Future Large Events to Confirm the Location of Large Historical Events? In US Geol. Survey Open File Rep. "The 1886 Charleston Earthquake and its implication for today".

Bell, G.D., and M. Chelliah, 2006. Leading Tropical Modes Associated with Interannual and Multidecadal Fluctuations in North Atlantic Hurricane Activity. *J. Climate*, V.19, p.590–612.

Blenkarn, K.A., and A.E. Knapp, 1969. Ice Conditions on the Grand Banks. Canadian Institute of Mining and Metallurgy, Special Volume 10, (Ice Seminar), Calgary, AB.

Borgman, L.E., 1973. Probabilities for the highest wave in a hurricane. J. Waterways, Harbors and Coastal Engineering Div., ASCE, p.185-207.

Chakrabarti, S.K., 1987. Hydrodynamics of Offshore Structures. Computational Mechanics Publications, Southhampton.

Canada Oil and Gas Lands Administration (COGLA)), 1987. Development of Seismic Hazard Maps for Eastern Canada Offshore Regions. Energy, Mines and Resources Canada, Technical Report No. 100 (prepared by Q.M. Atkinosn, A.B. Cammert, R. Gill and W.D.L. Finn).

Colbourne, E., 2002. Physical Oceanographic Conditions on the Newfoundland and Labrador Shelves during 2001. CSAS Res.Doc. 2002/023.

Colbourne, E.B., 2000. Oceanographic Conditions in NAFO Divisions 2J3KLMNO during 1999 with Comparisons to the Long-term (1961-1990) Average. Canadian Stock Assessment Secretariat Research Doc 2000/48, 50 p.

Colbourne, E.B., and K.D. Foote, 1994. Spatial Temperature and Salinity Fields over the Shelves of Newfoundland and Labrador. Can. Tech. Rep. Hydrog. Ocean Sci., V.160, 128 p.

Colbourne, E.B., and K.D. Foote, 2000. Variability of the Stratification and circulation on the Flemish Cap during the decades of 1950s and 1990s. J. Northw. Atl. Fish Sci., V.26, p.103-122.

Colbourne, E.B., D.R. Senciall, and K.D. Foote, 1996. Temperature, Salinity and Sigma. T. along the standard Flemish Cap transect. Can.Tech.Rep. Hydrog.Ocean Sci., V.172, 222p.

Colbourne, E.B., 2004. Decadal Changes in the Ocean Climate in Newfoundland and Labrador Waters from the 1950s to the 1990s**.** J. Northw. Atl. Fish. Sci., V.34, p.41–59.

Colbourne, E., B. deYoung, S. Narayanan, and J. Helbig, 1997. Comparison of hydrography and circulation on the Newfoundland Shelf during 1990–1993 with the long-term mean**.** Can. J. Fish. Aquat. Sci. V.54 (Suppl. 1), 1997.

Colbourne, E.B., and K.D. Foote, 2000. Variability of the Stratification and Circulation on the Flemish Cap during the Decades of the 1950s-1990s. J. Northw. Atl. Fish. Sci**.,** V.26, p.103–122.

Dawson, J., 1977. Freak Ocean Waves Are Episodic. New Scientist, V.73, p.7-9.

Deser, C., J.E. Walsh, and M.S. Timlin, 2000. Arctic sea ice variability in the context of recent wintertime atmospheric circulation trends. *Journal of Climate*, V.13**,** p.617–633.

Dobrocky Seatech, 1985. Field Data Report: Sea Ice Documentation in the Vicinity of the Hibernia Drilling Area. Report prepared for Mobil Oil Canada Ltd., Calgary, AB.

Drinkwater, K.F. and R.W. Trites, 1986. Monthly Means of Temperature and Salinity in the Grand Banks Region. Can. Tech. Rep. Fish. Aqu. Sci., V.1450, 111 p.

Environment Canada, 1997. The Canada Country Study: Climate Impacts and Adaptation, Atlantic Canada Summary.

Environment Canada, 2001. *Sea Ice Climatic Atlas: East Coast of Canada, 1971-2000.* Ottawa: Canadian Government Publishing.

Elsner, J.B., 2003. Tracking Hurricanes. Bulletin of the American Meteorological Society. V.84 p.353-356.

Elsner, J.B., and B.H. Bossak, 2004. "Hurricane landfall probability and climate", in Hurricanes and Typhoons: Past, Present, and Future, R. Murnane & K.-b. Liu, Eds., Columbia University Press.

Foo, S.H.C. and C.B. Crose, 1986. Evaluation of Seismicity and Earthquake Loading at Hibernia. Third Canadian Conference on Marine Geotechnical Engineering, V.1, p.55-85.

Foreman, M.G.G., 1978 (revised 2004). Manual for tidal heights analysis and prediction poufie Marine Science Report. 77-10. Institute of Ocean Science, Patricia Bay, 58 pp.

Forristall, G.Z., 1978. On the statistical distribution of wave heights in a storm. J. Geophys. Res., V.83, p.2353-2358.

Godin, G, 1980. Cotidal Charts for Canada. Marine Science Information Directorate. Man. Rep. Series, No. 55, Fisheries and Oceans Canada, 93 p.

Greenberg, D.A., and B.D. Petrie, 1988. The Mean Barotrophic Circulation on the Newfoundland Shelf and Slope 1951-1980. J. Geoph. Res., V.93 (C 12), PERD Project, 15541-15550.

Han G, and Z. Wang, 2006. Monthly mean circulation in the Flemish Cap Region: a Modeling Study, Estuarine and Coastal Modeling, ASCE. p.138-154.

Han, G., K. Ohashi, N. Chen, P.G. Myers, N. Nunes, J. Fischer, 2010. Decline and partial rebound of the Labrador Current 199302994. Monitoring ocean currents from altimetric and CTD data. J. Geophys., Res. V.115, C12012, doi:1029/2009/JC006091, 2010.

Harris, Erin. Personal Correspondence. Oceanweather, October 15, 2007.

Hart, R.E., and J.L. Evans, 2001. A Climatology of extratropical transition of Atlantic tropical cyclones. J. Climate, V.14, p.546-564.

Hasselmann, K., T.P. Barnett, E. Bouws, H. Carlson, D.E. Cartwright, K. Enke, J.E. Ewing, H. Gienapp, D.E. Hasselmann, P. Kruseman, A. Meerburg, P. Muller, D.J. Olbers, K. Richter, W. Sell and H. Walden, 1973. Measurements of the Wind-Wave Growth and Swell Decay during the Joint North Sea Wave Project (JONSWAP). Deutsche Hydrographische Zeitschrift, Reihe A (8), No. 12.

Helbig, J.A. and P. Brett, 1995. A Compendium of Satellite Tracked Drifting Buoy Observations Collected on the Labrador Shelf, Northeast Newfoundland Shelf, and Grand Banks. Unpublished Report.

Hukuda, H., R.J. Greatbach and A.E. Hay, 1989. A Simple Three-Dimensional Model of the Circulation off Newfoundland. J. Geoph. Res., V.94 (C9), p.12607-12618.

Kent, E.C., P.K. Taylor, B.S. Truscott and J.S. Hopkins, 1993. The Accuracy of Voluntary Observing Ships‟ Meteorological Observations – Results of the VSOP-NA. J. Atmosph. Oceanic Technol., V.10, p.591-608.

Krauss, W., R.H. Kase and H.H. Hinrichsen, 1990. The Branching of the Gulf Stream Southeast of the Grand Banks. J. Geoph. Res., V.95 (C8), p.13089-13103.

Lazier, J.R.N., 1982. Seasonable Variability and Salinity in the Labrador Current. J. Mar. Res. Sup. V.40, p.341-355.

Lazier, J.R.N. and D.G. Wright, 1993. Annual velocity Variations in the Labrador Current. J. Phys. Oceanog., V.23, p.659-678.

Laxon, S., N. Peacock, and D. Smith, 2003. High interannual variability of sea ice in the Arctic region. *Nature,* V.425**,** p.947–950.

LeBlond, P.H., 1982. Preliminary Review of Nonspectral Wave Properties: Grouping, Wave Breaking, and Freak waves. Canadian Contractor Report of Hydrography and Ocean Sciences, No. 1, Marine Environmental data Services Branch, Department of Fisheries and Oceans, Ottawa, 66 p.

LeBlond, P.H., S.M. Calisal, and M. Isaacson, 1982. Wave Spectra in Canadian Waters. Can. Tech. Rep. Hydro. Ocean Sci., V.6, 57 p.

Ledrew, B.R., and S.T. Culshaw, 1977. Ship in the Ice Data Report. C-CORE. St. John‟s, NF. Publication No. 77, 28 p.

Louis, J. P., B.D. Petrie, and P.C. Smith, 1982. Observations of Topographic Rossby Waves on the Continental Margin off Nova Scotia. J. Phys. Oceanog., V.12, p.47-55.

Makkonen, L., R.D. Brown, and P.T. Mitten, 1991. Comments on “Prediction of Vessel Icing for Near-Freezing Sea Temperatures”. Wea. Forecasting, V.6, p.565–567.

Marko, J.R., D.B. Fissel, P. Wadhams, P.M. Kelly, and R.D. Brown, 1994. "Iceberg Severity off Eastern North America: It‟s Relationship to Sea-Ice Variability and Climate Change." Journal of Climate, 7 p. 1335-1351.

Murty, T.S., 1977. Seismic Sea Waves – Tsunamis. Bull Fish. Res. Board Can V.198, 337 pp.

McCabe, G., M.P. Clark, M.C. Serreze, 2001. Trends in Northern Hemisphere Surface Cyclone Frequency and Intensity. *J. Climate*, V.14, p.2763–2768.

McLaren, A.S., 1989. The Under-Ice Thickness Distribution of the Arctic Basin as Recorded in 1958 and 1970, *J. Geophys. Res.*, 94(C4), 4971–4983.

McLaren, A.S., J.E. Walsh, T.H Bourke, R.L. Weaver, and W. Wittmann, 1992. Variability in se-ice thickness over the North Pole from 1977 to 1990, Nature, V.358, p.224-226.

McLellan, H.J., 1957. A Slope Water Survey – July 1954. Fish. Res. Board Can., Manuscript Reports of the Biological Stations, V.632, 49p.

Minsk, L.D., 1977. Ice Accumulation on Ocean Structures. CRREL Rep. 77-17, Cold Regions Research and Engineering Laboratory, Hanover, N.H., 42pp.

Muller, P., 1976. Parameterization of one-dimensional wind wave spectra and their dependence on the state of development. *Hamburger geophysikalische Einzelschrijten,* Heft 3 1. Hamburg : G. M. L. Wittenborn Sohne.

Murphy, D.L., W.E. Hanson, and R.L. Tuxhorn, 1991. Modifications to Ice Patrol‟s Mean Current Base. Report of the International Ice Patrol in the North Atlantic. US Coast Guard Bulletin, No. 76, CGC /188 /45.

Murty, T.S, 1977. Seismic Sea Waves. Fish. Res. Board Can., V.198, 337 p.

Narayanan, S., S. Prinsenberg and P.C. Smith, 1996. Current Meter Observations from the Labrador and Newfoundland Shelves and Comparisons with Barotrophic

Model Predictions and IIP Surface Currents. Atmosphere – Ocean, V.34, No. 1, 227-255.

Neumann, C.J., B.R. Jarvinen, C.J. McAdie, and J.D. Elms, 1993. Tropical cyclones of the North Atlantic Ocean, 1871–1992. National Climatic Data Center in cooperation with the National Hurricane Center, Coral Gables, FL, 193 pp. [Most recent track information available online at http://www.nhc.noaa.gov.]

Nolan-Ertec Ltd., 1981. Hibernia Gravity Base Structure, Preliminary Foundation Evaluation, Vol. A. Prepared for Mobil Oil Canada Ltd. by Hibernia Development Studies 1981.

Nolte, K.G., and M.E. Trethart, 1971. North Atlantic Sea Ice Survey. Report prepared by AMOCO Canada Petroleum Co. Ltd., Calgary, AB.

National Snow and Ice Data Center, 2009. *International Ice Patrol (IIP) Iceberg Sightings Data base.* Boulder, Colorado USA: National Snow and Ice Data Center/World Data Center for Glaciology. Digital media.

Oceans Ltd., 2001. White Rose Physical Environmental Data for Production Systems. Prepared for Husky Energy Inc., St. John‟s, NL, Canada.

Oceans Ltd., 2007. JONSWAP Peak Enhancement Factors at White Rose. Prepared for Husky Energy Inc., St. John‟s, NL, Canada.

Overland, J.E., C.H. Pease, R.W. Priesendorfer and A.L. Comiskey, 1986: Prediction of vessel icing. *Journal of Climate and Applied Meteorology*, V.25, p.1793-1806.

Overland, J.E., 1990. Prediction of vessel icing for near-freezing sea temperatures, *Weather and Climate*, V.5, p.62-77.

Pepin, P. and J.A. Helbig, 1997. Distributions and Drift of Atlantic Cod (Gadus morhua) Eggs and Larval on the Northeast Newfoundland Shelf. Can. J. Fish Aquat. Sci., V.4, p.670-685.

Petro-Canada, 1995. Development Application – Terra Nova Development: Environmental Impact Statement, prepared on behalf of the Terra Nova Proponents.

Petrie, B., K. Lonk and S. de Margerie, 1987. Tides on the Newfoundland Grand Banks. Atmosphere-Ocean, Vol.25, No. 1, 10-21.

Petrie, B., S. Akenhead, J. Lazier, and J. Loder, 1988. The cold intermediate layer on the Labrador and Northeast Newfoundland Shelves, 1978-1986. NAFO Sci. Counc. Stud., V.12, p.57-69.

Petrie, B. and A. Isenor, 1984. An analysis of Satellite – Tracked Drifter Observations Collected in the Grand Banks Region. Can. Tech. Rep. Hydrog. Ocean Sci., V.39, 64 p.

Petrie, B. and D. Warnell, 1988. Oceanographic and Meteorological Observations from the Hibernia Region of the Newfoundland Grand Banks. Canadian Data Report of Hydrography and Ocean Science, No. 69, 270 p.

Reitan, C.H., 1974. Frequency of Cyclones and Cyclogenesis for North America, 1951-1970. *Mon. Wea. Rev.,* V.102, p.861–868.

Rogers, E., and L.F. Bosart, 1986. An Investigation of Explosively Deepening Oceanic Cyclones. Monthly Weather Review, V.114, p.702-718.

Ross, C., 1980. The Drift of Satellite – Tracked Buoys on Flemish Cap, 1979-80. NAFO Sci. Council. Res. Doc. 80/Ix/127, 12 p.

Seaconsult Ltd, 1988. Terra Nova Development Studies. Physical Environmental Data for Production Systems at Terra Nova. Prepared for Petro-Canada Inc. and Terra Nova partners.

Stein, M., 2007. Oceanography of the Flemish Cap and Adjacent Waters. J. Northw. Atl. Fish. Sci., V.37, p.135-146.

Smith, P.C. and F.B. Schwing, 1991. Mean Circulation and Variability on the Eastern Canadian Continental Shelf. Continental Shelf Res., V.11, p.977-1012.

Smith, R., 1976. Giant Waves. J. Fluid Mechanics, V.77, p.417-431.

Soule, F.M., P.S. Bransom, and R.P. Dinsmore, 1951. Physical Oceanography of the Grand Banks Region and the Labrador Sea in 1951. Contribution No. 601, Collected Reprints of the Woods Hole Oceanographic Institution.

Swail, V.R., V.J. Cardone, M. Ferguson, D.J. Gummer, E.L. Harris, E.A. Orelup and A.T. Cox, 2006. *The MSC50 Wind and Wave Reanalysis*. 9th International Wind and Wave Workshop, September 25-29, 2006, Victoria, B.C.

Teagle, F., 1978. Nightmare Waves. Smithsonian, V.3, C21, 18 p.

Terra Nova Alliance, 1997. Design Environmental Criteria. TN-IM-PM50-X00-001.

United States Geological Survey, Conservation Division, 1979. OCS Platform Verification Program. Reston, Virginia.

U.S. Navy Marine Climatic Atlas of the World – Volume I North Atlantic Ocean (Revised 1974) by J.M. Meserve. Published by Direction of the Commander, Naval Weather Service Command.

Voorheis, G.M., K. Aagaard, and L.K. Coachman, 1973. Circulation Patterns near the Tail of the Grand Banks. J. Phys. Oceanog., V.3, p.397-405.

Wadhams, P., 1990. Evidence for thinning of the Arctic Ocean cover north of Greenland, Nature, V.345, p.795-797.

Wadhams, P., and N.R. Davis, 2000. Further evidence of thinning ice in the Arctic Ocean, Geophys. Res. Lett., V.27, p.3973-3976.

Winsor, P., 2001. Arctic sea ice thickness remained constant during the 1990s, *Geophys. Res. Lett.*, V.28(6), p.1039–1041.

Winterstein, S.R., T. Ude, C.A. Cornell, P. Jarager, and S. Haver, 1993. Environmental Parameters for Extreme Response: Inverse FORM with Omission Factors. ICOSSar-3, Paper No 509/11/3, Innsbruck, 3-12 August 1993.

World Meteorological Organization, 1998. Guide to Wave Analysis and Forecasting. WMO Pub., No. 702, Geneva.

Yao, T., T. Brown, and D. Fissel, 1992. Verification Study of Regional Sea Ice Models. Report by Active Sciences Ltd. to Ice Centre, Environment Canada, 286 p.

Yashayaev, I, and A. Clarke, 2006. Recent warming of the Labrador Sea. DFO AZMP Bulletin, No. 5, 2006.

Appendix 1
Wind Roses and
Wind Speed Frequency Distributions
for MSC50 GridPoint 11034

January

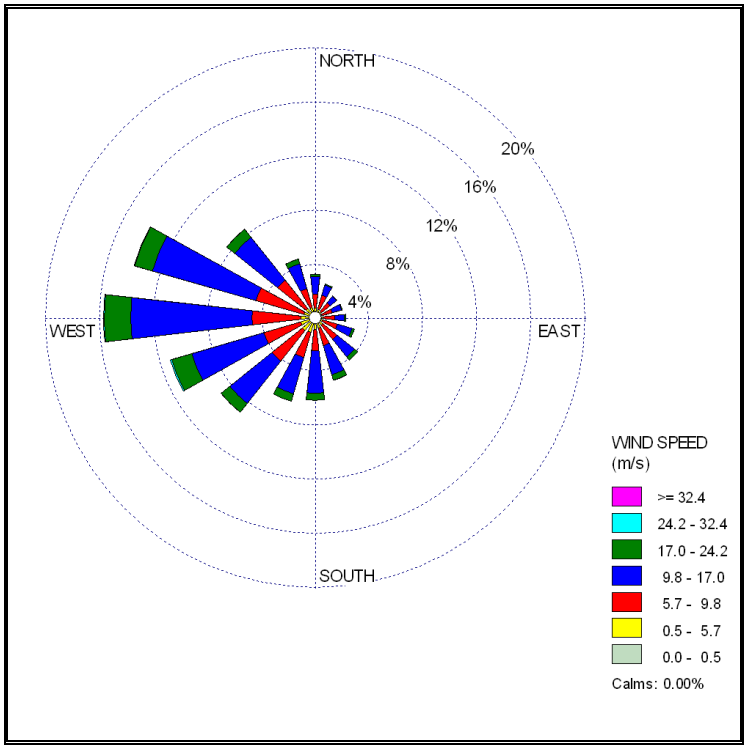
NORTH
20%
16%
12%
8%
4%
WEST
EAST
SOUTH
WIND SPEED
(m/s)
>= 32.4
24.2 - 32.4
17.0 - 24.2
9.8 - 17.0
5.7 - 9.8
0.5 - 5.7
0.0 - 0.5
Calms: 0.00%

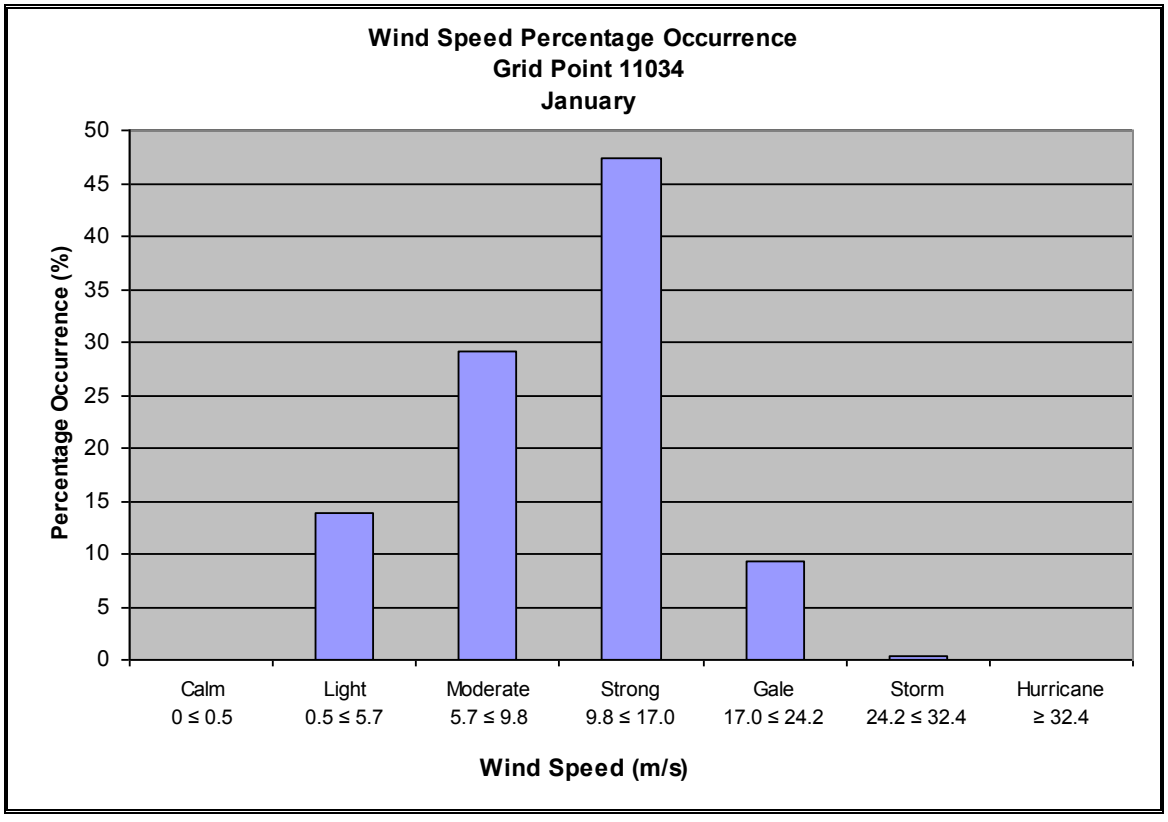
Wind Speed Percentage Occurrence
Grid Point 11034
January
Percentage Occurrence (%)
50
45
40
35
30
25
20
15
10
5
0
Calm
0 ≤ 0.5
Light
0.5 ≤ 5.7
Moderate
5.7 ≤ 9.8
Strong
9.8 ≤ 17.0
Gale
17.0 ≤ 24.2
Storm
24.2 ≤ 32.4
Hurricane
≥ 32.4
Wind Speed (m/s)

February

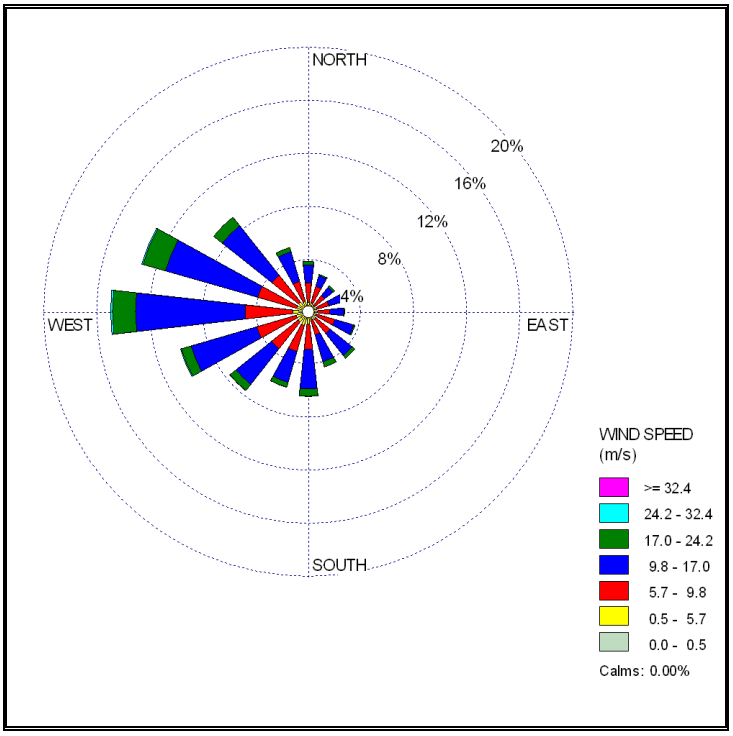
NORTH
20%
16%
12%
8%
4%
WEST
EAST
SOUTH
WIND SPEED
(m/s)
>= 32.4
24.2 - 32.4
17.0 - 24.2
9.8 - 17.0
5.7 - 9.8
0.5 - 5.7
0.0 - 0.5
Calms: 0.00%

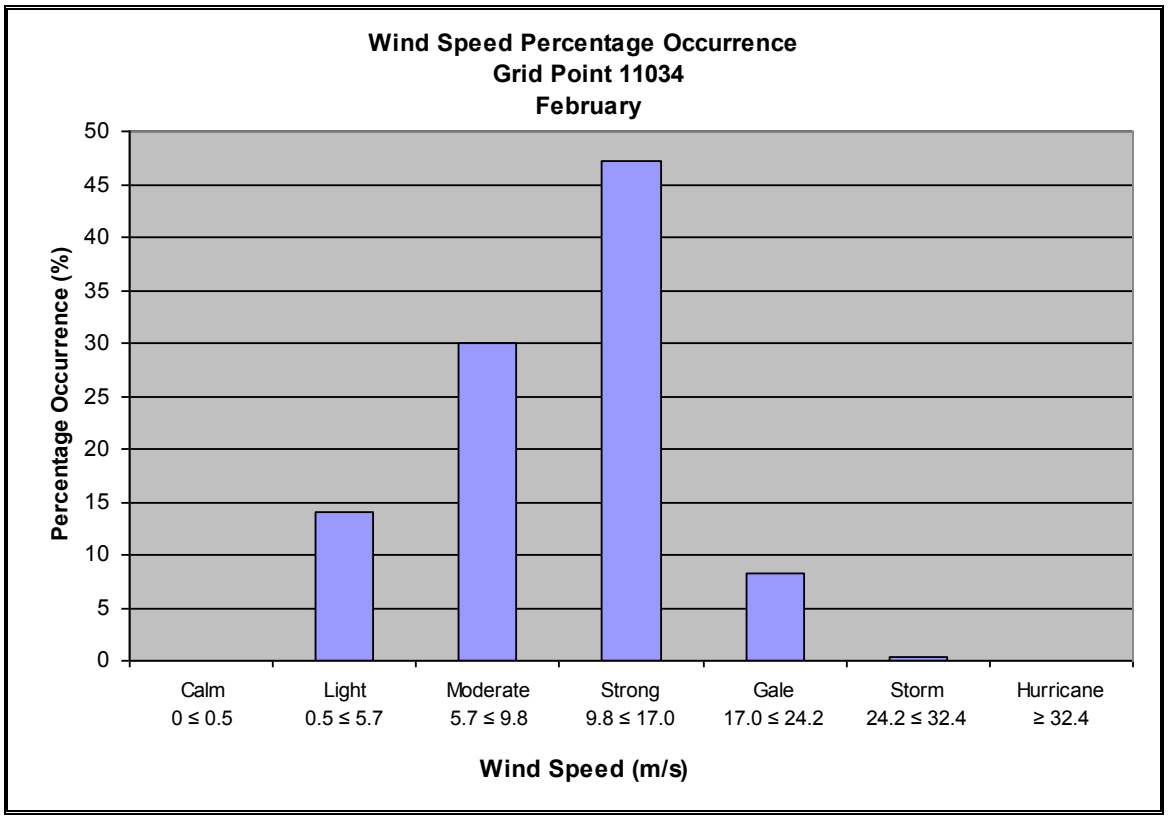
Wind Speed Percentage Occurrence
Grid Point 11034
February
Percentage Occurrence (%)
50
45
40
35
30
25
20
15
10
5
0
Calm
0 ≤ 0.5
Light
0.5 ≤ 5.7
Moderate
5.7 ≤ 9.8
Strong
9.8 ≤ 17.0
Gale
17.0 ≤ 24.2
Storm
24.2 ≤ 32.4
Hurricane
≥ 32.4
Wind Speed (m/s)

March

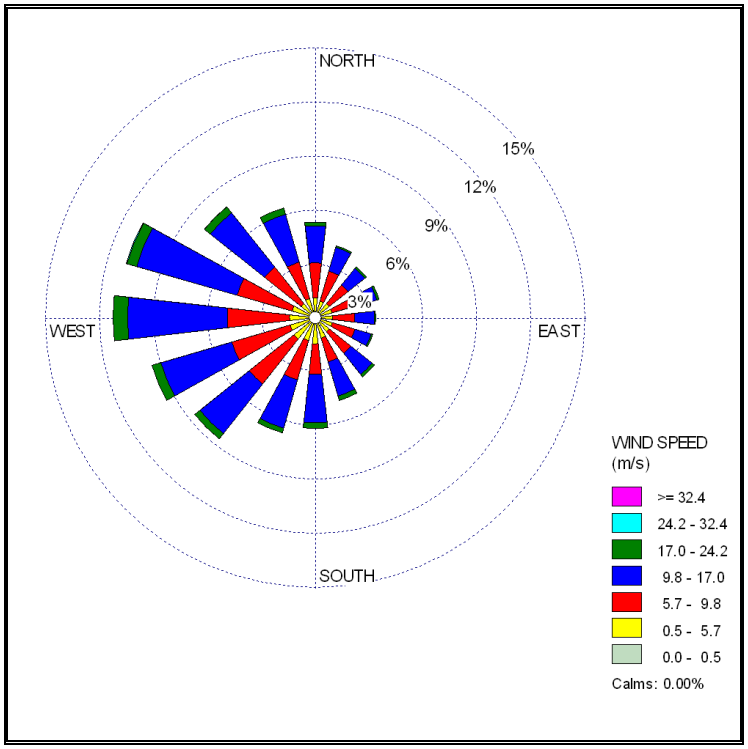
NORTH
15%
12%
9%
6%
3%
WEST
EAST
SOUTH
WIND SPEED
(m/s)
>= 32.4
24.2 - 32.4
17.0 - 24.2
9.8 - 17.0
5.7 - 9.8
0.5 - 5.7
0.0 - 0.5
Calms: 0.00%

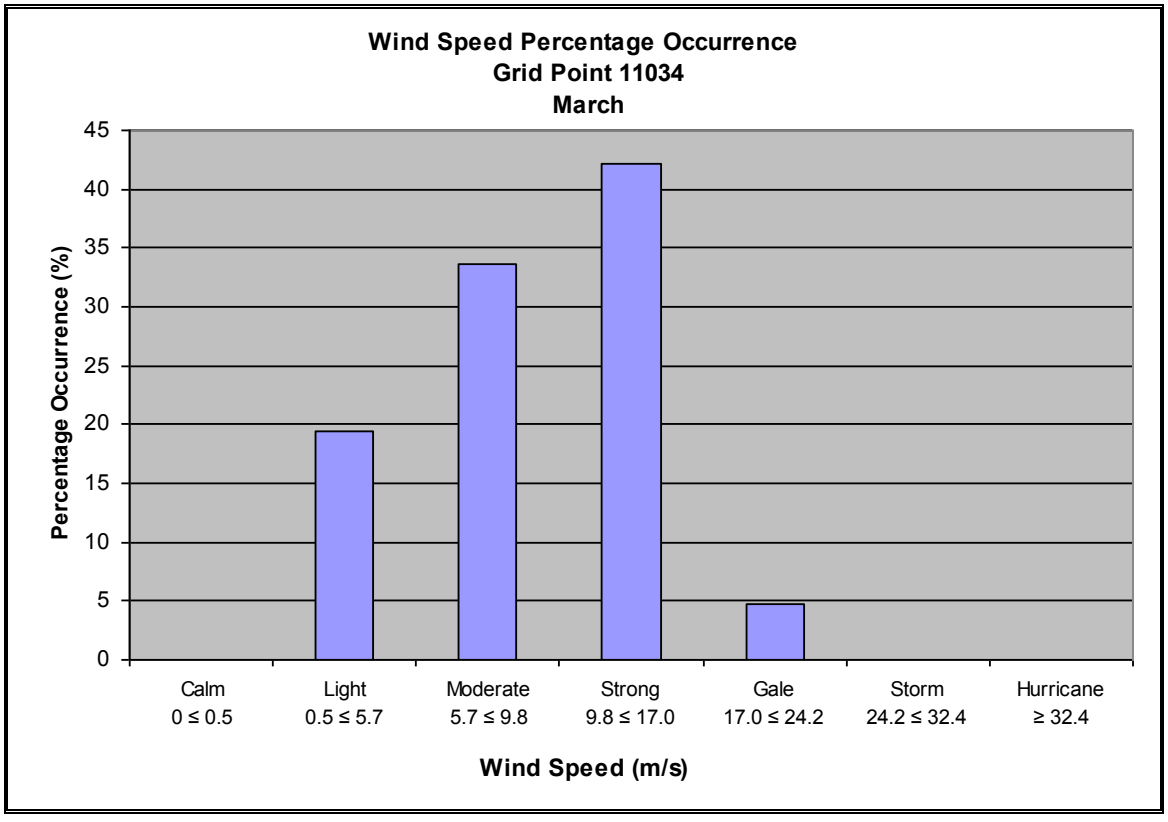
Wind Speed Percentage Occurrence
Grid Point 11034
March
Percentage Occurrence (%)
45
40
35
30
25
20
15
10
5
0
Calm
0 ≤ 0.5
Light
0.5 ≤ 5.7
Moderate
5.7 ≤ 9.8
Strong
9.8 ≤ 17.0
Gale
17.0 ≤ 24.2
Storm
24.2 ≤ 32.4
Hurricane
≥ 32.4
Wind Speed (m/s)

April

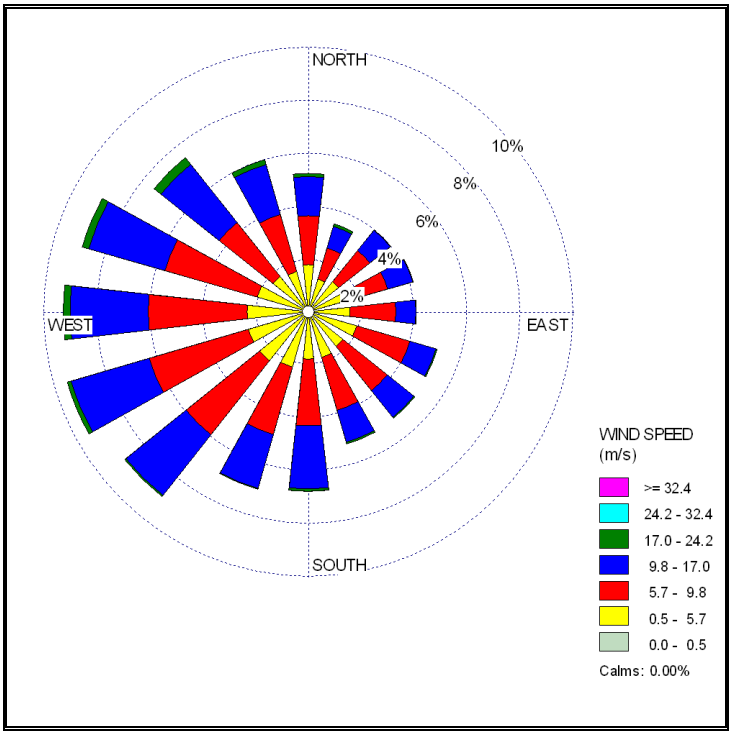
NORTH
EAST
SOUTH
WEST
2%
4%
6%
8%
10%
WIND SPEED
(m/s)
>= 32.4
24.2 - 32.4
17.0 - 24.2
9.8 - 17.0
5.7 - 9.8
0.5 - 5.7
0.0 - 0.5
Calms: 0.00%

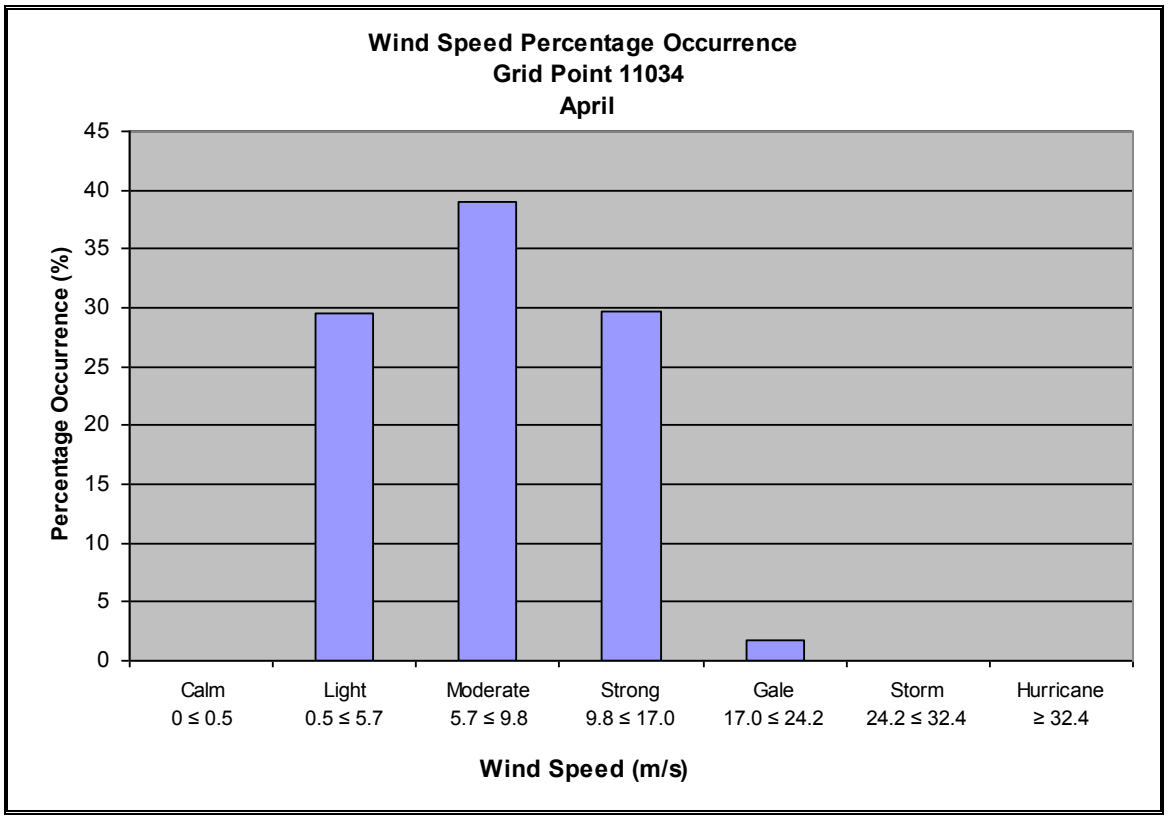
Wind Speed Percentage Occurrence
Grid Point 11034
April
Percentage Occurrence (%)
0
5
10
15
20
25
30
35
40
45
Calm
0 ≤ 0.5
Light
0.5 ≤ 5.7
Moderate
5.7 ≤ 9.8
Strong
9.8 ≤ 17.0
Gale
17.0 ≤ 24.2
Storm
24.2 ≤ 32.4
Hurricane
≥ 32.4
Wind Speed (m/s)

May

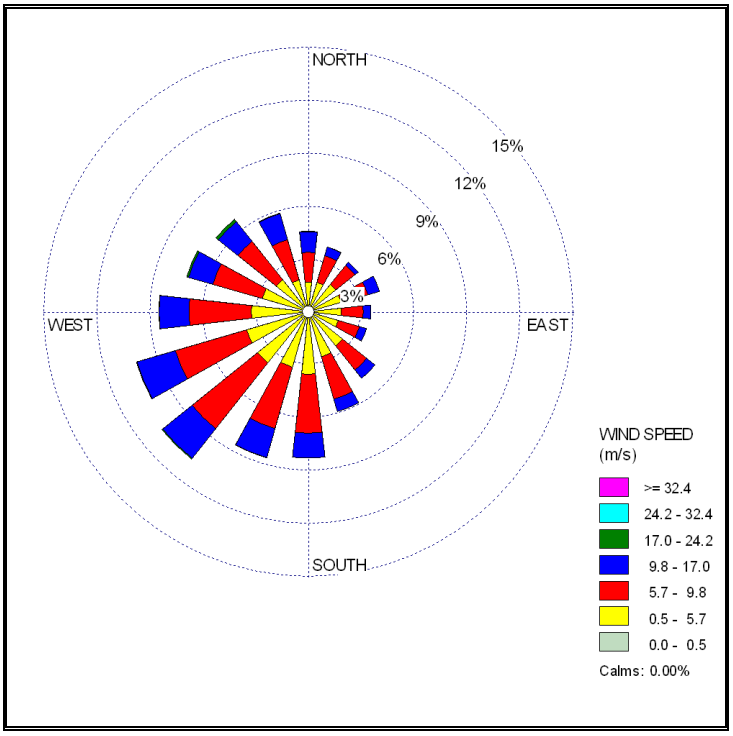
NORTH
15%
12%
9%
6%
3%
WEST
EAST
SOUTH
WIND SPEED
(m/s)
>= 32.4
24.2 - 32.4
17.0 - 24.2
9.8 - 17.0
5.7 - 9.8
0.5 - 5.7
0.0 - 0.5
Calms: 0.00%

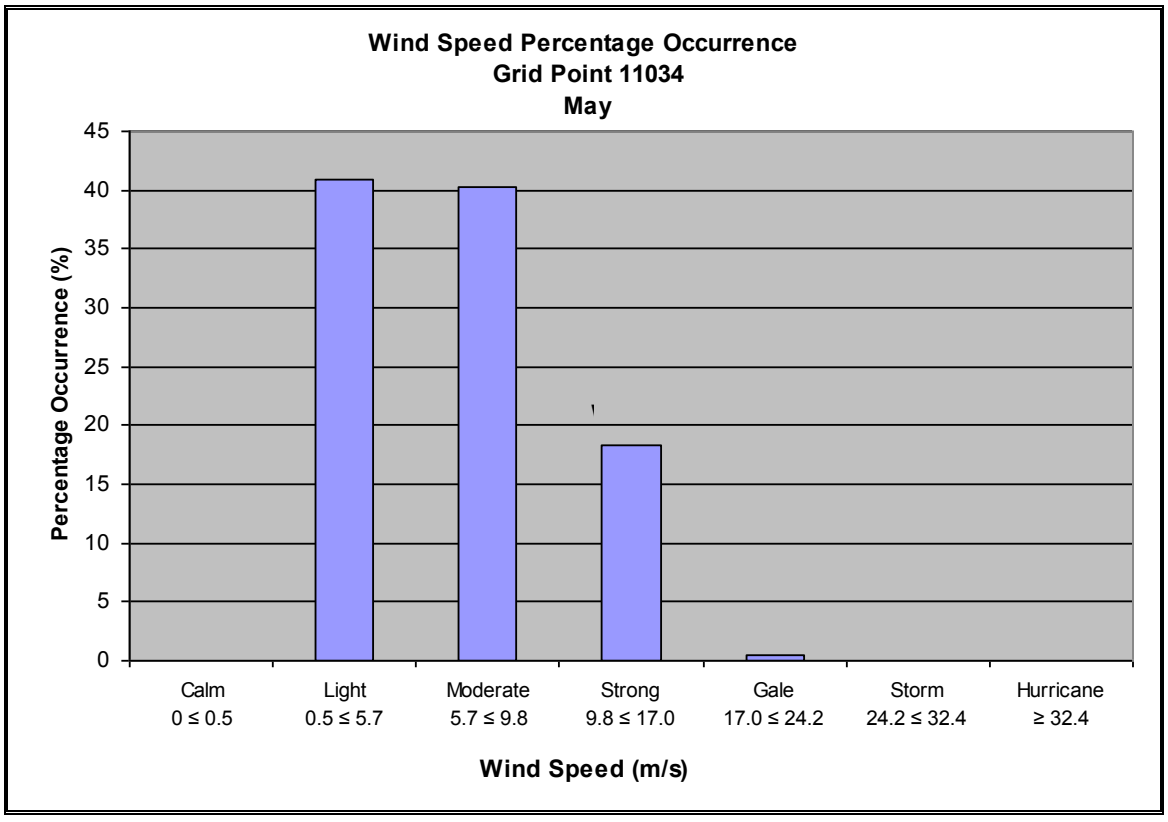
Wind Speed Percentage Occurrence
Grid Point 11034
May
Percentage Occurrence (%)
45
40
35
30
25
20
15
10
5
0
Calm
0 ≤ 0.5
Light
0.5 ≤ 5.7
Moderate
5.7 ≤ 9.8
Strong
9.8 ≤ 17.0
Gale
17.0 ≤ 24.2
Storm
24.2 ≤ 32.4
Hurricane
≥ 32.4
Wind Speed (m/s)

June

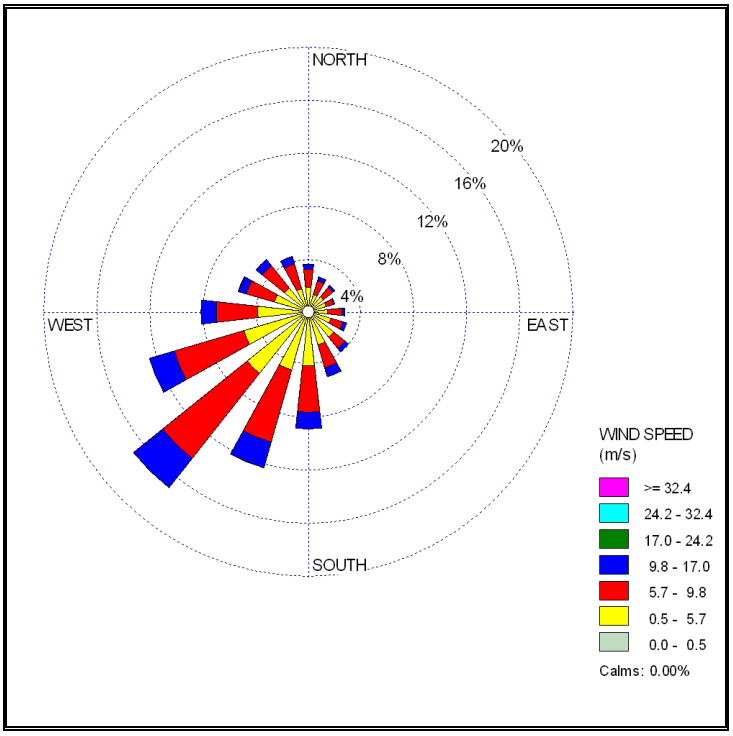
NORTH
20%
16%
12%
8%
4%
WEST
EAST
SOUTH
WIND SPEED
(m/s)
>= 32.4
24.2 - 32.4
17.0 - 24.2
9.8 - 17.0
5.7 - 9.8
0.5 - 5.7
0.0 - 0.5
Calms: 0.00%

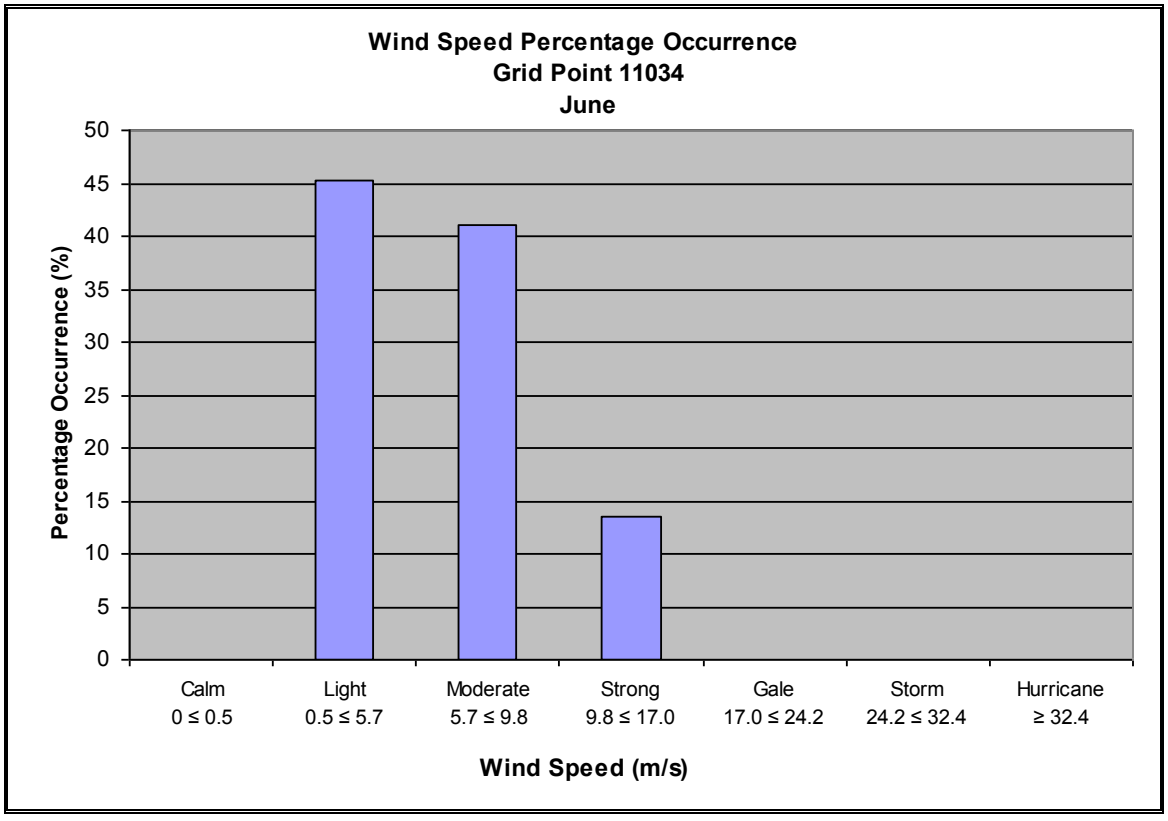
Wind Speed Percentage Occurrence
Grid Point 11034
June
Percentage Occurrence (%)
50
45
40
35
30
25
20
15
10
5
0
Calm
0 ≤ 0.5
Light
0.5 ≤ 5.7
Moderate
5.7 ≤ 9.8
Strong
9.8 ≤ 17.0
Gale
17.0 ≤ 24.2
Storm
24.2 ≤ 32.4
Hurricane
≥ 32.4
Wind Speed (m/s)

July

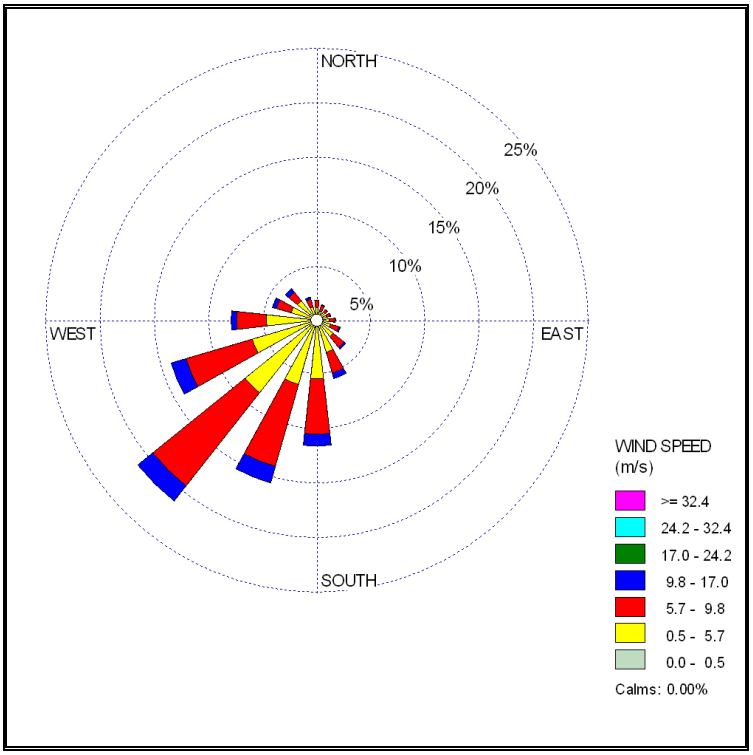
NORTH
25%
20%
15%
10%
5%
WEST
EAST
SOUTH
WIND SPEED
(m/s)
>= 32.4
24.2 - 32.4
17.0 - 24.2
9.8 - 17.0
5.7 - 9.8
0.5 - 5.7
0.0 - 0.5
Calms: 0.00%

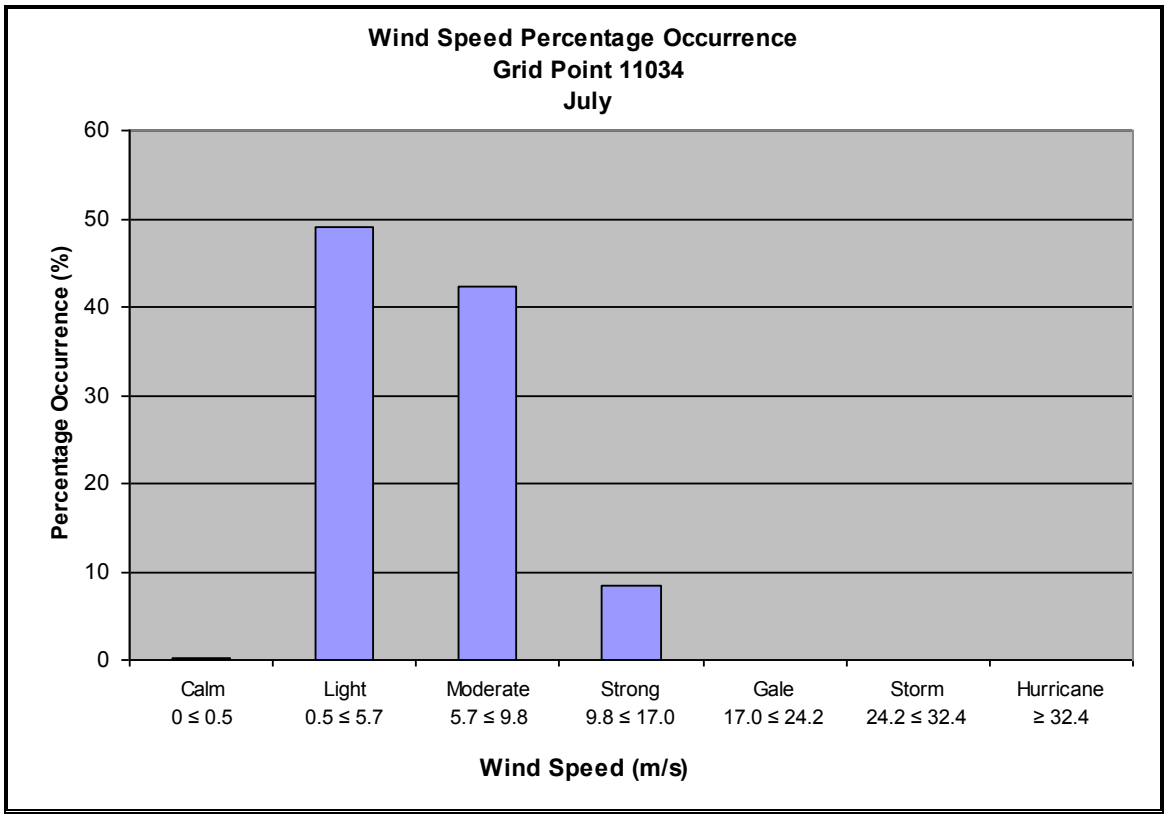
Wind Speed Percentage Occurrence
Grid Point 11034
July
Percentage Occurrence (%)
60
50
40
30
20
10
0
Calm
0 ≤ 0.5
Light
0.5 ≤ 5.7
Moderate
5.7 ≤ 9.8
Strong
9.8 ≤ 17.0
Gale
17.0 ≤ 24.2
Storm
24.2 ≤ 32.4
Hurricane
≥ 32.4
Wind Speed (m/s)

August

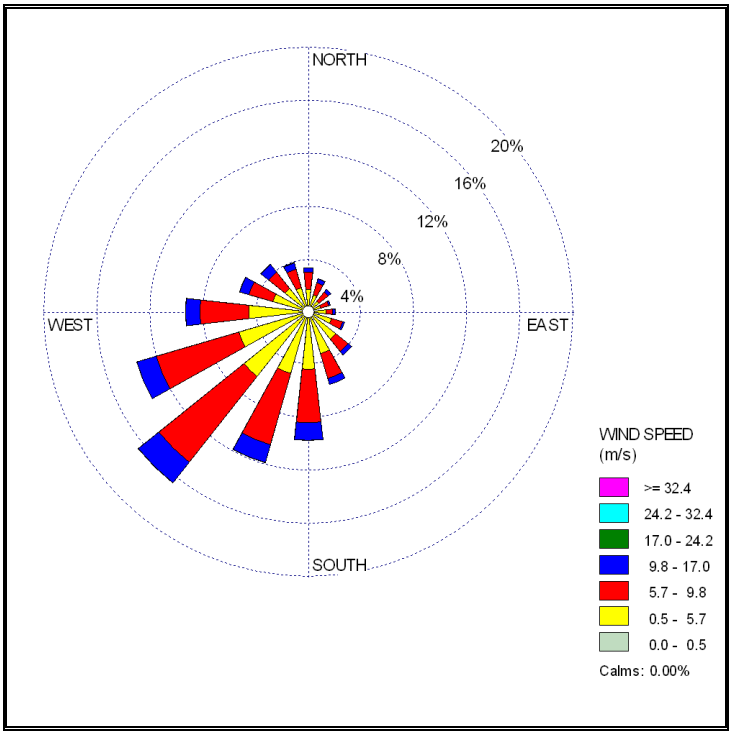
NORTH
20%
16%
12%
8%
4%
WEST
EAST
SOUTH
WIND SPEED
(m/s)
>= 32.4
24.2 - 32.4
17.0 - 24.2
9.8 - 17.0
5.7 - 9.8
0.5 - 5.7
0.0 - 0.5
Calms: 0.00%

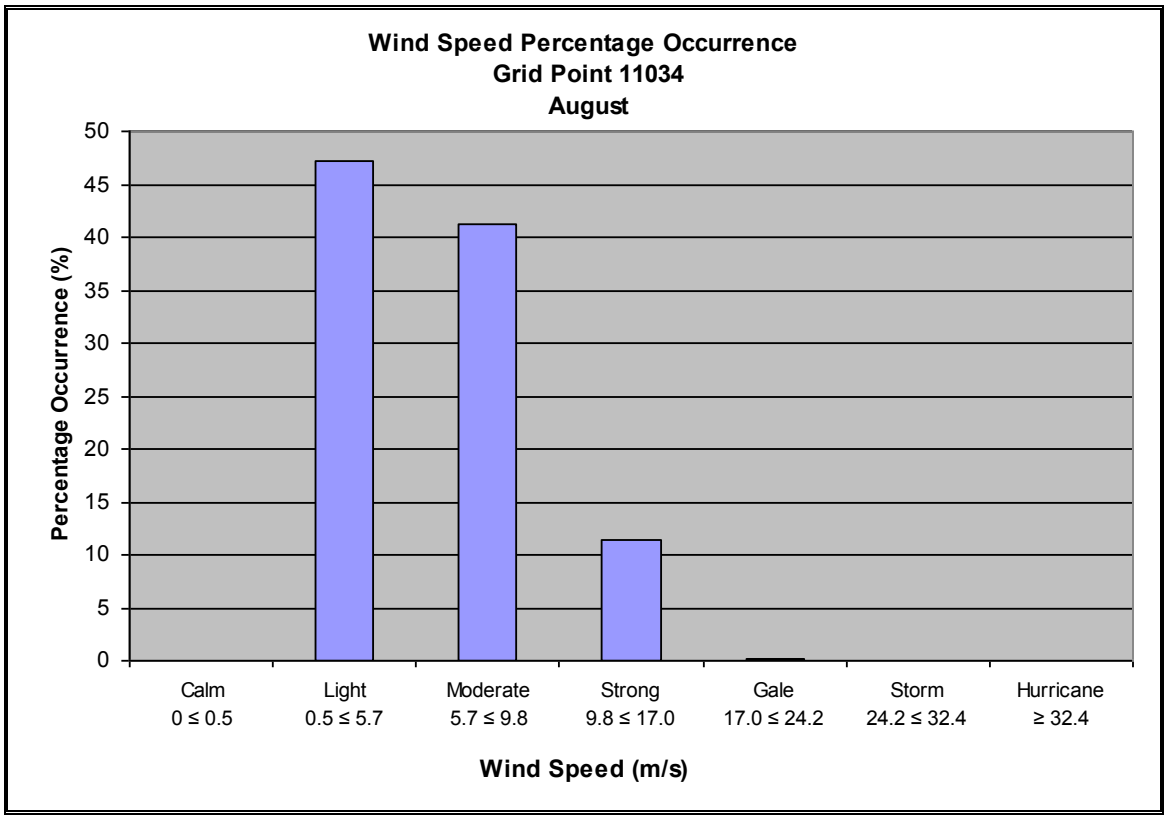
Wind Speed Percentage Occurrence
Grid Point 11034
August
Percentage Occurrence (%)
50
45
40
35
30
25
20
15
10
5
0
Calm
0 ≤ 0.5
Light
0.5 ≤ 5.7
Moderate
5.7 ≤ 9.8
Strong
9.8 ≤ 17.0
Gale
17.0 ≤ 24.2
Storm
24.2 ≤ 32.4
Hurricane
≥ 32.4
Wind Speed (m/s)

September

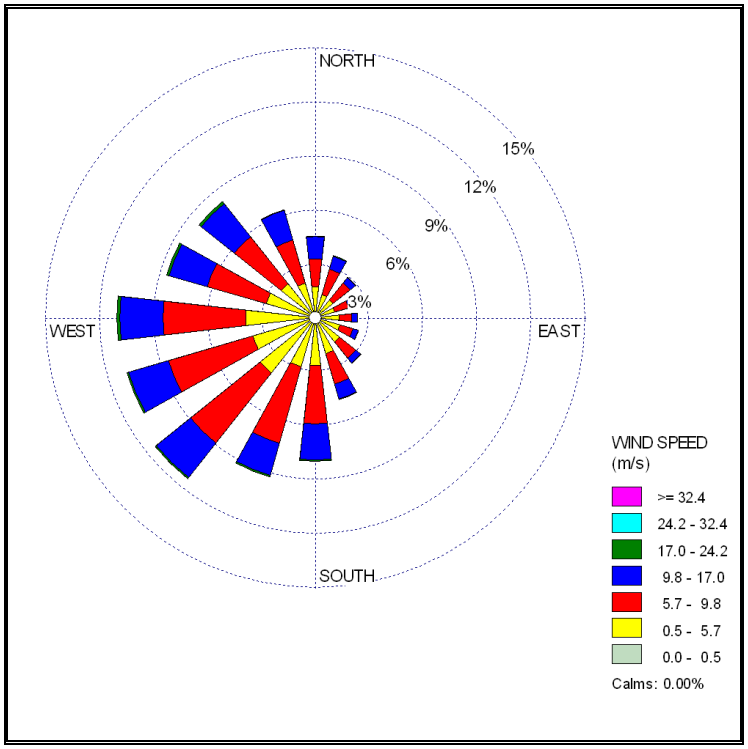
NORTH
15%
12%
9%
6%
3%
WEST
EAST
SOUTH
WIND SPEED
(m/s)
>= 32.4
24.2 - 32.4
17.0 - 24.2
9.8 - 17.0
5.7 - 9.8
0.5 - 5.7
0.0 - 0.5
Calms: 0.00%

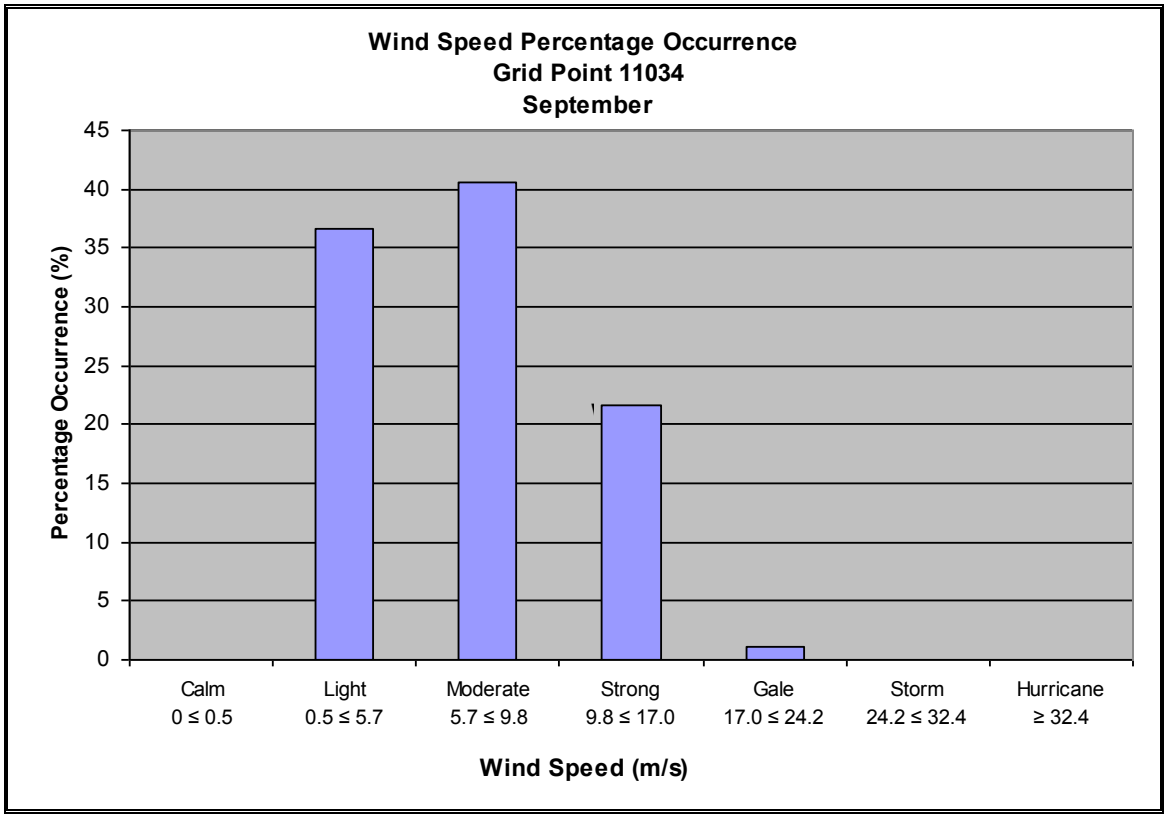
Wind Speed Percentage Occurrence
Grid Point 11034
September
Percentage Occurrence (%)
45
40
35
30
25
20
15
10
5
0
Calm
0 ≤ 0.5
Light
0.5 ≤ 5.7
Moderate
5.7 ≤ 9.8
Strong
9.8 ≤ 17.0
Gale
17.0 ≤ 24.2
Storm
24.2 ≤ 32.4
Hurricane
≥ 32.4
Wind Speed (m/s)

October

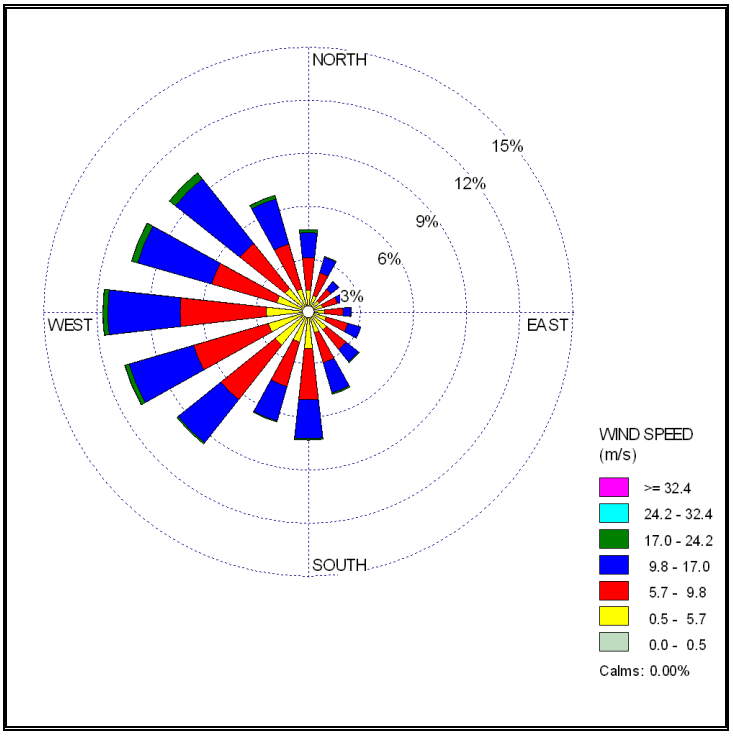
NORTH
15%
12%
9%
6%
3%
WEST
EAST
SOUTH
WIND SPEED
(m/s)
>= 32.4
24.2 - 32.4
17.0 - 24.2
9.8 - 17.0
5.7 - 9.8
0.5 - 5.7
0.0 - 0.5
Calms: 0.00%

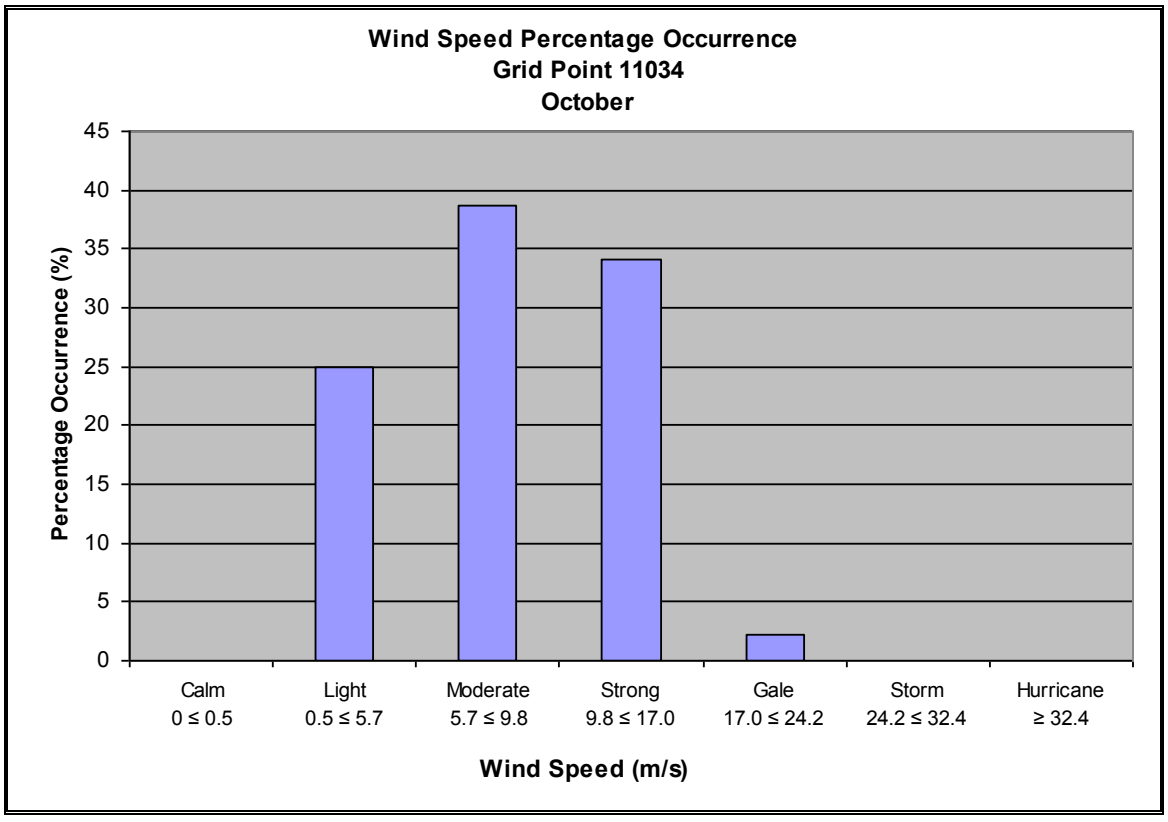
Wind Speed Percentage Occurrence
Grid Point 11034
October
Percentage Occurrence (%)
45
40
35
30
25
20
15
10
5
0
Calm
0 ≤ 0.5
Light
0.5 ≤ 5.7
Moderate
5.7 ≤ 9.8
Strong
9.8 ≤ 17.0
Gale
17.0 ≤ 24.2
Storm
24.2 ≤ 32.4
Hurricane
≥ 32.4
Wind Speed (m/s)

November

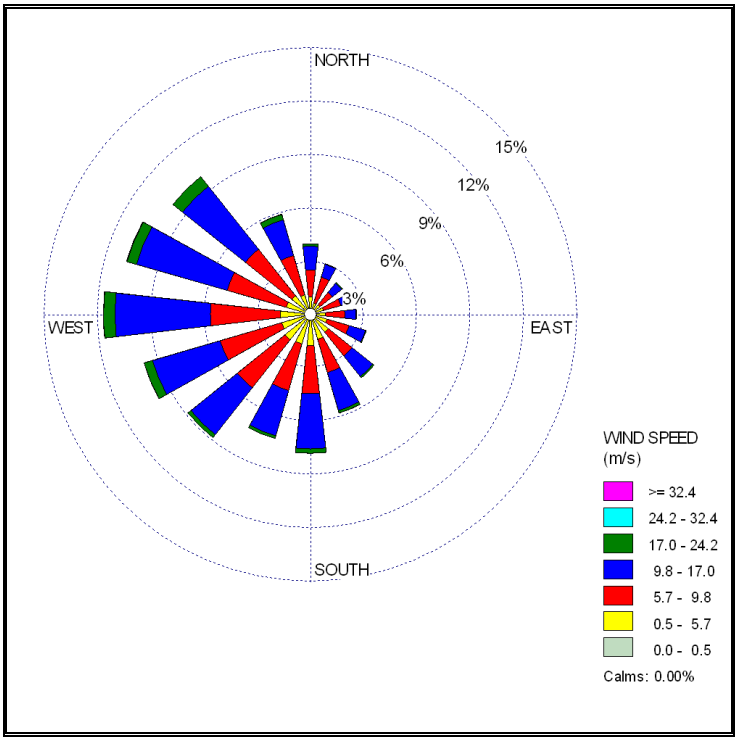
NORTH
15%
12%
9%
6%
3%
WEST
EAST
SOUTH
WIND SPEED
(m/s)
>= 32.4
24.2 - 32.4
17.0 - 24.2
9.8 - 17.0
5.7 - 9.8
0.5 - 5.7
0.0 - 0.5
Calms: 0.00%

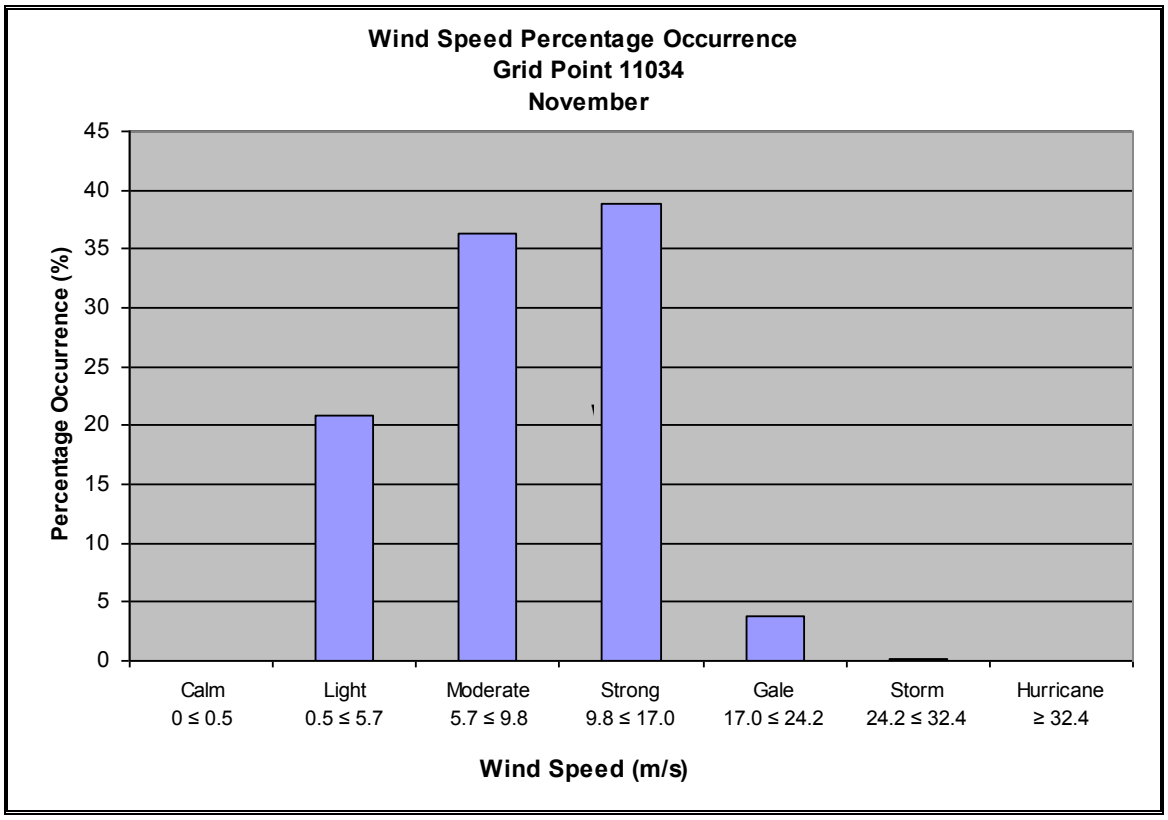
Wind Speed Percentage Occurrence
Grid Point 11034
November
Percentage Occurrence (%)
45
40
35
30
25
20
15
10
5
0
Calm
0 ≤ 0.5
Light
0.5 ≤ 5.7
Moderate
5.7 ≤ 9.8
Strong
9.8 ≤ 17.0
Gale
17.0 ≤ 24.2
Storm
24.2 ≤ 32.4
Hurricane
≥ 32.4
Wind Speed (m/s)

December

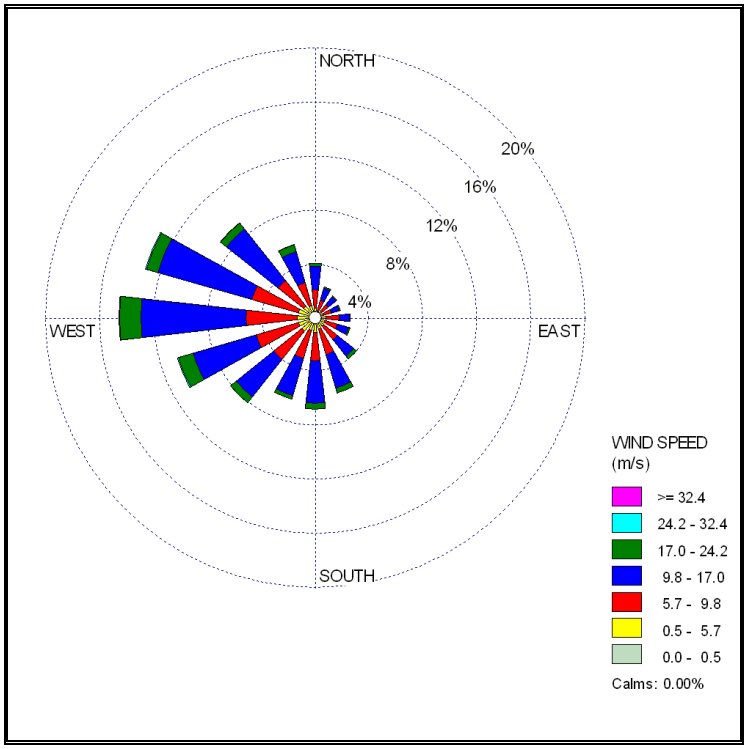
NORTH
20%
16%
12%
8%
4%
WEST
EAST
SOUTH
WIND SPEED
(m/s)
>= 32.4
24.2 - 32.4
17.0 - 24.2
9.8 - 17.0
5.7 - 9.8
0.5 - 5.7
0.0 - 0.5
Calms: 0.00%

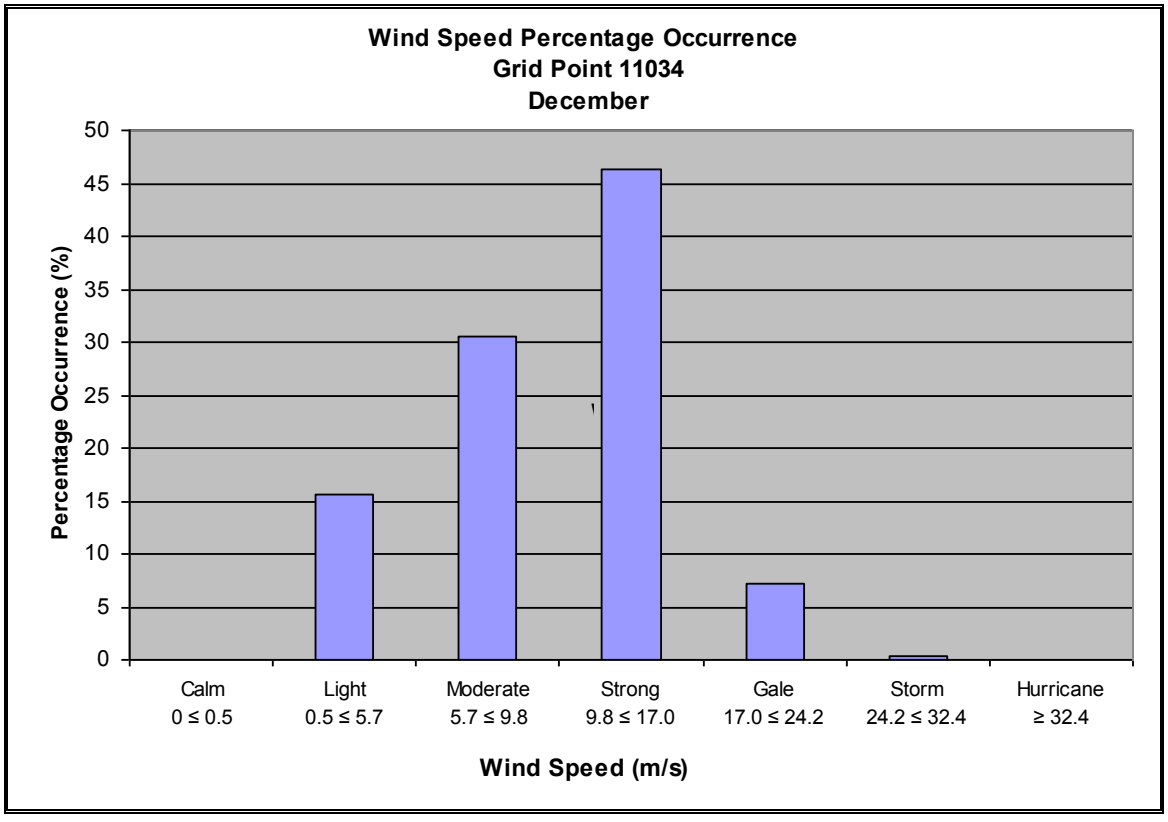
Wind Speed Percentage Occurrence
Grid Point 11034
December
Percentage Occurrence (%)
50
45
40
35
30
25
20
15
10
5
0
Calm
0 ≤ 0.5
Light
0.5 ≤ 5.7
Moderate
5.7 ≤ 9.8
Strong
9.8 ≤ 17.0
Gale
17.0 ≤ 24.2
Storm
24.2 ≤ 32.4
Hurricane
≥ 32.4
Wind Speed (m/s)

Appendix 2
Wave Roses
and
Wave Height Frequency Distributions
for MSC50 GridPoint 11034

January

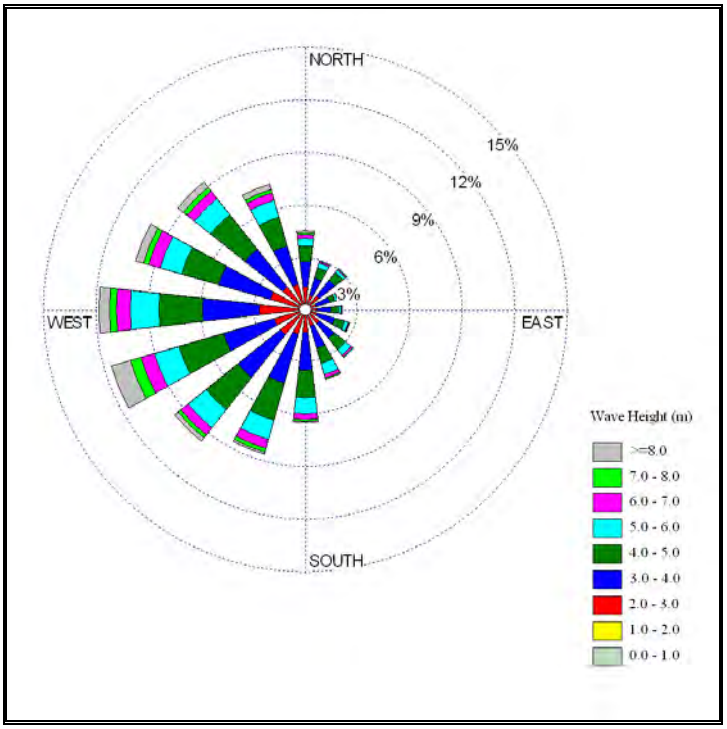
NORTH
15%
12%
9%
6%
3%
WEST
EAST
SOUTH
Wave Height (m)
>=8.0
7.0 - 8.0
6.0 - 7.0
5.0 - 6.0
4.0 - 5.0
3.0 - 4.0
2.0 - 3.0
1.0 - 2.0
0.0 - 1.0

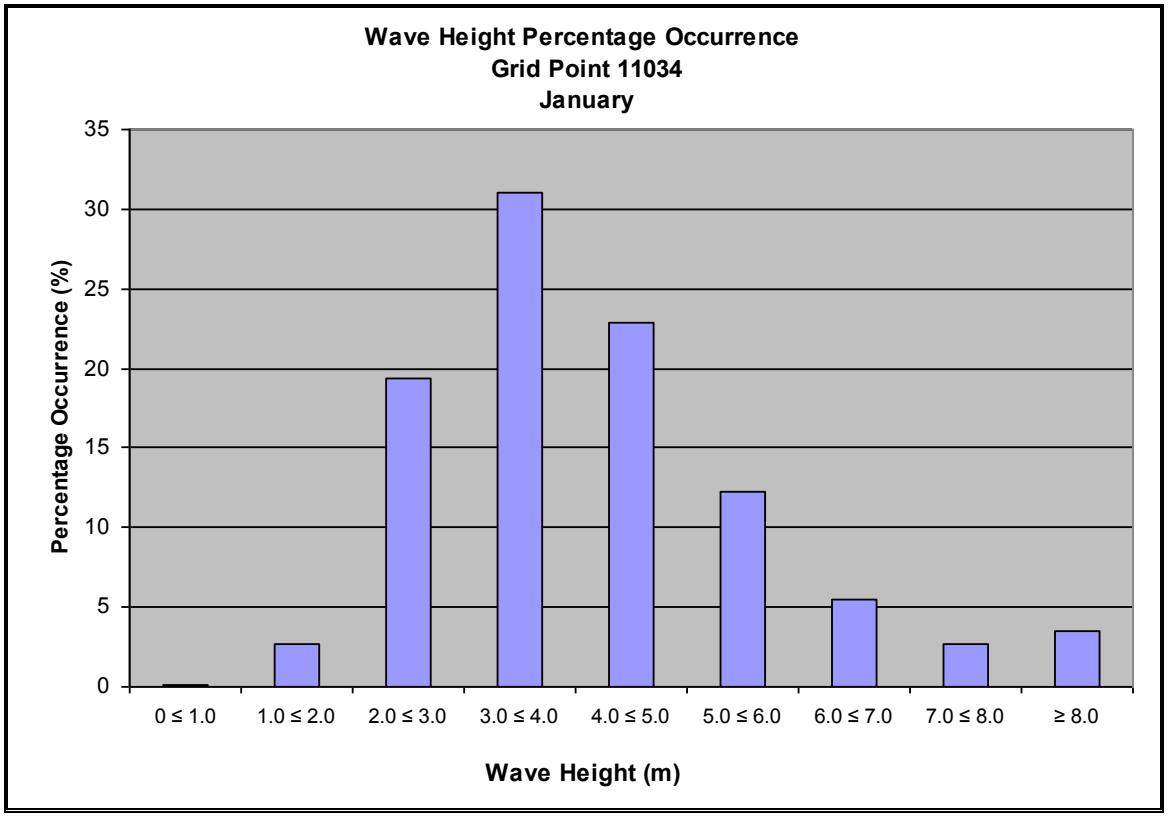
Wave Height Percentage Occurrence
Grid Point 11034
January
Percentage Occurrence (%)
35
30
25
20
15
10
5
0
0 ≤ 1.0
1.0 ≤ 2.0
2.0 ≤ 3.0
3.0 ≤ 4.0
4.0 ≤ 5.0
5.0 ≤ 6.0
6.0 ≤ 7.0
7.0 ≤ 8.0
≥ 8.0
Wave Height (m)

February

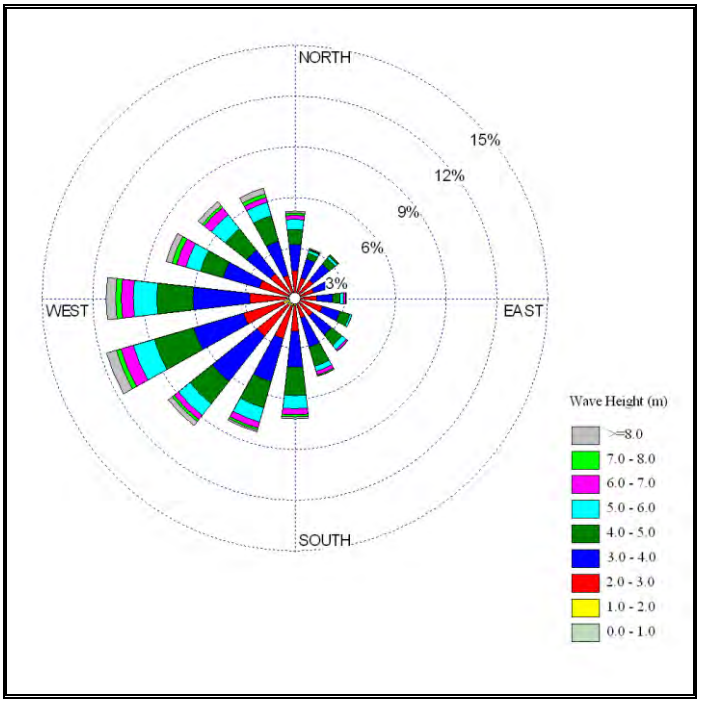
NORTH
15%
12%
9%
6%
3%
WEST
EAST
SOUTH
Wave Height (m)
>=8.0
7.0 - 8.0
6.0 - 7.0
5.0 - 6.0
4.0 - 5.0
3.0 - 4.0
2.0 - 3.0
1.0 - 2.0
0.0 - 1.0

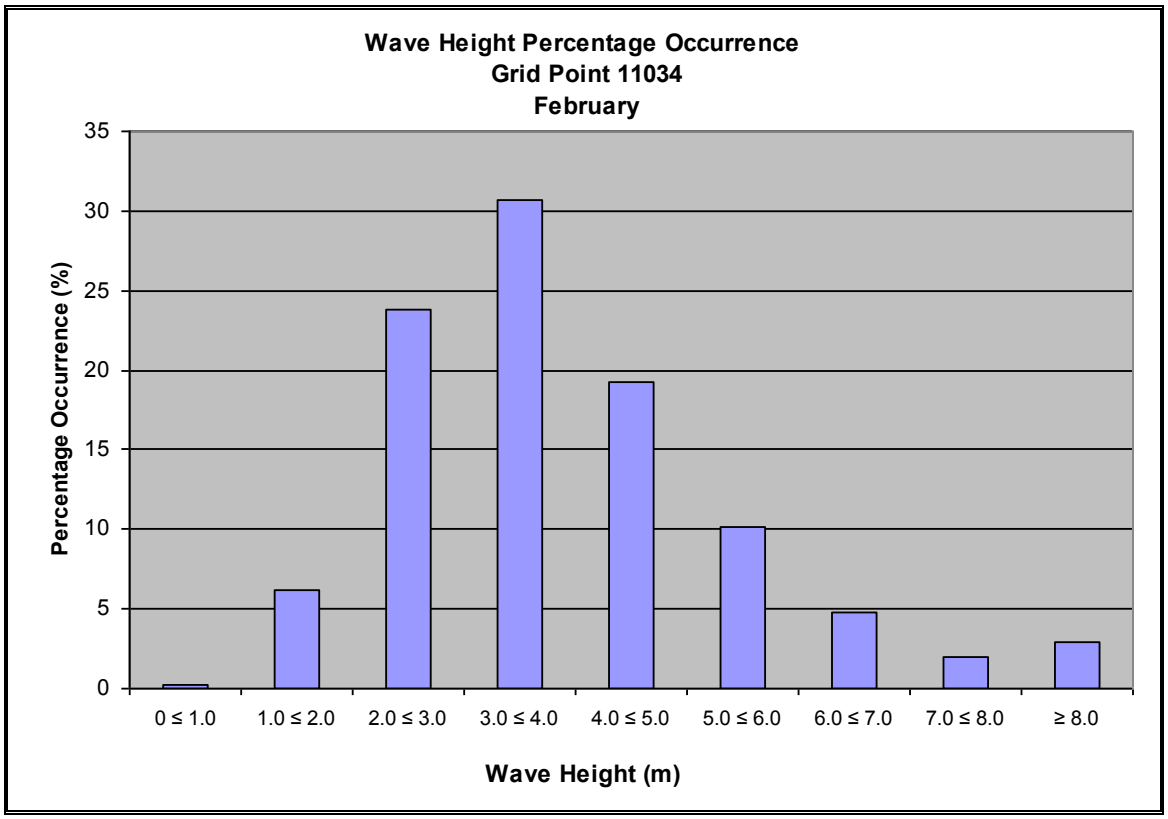
Wave Height Percentage Occurrence
Grid Point 11034
February
Percentage Occurrence (%)
35
30
25
20
15
10
5
0
0 ≤ 1.0
1.0 ≤ 2.0
2.0 ≤ 3.0
3.0 ≤ 4.0
4.0 ≤ 5.0
5.0 ≤ 6.0
6.0 ≤ 7.0
7.0 ≤ 8.0
≥ 8.0
Wave Height (m)

March

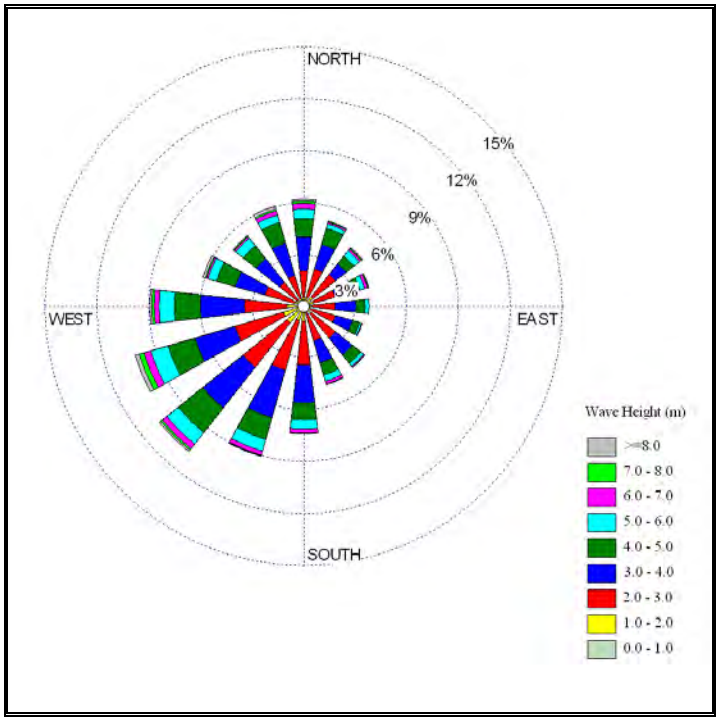
NORTH
15%
12%
9%
6%
3%
WEST
EAST
SOUTH
Wave Height (m)
>=8.0
7.0 - 8.0
6.0 - 7.0
5.0 - 6.0
4.0 - 5.0
3.0 - 4.0
2.0 - 3.0
1.0 - 2.0
0.0 - 1.0

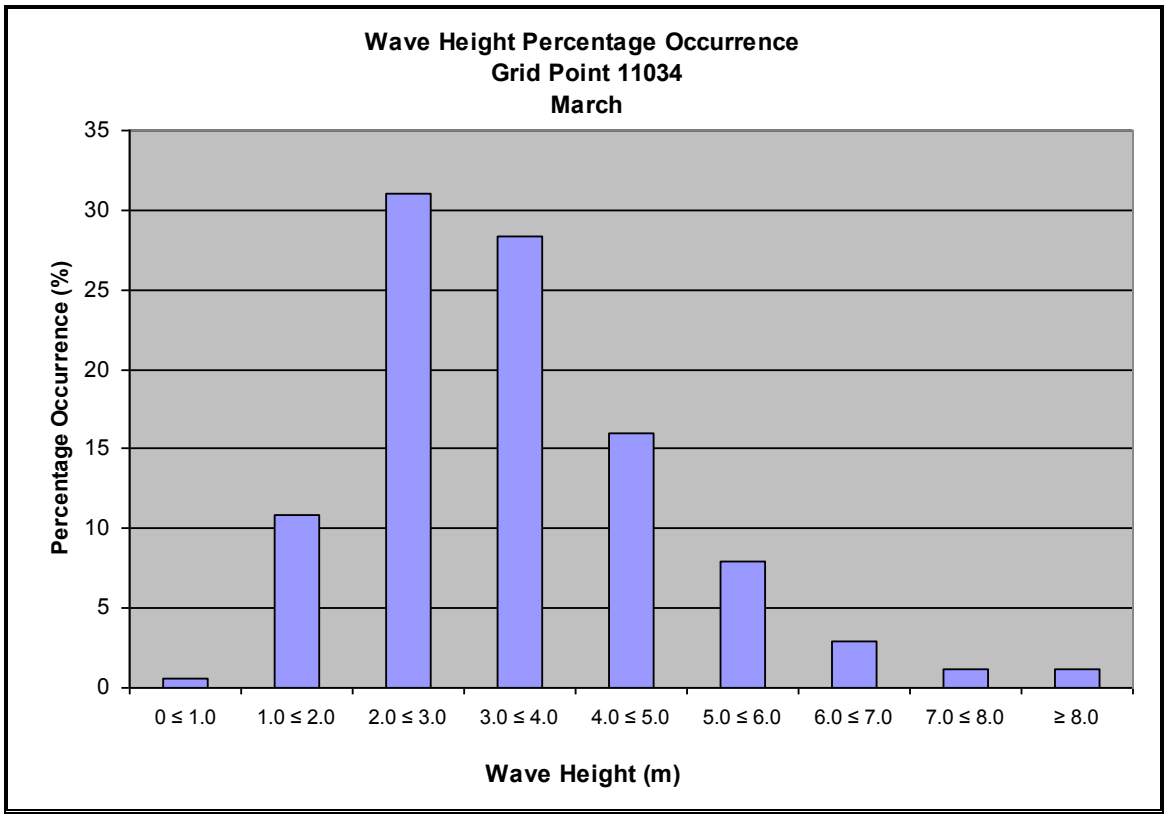
Wave Height Percentage Occurrence
Grid Point 11034
March
Percentage Occurrence (%)
35
30
25
20
15
10
5
0
0 ≤ 1.0
1.0 ≤ 2.0
2.0 ≤ 3.0
3.0 ≤ 4.0
4.0 ≤ 5.0
5.0 ≤ 6.0
6.0 ≤ 7.0
7.0 ≤ 8.0
≥ 8.0
Wave Height (m)

April

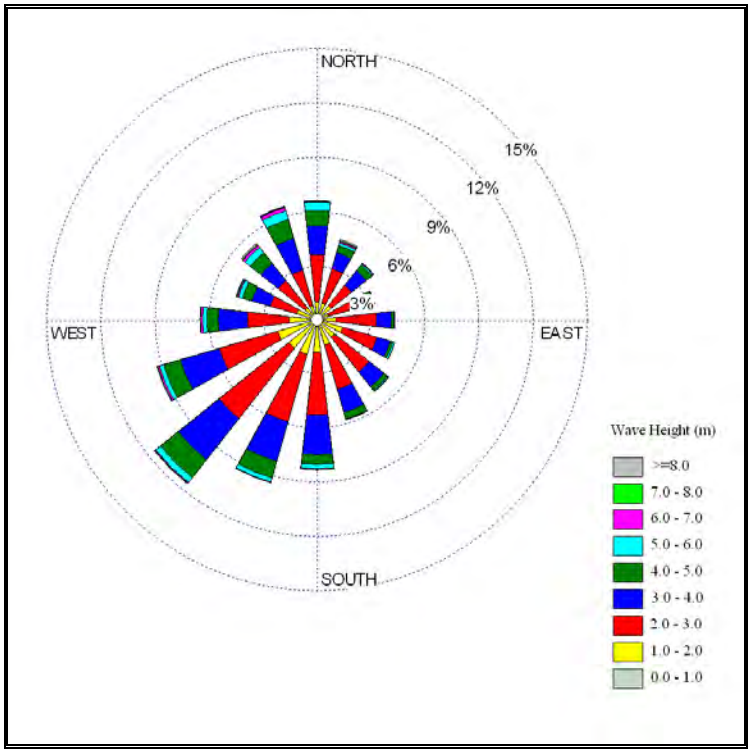
NORTH
15%
12%
9%
6%
3%
WEST
EAST
SOUTH
Wave Height (m)
>=8.0
7.0 - 8.0
6.0 - 7.0
5.0 - 6.0
4.0 - 5.0
3.0 - 4.0
2.0 - 3.0
1.0 - 2.0
0.0 - 1.0

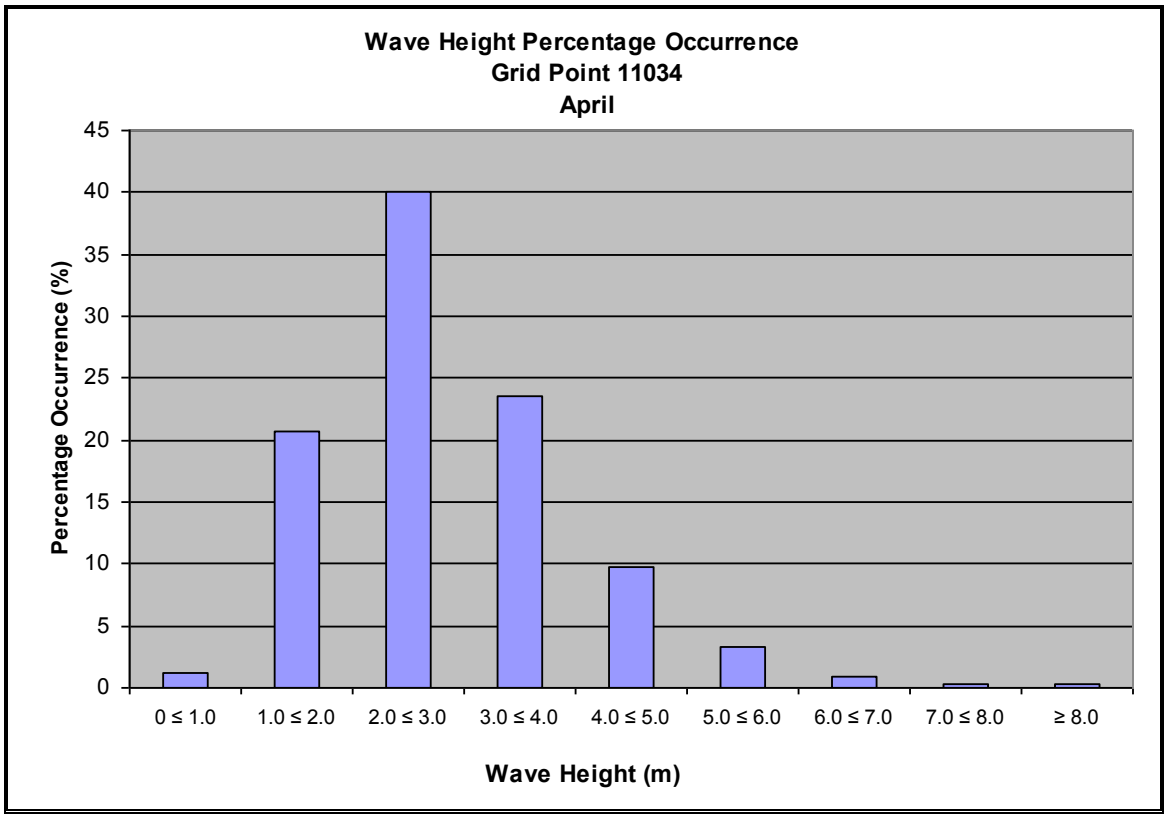
Wave Height Percentage Occurrence
Grid Point 11034
April
Percentage Occurrence (%)
45
40
35
30
25
20
15
10
5
0
0 ≤ 1.0
1.0 ≤ 2.0
2.0 ≤ 3.0
3.0 ≤ 4.0
4.0 ≤ 5.0
5.0 ≤ 6.0
6.0 ≤ 7.0
7.0 ≤ 8.0
≥ 8.0
Wave Height (m)

May

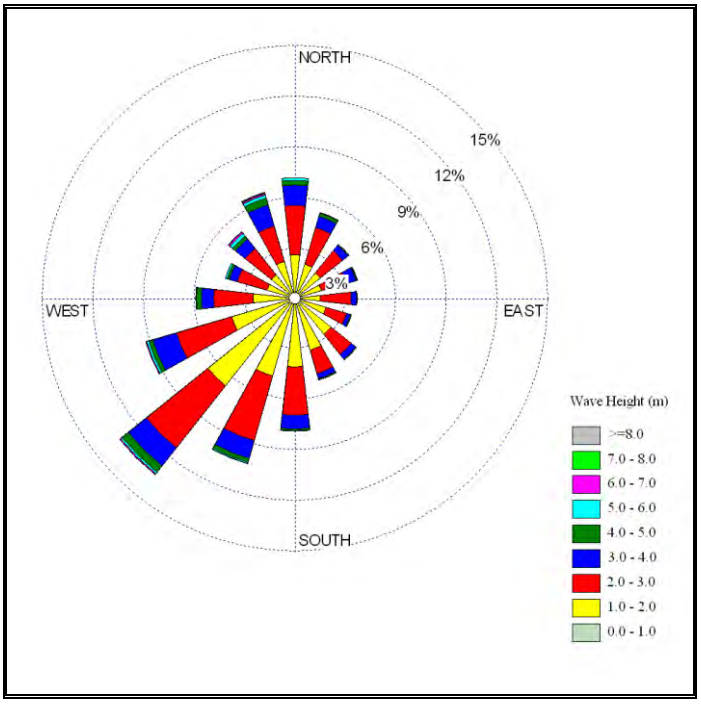
NORTH
15%
12%
9%
6%
3%
WEST
EAST
SOUTH
Wave Height (m)
>=8.0
7.0 - 8.0
6.0 - 7.0
5.0 - 6.0
4.0 - 5.0
3.0 - 4.0
2.0 - 3.0
1.0 - 2.0
0.0 - 1.0

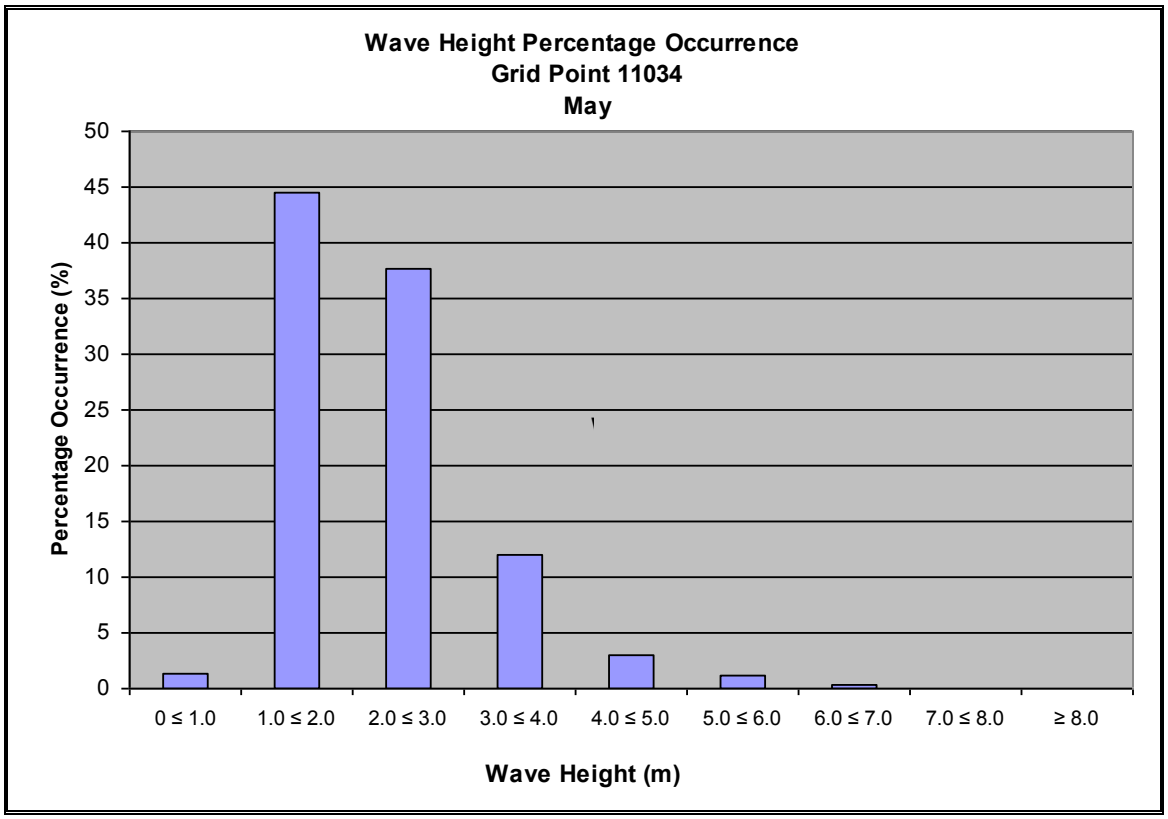
Wave Height Percentage Occurrence
Grid Point 11034
May
Percentage Occurrence (%)
50
45
40
35
30
25
20
15
10
5
0
0 ≤ 1.0
1.0 ≤ 2.0
2.0 ≤ 3.0
3.0 ≤ 4.0
4.0 ≤ 5.0
5.0 ≤ 6.0
6.0 ≤ 7.0
7.0 ≤ 8.0
≥ 8.0
Wave Height (m)

June

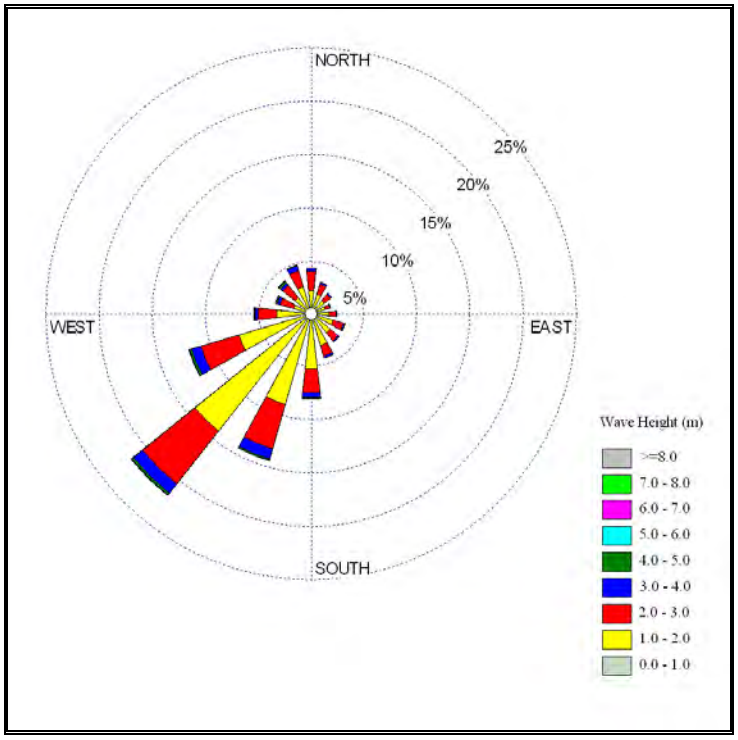
NORTH
25%
20%
15%
10%
5%
WEST
EAST
SOUTH
Wave Height (m)
>=8.0
7.0 - 8.0
6.0 - 7.0
5.0 - 6.0
4.0 - 5.0
3.0 - 4.0
2.0 - 3.0
1.0 - 2.0
0.0 - 1.0

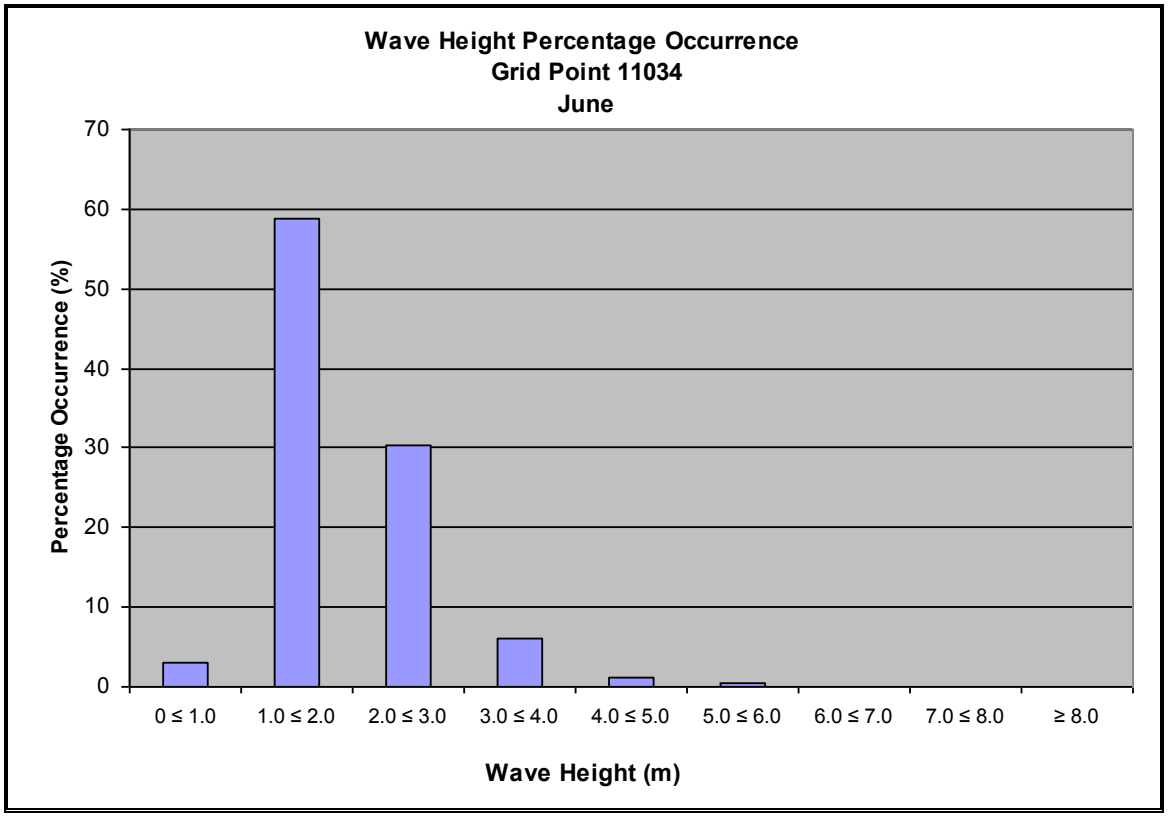
Wave Height Percentage Occurrence
Grid Point 11034
June
Percentage Occurrence (%)
70
60
50
40
30
20
10
0
0 ≤ 1.0
1.0 ≤ 2.0
2.0 ≤ 3.0
3.0 ≤ 4.0
4.0 ≤ 5.0
5.0 ≤ 6.0
6.0 ≤ 7.0
7.0 ≤ 8.0
≥ 8.0
Wave Height (m)

July

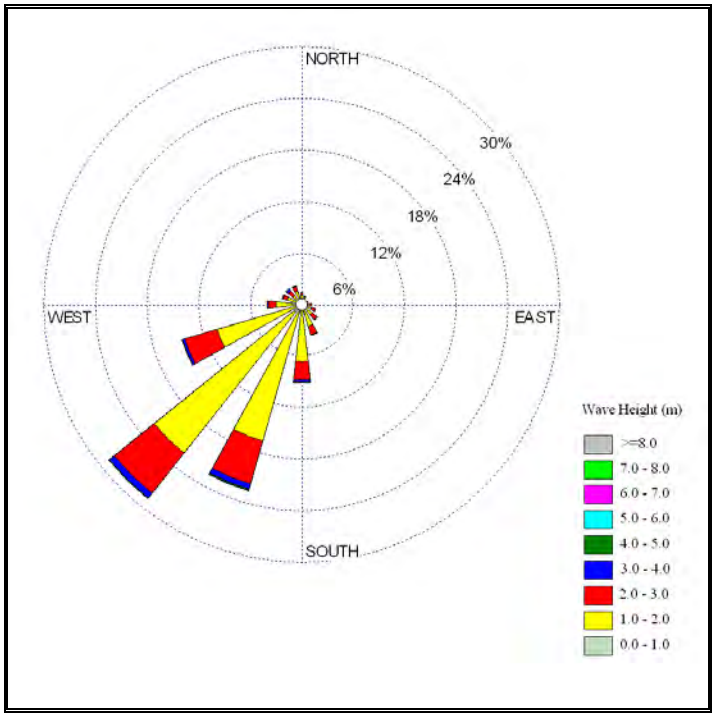
NORTH
30%
24%
18%
12%
6%
WEST
EAST
SOUTH
Wave Height (m)
>=8.0
7.0 - 8.0
6.0 - 7.0
5.0 - 6.0
4.0 - 5.0
3.0 - 4.0
2.0 - 3.0
1.0 - 2.0
0.0 - 1.0

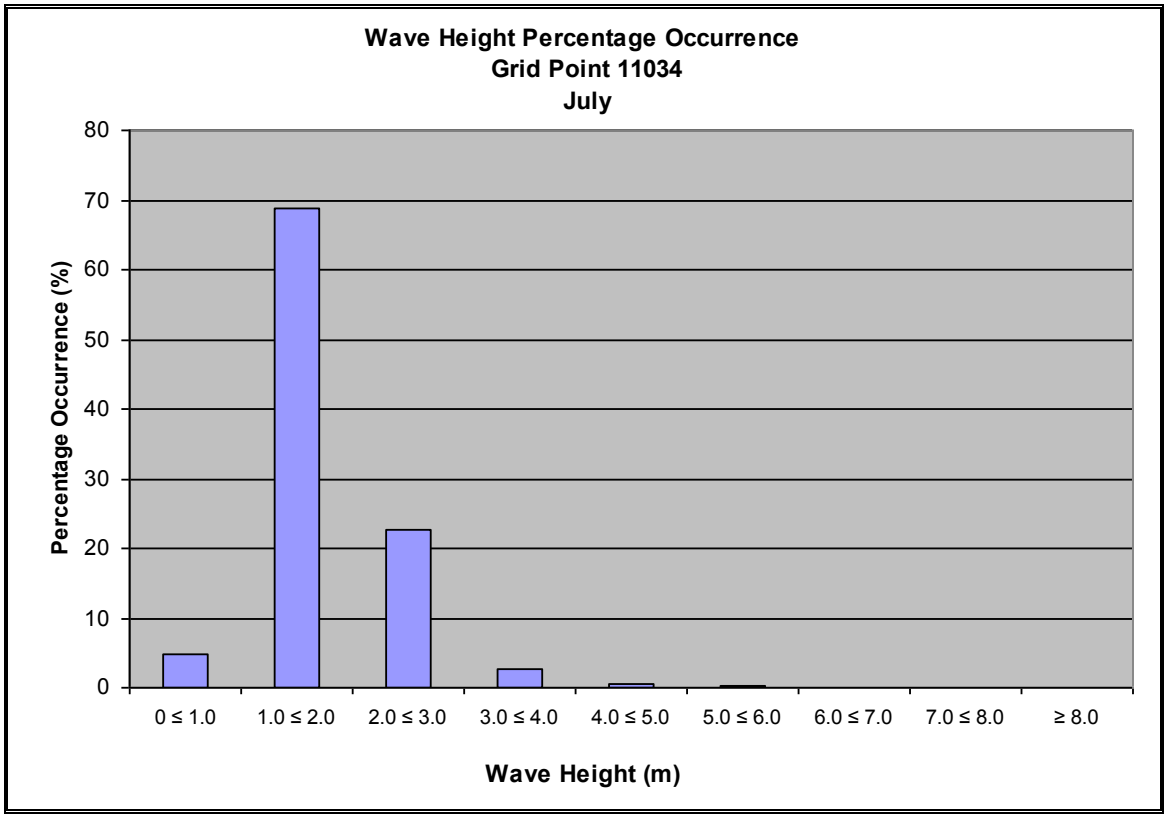
Wave Height Percentage Occurrence
Grid Point 11034
July
Percentage Occurrence (%)
80
70
60
50
40
30
20
10
0
0 ≤ 1.0
1.0 ≤ 2.0
2.0 ≤ 3.0
3.0 ≤ 4.0
4.0 ≤ 5.0
5.0 ≤ 6.0
6.0 ≤ 7.0
7.0 ≤ 8.0
≥ 8.0
Wave Height (m)

August

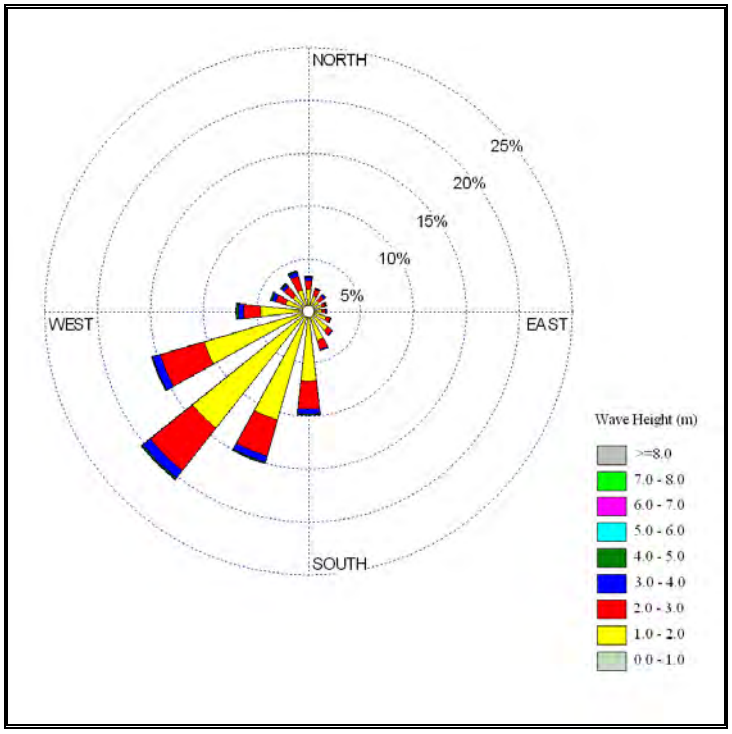
NORTH
25%
20%
15%
10%
5%
WEST
EAST
SOUTH
Wave Height (m)
>=8.0
7.0 - 8.0
6.0 - 7.0
5.0 - 6.0
4.0 - 5.0
3.0 - 4.0
2.0 - 3.0
1.0 - 2.0
0.0 - 1.0

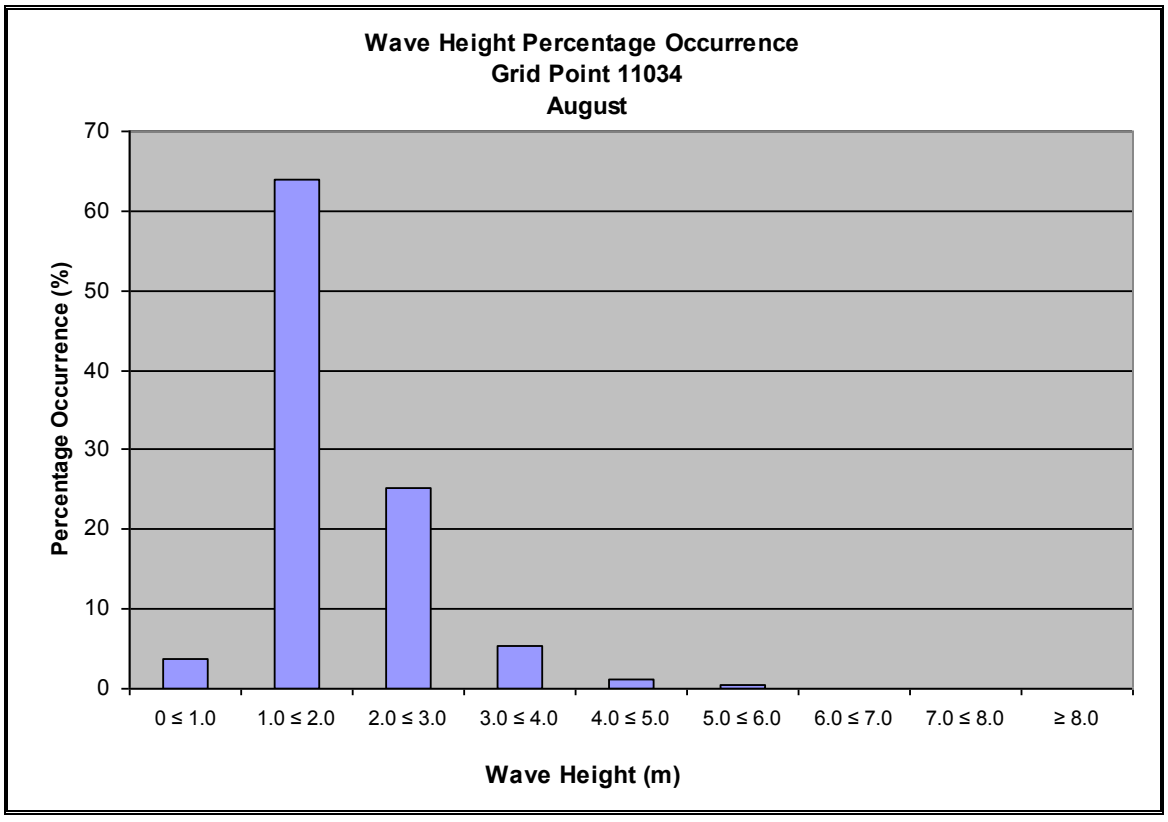
Wave Height Percentage Occurrence
Grid Point 11034
August
Percentage Occurrence (%)
70
60
50
40
30
20
10
0
0 ≤ 1.0
1.0 ≤ 2.0
2.0 ≤ 3.0
3.0 ≤ 4.0
4.0 ≤ 5.0
5.0 ≤ 6.0
6.0 ≤ 7.0
7.0 ≤ 8.0
≥ 8.0
Wave Height (m)

September

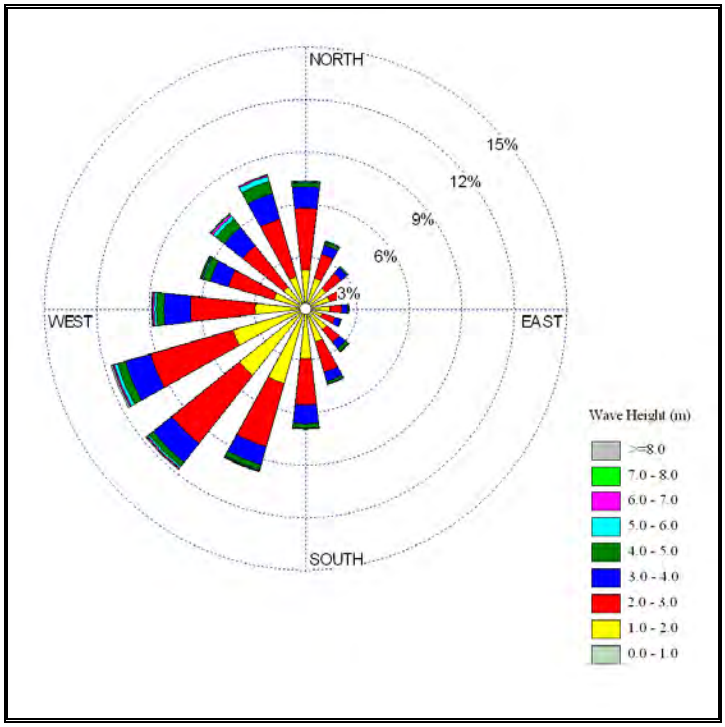
NORTH
15%
12%
9%
6%
3%
WEST
EAST
SOUTH
Wave Height (m)
>=8.0
7.0 - 8.0
6.0 - 7.0
5.0 - 6.0
4.0 - 5.0
3.0 - 4.0
2.0 - 3.0
1.0 - 2.0
0.0 - 1.0

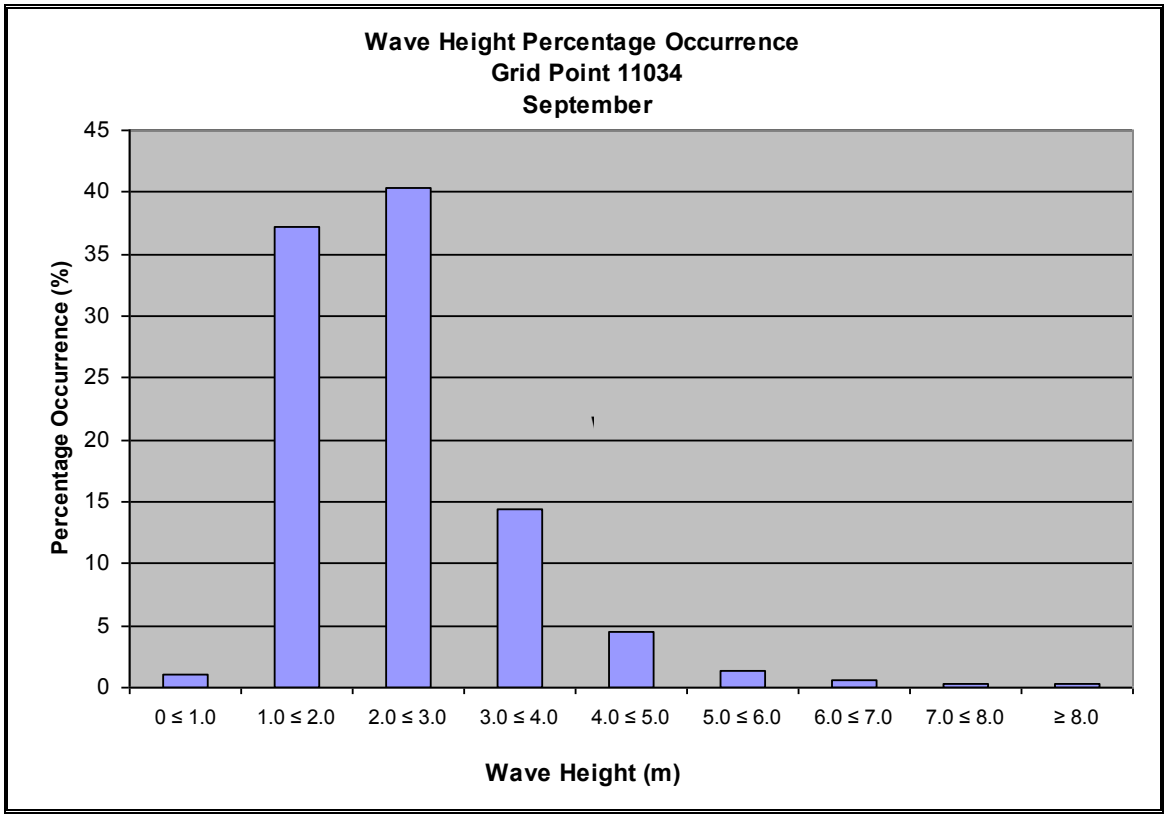
Wave Height Percentage Occurrence
Grid Point 11034
September
Percentage Occurrence (%)
45
40
35
30
25
20
15
10
5
0
0 ≤ 1.0
1.0 ≤ 2.0
2.0 ≤ 3.0
3.0 ≤ 4.0
4.0 ≤ 5.0
5.0 ≤ 6.0
6.0 ≤ 7.0
7.0 ≤ 8.0
≥ 8.0
Wave Height (m)

October

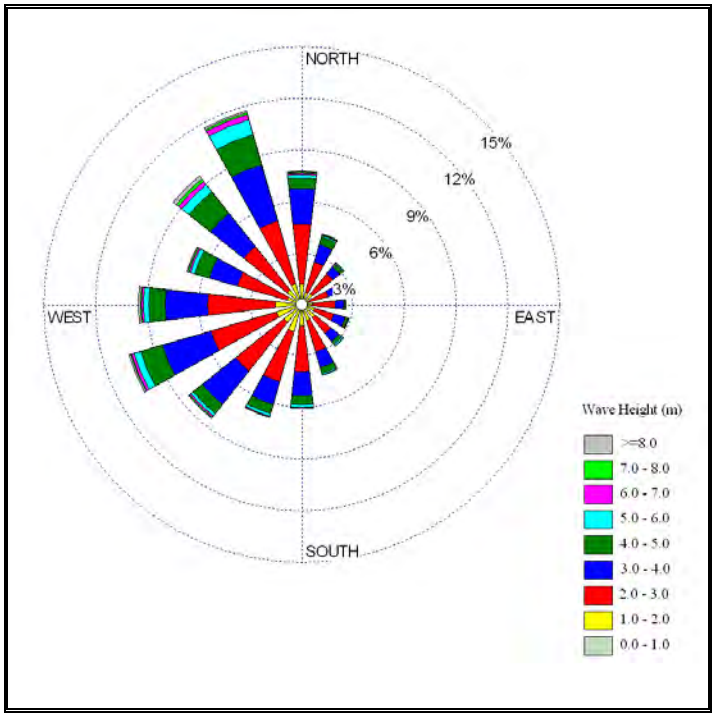
NORTH
15%
12%
9%
6%
3%
WEST
EAST
SOUTH
Wave Height (m)
>=8.0
7.0 - 8.0
6.0 - 7.0
5.0 - 6.0
4.0 - 5.0
3.0 - 4.0
2.0 - 3.0
1.0 - 2.0
0.0 - 1.0

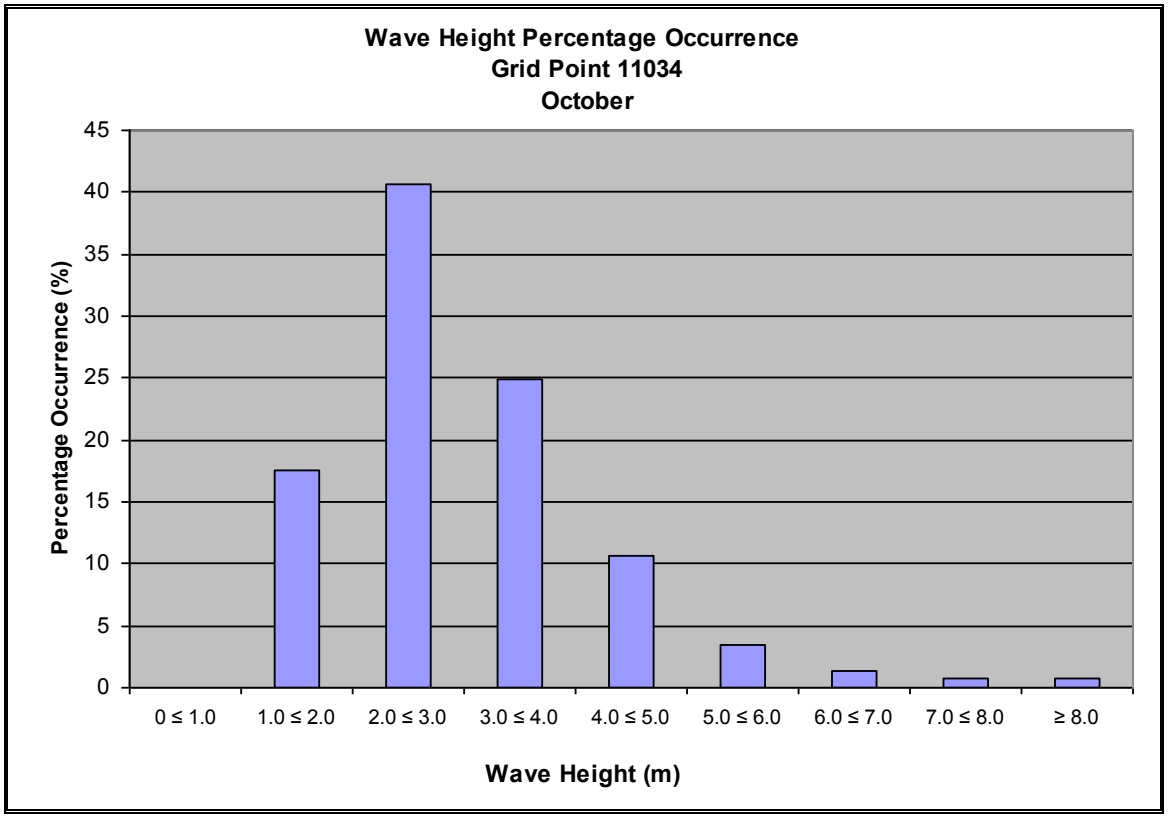
Wave Height Percentage Occurrence
Grid Point 11034
October
Percentage Occurrence (%)
45
40
35
30
25
20
15
10
5
0
0 ≤ 1.0
1.0 ≤ 2.0
2.0 ≤ 3.0
3.0 ≤ 4.0
4.0 ≤ 5.0
5.0 ≤ 6.0
6.0 ≤ 7.0
7.0 ≤ 8.0
≥ 8.0
Wave Height (m)

November

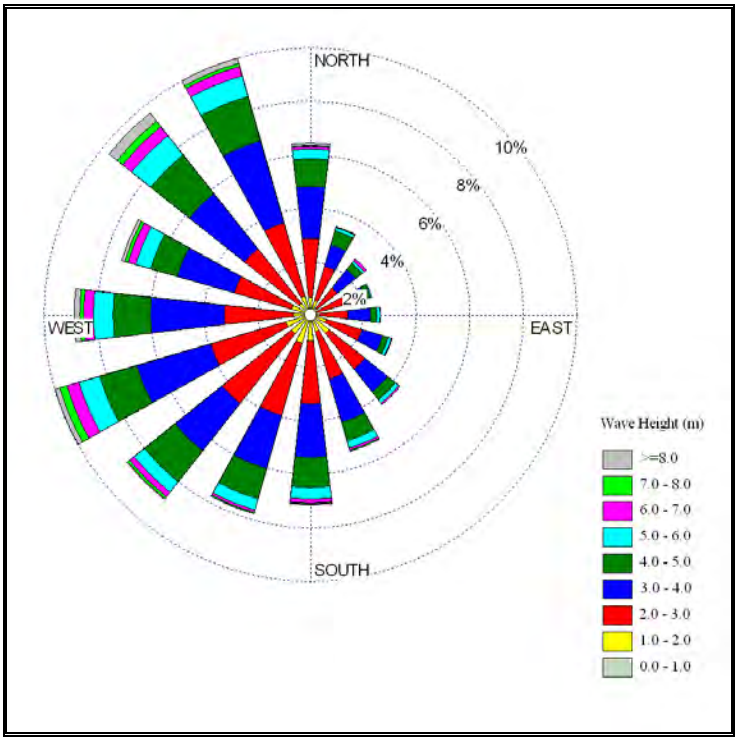
NORTH
EAST
SOUTH
WEST
2%
4%
6%
8%
10%
Wave Height (m)
>=8.0
7.0 - 8.0
6.0 - 7.0
5.0 - 6.0
4.0 - 5.0
3.0 - 4.0
2.0 - 3.0
1.0 - 2.0
0.0 - 1.0

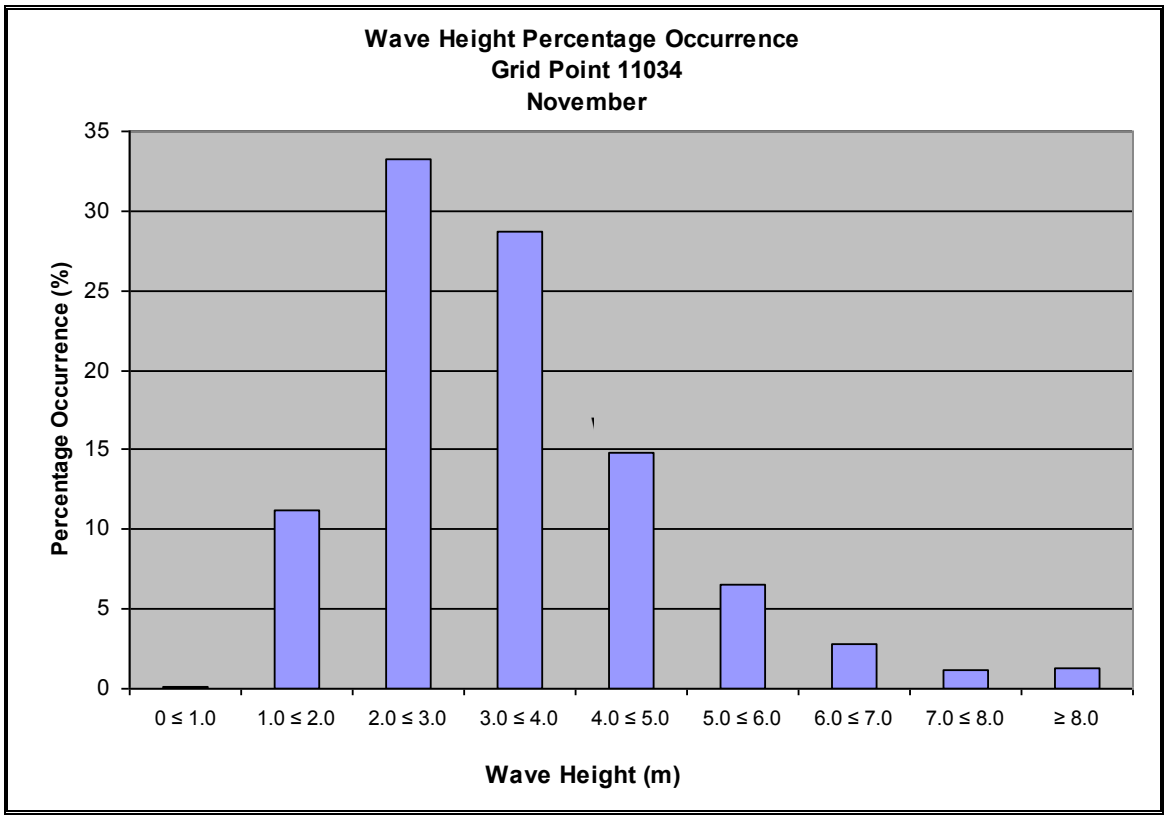
Wave Height Percentage Occurrence
Grid Point 11034
November
Percentage Occurrence (%)
0
5
10
15
20
25
30
35
0 ≤ 1.0
1.0 ≤ 2.0
2.0 ≤ 3.0
3.0 ≤ 4.0
4.0 ≤ 5.0
5.0 ≤ 6.0
6.0 ≤ 7.0
7.0 ≤ 8.0
≥ 8.0
Wave Height (m)

December

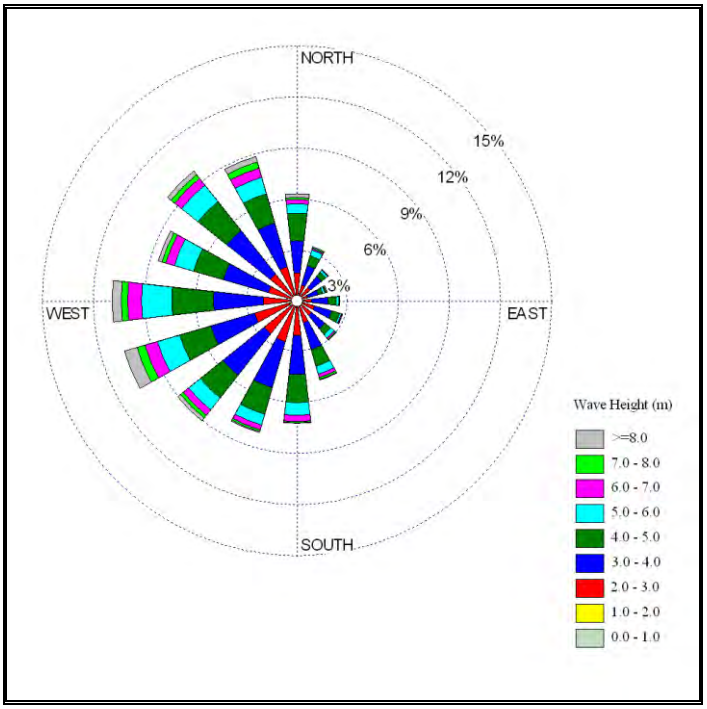
NORTH
15%
12%
9%
6%
3%
WEST
EAST
SOUTH
Wave Height (m)
>=8.0
7.0 - 8.0
6.0 - 7.0
5.0 - 6.0
4.0 - 5.0
3.0 - 4.0
2.0 - 3.0
1.0 - 2.0
0.0 - 1.0

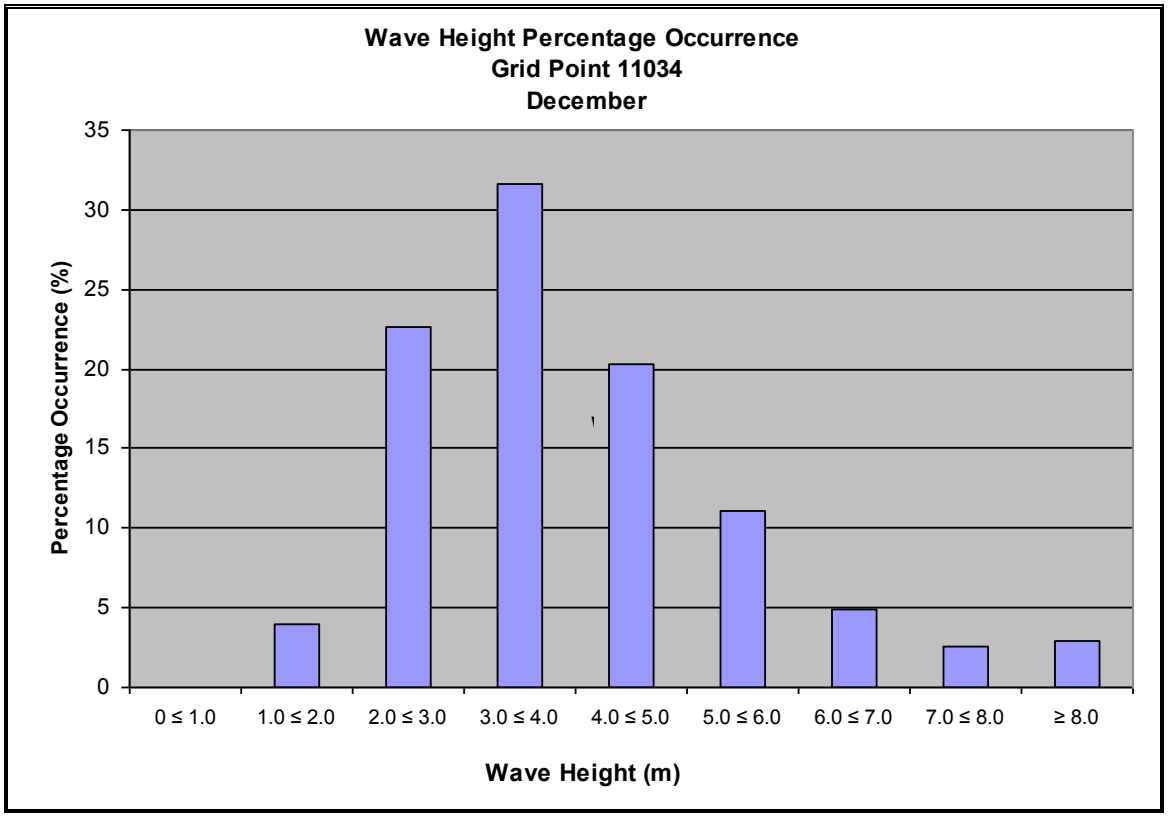
Wave Height Percentage Occurrence
Grid Point 11034
December
Percentage Occurrence (%)
35
30
25
20
15
10
5
0
0 ≤ 1.0
1.0 ≤ 2.0
2.0 ≤ 3.0
3.0 ≤ 4.0
4.0 ≤ 5.0
5.0 ≤ 6.0
6.0 ≤ 7.0
7.0 ≤ 8.0
≥ 8.0
Wave Height (m)

Appendix 3
Monthly Joint Probabilities of Extreme wave Heights and Spectral Peak Period for MSC50 GridPoint 11034

January Environmental Contours for Grid Point 11034 46.7°N 48.1°W
Data from MSC50 Hindcast 1954 - 2009

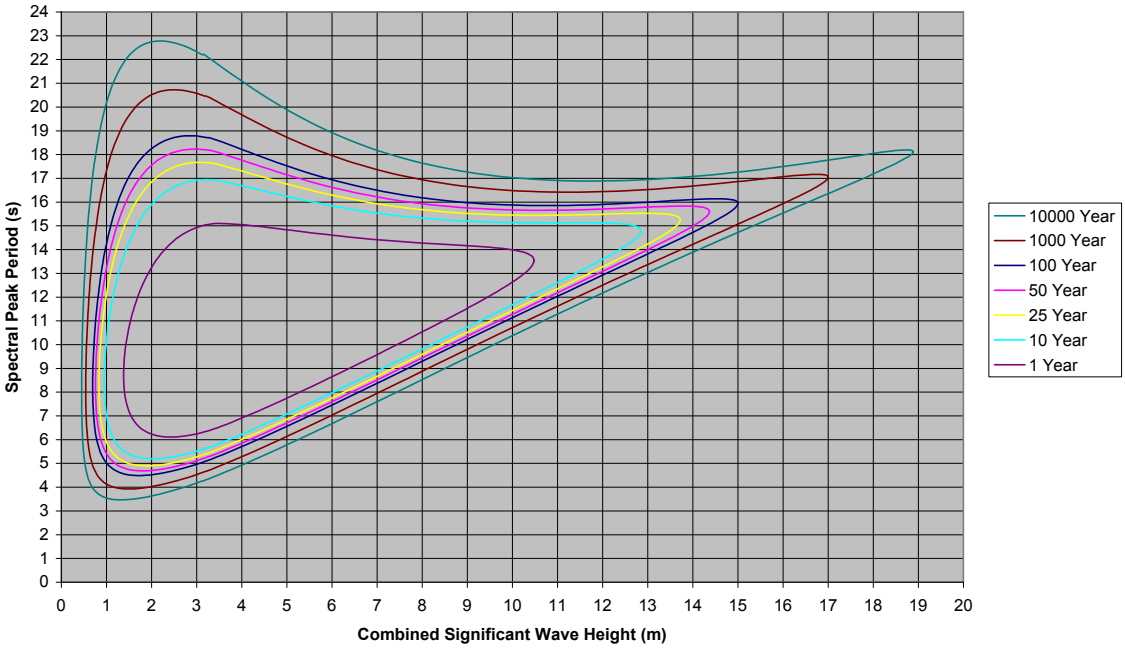

February Environmental Contours for Grid Point 11034 46.7°N 48.1°W
Data from MSC50 Hindcast 1954 - 2009

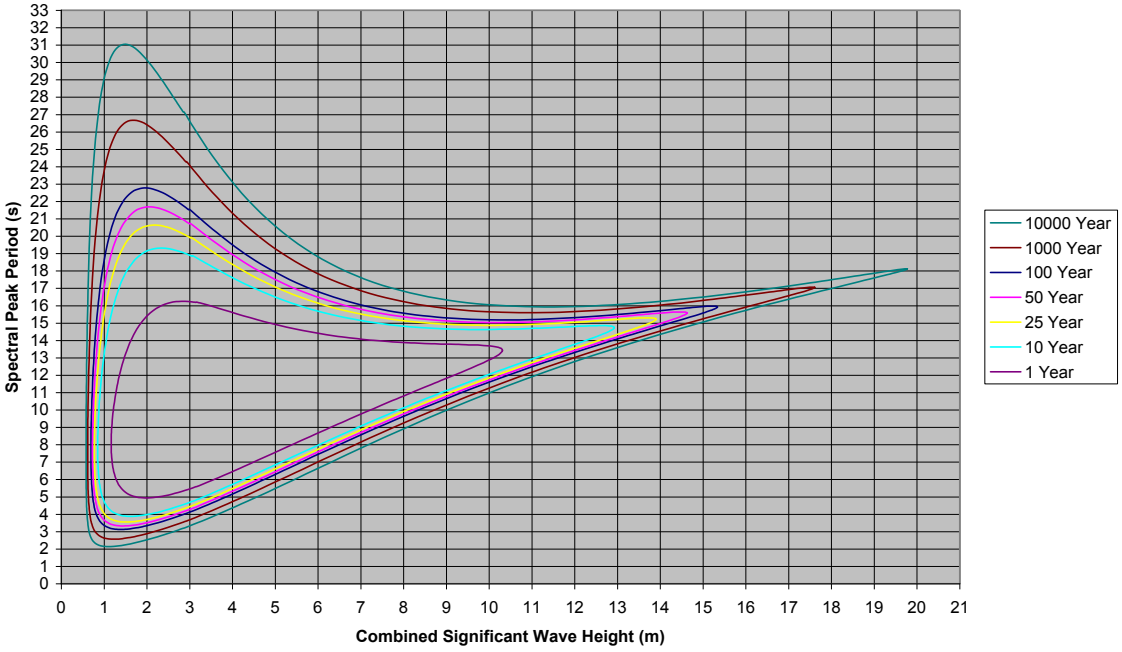

March Environmental Contours for Grid Point 11034 46.7°N 48.1°W
Data from MSC50 Hindcast 1954 - 2009

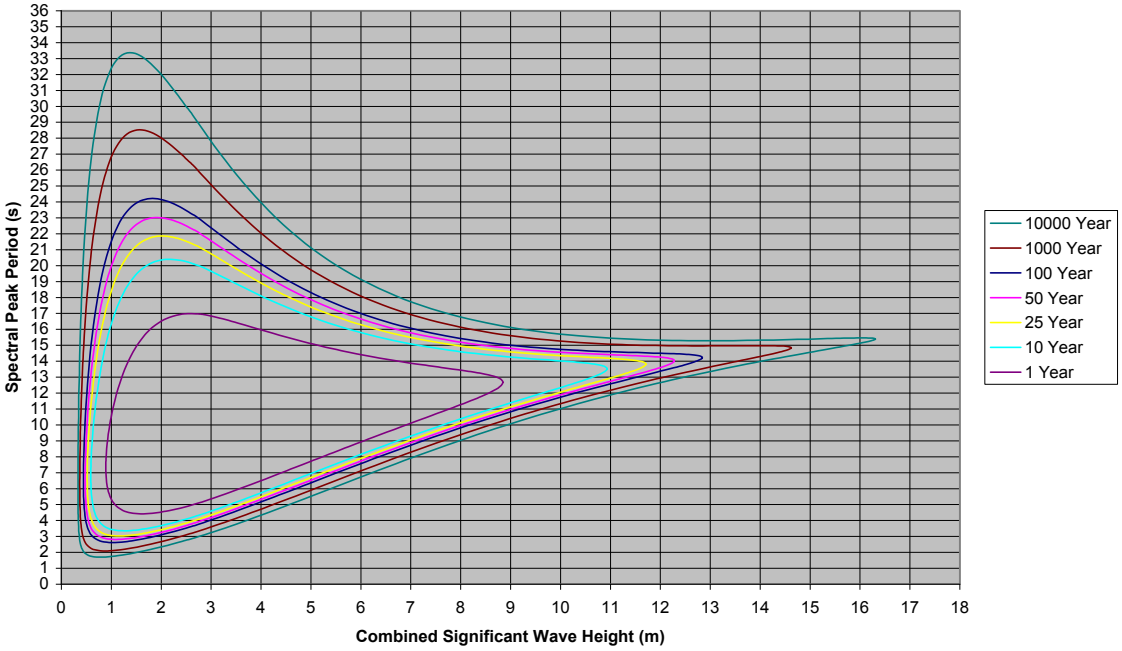

April Environmental Contours for Grid Point 11034 46.7°N 48.1°W
Data from MSC50 Hindcast 1954 - 2009

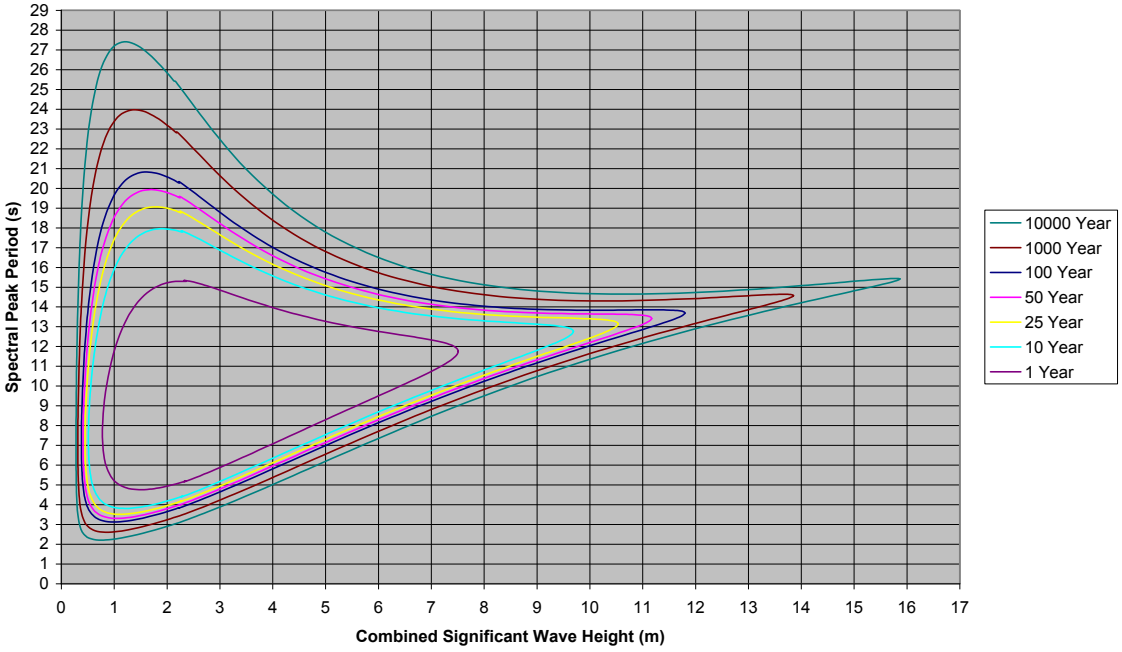

May Environmental Contours for Grid Point 11034 46.7°N 48.1°W
Data from MSC50 Hindcast 1954 - 2009

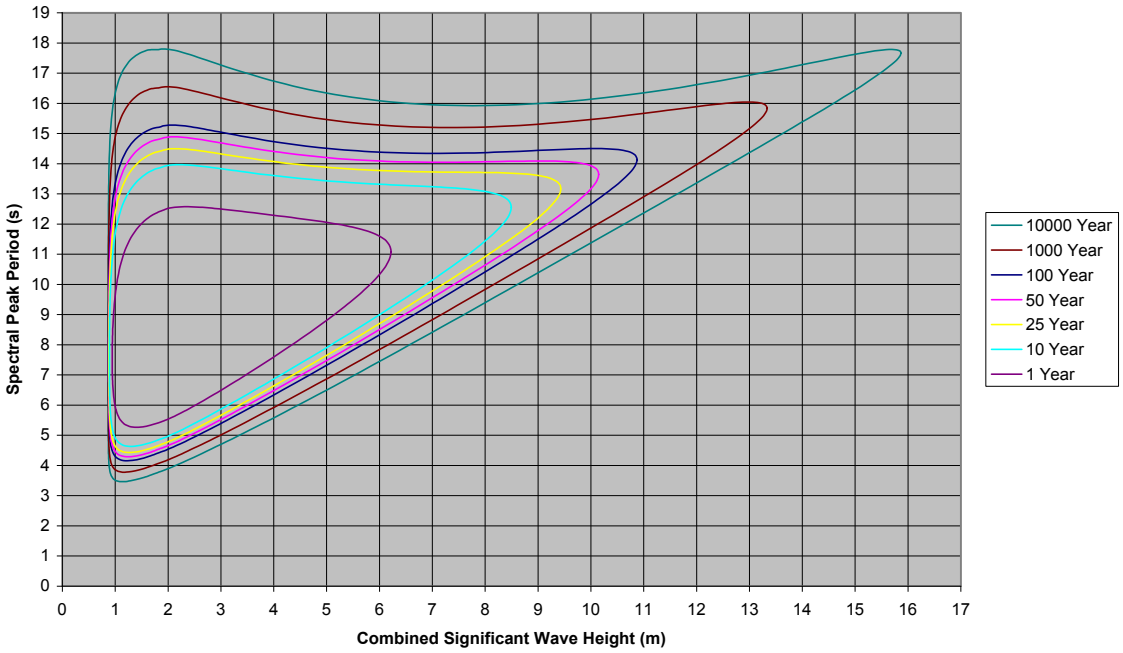

June Environmental Contours for Grid Point 11034 46.7°N 48.1°W
Data from MSC50 Hindcast 1954 - 2009

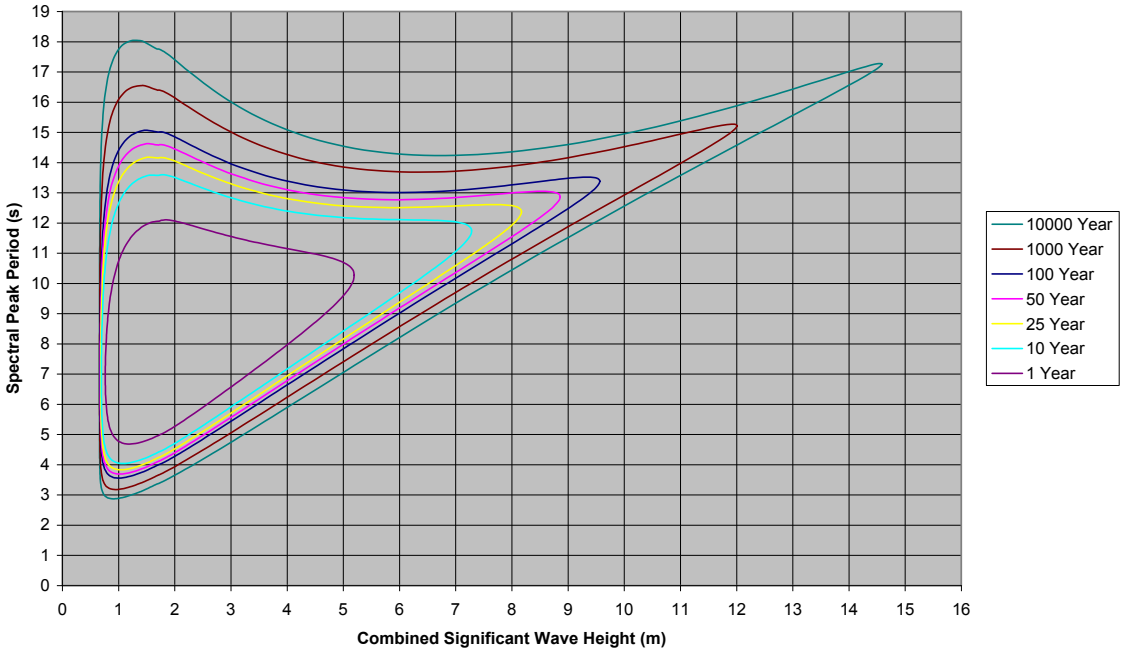

July Environmental Contours for Grid Point 11034 46.7°N 48.1°W
Data from MSC50 Hindcast 1954 - 2009

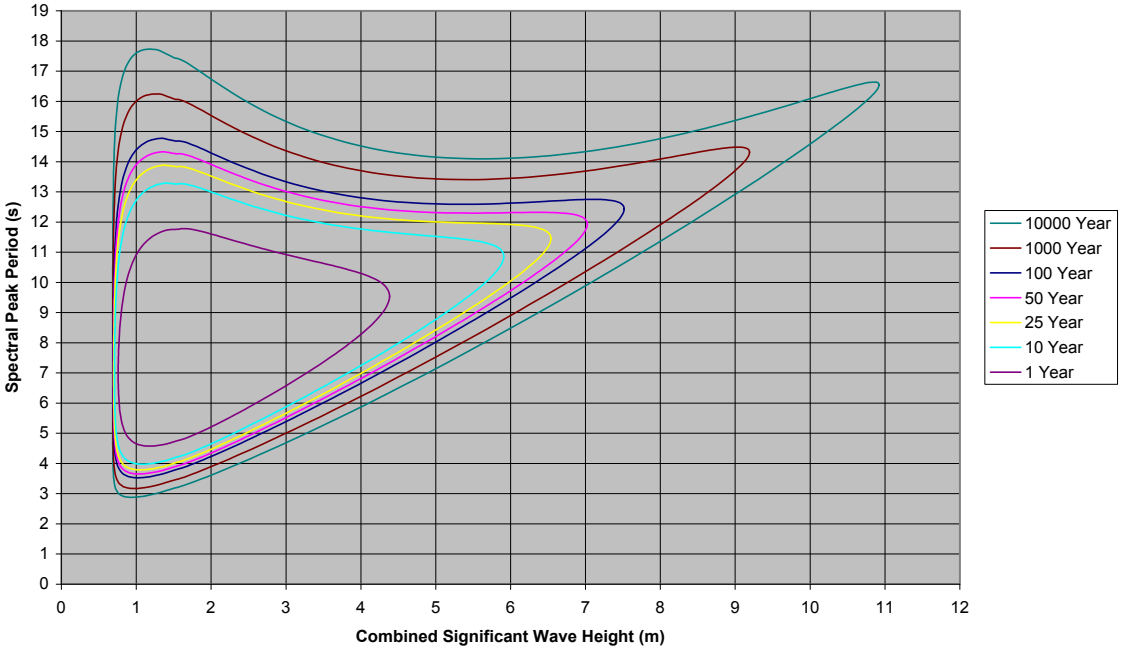

August Environmental Contours for Grid Point 11034 46.7°N 48.1°W
Data from MSC50 Hindcast 1954 - 2009

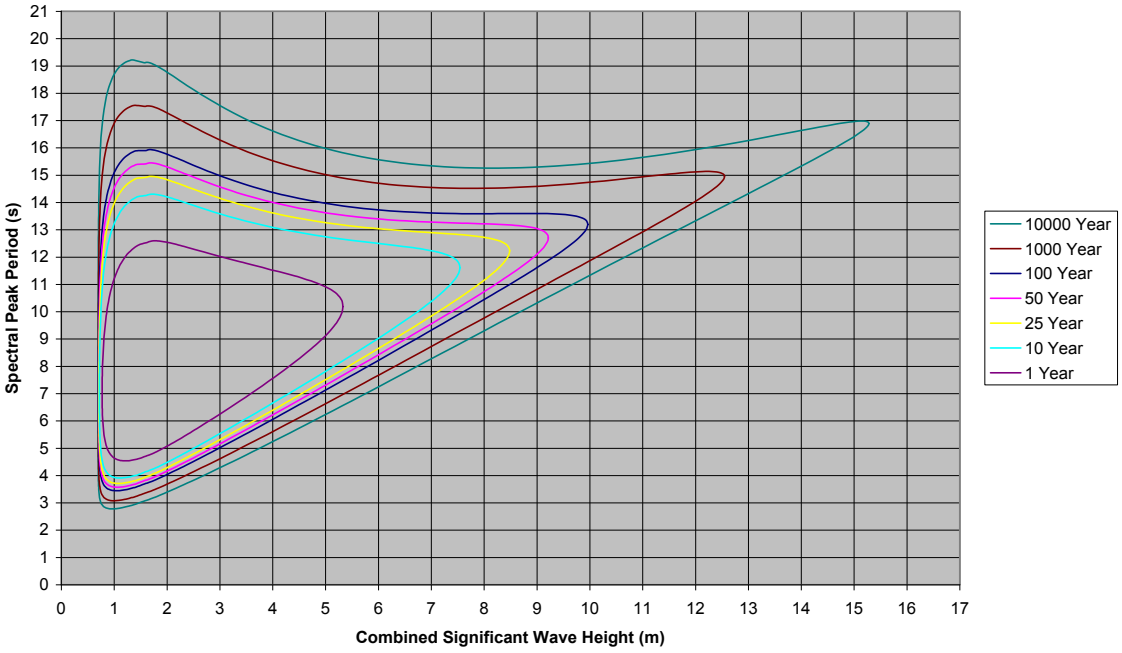

September Environmental Contours for Grid Point 11034 46.7°N 48.1°W
Data from MSC50 Hindcast 1954 - 2009

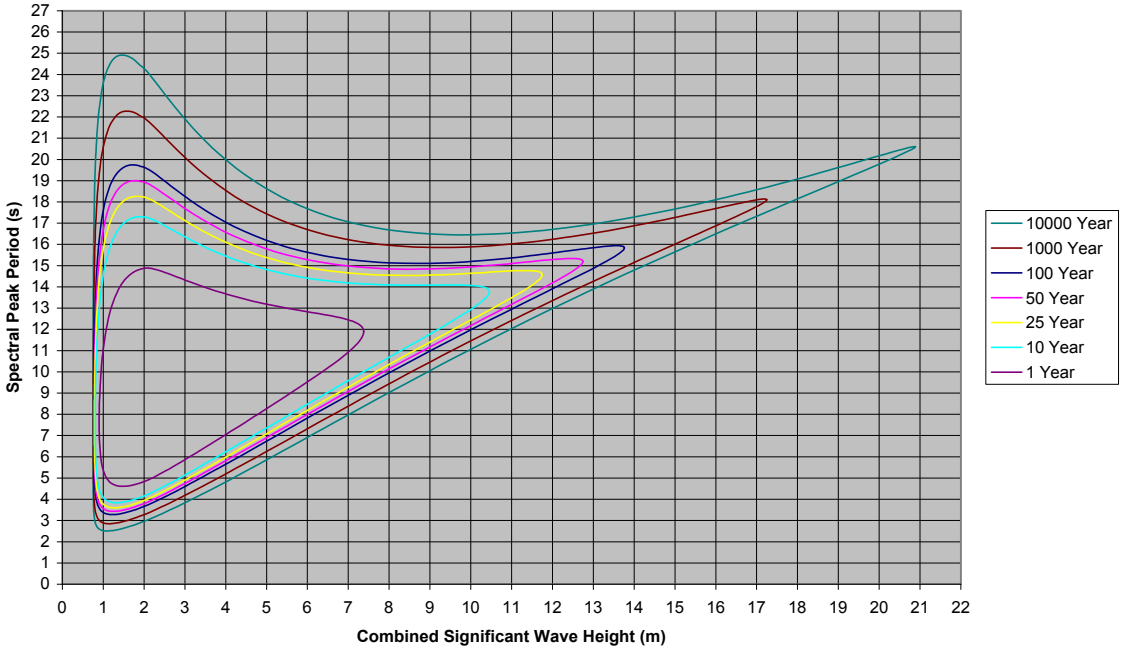

October Environmental Contours for Grid Point 11034 46.7°N 48.1°W
Data from MSC50 Hindcast 1954 - 2009

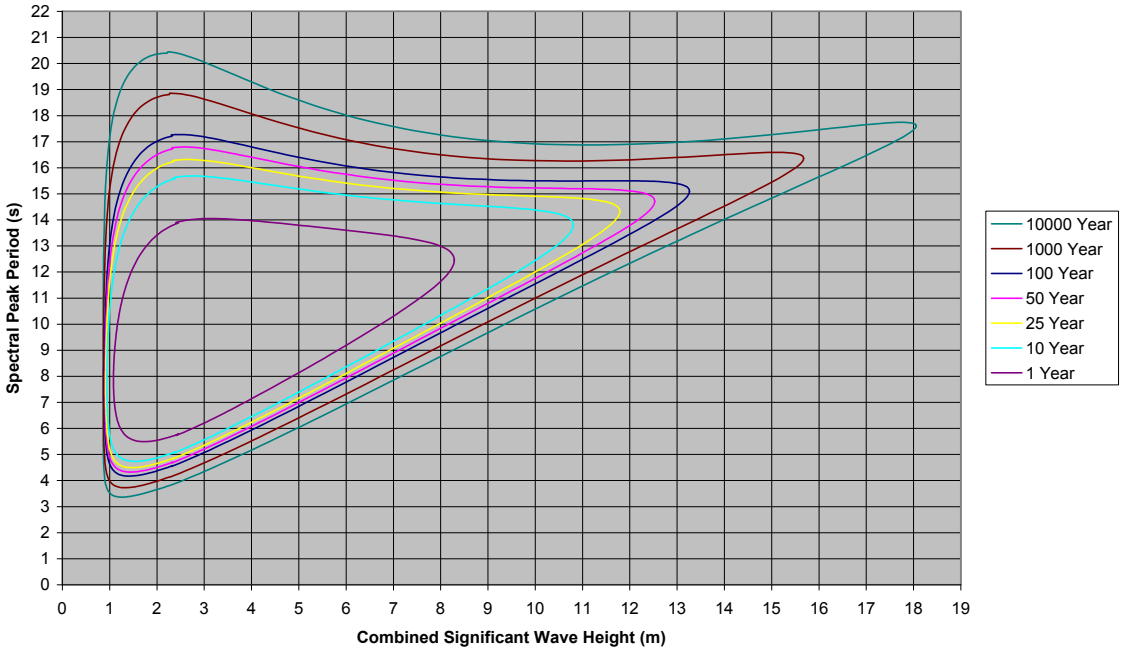

November Environmental Contours for Grid Point 11034 46.7°N 48.1°W
Data from MSC50 Hindcast 1954 - 2009

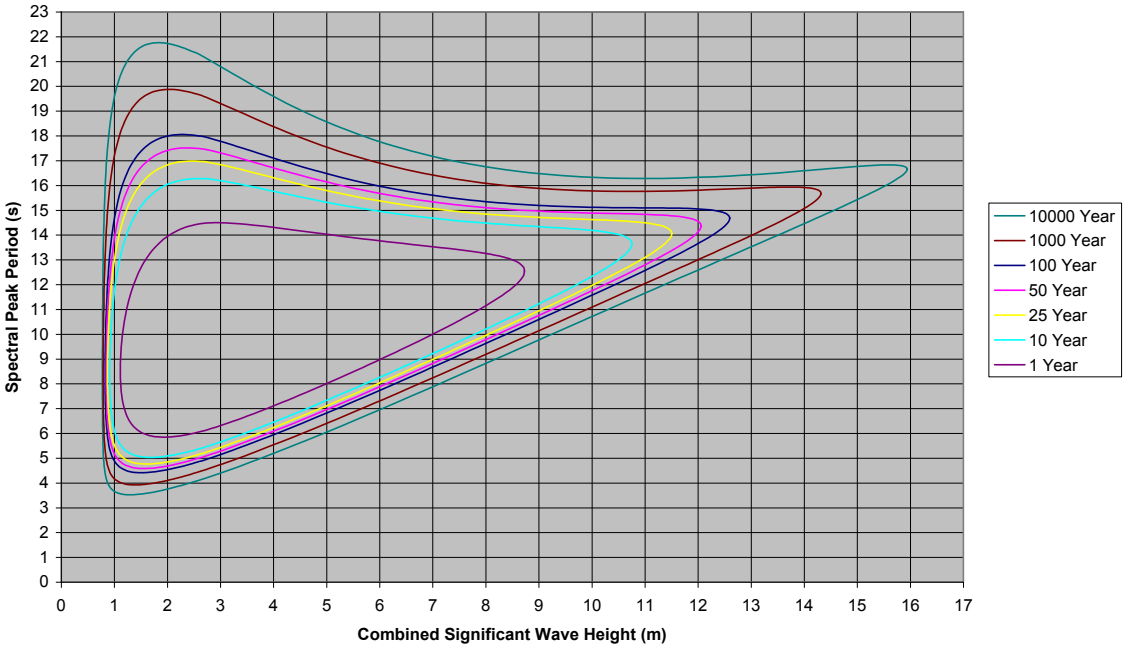

December Environmental Contours for Grid Point 11034 46.7°N 48.1°W
Data from MSC50 Hindcast 1954 - 2009